31 October 2008 | $10

# Science

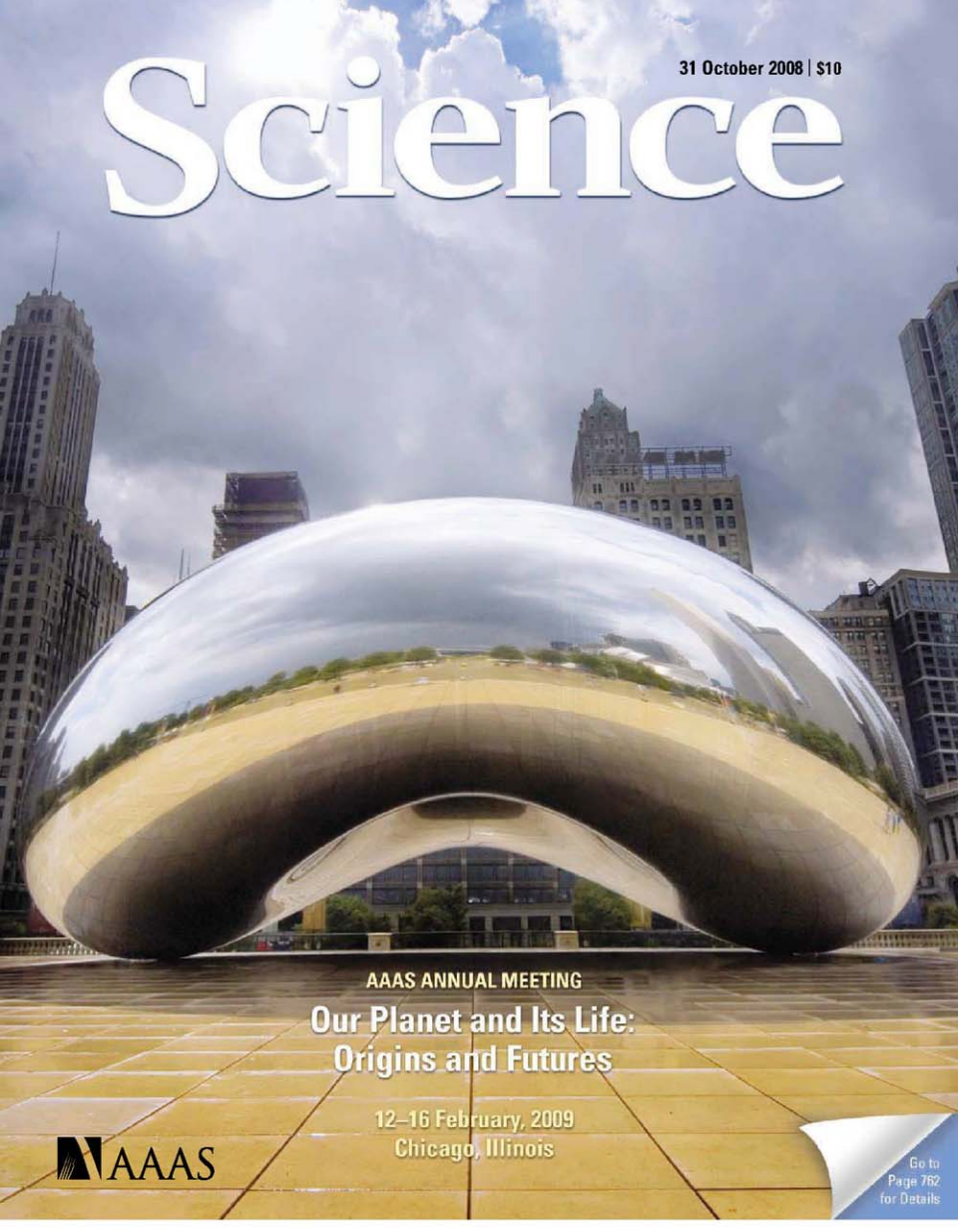

AAAS ANNUAL MEETING

## Our Planet and Its Life: Origins and Futures

12–16 February, 2009
Chicago, Illinois

AAAS

Go to Page 762 for Details

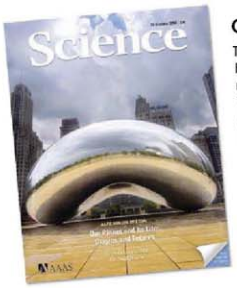


## COVER

The mirror-like surface of Anish Kapoor's sculpture "Cloud Gate" reflects the cityscape of Chicago. The theme of the AAAS Annual Meeting in Chicago, 12 to 16 February 2009, acknowledges the 150th anniversary of Charles Darwin's *On the Origin of Species*, and the meeting starts on his 200th birthday. See the preliminary program beginning on page 762.

***Image: Paul Sampson***

## DEPARTMENTS



## EDITORIAL



## NEWS OF THE WEEK



## NEWS FOCUS



## LETTERS




664

## BOOKS *ET AL.*

*Political Science*




677

## EDUCATION FORUM



## PERSPECTIVES



CONTENTS continued >>

## SCIENCE EXPRESS

www.sciencexpress.org

CHEMISTRY

**Time-Resolved Dynamics in $N_2O_4$ Probed Using High Harmonic Generation**
*W. Li* et al.
Electrons can be ejected from multiple orbitals of $N_2O_4$ by exploiting different stages in its excited vibrations, yielding an attosecond light probe of molecular dynamics.
10.1126/science.1163077

BIOCHEMISTRY

**Structural Evidence for Common Ancestry of the Nuclear Pore Complex and Vesicle Coats**
*S. G. Brohawn* et al.
The protein complex that controls entry and exit from the cell nucleus shares a structural element with vesicle coat proteins, suggesting that it is built around a lattice-like scaffold.
10.1126/science.1165886

**LETTER: European Union and NIH Collaborate**
*E. A. Zerhouni and J. Potočnik*
10.1126/science.1167667

MICROBIOLOGY

**BREVIA: Bat White-Nose Syndrome: An Emerging Fungal Pathogen?**
*D. S. Blehert* et al.
Bats that died en masse in New York state while they were hibernating were infected with a cold-tolerant fungus.
10.1126/science.1163874

CHEMISTRY

**High Harmonic Generation from Multiple Orbitals in $N_2$**
*B. K. McFarland, J. P. Farrell, P. H. Bucksbaum, M. Gühr*
Electron ejection from multiple $N_2$ orbitals, controlled by the molecule's orientation relative to a laser, produces attosecond light spectra that can reveal molecular dynamics.
10.1126/science.1162780

## PERSPECTIVES *CONTINUED...*



## TECHNICAL COMMENT ABSTRACTS

PHYSIOLOGY



## REVIEW

BIOCHEMISTRY



## BREVIA

MICROBIOLOGY



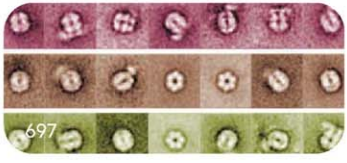


## RESEARCH ARTICLES

CELL BIOLOGY



BIOCHEMISTRY



## REPORTS

PLANETARY SCIENCE



PHYSICS



MATERIALS SCIENCE



**CONTENTS** continued >>

## REPORTS *CONTINUED...*



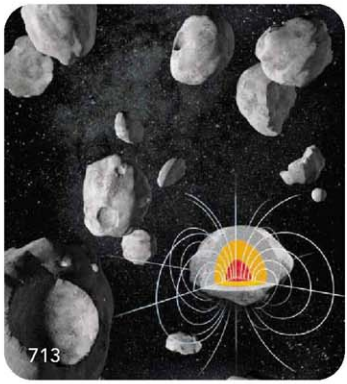




AAAS ADVANCING SCIENCE, SERVING SOCIETY

**SCIENCE** (ISSN 0036-8075) **is published weekly on Friday, except the last week in December, by the American Association for the Advancement of Science, 1200 New York Avenue, NW, Washington, DC 20005.** Periodicals Mail postage (publication No. 484460) paid at Washington, DC, and additional mailing offices.  Domestic individual membership and subscription ($1 issues): $144 ($74 allocated to subscription). Domestic institutional subscription ($1 issues): $770; Foreign postage extra: Mexico, Caribbean (surface mail) $55; other countries (air assist delivery) $85. First class, airmail, student, and emeritus rates on request. Canadian rates with GST available upon request, GST #125488322. Publications Mail Agreement Number 1069624. SCIENCE is printed on 30 percent post-consumer recycled paper. **Printed in the U.S.A.**

**Change of address:** Allow 4 weeks, giving old and new addresses and 8-digit account number. **Postmaster:** Send change of address to AAAS, P.O. Box 96178, Washington, DC 20090–6178. **Single-copy sales:** $10.00 current issue, $15.00 back issue prepaid (includes surface postage; bulk rates on request. **Authorization to photocopy** material for internal or personal use under circumstances not falling within the fair use provisions of the Copyright Act is granted by AAAS to libraries and other users registered with the Copyright Clearance Center (CCC) Transactional Reporting Service, provided that $20.00 per article is paid directly to CCC, 222 Rosewood Drive, Danvers, MA 01923. The identification code for Science is 0036-8075. Science is indexed in the *Reader's Guide to Periodical Literature* and in several specialized indexes.

Printed on 30% post-consumer recycled paper.

CONTENTS continued >>

## SCIENCE**NOW**

www.sciencenow.org

HIGHLIGHTS FROM OUR DAILY NEWS COVERAGE

**Viagra Stands Firm Against Muscular Dystrophy**
Famous anti-impotence pill might compensate for muscle-weakening enzyme deficiency.

**Thanks for Erasing the Memories**
Combination of genetic engineering and drugs wipes out specific memories in mice.

**Not Your Garden-Variety Tomato**
Researchers engineer cancer-fighting purple tomatoes.

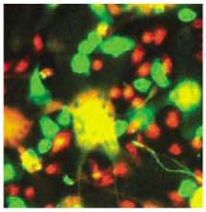

Programming macrophages to fuse.

## SCIENCE **SIGNALING**

www.sciencesignaling.org

THE SIGNAL TRANSDUCTION KNOWLEDGE ENVIRONMENT

**RESEARCH ARTICLE: Essential Role of DAP12 Signaling in Macrophage Programming into a Fusion-Competent State**
*L. Helming, E. Tomasello, T. R. Kyriakides, F. O. Martinez, T. Takai, S. Gordon, E. Vivier*
Signaling through the DAP12 adaptor triggers a gene expression profile that makes macrophages competent to fuse and form multinucleated giant cells.

**PROTOCOL: High-Resolution Imaging of Redox Signaling in Live Cells Through an Oxidation-Sensitive Yellow Fluorescent Protein**
*G. Maulucci, V. Labate, M. Mele, E. Panieri, G. Arcovito, T. Galeotti, H. Østergaard, J. R. Winther, M. De Spirito, G. Pani*
Measure and visualize intracellular changes in the redox state.

**JOURNAL CLUB: The HIF-1α-C/EBPα Axis**
*H. P. Janardhan*
Interactions between HIF-1α and C/EBPα may mediate reciprocal functional effects.

**PODCAST**
*R. Linding and A. M. VanHook*
Rune Linding explains how combining NetPhorest with a genetic screen enables researchers to gain insight into the relationships among the identified players.

CREDITS: (SCIENCE CAREERS) NIH; (SCIENCE SIGNALING) LAURA HELMING/TECHNICAL UNIVERSITY MUNICH/GERMANY

Enthusiasm for virology.

## SCIENCE **CAREERS**

www.sciencecareers.org/career_development

FREE CAREER RESOURCES FOR SCIENTISTS

**The Pathways to Independence Award: Early Returns**
*S. Carpenter*
NIH's new transition awards program seems to be achieving its goal.

**The Other Life Sciences Industry**
*C. Mintz*
The medical devices and diagnostics industry is underappreciated as a life sciences career destination.

**A Virologist With a Contagious Enthusiasm**
*E. Pain*
French virologist Ali Saib is praised for his research achievements and efforts to attract a diversity of people to science.

**From the Archives: Lab Dynamics—Science at the Balcony**
*C. M. Cohen and S. L. Cohen*
How you discuss content or data can be as important as the content or data itself.

## SCIENCE**PODCAST**

www.sciencemag.org/multimedia/podcast

FREE WEEKLY SHOW

Download the 31 October *Science* Podcast to hear about how the bacterium *Wolbachia* protects insects from virus-induced death, academic freedom in China, and more.

***Separate individual or institutional subscriptions to these products may be required for full-text access.***

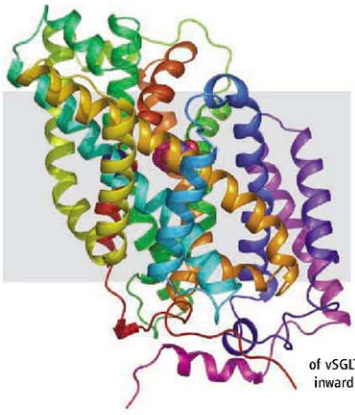

## << Transporter in Action

Secondary active transporters couple transport of substrate to an ion gradient. Transport is proposed to occur through an alternating access mechanism in which a substrate binding site located toward the center of the protein has alternating access to either side of the membrane. Structures of two secondary transporters, the leucine transport protein LeuT and the galactose transport protein vSGLT, are available, but in both structures the substrate is occluded from both sides of the membrane. Now **Weyand *et al.*** (p. 709, published online 16 October) report outward facing open and substrate-bound occluded conformations for a nucleobase transporter. Comparison of the outward facing conformations with the inward facing substrate occluded conformation of vSGLT suggests a structural model for how alternate opening and closing of inward and outward facing cavities is achieved.

## Clocking Clock Components

Like most cells and organisms, cyanobacteria contain a circadian clock that helps to optimize its metabolism for the daily cycles of light, dark, and temperature. This clock can be reconstituted in vitro with just three protein components—KaiA, KaiB, and KaiC. **Johnson *et al.*** (p. 697) review how the high-resolution structures of these proteins show that their interactions result in conformational changes and phosphorylation events over a 24-hour period. Sequential phosphorylation of two amino acids in KaiC may be enforced by the structure of the protein, causing a built-in ratcheting mechanism that drives the oscillator unidirectionally. Thus, the structural features of the three essential clock components, combined with biochemical and biophysical data, reveal molecular mechanisms of biological timekeeping.

## Getting Angrite

Angrites are a type of primitive meteorite from some of the earliest formed planetesimals in our solar system. **Weiss *et al.*** (p. 713) show that angrites preserve a remnant magnetic field that was probably generated internally. These fields were perhaps as large as 20% of that of Earth. Thus it seems that, even in these small primitive bodies, a molten iron core formed rapidly after the formation of the solar system.

## Sediments in Motion

Many models of Earth surface dynamics employ some criteria for determining the conditions that lead to particle entrainment, when oscillating or flowing objects move in step together. An example of this is the dislodging of particles from a sedentary bed into a mildly turbulent flowing stream. In general this has been modeled by considering the time-average boundary shear, which is connected to the maximum force impacts on the particles. **Diplas *et al.*** (p. 717) show that this criterion is not sufficient, and that instead one should consider the impulse, which is a combination of the force and duration, in determining sediment motion.

## Lithographic Liquids

The ability to use polymers for nanometer-scaled imprint lithography depends on being able to control their flow and final dimensions as they are squeezed into shape. One might expect that longer polymers would always show the highest viscosities, because they can form the greatest number of entanglements, and that increasing the applied strain should act on all molecular sizes in a similar way. **Rowland *et al.*** (p. 720, published online 2 October; see the Perspective by **Soles and Ding**) studied a series of polystyrene polymers compressed by a flat rigid die and observed unusual, nonlinear behavior for the thinnest films, where the dimensions of the film approach the unconstrained dimensions of the polymer chains. Thus, at the smallest dimensions, it may be easiest to process very long polymers, which may provide the best lithographic resolution.

## $NO_X$

Atmospheric nitrogen oxides ($NO_2$ + NO, collectively referred to as $NO_X$) are important in the environment, where $NO_2$ is a precursor for nitrate, an essential macronutrient for plants, as well as in the atmosphere, where they are important components of the ozone cycle and particle formation. Although much attention has been paid to regulating the emission of $NO_X$, its atmospheric concentration is increasing globally, even in very remote regions, due to continued and increasing emissions in some parts of the world and long-range transport. **Morin *et al.*** (p. 730) present results of isotopic measurement of N and O in atmospheric nitrate from the High Arctic, which reveal how a combination of transport and springtime photochemical emissions of reactive nitrogen from the snowpack produce an overwhelming flux of $NO_X$. This is important in the process of evaluating pollution threats to the air quality and ecosystems of that region and for understanding the potential impact on climate and biodiversity.

## Emergence of Modern Human Behavior

The time and rate at which modern humans colonized the planet, and the interactions that they had with the indigenous biota, remains a source of continuing debate. **Jacobs *et al.*** (p. 733) report new and precise ages for two short-lived bursts of technological innovation associated with the emergence of modern human behavior during the southern African Middle Stone Age. These key archaeological events cannot be explained by environmental factors alone, but were contemporaneous with—and may have catalyzed—the prehistoric expansion of human populations within Africa and the first successful exodus of people 80 to 60 thousand years ago.

*Continued on page 647*

CREDITS (TOP TO BOTTOM): WEYAND ET AL.; SAMUEL MORIN

*Continued from page 645*

## Tuna Mix

Bluefin Tuna are split into two populations. The western population spawns in the Gulf of Mexico and the eastern population spawns in the Mediterranean Sea. The western population is in a particularly vulnerable state, and conservation management zones that are currently arbitrarily demarked by 45°W longitude do not seem to be alleviating the population decline. In an attempt to find out why tuna management is ineffective, **Rooker *et al.*** (p. 742, published online 2 October) have taken cores from otoliths in the fishes' ears and measured carbon and oxygen isotope ratios to obtain a chemical signature characteristic of the fishes' birthplace. Adolescent fish from both populations, oblivious to the 45°W management boundary, mix on their extensive migrations to feed in the Atlantic Ocean. As the tuna mature they exhibit a strong tendency to return, like salmon, to their birthplace to spawn. Unexpectedly, the waters around the Gulf of Maine and St. Lawrence were refugia for mature adults from the western population, which may have implications for revising tuna management across international boundaries.

## Mussels and Self-Organization

The concept of spatial self-organization, where small-scale interactions between individual organisms drive large-scale spatial patterns, is the main explanation for coherent spatial patterns in a wide range of terrestrial and aquatic ecosystems. **Van de Koppel *et al.*** (p. 739) present an experimental test of the mechanisms underlying spatial self-organization in an ecosystem—mussels on the seabed. Regular spatial patterns emerge in a mussel bed under experimentally controlled conditions, which modeling suggests arise from interactions between individual mussels. A subsequent field study showed the positive effects of self-organization on ecosystem-level processes, in particular, secondary production and resistance to wave disturbance, pointing to the need for conservation of spatial structure within ecosystems.

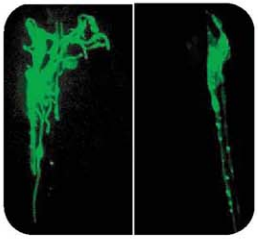

## Of Glia and Senses

Sensory organs are the main conduit by which an animal perceives its environment, and these organs have been remarkably conserved in anatomy, morphology, and molecular biology from *Caenorhabditis elegans* to humans. To explore the role of glial cells in sensory perception **Bacaj *et al.*** (p. 744; see the Perspective by **Reichenbach and Pannicke**) examined their functions in the amphid, the largest *C. elegans* sense organ, and revealed essential functions for glia in regulating neuronal morphology and activity. The sheath glial cell of the amphid is required for several functional aspects of the ensheathed sensory neurons.

## HARPing On

The complementarity of DNA and RNA is of great utility for the conveyance of genetic information, as well as (mainly in the case of RNA) the formation of secondary and tertiary structure critical for function. Still, for the information to be read, or the structures to be assembled or disassembled, the base-paired strands of nucleic acid need to be pulled asunder. This feat is carried about by a ubiquitous class of enzymes known as helicases. **Yusufzai and Kadonaga** (p. 748) have now characterized precisely the opposite activity, a human enzyme, HARP (HepA-related protein), a distant member of the SNF2 family of ATP-driven molecular motor proteins, that uses ATP to zip up stably separated strands of DNA. Mutations in HARP result in Schimke immuno-osseous dysplasia, a fatal autosomal recessive disorder. In patients, the severity of the disease correlates with the loss of reverse helicase activity of the enzyme.

## TRPM7 and T Cell Development

The transient receptor potential melastatin-like 7 (TRPM7) protein is a membrane ion channel that conducts $Ca^{2+}$ and $Mg^{2+}$ ions. Its physiological role has been proposed to be essential for $Mg^{2+}$ uptake and homeostasis of $Mg^{2+}$ concentrations in whole animals. To examine the physiological roles of the channel in vivo, **Jin *et al.*** (p. 756) studied mice in which the channel was specifically depleted from the T cell lineage. The results suggest that TRPM7 is required for a developmentally important step in thymic maturation of T cells.

CREDITS: (TOP TO BOTTOM) BACAJ ET AL.

Wen Jiabao is Premier of the State Council of the People's Republic of China.*

# Science and China's Modernization

THE HISTORY OF MODERNIZATION IS IN ESSENCE A HISTORY OF SCIENTIFIC AND TECHNOLOGICAL progress. Scientific discovery and technological inventions have brought about new civilizations, modern industries, and the rise and fall of nations. China is now engaged in a modernization drive unprecedented in the history of humankind.

Over the past half century, China has made great achievements in basic science and technological innovation. It now ranks among the top nations in the annual number of papers published internationally and patent applications filed. China has also made achievements in such areas as manned space flight, high-performance computers, super–large-scale integrated circuits, and third-generation telecommunications technology. High-tech industry has experienced rapid growth, accounting for over 15% of the manufacturing industry.

Francis Bacon, the 16th-century English philosopher, referred to science as a means to improve humankind's lot. Today, the hybrid rice variety developed by Chinese scientists has been adopted for planting in over three million hectares and has become a "golden key" to meeting China's own food needs and boosting world cereal production. Scientific and technological development in the realm of health has also increased average life expectancy in China to that in developed countries.

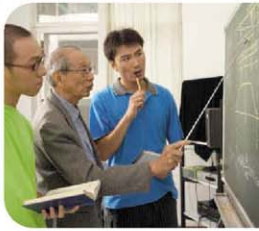

To encourage further innovation, the Chinese government has formulated a Mid- to Long-Term Plan for Development of Science and Technology (2006–2020), which highlights research in the basic sciences and frontier technologies, with priority given to energy, water resources, and environmental protection. We strive to develop independent intellectual property rights in areas of information technology and new materials, while strengthening the application of biotechnology to agriculture, industry, population, and health.

The future of China's science and technology depends fundamentally on how we attract, train, and use young scientific talents today. Thus, at the core of our science and technology policy is attracting a diverse range of talents, especially young people, into science and providing them with an environment that brings out the best of their creative ideas.

In the field of science and technology, we will intensify institutional reform, restructure scientific research, rationally allocate public resources, and enhance innovation capability. We advocate free academic debate under a lively academic atmosphere, where curiosity-driven exploration is encouraged and failure tolerated.

Science has no boundaries. China's endeavors in science and technology need to be more integrated with those of the world, and the world needs a China that is vibrant and able to deliver more in science and technology. Just as collisions generate sparks, exchange and communication enrich imagination and creativity. Many Chinese scientists have stepped into the international academic arena, where they and their foreign colleagues learn from each other and jointly contribute to the worldwide development of science and technology.

To encourage the learning and application of science among the general public, we need to embrace a scientific culture by promoting scientific rationality while cherishing Chinese cultural heritage. Enlightened by science, the rich and profound Chinese culture is bound to shine more gloriously.

I firmly believe that science is the ultimate revolution. At a time when the current global financial turmoil is dealing a heavy blow to the world economy, it has become all the more important to rely on scientific and technological progress to promote growth in the real economy. Economic and social development must rely on science and technology, and science and technology must serve economic and social development. We will rely on science and technology to promote economic restructuring, transform development patterns, safeguard food and energy security, and address global climate change. We are confident that China will reap a rich harvest in science and technology and that this will have positive and far-reaching effects on human civilization and the well-being of humankind.

**– Wen Jiabao**

10.1126/science.1166843

* See *Science*'s interview with Wen Jiabao, 17 October 2008, p. 362.

CREDITS: (TOP) AP; (RIGHT) GETTY IMAGES

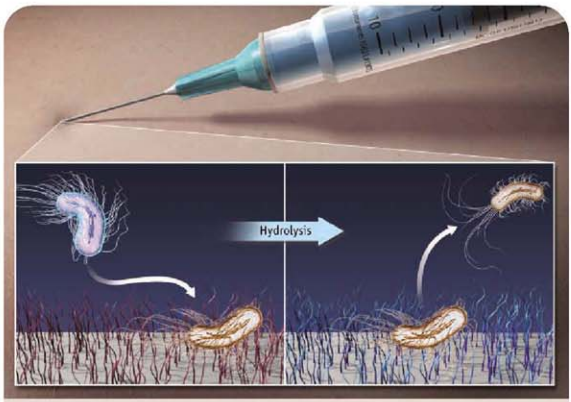


CHEMISTRY

## Catch, Kill, and Release

During the implantation or insertion of medical devices such as catheters, pathogenic microbes may be introduced into the patient. Once implanted, microbes may attach to the surface of the device to form a biofilm, a common cause of device failure. To overcome these problems, several strategies have been used to create coatings that are either antimicrobial or nonfouling. Cheng *et al.* now report a coating that combines both properties, switching from antimicrobial to nonfouling upon hydrolysis. Specifically, they apply a poly(methacrylate) derivative with cationic side chains that become zwitterionic upon conversion of a terminal ester to a carboxylate. Within 1 hour of exposure to the initially prepared coating, 99.9% of attached *Escherichia coli* bacteria were dead. Over the course of the next 2 to 8 days, the coating slowly hydrolyzed, releasing 98% of the dead microbial cells. The nonfouling nature of the hydrolyzed coating prevents further attachment of microbial cells and formation of a biofilm. By tuning the hydrolysis rate of the coating, it should be possible to adapt it to a range of applications in implantable medical devices. — JFU

*Angew. Chem. Int. Ed.* **47**, 10.1002/anie.200803570 (2008).

ECOLOGY

## Early Life Experiences

The decline of Columbia River salmon may be one sign of the human impact on fisheries, and it has been argued that some of the Columbia River dams should be removed in order to reduce the hazards encountered by salmon smolts as they make their way from the spawning grounds to the sea. In order to assess migration losses in the Thompson-Fraser (which is not dammed) and the Snake-Columbia (which is) river systems in North America, Welch *et al.* measured the survival rate of Chinook and steelhead smolts with implanted acoustic tags. Surprisingly, their data suggest that the survival rates of juvenile fish making these journeys are comparable; in fact, they are somewhat higher in the hydroelectric power–generating portion of the Columbia. Two corollaries to be examined are (i) whether the Fraser River imposes an unidentified toll on juvenile survival, and (ii) whether the transit through the systems of dams exacts a later cost in terms of ocean mortality. — LMZ

*PLoS Biol.* **6**, e265 (2008).

ECOLOGY

## A Diversity of Consumers

The vulnerability of coral reefs to human interference has become only too apparent. Caribbean reefs in particular have been battered by climate change, overfishing, and the excessive growth of seaweed (macroalgae). In order to isolate a key factor that improves reef health even under environmental challenge, Burkepile and Hay corralled herbivorous parrotfish and surgeonfish, alone and in combination, in cages on reefs off the Florida Keys. The outcomes: No fish, and seaweed takes over; add two fish species, and the algae are kept under control and coral cover increases. Alongside ocean surgeonfish, the redband parrotfish were particularly effective consumers of early algal colonizers because the surgeonfish removed the less abundant species of algae that the parrotfish found distasteful. Not all parrotfish were the same: Princess parrotfish preferred the mat-forming seaweeds, and redbands grazed the taller species.

*Continued on page 653*


Ocean surgeon fish.

PHYSICS

## Purifying X-ray Pulses

Static structural information on solids is now routinely obtained in exquisite detail using coherent x-rays at synchrotron facilities. Probing of the dynamics of structural and electronic phase transitions can also be achieved using pulses of x-rays on the relevant time scales—picosecond and femtosecond—but the generation of such x-ray pulses is not trivial and the techniques are still under development. The usual route to obtain pulses of light is to use a cavity, with the output period of the pulses on the order of the return transit time of the cavity. However, it has been difficult to control the phase of the cycling x-rays within the cavity, leading to incoherent pulses. Based on the principle of reflection and trapping within the cavity, but using diffraction from crystallographic planes of silicon, Chen *et al.* have developed a Fabry-Perot type of cavity for x-rays. They demonstrate the ability to maintain coherence and form standing waves within the cavity, obtaining promising results toward the goal of obtaining a high-brightness source of quasi-coherent x-ray pulses for probing the dynamics of structural and electronic transitions. — ISO

*Appl. Phys. Lett.* **93**, 141105 (2008).

*Helen Pickersgill and Chris Surridge are locum editors in *Science*'s editorial department.

CREDITS (TOP TO BOTTOM): C. NICKEL/*SCIENCE*; DEBON BURKEPILE

Continued from page 651

These experiments underline the importance of grazer diversity to coral reef health, especially in the Caribbean. — CA

*Proc. Natl. Acad. Sci. U.S.A.* **105**, 16201 (2008).

BIOPHYSICS

## Swimming in Sand

Several species of lizard are capable of traveling for long distances beneath the surface of desert sands. Most have very reduced, or even absent, limbs and adopt a serpentine motion akin to the swimming of water snakes. In contrast, the sandfish lizard (*Scincus scincus*) of North Africa and the Arabian peninsula has well-developed limbs that it was assumed were held tightly against its body when moving through sand.

Baumgartner *et al.* used nuclear magnetic resonance imaging to observe sandfish movement directly and found that they actually propel

themselves with their limbs. Unlike a swimming snake, which drives its near-stationary head forward with sinusoidal movements of its body that increase in amplitude toward its tail, the whole body of the sandfish underwent sinusoidal oscillations with a frequency of 3 Hz and an amplitude of around half its body length. The oscillations of the lizard's body act to fluidize the surrounding sand, an effect well known to engineers dealing with granular media. Using a vibrating metal rod of similar dimensions to a sandfish, the authors confirmed that the resistance to motion through dry sand dropped dramatically when horizontal oscillations were faster than 2.5 Hz. Within this localized volume of fluidized sand the sandfish swims by paddling its fore and hind limbs in synchrony with the flexing of its body. — CS*

*PLoS ONE* **3**, e3309 (2008).

DEVELOPMENT

## Giving a Twist to Twist

Cells initiate and are subject to a great many morphogenetic movements—such as migration, stretching, and invagination—during early embryogenesis. The mechanics at play when cells shuffle around may serve not only to get them to the right place at the right time but also to regulate gene expression.

Desprat *et al.* tested this idea using physical means to mimic deformation forces during early gastrulation in *Drosophila*. In wild-type embryos, the expression of Twist increases when stomodeal cells are compressed during germ band extension. After experimentally eliminating the natural compressing forces by ablating the most dorsal cells, the authors mechanically perturbed the embryos either by using a needle to create a 20-μm indentation or by using magnetic tweezers to apply a force of 60 nN to a ferrofluid injected just before cellularization (and then captured by the newly formed anterodorsal cells). At the molecular level, reproducing stomodeum compression via these mechanical manipulations resulted in the nuclear localization of Armadillo, which led to elevated Twist expression that in turn was necessary for differentiation of the fly midgut. These results demonstrate the potential that the experimental manipulation of tissue deformation holds for the study of molecular and physiological responses. — BAP

*Dev. Cell* **15**, 470 (2008).

CELL BIOLOGY

## Talking About Stress

Cells encounter many different forms of stress and have evolved a variety of methods to deal with them. They tackle relatively minor stresses, such as excessive heat or insufficient oxygen (hypoxia), by forming cytoplasmic stress granules, which prevent the accumulation of defective proteins that can irreparably damage the cell. However, some stresses, including x-rays and DNA-damaging agents, are insurmountable, and the cell acknowledges defeat by killing itself in a process called apoptosis. This is triggered via the intracellular signaling cascades known as the stress-activated p38 and JNK MAPK (SAPK) pathways. Whether and how these two mechanisms of stress management are connected was unknown.

Arimoto *et al.* find that the formation of stress granules in response to minor stresses specifically inhibits the SAPK-mediated cell death response, indicating a connection between the two pathways. They found that the signaling scaffold protein RACK1 is required for the apoptotic response by binding directly to a protein in the SAPK pathway. However, during minor stresses RACK1 becomes sequestered within the cytoplasmic stress granules, thereby inhibiting apoptosis. The authors also showed that when cells are exposed to both types of stresses simultaneously, SAPK-mediated apoptosis is blocked. This mechanism of cross talk between two stress-management pathways could explain in part why cancer cells, which live under the constant minor stress of hypoxia, are resistant to apoptosis induced by radiotherapy and chemotherapy. — HP*

*Nat. Cell Biol.*, 10.1038/ncb1791 (2008).

CREDIT: FRANK GREENAWAY/GETTY IMAGES

www.sciencemag.org

# Science

1200 New York Avenue, NW
Washington, DC 20005
Editorial: 202-326-6550, FAX 202-289-7562
News: 202-326-6581, FAX 202-371-9227
Bateman House, 82-88 Hills Road
Cambridge, UK CB2 1LQ
+44 (0) 1223 326500, FAX +44 (0) 1223 326501

**Subscription Services** For change of address, missing issues, new orders and renewals, and payment questions: 866-434-AAAS (2227) or 202-326-6417, FAX 202-842-1065. Mailing addresses: AAAS, P.O. Box 96178, Washington, DC 20090-6178 or AAAS Member Services, 1200 New York Avenue, NW, Washington, DC 20005

**Institutional Site Licenses** please call 202-326-6755 for any questions or information

**Reprints:** Author inquiries 800-635-7181
Commercial inquiries 803-359-4578

**Permissions** 202-326-7074, FAX 202-682-0816

**Member Benefits** AAAS/Barnes&Noble.com bookstore www.aaas.org/bn; AAAS Online Store www.aplsource.com/aaas/ code MKB6; AAAS Travels: Betchart Expeditions 800-252-4910; Apple Store www.apple/epptstore/aaas; Bank of America MasterCard 1-800-833-4262 (priority code FAA3YU); Cold Spring Harbor Laboratory Press Publications www.cshlpress.com/affiliates/aaas.htm; GEICO Auto Insurance www.geico.com/landingpage/go51.htm?logo=17624; Hertz 800-654-2200 CDP#343457; Office Depot https://bsd.officedepot.com/portalLogin.do; Seabury & Smith Life Insurance 800-424-9883; Subaru VIP Program 202-326-6417; VIP Moving Services www.vipmayflower.com/domestic/index.html; Other Benefits: AAAS Member Services 202-326-6417 or www.aaasmember.org.

| | |
|---|---|
| science_editors@aaas.org | (for general editorial queries) |
| science_letters@aas.org | (for queries about letters) |
| science_reviews@aaas.org | (for returning manuscript reviews) |
| science_bookrevs@aaas.org | (for book review queries) |

Published by the American Association for the Advancement of Science (AAAS), *Science* serves its readers as a forum for the presentation and discussion of important issues related to the advancement of science, including the presentation of minority or conflicting points of view, rather than by publishing only material on which a consensus has been reached. Accordingly, all articles published in *Science*—including editorials, news and comment, and book reviews—are signed and reflect the individual views of the authors and not official points of view adopted by AAAS or the institutions with which the authors are affiliated.

AAAS was founded in 1848 and incorporated in 1874. Its mission is to advance science, engineering, and innovation throughout the world for the benefit of all people. The goals of the association are to: enhance communication among scientists, engineers, and the public; promote and defend the integrity of science and its use; strengthen support for the science and technology enterprise; provide a voice for science on societal issues; promote the responsible use of science in public policy; strengthen and diversify the science and technology workforce; foster education in science and technology for everyone; increase public engagement with science and technology; and advance international cooperation in science.

**Information for Authors**
See pages 634 and 635 of the 1 February 2008 issue or access www.sciencemag.org/about/authors

EDITOR-IN-CHIEF **Bruce Alberts**
EXECUTIVE EDITOR **Monica M. Bradford**
DEPUTY EDITORS **R. Brooks Hanson, Barbara R. Jasny, Katrina L. Kelner**
NEWS EDITOR **Colin Norman**

**Editorial supervisory senior editor** Phillip D. Szuromi; **senior editor/perspectives** Lisa D. Chong; **senior editors** Gilbert J. Chin, Pamela J. Hines, Paula A. Kiberstis (Boston), Marc S. Lavine (Toronto), Beverly A. Purnell, L. Bryan Ray, Guy Riddihough, H. Jesse Smith, Valda Vinson; **associate editors** Jake S. Yeston, Laura M. Zahn; **online editor** Stewart Wills; **associate online editors** Robert Frederick, Tara S. Marathe; **web content director** Martyn Green; **book review editor** Sherman J. Suter; **associate letters editor** Jennifer Sills; **editorial manager** Cara Tate; **senior copyeditors** Jeffrey E. Cook, Cynthia Howe, Harry Jach, Barbara P. Ordway, Trista Wagoner; **copyeditors** Chris Filiatreau, Lauren Kmec; **editorial coordinators** Carolyn Kyle, Beverly Shields; **publications assistant** Ramatoulaye Diop, Joi S. Granger, Jeffery Hearn, Lisa Johnson, Scott Miller, Jerry Richardson, Jennifer A. Seibert, Brian White, Anita Wynn; **editorial assistants** Carlos L. Durham, Emily Gutse, Patricia M. Moore; **executive assistant** Sylvia S. Kihara; **administrative support** Maryrose Madrid

**News deputy news editors** Robert Coontz, Elliot Marshall, Jeffrey Mervis, Leslie Roberts; **contributing editors** Elizabeth Culotta, Polly Shulman; **news writers** Yudhijit Bhattacharjee, Adrian Cho, Jennifer Couzin, David Grimm, Constance Holden, Jocelyn Kaiser, Richard A. Kerr, Eli Kintisch, Andrew Lawler (New England), Greg Miller, Elizabeth Pennisi, Robert F. Service (Pacific NW), Erik Stokstad; **intern** Rachel Zelkowitz; **contributing correspondents** Jon Cohen (San Diego, CA), Daniel Ferber, Ann Gibbons, Robert Koenig, Mitch Leslie, Charles C. Mann, Virginia Morell, Evelyn Strauss, Gary Taubes; **copy editors** Linda B. Felaco, Melvin Gatling, Melissa Ratmondi; **administrative assistant** Sharmaine Mack, Fannie Groom; **interns** New England: 207-549-7755, San Diego, CA: 760-942-3252, FAX 760-942-4979, Pacific Northwest: 503-963-1940

**Production director** James Landry; **senior manager** Wendy K. Shank; **assistant manager** Rebecca Doshi; **senior specialists** Steve Forrester, Chris Redwood; **specialist** Anthony Rosen; **prepflight director** David M. Tompkins; **manager** Marcus Spiegler; **specialist** Jessie Mudjitaba

**Art director** Yael Kats; **associate art director** Aaron Morales; **illustrators** Chris Bickel, Katharine Sutliff; **senior art associates** Holly Bishop, Laura Creveling, Preston Huey, Nayomi Kevithyagalla; **associate** Jessica Newfield; **photo editor** Leslie Bitzard

**Science International**

**Europe** (science@science-int.co.uk) **editorial: international managing editor** Andrew M. Sugden; **senior editor/perspectives** Julia Fahrenkamp-Uppenbrink; **senior editor** Caroline Ash, Stella M. Hurtley, Ian S. Osborne, Peter Stern; **editorial support** Deborah Dennison, Rachel Roberts, Alice Whaley; **administrative support** John Cannell, Janet Clements; **news: europe news editor** John Travis; **deputy news editor** Daniel Clery; **contributing correspondents** Michael Balter (Paris), John Bohannon (Vienna), Martin Enserink (Amsterdam and Paris), Gretchen Vogel (Berlin); **intern** Sara Coelho

**Asia** Japan Office: Asca Corporation, Eiko Ishioka, Fusako Tamura, 1-8-13, Hirano-cho, Chuo-ku, Osaka-shi, Osaka, 541-0046 Japan; +81 (0) 6 6202 6272, FAX +81 (0) 6 6202 6271; asca@os.gulf.or.jp; **asia news editor** Richard Stone (Beijing; rstone@aaas.org); **contributing correspondents** Dennis Normile (Japan: +81 (0) 3 3391 0630, FAX +81 (0) 3 5936 3531; dnormile@gol.com); Hao Xin (China: +86 (0) 10 6307 4439 or 6307 3676, FAX +86 (0) 10 6307 4358; dindyhao@gmail.com); Pallava Bagla (South Asia: +91 (0) 11 2271 2896; pbagla@vsnl.com)

EXECUTIVE PUBLISHER **Alan I. Leshner**
PUBLISHER **Beth Rosner**

**Fulfillment Systems and Operations** (membership@aaas.org): **director** Waylon Butler; **senior systems analyst** Jonny Blaker; **customer service supervisor** Pat Butler; **specialists** Latoya Casteel, LaWonda Crawford, Vicki Linton, April Marshall; **data entry supervisor** Cynthia Johnson; **specialists** Tamika Hill, Elenzo Bowden

**Business Operations and Administration director** Deborah Rivera-Wienhold; **assistant director, business operations** Randy Yi; **manager, business analysis** Michael LoBue; **manager, business operations** Jessica Tierney; **financial analysts** Patti Paimanet, Celeste Troxler; **rights and permissions: administrator** Emilie David; **associate** Elizabeth Sandler; **marketing director** John Meyers; **marketing manager** Allison Pritchard; **marketing associates** Aimee Aponte, Alison Chandler, Mary Ellen Crowley, Marcia Leach, Julianne Weiga, Wendy Wise; **international marketing manager** Wendy Sturley; **marketing executive** Jennifer Reeves; **membership number services executive** Linda Rusk; **site license sales director** Tom Ryan; **sales manager** Russ Edra; **sales and customer service** Iquo Edim, Kiki Forsythe, Catherine Holland, Phillip Smith, Phillip Tsolakidis; **corporate relations director** Ellen Bermudette-Moran; **electronic media: manager** Elizabeth Hartman; **project manager** Trista Snyder; **assistant manager** Lisa Stanford; **senior production specialists** Christopher Coleman, Walter Jones; **production specialists** Michele Johnston, Kimberly Oster

**Advertising director, worldwide ad sales** Bill Moran

**Product** (science_advertising@aaas.org): **midwest** Rick Bongiovanni: 330-405-7080, FAX 330-405-7081; **west coast/w. canada** Teola Young: 650-964-2266; **east coast/e. canada** Laurie Faraday: 508-747-9395, FAX 617-507-8189; **ukeurope/asia** Tracy Holmes: +44 (0) 1223 326525, FAX +44 (0) 1223 326532; **japan** Mashy Yoshikawa: +81 (0) 3 3235 5961, FAX +81 (0) 3 3235 5852; **senior traffic associate** Delandra Simms

**Commercial Editor** Sean Sanders: 202-326-6430

**Project Director, Outreach** Brianna Blaser

**Classified** (advertise@sciencecareers.org): **us: recruitment sales manager** Ian King: 202-326-6528, FAX 202-289-6742; **inside sales manager: midwest/canada** Daryl Anderson: 202-326-6543; **inside sales representative** Karen Foote: 202-326-6740; **key account manager** Joribah Abic: **northeast** Abeni Fleming: 202-326-6578; **southeast** Tina Burks: 202-326-6577; **west** Nicholas Hinrichsen: 202-326-6533; **sales coordinators** Erika Foard, Rohan Edmonson, Shirley Young; **international: sales manager** Tracy Holmes: +44 (0) 1223 326525, FAX +44 (0) 1223 326532; **sales** Dan Pennington, Alex Palmer, Alessandra Sorgente; **sales assistant** Louise Moore; **japan** Mashy Yoshikawa: +81 (0) 3 3235 5961, FAX +81 (0) 3 3235 5852; **advertising production operations manager** Deborah Tompkins; **senior production specialists** Robert Buck, Amy Hardcastle; **senior traffic associate** Christine Hall; **publications assistant** Mary Lagnaoui

**AAAS Board of Directors retiring president, chair** David Baltimore; **president** James J. McCarthy; **president-elect** Peter C. Agre; **treasurer** David E. Shaw; **chief executive officer** Alan I. Leshner; **board** Lynn W. Enquist, Susan M. Fitzpatrick, Alice Gast, Linda P. B. Katehi, Nancy Knowlton, Cherry A. Murray, Thomas D. Pollard, Thomas A. Woolsey

AAAS
ADVANCING SCIENCE, SERVING SOCIETY


Psychologists at the University of Hertfordshire, U.K., last week unveiled what they are billing as "the world's most relaxing room." The 160-square-meter space, bathed in green lights with an artificially lit blue sky, is furnished with soft mats and lavender-scented pillows "to create a relaxing environment with no sense of threat," explains the project's mastermind Richard Wiseman.

The design is based on research on the effects of light, scent, and music in relaxation. "Cold colors such as blue and green tend to be perceived as calming, whereas warm colors can be perceived as arousing," explains Birgitta Gatersleben, an environmental psychologist from the University of Surrey in Guildford, U.K. Lavender is said to reduce anxiety and induce sleep by lowering the levels of the stress hormone cortisol. The room also features specially composed music with a slow, steady beat and low-frequency tones.

So far, the room's 200 visitors have given it mixed reviews. "Some people absolutely love it and can't have enough of it," Wiseman says. "But people who thrive on and need stress to work absolutely hate it."

The project was designed to be easy to replicate in offices and other real-life environments. "I would like to see relaxation rooms in public spaces," Wiseman adds. "If we pay 20p to use a toilet in King's Cross train station, why not pay for 20 minutes of peace?"

## A Bank for China's Wild Plants

A new seed bank, occupying vaults under China's Kunming Institute of Botany, opened this week in Yunnan Province. The Southwest China Germplasm Bank of Wild Species, a joint project of the Chinese Academy of Sciences and the U.K.'s Kew Millennium Seed Bank Project (MSBP), will preserve seeds from some 4000 species of endemic Chinese plants, including many threatened species.

This is especially important for Southwestern China, which is "increasingly under threat from agricultural and industrial development," says Hugh Pritchard, head of research at MSBP.

## Whipping Up a Diagnosis

Take a $2.50 hand-cranked eggbeater, remove one rotor, and you've got a centrifuge that can help health workers diagnose diseases in poor countries, Harvard University chemist George Whitesides and colleagues write in a paper published online this month in the journal *Lab on a Chip*. Some diagnostic tests—such as for hepatitis B—use plasma, the liquid component of blood. Plasma is usually prepared by removing cells from the blood in a centrifuge, but such machines are expensive and use electricity.

So the Harvard team put 100 milliliters of blood in a short piece of very thin polyethylene tubing, sealed both ends by melting them over a candle flame, and taped the tube to the eggbeater's rotor. When cranked at a comfortable speed, the contraption separated cells from plasma in about 10 minutes. Very little plasma is required for most tests, so a few minutes of "beating" is usually enough, says co-author Malancha Gupta. Furthermore, you can tape as many as 20 samples at time to the rotor.

The idea isn't entirely new, says Bart Knols, a malaria researcher at Wageningen University in the Netherlands; one previously proposed centrifuge was inspired by a children's game involving spinning a button with threads.

## RETURN OF THE POPULATION BOMB

At a time when some developed nations are paying citizens to bolster flagging birthrates (*Science*, 30 June 2006, p. 1894), a grass-roots group of scientists and environmentalists is calling for a new push to limit human numbers.

Overpopulation is threatening life as we know it on the planet, say members of a movement called Global Population Speak Out (http://gpso.wordpress.com/), which aims to persuade at least 50 "respected voices" to "speak out in some way" about the problem for a month next year.

"The hope is to concentrate these informed researchers' messages about population during the month of February so we can make a bit of a dent in this taboo" surrounding the subject, says the movement's organizer John Feeney, an environmental writer in Boulder, Colorado. Global population, now at about 6.7 billion, is expected to reach 9.1 billion by 2050, says Feeney, and that's the United Nations' "medium" projection.

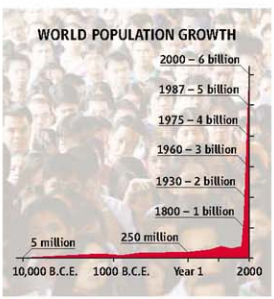


So far, Feeney says 46 people have pledged to speak out or endorse the movement, including botanist Peter Raven, director of the Missouri Botanical Garden in St. Louis; Cornell University entomologist David Pimentel; and entomologist Paul Ehrlich of Stanford University in Palo Alto, California, author of the 1968 book *The Population Bomb*. Although some of Ehrlich's most dire predictions haven't come to pass, others—namely, mass extinctions, as well as horrors he didn't mention, such as destruction of rainforests and coral reefs from climate change—appear to be well under way.

CREDITS (TOP TO BOTTOM): UNIVERSITY OF HERTFORDSHIRE; ROYAL SOCIETY OF CHEMISTRY; CHERYL RAVELO/REUTERS; SOURCE: SUSTAINABLESCALE.ORG

# Two Cultures

**GLASSY COSMOS.** When Josiah McElheny, a New York–based glass artist, told Ohio State University, Columbus, cosmologist David Weinberg that he wanted to create sculptures depicting the history of the universe, Weinberg's first reaction was: "Good luck. It's hard enough trying to convey that in an hour to an undergraduate class." But Weinberg soon overcame his skepticism and has spent the past 4 years helping McElheny with two pieces that went on display this month at the White Cube in London and the Andrea Rosen Gallery in New York City, respectively.

The sculptures, *Island Universe* and *The End of The Dark Ages*, show galaxy clusters and quasars at different times in the universe's history. The details mirror trends predicted by cosmological equations: "The earliest [closest in] galaxies are small disks in groups of one to three; farther out, there is a shift towards larger galaxies, more ellipticals, and larger clusters," Weinberg says. The works "don't wear their intellectual depth on their sleeve," he adds. "But if you spend time with them, you can tell that it is there."

## MOVERS

**WIDER VIEW.** After 14 years leading the Joint United Nations Programme on HIV/AIDS (UNAIDS) in Geneva, Switzerland, epidemiologist Peter Piot has decided to head the new Institute for Global Health at Imperial College London.

Piot says the institute, which at this point has only core funding from the school, will reach beyond the traditional global health realms of epidemiology and infectious diseases. He envisions the institute as a "hub" for researchers from the school's programs in public health, business, and engineering. He also hopes to explore how economic development can lead to changes in health by, for example, changing dietary habits. "India may soon have the largest number of overweight people and malnourished people in one country," says Piot. "How do you deal with it?"

Piot, who plans to start the job in May, will conduct research himself at the institute and will recruit some new faculty. U.N. Secretary-General Ban Ki-moon is expected to choose Piot's replacement from among a list of three candidates presented to him this week.

The European University Association (EUA) has elected Swiss legal scholar and former university administrator **Jean-Marc Rapp** as its new president. Rapp, a former rector of the University of Lausanne, Switzerland, is currently an EUA vice president. He won 65% of the vote against Sijbolt Noorda, president of the Association of Universities in the Netherlands. Rapp succeeds Austrian economist Georg Winckler. EUA represents more than 800 universities and 34 national rectors' conferences.

CREDITS (TOP LEFT): SOURCE: DAVID WEINBERG; JOSIAH MCELHENY; TOP RIGHT: SOURCE: WALTER ALVAREZ; UNAIDS; EUA

## Three Q's >>

American geologist **Walter Alvarez** has won the $250,000 Vetlesen Prize for bringing catastrophism back to the geological sciences. In 1980, Alvarez—now a professor at the University of California, Berkeley—his father and Nobel Prize winner, Luis Alvarez, and two colleagues proposed that a huge asteroid impact had wiped out the dinosaurs. Many geoscientists were skeptical because the idea that instantaneous devastation could explain the rock record had been rejected by researchers a century earlier. But over the years, the Alvarez theory has prevailed.

**Q: How quickly did you realize you were heading off the beaten track?**
It took a while to dawn on me that what we were finding was at odds with all the training that I'd had [and that] maybe Earth history could be exciting, not just this slow, uniformitarian stuff.

**Q: Do you still have to actively defend it?**
I don't feel the need to nail it down until everybody agrees. I was involved for 20 years. It was time to come full circle back to global tectonics.

**Q: What did you take away from the experience?**
A chance for a broader understanding of Earth history. I'm giving a course on the history of everything in the past called "Big History: Cosmos, Earth, Life, and Humanity."

Got a tip for this page? E-mail people@aaas.org

Cave bear decoded
662

Embryo bill advances in the U.K.
663

U.S. ELECTION

# Scientists Plant Grass-Roots Effort For Obama in Final Days of Contest

As a graduate student at Iowa State University in Ames, physicist Bernice Durand worked for antiwar candidate Eugene McCarthy in 1968 in his failed bid for the Democratic nomination for U.S. president. Four decades later, the recently retired University of Wisconsin, Madison, professor and administrator has jumped back into the political fray on behalf of Senator Barack Obama. This time around, Durand is using a career's worth of contacts and organizational skills to build an unusual national grass-roots effort, focused on scientific issues, for the Democratic candidate.

**Science** and the **2008 Campaign**

Since September, Durand has worked with more than three dozen scientists who have placed articles or letters in 50-plus newspapers in 20 states, most of them considered still up for grabs. The scientists have also appeared on a handful of radio shows and been interviewed by reporters covering the campaign. "I feel I'm doing something that will make the country better," says Durand. "On issues of science, on support for research, and on his interactions with the scientific community, there's no contest compared to [Senator John] McCain," she says.

Political analysts say Obama has captured the lion's share of visible support among scientists. "It's an enthusiasm chasm," says Michael Stebbins, president of the Scientists and Engineers for America (SEA) Action Fund, which set up a channel on YouTube for scientists of both political persuasions to explain their choice. As of press time, 22 videos have been posted—all by Obama supporters. "It's been frustrating. We want scientists to come out and say why they're voting for McCain," says Stebbins, who has volunteered for the Obama campaign in addition to continuing his SEA efforts.

Durand traces her recent activism to conversations with colleagues this summer at the Aspen Center for Physics in Colorado. They passed along her name to physicist Donald Lamb of the University of Chicago in Illinois, who has helped organize the Obama campaign's scientific advisory committees (*Science*, 26 September, p. 1762). Lamb then invited Durand to launch the network.

Durand, who was eager to take up a new challenge after her retirement, estimates that she's spending 45 hours a week on the project. She's written more than 1000 e-mails aimed at building the network, recruiting authors, and providing suggestions on their draft articles or letters. The Obama campaign, which declined comment for this story, has kept the effort at arm's length. "It's a grass-roots thing," says Lamb, who spent last week working to get out the vote in northern Virginia.

The pieces typically emphasize local concerns. In an op-ed published earlier this month in *The Virginian-Pilot*, Francis Collins, who in August stepped down as director of the National Human Genome Research Institute at the National Institutes of Health (NIH) in Bethesda, Maryland, described himself as "a citizen, a scientist, a physician, and a son of Virginia." The author explains why he supports Obama's "science, technology and innovation agenda," which includes doubling the NIH budget, and notes that NIH "supports most biomedical research in our premier universities—including many in Virginia."

Many of the letter writers have also mentioned the list of U.S. Nobel Prize winners, now up to 70, who have endorsed Obama. "[I'm] not sure people up here would have heard about that otherwise," says Brian Black, a biology professor at Bay de Noc Community College in Escanaba, Michigan, whose letter has been published in four papers located in the state's sparsely populated and Republican-leaning northern regions. "I'm sure there are those who think I'm a nut."

Some scientists believe that their training prepares them to be effective political communicators. "A lot of interacting with voters involves studying the issues, developing a coherent and logical argument, and articulating one's ideas. And thinking on one's feet. And this is what scientists are trained to do," says Daniel Holz, a physicist at Los Alamos National Laboratory in New Mexico. But Dartmouth College cosmologist Robert Caldwell was a little disappointed when four New Hampshire papers rejected his letters. He wonders if the "footnotes and references" he included to bolster his arguments hurt his chances. "They probably added to the word count," he says.

Campaign donation records indicate that some scientists are supporting McCain, but *Science* could not find any evidence of grass-roots efforts by scientists on his behalf. (The McCain campaign did not

PITCHING FOR OBAMA

Note: Several participants have also posted blogs, appeared on radio shows, and been interviewed by reporters covering the campaign.

**Battle stations.** Scientists have proclaimed their support for Obama in 47 newspapers from states in which the presidential candidates are actively campaigning.

SOURCE: BOTTOM: BERNICE DURAND

China's long science march
664

Progress against a puzzling disease
667

reply to requests for comment.) One donor, mathematician Nakhle Asmar of the University of Missouri, Columbia, says "national security" was the reason he gave McCain $2300, the maximum allowed from an individual for the general election. Has he done anything more for the candidate? "I don't have time," he says, adding that he believes "both [candidates] will be good for education and science."

Some who have volunteered for Obama say they would have preferred to remain nonpartisan but that the stakes are too high. Holz, who has written to local papers, recorded YouTube videos, and canvassed for Obama, worries that such activism could "compromise the scientific enterprise" by politicizing it. But the bigger problem, he says, is that "the scientific enterprise has already been compromised and politicized by Republicans." White House science adviser John Marburger says he opposes "scientists using science to support their partisan views." The problem, he says, is that they could "lose credibility with the public."

Durand doesn't pretend to know if her efforts have helped Obama. But she's got her fingers crossed. "I feel so much more optimistic now than I did in 1968," she says.

–ELI KINTISCH

SELF-EXPERIMENTATION

# Eat, Drink, and Be Wary: A Sugar's Sour Side

In 2001, Ajit Varki's dream came true when he drank an extract from pig spit. Varki's strange culinary excursion was part of an experiment that he believed might help explain the unique susceptibility humans have to some infectious diseases, cancers, and heart ailments.

A prominent researcher in the dual disciplines of sugar biology and evolutionary biology, Varki first purchased a few kilos of glands taken from the jaws of pigs. Next, his lab at the University of California, San Diego (UCSD), minced and homogenized them to extract the mucins. From these mucins, proteins secreted by mucosal surfaces, they plucked off a sugar called Neu5Gc for short. And that's what Varki's sweet tooth craved.

Neu5Gc, which is also known as a sialic acid, is made by chimpanzees and many other mammals but not humans, and Varki's group earlier had found the genetic mutation that prevents us from making it. Varki suspected that when we are exposed to Neu5Gc, it incorporates into our cells, where it somehow makes humans more susceptible to a variety of diseases. The first step was to figure out how it entered the body—thus, the pig spit experiment.

Varki reasoned that Neu5Gc could enter humans through food that contains it, such as red meat and milk products. To prove it, he proposed ingesting huge amounts of pig Neu5Gc and seeing where it went. But when Varki asked his institutional review board for permission to drink the Neu5Gc, some members balked. "I was at first told that self-experimentation was not allowed any more," says Varki. He assured them that he would assess results using objective measures such as mass spectrometry to prove its presence—

**Diet-conscious.** Ajit Varki long suspected a link between disease and Neu5Gc in red meats and dairy products.

CREDIT: SAM HODGSON/VOICE OF SAN DIEGO

and he slyly asked if any members of the committee wanted to be the volunteers, he recalls. They gave him a green light.

To establish a baseline, Varki restricted what he put in or on his body for 2 days before the experiment: no red meats, milk products, or lanolin shampoos, all of which contain Neu5Gc. Then he checked into a clinical research center at UCSD and drank 150 milligrams of the Neu5Gc dissolved in 100 milliliters of water. "It was slightly sweet and sour, slightly acidic," says Varki, pig-spit connoisseur. He wasn't particularly worried that the Neu5Gc (full name, *N*-glycolylneuraminic acid) would make him sick. "It was like eating 14 pork steaks," he says. "People do that on July 4th." But to be safe, the clinical center kept him under observation all day, taking blood samples every 2 hours. No side effects surfaced. Urine, saliva, and hair trimmings over the next week all showed increased levels of Neu5Gc. Closer analyses showed that his cells had actually taken it up and incorporated it on their surfaces, as they do with other sialic acids in the synthesis of new glycans. Two of Varki's colleagues did the same self-experiment with similar results, which they published in the 14 October 2003 issue of the *Proceedings of the National Academy of Sciences*. "There's no other example I know of where you eat something foreign that outfoxes the biochemical systems and becomes part of you, no different from molecules made in your body," Varki says. ▸

Varki has since taken that observation a step further. This week, *Nature* is publishing a new study online, led by Varki and two teams of researchers in Australia, that strongly ties Neu5Gc to a human disease and ingestion of red meat. "It's a very concrete example of how our susceptibility to disease might be governed by our diet," says Carolyn Bertozzi, a carbohydrate chemist at UC Berkeley. "Ajit is an incredibly creative guy. Sometimes he's chasing strange meteors and comets, and sometimes he hits something. This is a really interesting story, and I'm very excited by it."

Varki has long wondered why chimpanzees and humans are genetically so similar but suffer from different diseases, and he sees Neu5Gc as one key to solving that mystery. But so far, speculations have outnumbered evidence. "He's been looking for that direct link with disease, and it's been elusive," says Bertozzi. That is, until the new *Nature* study, which she says is thoroughly convincing.

Neu5Gc connected Varki and his Australian collaborators through a circuitous route that dates back to the death of several children in 1993 who ate tainted hamburgers from Jack in the Box restaurants in the United States. The culprit was later identified as a deadly strain of the gut bacteria *Escherichia coli*, known as 0157:H7. A toxin secreted by this *E. coli*, Shiga, can lead to hemolytic-uremic syndrome (HUS), which causes kidney failure. Molecular microbiologists James and Adrienne Paton, a husband-and-wife team at the University of Adelaide in Australia, subsequently discovered several other Shiga-producing *E. coli* that caused HUS outbreaks there, and one secreted a second toxin as well, subtilase cytotoxin (SubAB).

Toxins must first bind to the surface of a cell to do their damage, which led the Patons to David Smith of Emory University School of Medicine in Atlanta, Georgia, who specializes in matchmaking ligands and receptors. Smith found that SubAB has a high affinity for Neu5Gc, and he told the Patons about Varki's work. Their subsequent collaborative studies make a compelling case that when humans eat meat or dairy products that have high levels of Neu5Gc, it becomes incorporated into their cell surfaces, and SubAB can bind to it. "It's the first time we've seen an example of a component in food being the preferred receptor for a bacterial toxin," says James Paton.

The researchers next showed precisely how Neu5Gc binds to the toxin, which included crystallizing SubAB, an intensive effort done in Jamie Rossjohn's lab at Monash University near Melbourne.

**Got Neu5Gc?** Varki and two colleagues drank Neu5Gc extracted from these buckets of pig glands.

Human cells fed Neu5Gc also became much more susceptible to SubAB, the team found. And mouse experiments further clarified the connections between SubAB, Neu5Gc, and disease.

So consider the delicious irony. *E. coli* that produces the SubAB toxin contaminates red meat and milk products. Humans who ingest these foods incorporate Neu5Gc into their cells, making them hypersusceptible to SubAB—and much more likely to become seriously ill from the toxin.

Although these insights have no immediate practical application, Varki hopes they may open a door that eventually helps explain and even thwart major diseases. Some forms of Neu5Gc are seen as foreign by the human immune system, and we sometimes create antibodies to it. Varki suspects that these antibodies may contribute to autoimmune diseases, cancers, and heart problems seen in humans but not in chimps. Pathogens can also directly bind to Neu5Gc on cell surfaces, and one strain of the malaria parasite does just that, readily causing disease in chimps but not humans. Paton suggests that the greatest impact of the new findings may be in sparking epidemiological studies of, say, vegans, that prove these links. Any way you look at it, Neu5Gc proves the point like never before: You are what you eat. **–JON COHEN**

CREDIT: PASCAL GAGNEUX

## Panel OKs Anthrax Shots for First Responders

A U.S. scientific panel thinks that police, firefighters, people who work with hazardous materials, and others running the risk of exposure to an anthrax infection may be offered the vaccine against the fatal disease. That suggestion, from an advisory panel to the U.S. Centers for Disease Control and Prevention (CDC), is a departure from current policies.

Anthrax vaccination is compulsory for military personnel serving in risk areas overseas. Although most experts believe the vaccine—six shots over a period of 18 months—is safe, some service members believe it has made them ill, and some have filed lawsuits. Relying on new safety data, CDC's Advisory Committee on Immunization Practices agreed on 22 October that first-responder agencies "may choose to offer" their staff the vaccines on a voluntary basis—but it stopped short of recommending they do so.

That caution reflects the panel's inability to assess the risk of future attacks, says the committee's chair, Dale Morse, who adds that the job site and duties affect a worker's risk of contracting anthrax as well. "We believe it's very low, but we can't say it's zero," Morse says. Meryl Nass, an internist at Mount Desert Island Hospital in Bar Harbor, Maine, who strongly opposes the military program, believes the recommendations will put more people at risk for adverse events. No first responders became infected during the 2001 anthrax letter attacks, which killed five people. **–MARTIN ENSERINK**

## HAL the Cosmologist

Physicists know that the gravity from huge strands of dark matter distorts the images of distant galaxies and makes them tend to align, a bit like fish in a school. Now, computer scientists may help them to find new algorithms to measure that "weak lensing" distortion, which could be used to probe the mysterious dark energy that's accelerating the expansion of the universe. The competitors in the GRavitational lEnsing Accuracy Test 2008 (GREAT08) PASCAL Challenge will analyze a simulated data set of 30 million galaxies, preparation for the billions of galaxies that cosmologists expect to survey in coming decades. The challenge is the latest from the PASCAL Network, a consortium sponsored by the European Union. John Shawe-Taylor, a computer scientist at University College London, says the contest pushes machine learning in new directions by emphasizing large data sets and high precision. **–ADRIAN CHO**

EVOLUTION

# Two Sets of Cave Bear DNA Uncover the Bear Facts

What kind of bear was Winnie-the-Pooh? Author A. A. Milne christened the fictional character after the teddy bear of his son, who in turn had borrowed the name from an American black bear in the London Zoo called Winnipeg. Yet for decades, researchers have argued about whether Winnipeg's scientific name should be *Ursus americanus* or *Euarctos americanus*. Indeed, although there are only eight species of living bears, scientists have come up with at least half a dozen versions of the bear family tree.

Now a paper published by the *Proceedings of the National Academy of Sciences* (*PNAS*) online this week helps untangle bear phylogeny by presenting "the first mitochondrial genome" from the extinct cave bear, *Ursus spelaeus*. But another paper, published with little fanfare last July, also reported the complete mitochondrial DNA (mtDNA) of the cave bear, as well as that of the extinct American short-faced bear, *Arctodus simus*. The two teams are arguing about scientific priority. But for the bears, this means that two sets of data now illuminate their family tree, although the studies disagree about the timing of bear evolution.

Both teams independently leaped a major technological hurdle, adds evolutionary biologist Hervé Bocherens of the University of Tübingen in Germany: They sequenced the first complete mitochondrial genomes from specimens that are tens of thousands of years old but not preserved in permafrost. "This opens the field of complete mitochondrial sequencing to a very wide range of extinct species," says Bocherens.

Researchers had already sequenced the mtDNA genome in all eight living species of bears and used the genetic differences among them to create family trees. But because the bears underwent a rapid and fairly recent radiation, those variations are not great. To have confidence in their trees, researchers needed data from extinct animals.

They got it twice over. In this week's paper, a team led by biologist Jean-Marc Elalouf of the Atomic Energy Commission in Saclay, France, reported cave bear mtDNA from a celebrated source: a 32,000-year-old sternum bone from France's Chauvet Cave, site of the oldest known cave art (*Science*, 15 August, p. 904). In another paper back in July, evolutionary biologist Michael Hofreiter of the Max Planck Institute for Evolutionary Anthropology in Leipzig, Germany, reported in *BMC Evolutionary Biology* that his team had extracted mtDNA from a 44,000-year-old cave bear femur found in Austria; the team also reported the mtDNA genome of a 22,000-year-old American giant short-faced bear from Canada.

Hofreiter's team sent its paper first to *PNAS*, on 11 December 2007, but it was rejected without review, say Hofreiter and *PNAS* Editor-in-Chief Randy Schekman. Elalouf's paper, which Schekman says was handled by a different member of the *PNAS* editorial board, was submitted on 1 July 2008 and accepted the following month. Elalouf argues that although his team's paper is second, they submitted their sequence to GenBank—the National Institutes of Health's repository for DNA sequences—back on 4 December 2007.

**Not your average bear.** Ancient DNA from the extinct cave bear reveals their family tree.

CREDIT: DE AGOSTINI PICTURE LIBRARY/GETTY IMAGES

Hofreiter's team didn't submit its cave bear sequence to GenBank until 23 June 2008, shortly before its paper appeared. Schekman says that Elalouf has now agreed to add a "note in proof" to the print edition of *PNAS*, which will be published shortly, acknowledging the Hofreiter group's earlier paper; Hofreiter says that solution will satisfy his group's concerns.

Whatever the priority, both groups agree on the outline of the bear family tree. They confirm that the giant panda was the first species to split off from the lineage leading to later bears, and both conclude that the cave bear shared a common ancestor with the brown bear and the polar bear, which turn out to be closely related to each other. Moreover, both teams slash the number of genera of living bears from seven in some schemes, to three for the Hofreiter group and four for the Elalouf group. They assign most species—including Winnipeg's—to the genus *Ursus*.

Adding data from the two extinct bears provides a "robust" tree that is "important for understanding the evolutionary history of this mammalian family," says Ya-ping Zhang, an evolutionary geneticist at the Kunming Institute of Zoology in China, who published the complete mtDNA genomes of five living bears in 2007.

Yet when it comes to the timing of the recent bear radiation, the two groups part company. Elalouf concludes that it was only about 2 million to 3 million years ago, using a previous estimate of the giant panda's divergence at 12 million years ago as a chronological anchor point. Hofreiter's team anchors its tree with the much earlier divergence of the harbor seal and finds that the panda split off earlier, about 19 million years ago, and that the rest of the bears radiated about 5 million years ago. He notes that some aspects of climate changed dramatically about that time, when the Bering Strait opened and the Mediterranean Sea became drier. Other mammals also showed dramatic changes at this time, such as the split between the human and ape lineages.

Researchers outside the fray are divided. "I would not take the divergence time too seriously in either paper," says Xiaoming Wang, a paleontologist at the Natural History Museum of Los Angeles County in California. Wang adds that more research on the bears' nuclear genomes, which is still at an early stage, will be necessary to fine-tune the chronology. For now, at least, Winnie-the-Pooh should be happy to have his true scientific name at last.

–MICHAEL BALTER

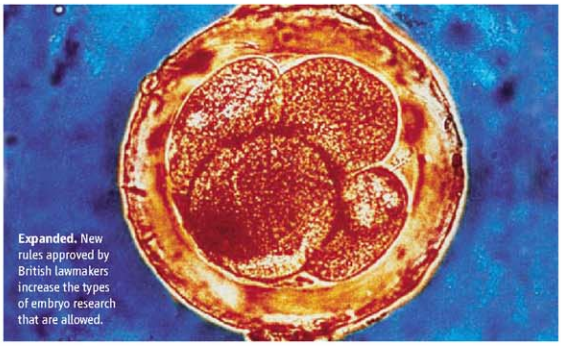

**Expanded.** New rules approved by British lawmakers increase the types of embryo research that are allowed.

BIOETHICS

# U.K. Approves New Embryo Law

With the enthusiastic support of the scientific community, the British House of Commons has overwhelmingly approved a wide-ranging bill that expands the country's rules governing work with human embryos. The new standards, which have dismayed opponents of embryo research, spell out the kinds of research governed by the country's Human Fertilisation and Embryology Authority (HFEA). The 22 October vote in the Commons, which favored the bill 355 to 129, was considered its most significant hurdle, although the bill still needs final approval from the House of Lords.

The bill updates the 1990 regulations establishing HFEA and a 2001 law governing nuclear transfer, as well as other regulations pertaining to reproductive technologies. It allows several kinds of research that were not covered previously, including interspecies nuclear transfer, in which scientists attempt to create an "admixed embryo" by fusing a human cell and an enucleated animal egg. Some scientists hope to use such embryos to derive embryonic stem (ES) cells. HFEA has already granted three licenses for such work, but opponents had challenged the licenses in court, charging that the agency had no legal authority to grant them. The new bill provides that authority.

The bill also says that HFEA can grant licenses for research to create transgenic embryos carrying human and animal genes or to create chimeric embryos by mixing human and animal eggs or sperm. Opponents have claimed that the bill authorizes the creation of "humanzees." But scientists "made a huge effort to allay fears that this was going to lead to real human hybrids," says stem cell expert Stephen Minger of King's College London. (The bill forbids allowing any human-animal embryos to develop for longer than 14 days or implanting one in a human or animal womb.) Their lobbying paid off. "Many people said, 'I am naturally queasy about this. I would have voted against it, but you guys have made such a strong case I can't see any reason not to vote for it,'" Minger says.

Developmental geneticist Robin Lovell-Badge of the National Institute for Medical Research in London says experiments mixing human sperm and, for example, transgenic mouse eggs can yield important insights into the process of fertilization. Researchers hoping to test new methods of storing human sperm or new contraceptives that target fertilization will also benefit.

Some politicians had argued that induced pluripotent stem cells, which are ES-like cells that are reprogrammed using a cocktail of specific genes instead of an oocyte, render interspecies nuclear transfer unnecessary. Minger and Lovell-Badge cite important reasons to pursue the technique, for instance, to compare the ES cells that result from both processes. Studying nuclear transfer—without having to rely on scarce human oocytes—also offers the best chance for teasing apart exactly what happens to turn back the clock of an adult cell and allow it to direct the process of development again, Minger says.

–GRETCHEN VOGEL

CREDIT: EDELMAN/PHOTO RESEARCHERS INC.

## China Stakes Genetic Claims

**BEIJING**—China is moving to better secure its genetic riches. The National People's Congress (NPC) is reviewing amendments to a patent law that would require applicants to disclose the origins of genetic resources when such materials are essential to the claimed intellectual property. The provision should make it easier to be fair to sources of genetic resources as well as inventors as mandated by the Convention on Biological Diversity, to which China is a party. But the amended patent law is silent on protecting the rights of indigenous people over their own genetic resources and traditional knowledge, a point that GRAIN, an environmental nonprofit based in Spain, wants to change. NPC is expected to complete its work by early next year. –RICHARD STONE

## Star Wars in Florida

Just days before the U.S. presidential election, both presidential campaigns desperately sought to assure Florida voters that their man will boost spending for NASA, a major employee in the battleground state. Both candidates have promised to spend $2 billion to ease the disruption to the work force resulting from a gap between retiring the space shuttle and building a new launcher. "If I'm elected president, I won't cut NASA funds like Senator [Barack] Obama [D–IL]," Senator John McCain (R–AZ) said last week in Melbourne, Florida. But McCain also repeated his intention to freeze spending for all programs except defense, Social Security, and health care. "It seems Senator McCain isn't committed to exempting NASA from his proposed spending freeze," said the Obama campaign in response. –ANDREW LAWLER

## How to Age Gracefully

The U.S. National Institute on Aging (NIA) in Bethesda, Maryland, has launched a 12,000-person study to better understand what contributes to disability in the elderly. Whereas previous studies have examined the use of government-funded medical services, the new study will assess everything from medical records to lifestyle choices to understand why some people age more effortlessly than others. This week, NIA announced that the Johns Hopkins Bloomberg School of Public Health (JHSPH) in Baltimore will run the $24 million study. The ultimate goal is to gather reams of data that will help us "understand disability trends and how these are playing out in different parts of the population," says JHSPH health policy researcher Judith Kasper, who's leading the study. –RACHEL ZELKOWITZ

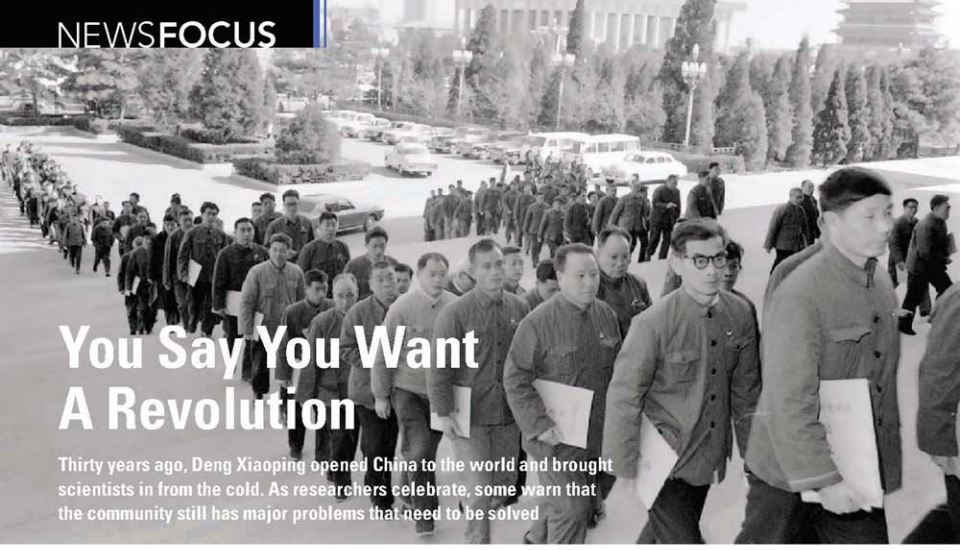

# You Say You Want A Revolution

**Thirty years ago, Deng Xiaoping opened China to the world and brought scientists in from the cold. As researchers celebrate, some warn that the community still has major problems that need to be solved**

**BEIJING**—After Lu Yongxiang began a third term as president of the Chinese Academy of Sciences (CAS) last March, a TV talk show host asked the former varsity soccer player which question he would like to answer first: When can Chinese scientists win the Nobel Prize? Or when can the national men's soccer team win the World Cup?

In both cases, Lu responded, the challenges are similar. China's scientific community and its much-derided men's national soccer team must build stronger foundations. For a China-based scientist to win a Nobel Prize or the soccer team to win the World Cup, Lu said, both need more money, more talent, and an environment that encourages innovation.

In the 30 years since Deng Xiaoping and other leaders opened China to the outside world, China's science, like its economy, has grown immensely. According to the Organisation for Economic Co-Operation and Development's publication *Main Science and Technology Indicators 2008*, China's $87 billion R&D expenditure in 2006, in purchasing power parity dollars, was higher than all countries except the United States and Japan, and only the United States has more researchers—1,387,882 compared with China's 1,223,756. Officials with China's Ministry of Science and Technology (MOST) like to point out that China is now second only to the United States in the number of publications in international journals.

But in many ways, China punches below its weight in science. "Our country has not made contributions proportionate with its overall strength," neuroscientist Rao Yi of Peking University and structural biologist Shi Yigong of Tsinghua University wrote in a recent editorial in the newspaper *Huanqiu Shibao*. They and others argue that China's rising R&D investments are being misspent on facilities and megaprojects that are driven by special interests, creating an illusion of grandeur rather than bringing China closer to the forefront of international research.

Also disturbing is that many Chinese scientists exhibit a surprising lack of curiosity, asserts Rao, who says he has endured "intellectual starvation" since returning to his homeland last year from Northwestern University's Feinberg School of Medicine in Chicago, Illinois. Although many scientists eagerly showcase their own work at conferences, Rao says, few discuss ideas informally or show up at seminars to listen to colleagues—interactions that inspire creativity in the West. "True collaborations are rare, and motivations for science are driven by temporary and relatively easy goals," he says.

Another damning assessment comes from theoretical physicist and former president of CAS Zhou Guangzhao. In China, he says, "success is often scored by quantity rather than quality." For that reason, Zhou contends, most Chinese scientists are content to follow well-trodden paths and churn out routine papers rather than strive for fundamental breakthroughs. Deference to status also makes it difficult for junior researchers to challenge academicians or science mandarins. That wasn't so in the 1950s and 1960s, when Zhou was working on China's atomic bomb project; then, he says, scientists treated one another as equals and worked collectively toward the goal of strengthening China. These days, many scientists say, there is greater freedom in society, but a market economy has made private interests the driving force of science, supplanting the idealism that inspired earlier generations of researchers.

Although public discussion about systemic problems in Chinese science runs up against censorship in state newspapers and TV—the government's voice—the blogosphere now provides a largely unfettered forum. "Blogs and the Internet as a whole are changing China's political discourse," says Cao Cong, a senior research associate at the Neil D. Levin Graduate Institute of International Relations and Commerce in New York City. Cao, a blogger on ScienceNet.cn, hopes that "positive and constructive opinions raised in the blogosphere" will receive official attention. This seems to be happening. Earlier this month, Chinese media reported that Premier Wen Jiabao, alerted by a journalist's blog about a cover-up of a disaster in Shanxi Province—where a mudslide caused by dumping mining waste killed more than 40 people in August—sent a team to

CREDIT: LI SHENGNAN, *CHINA FEATURES*/XINHUA PHOTOS

**On the march.** Scientists arriving at the Great Hall of the People for the transformative "Spring of Science" conference.

investigate. Zhao Yan, editor-in-chief of ScienceNet.cn, hopes the site's 1400-plus bloggers may spark a bottom-up reform not just in matters of public safety and governance but also in science and technology, about which frank talk among peers is sorely needed.

### A time of revival

China's reforms and opening up followed the decade-long turmoil known as the Great Proletarian Cultural Revolution launched by Mao Zedong in 1966. Seeking to rid the country of what he labeled as feudal, bourgeois, and foreign influences, Mao closed universities and banished professors to the countryside to work as peasants. Research was halted, except in areas that served national needs such as defense.

Careers like that of Chen Jia'er, a young physicist in the 1960s, were thrown into reverse. After 3 years as an exchange researcher in nuclear physics at the University of Oxford in the U.K., Chen returned home in 1966, hoping to build a heavy-ion research program. Instead, he was branded a "reactionary academic authority" and sent for reeducation to a village in eastern China, where he laid railroad tracks, raised pigs, and worked odd jobs for almost a decade.

Mao's death in 1976 and the subsequent purge of the coterie led by Mao's widow released China from its ideological straitjacket. One of the first reform steps Deng took was to rehabilitate scientists from a class to be "won over, reeducated, and transformed" to vital members of society whose knowledge and expertise would help modernize the country. Scientists such as Chen were brought in from the cold.

In a keynote speech at the first National Science and Technology Convention in Beijing in March 1978, Deng declared that "science and technology is a productive force." The "Spring of Science," as the founding and then–CAS president Guo Moruo poetically pronounced, had arrived. Many scientists recall that time fondly. It was "the turning point of my life," says Chen, who served as president of China's National Natural Science Foundation (NSFC) from 2000 to 2003.

Deng's call for modernization posed a daunting challenge. For some like Peking University biochemist Gu Xiaocheng, it meant racing to recoup lost ground. Gu had been one of the few professors permitted to remain in Beijing during the Cultural Revolution. She was part of a team that set out to synthesize insulin, a project considered in the national interest. They succeeded in 1965 and tried to determine insulin's crystal structure. But even for this elite group, "no international journals were available to us," Gu says. After the Cultural Revolution in the late 1970s, "when I saw *Science* again after so long, I thought, 'They're speaking a different language.' We really didn't know how to catch up."

Since then, China has worked to reform its R&D system, but these efforts have been top-down and often flawed, says He Zuoxiu of CAS's Institute of Theoretical Physics here. In the 1980s, then-Premier Zhao Ziyang wanted the marketplace to decide what research was needed and directed CAS to focus on applied research. The leadership "confused applied research with product development," He says, and the resulting tendency to ignore basic research has weakened the country's ability to innovate. Chinese leaders abandoned Mao's idea of self-reliance and expected the country to acquire advanced technologies from multinational companies in exchange for giving them market access. Zhao infamously told Chinese scientists in 1985 to "go up hills and pick peaches," reflecting his belief that China could simply reap the fruits of research done in other countries. But without accumulating one's own knowledge, says Chen, "it's impossible to have new ideas or really know how to apply them."

A second major reform came in the late 1990s, when "indigenous innovation" became a buzzword. Former president of China Jiang Zemin called on scientists to focus their efforts on national needs, "to do [research in some areas] and not to do [it in others]." In response, in 1998 Lu launched CAS's Knowledge Innovation Project (KIP). Under that banner, Lu reduced the number of CAS institutes from more than 100 to about 80 and its 80,000 work force to 48,000 (*Science*, 23 February 2001, p. 1477). The streamlining, Lu says, made institutes "more active and dynamic."

The innovation project achieved some positive results: "Our facilities were dilapidated before, but now many new buildings rival those at universities," says Wang Zhizhen of CAS's Institute of Biophysics here. The work force is much younger than it was a decade ago, and most researchers have studied abroad. Some institutes, especially newer ones, such as the Institute of Neuroscience established in 1999, compete at an international level, says Lu.

But for many older institutes, the drastic work-force reduction only looks good on paper. These institutes must use money allocated to a smaller payroll to support retirees and staff members not counted as KIP personnel. To accomplish this, institutes collect "head taxes" from principal investigators with grants to augment PIs' salaries, based on their productivity, and to pay junior researchers and grad students. Although basic salaries for PIs are fixed at several thousand dollars a year, productivity-based supplements can boost annual incomes to well over $30,000. For grad students, the basic stipend is about $500 a year; those lucky enough to receive supplemental pay may get an additional $3000.

Grants are golden because they provide the lion's share of productivity-based pay, even though many funders explicitly forbid using grant money this way. Institutes account for the payments as user fees, processing fees, or collaboration fees, according to several researchers who asked to remain anonymous to avoid retribution. These scientists estimate that about 10% of total grant money at well-funded institutions, and as much as 50% at poorer ones, is spent on salaries. As a result, some PIs go after grants beyond what's needed for research and outside their areas of expertise, says Zhao Zhongxian of the Institute of Physics here.

To combat this problem, Zhou says salaries should be capped and the portion


**Eager to learn.** Some students of Peking University's first post–Cultural Revolution freshman class in 1978.

CREDIT: CHINA FEATURES/XINHUA PHOTOS

from grants should not exceed 3 months' worth of PI pay, as many U.S. research universities stipulate. A few Chinese institutes have adopted this approach. The Institute of Physics, Zhao says, has changed its formula for productivity-based pay such that a PI's salary does not increase linearly with the amount of grant money.

Publications also contribute to a researcher's productivity-based pay. Institutes determine publication bonuses differently, but most take into account the impact factors of journals in which papers are published. CAS's Institute of Chemistry follows a typical formula in China: A paper in *Science* or *Nature* fetches $2500 or more; a paper published in journals such as *Physical Review Letters* (*PRL*) and the *Journal of the American Chemical Society* (*JACS*) brings about $1300; papers in journals with impact factors greater than three bring about $500; and papers in journals with impact factors under three are awarded less than $200. Bonuses are divvied according to the authors' contributions. Universities also pay productivity-based salaries to professors.

*The Spring of Science conference was "the turning point of my life."*

—CHEN JIA'ER, FORMER PRESIDENT, NSFC

A few institutes, including the Institute of Neuroscience, do not pay publication bonuses, whereas some, such as the Institute of Physics, have de-emphasized publication bonuses and only award several thousand dollars to papers published in four journals: *Science*, *Nature*, *PRL*, and *JACS*.

### Quantity trumps quality

Both productivity-based pay and the way Chinese researchers are evaluated emphasize quantity over quality. This is partly because Chinese scientists are often fearful of giving offense if they critique a colleague's work truthfully, Zhao says. Instead, number-based evaluation is considered more objective and has gained popularity. To break the expectation of guaranteed employment regardless of performance—the "iron rice bowl"—Nanjing University in the early 1980s began to use the Science Citation Index (SCI) to measure the productivity of its professors. Since then, universities and research institutes have been ranked annually based on how many SCI papers they churn out. Science ministry grant applications often require PIs to state how many SCI papers they intend to publish, and researchers are promoted and occasionally demoted based on the number of their publications.

The top-performing one-third of CAS institutes has adopted a system of international review. For example, since 2003, the Institute of Genetics and Developmental Biology (IGDB) here has been using outside reviewers to evaluate PIs in its three main research areas. The institute invites a scientist from abroad to recruit a panel of reviewers for each area, says IGDB developmental biologist Zhang Jian. The panel anonymously reviews packages prepared by PIs and conducts a site visit to talk to scientists, research staff, and students. The visitors also give constructive comments to the lab under review. Reviews are conducted every 5 years; a few investigators have been forced out primarily because of the reviews, says Zhang.

### Speaking out

To Xu Liangying, a retired science historian here, the root cause of the problem in China's scientific community is Deng's declaration 30 years ago of science and technology as a productive force, now an official mantra. Since then, the Chinese words for "science" and "technology" have been fused into "scitech," which in common usage solely connotes technology. In China, science is expected to contribute directly to economic development and not to the pursuit of truth and knowledge, asserts Xu.

Xu has always spoken his mind, even though it has cost him dearly. In the late 1950s, he was branded a "rightist" and banished to his ancestral village in Anhui Province. For more than 2 decades, Xu toiled in the fields during the day and translated the collected works of Einstein into Chinese during his spare time. After being allowed back into CAS in 1978, he became China's foremost Einstein scholar. He also took up the cause of human rights in China. Xu was put under house arrest for a time in 1989 after writing an open letter, and collecting signatures for it, that called on the Central Committee of the Communist Party to release political prisoners and allow freedom of speech. Last April, the American Physical Society awarded Xu the Andrei Sakharov Prize for a "lifetime's advocacy of truth, democracy, and human rights."

These days, speaking one's mind is not nearly as risky. Peking University's Rao was allowed to come back to China after he and others wrote an article in *Nature*'s China Supplement in 2004 that advocated stripping MOST of its power to administer research funds and making the ministry an advisory body. Rao says China needs an impartial science and technology board to advise the State Council on policy and funding priorities. The board, he says, should be made up of people free of institutional conflicts of interest, replacing an existing science and technology group under the premier that consists of ministers who inevitably want more money for their own ministries.

Theoretical physicist He Zuoxiu of CAS agrees and says MOST failed to curb institutional interest when it led the formulation of China's mid- to long-term science and technology plan. "The plan does not represent true national interest; it is a balancing act among interest cliques," says He. One of the plan's biggest flaws, he says, is its backing of "megaprojects" advocated by individual ministries and scientists (*Science*, 17 March 2006, p. 1548). Even though China needs to invest more heavily in renewable energy, an area critical for sustainable development, the plan hardly mentions it, He notes. Because the country's top leaders emphasize R&D for national needs, scientists often promote their own research as aligned with such needs, says Rao. Some use political clout and connections to designate their own projects or those of associates and friends as "top national priorities," he says.

Many researchers discuss such issues openly on ScienceNet.cn, a Web site that has been running for fewer than 2 years and boasts tens of thousands of readers per day. The site's bloggers do not hide behind pseudonyms, which sets it apart from most Internet forums and blog sites in China. "Scientists have no problem with using real names," says Zhao, "because they want to be responsible for what they say."

These bloggers call for systemic reforms to curb special interests in setting research priorities, to make the funding system more transparent and fair, and to liberate scientists from meaningless evaluations imposed by administrators. These cries for reform offer a glimpse of what could happen in the future, as a new generation that has prospered in Deng's reformed China pushes its way into the ranks and pressures science leaders to live up to their expectations.

—HAO XIN

With reporting by Richard Stone.

CREDIT: COURTESY OF CHEN JIAER

BIOMEDICAL RESEARCH

# More Than Skin Deep

**Scientists still don't know what causes scleroderma, a complex disease often marked by toughening skin and widespread internal fibrosis, but they're developing potential treatments nonetheless**

At age 19, Barbara Lowe didn't think much of it when one of her fingers temporarily turned completely white during a lunch break at work. "My friends thought it was a party trick," says Lowe. Twenty years later, however, the party trick had taken a serious turn. Most of her fingers and toes were suffering bouts of poor blood flow, and searing heartburn and lingering colds constantly hampered her. When she was taken to the hospital for pneumonia, doctors finally gave her symptoms a name: scleroderma. "I didn't know anyone who had it other than myself. My GP [general practitioner] couldn't tell me a lot of about it," says Lowe. "You're kind of completely on your own with the disease. People just don't know what it is."

Although scleroderma affects as many as 300,000 Americans and kills roughly 10,000 every year, this autoimmune disease remains an enigma and far from the public's radar. Its cause—or causes—remains murky. Genetic and environmental studies have yielded few clues, as the disease seems to strike almost at random.

Scleroderma was formally discovered in 1754 by Carlo Curzio, an Italian doctor who described treating a woman with thick, stiff skin—the symptom from which scleroderma gets its name (from Greek meaning "hard skin"). This skin condition, along with the circulation problem that Lowe experienced, known as Raynaud syndrome, are the classic signs of the disease—and many people with scleroderma suffer from only these disabling, not deadly, symptoms.

Another hallmark of scleroderma is that patients suffer a diverse array of symptoms, leading many physicians to consider the condition a constellation of disorders. In bad cases of systemic scleroderma, the most severe form of the disease, inflammation and fibrotic scar tissue flare up in multiple organs, blood vessels narrow and harden, and traitorous immune cells attack a person's own flesh. The dizzying complexity of scleroderma has kept scientists both frustrated and fascinated for decades. "The problem is we don't really understand what the primary basis is of the disease," says Robert Lafyatis, a rheumatologist at Boston University (BU) School of Medicine. "We don't know if it's a vascular disease, a fibrotic disease, or an immune disease."

At a recent meeting in Cambridge, U.K., Lafyatis and several hundred scleroderma investigators gathered* to compare notes and chart the field's progress. Despite continued bewilderment about what causes the disease, there was good news to report. In the 1980s, physicians began effectively treating the kidney problems that then killed most scleroderma patients. New insights into the disease's molecular underpinnings are helping to tackle other dangerous symptoms, too. Some researchers are even finding that "rebooting" a person's immune system with stem cell therapy may completely eliminate the systemic fibrosis that continues to kill many people. "There's been a change from nihilism to a bright light at the end of the tunnel," says Alan Tyndall, a rheumatologist at the University of Basel in Switzerland. "As medical students [in the 1960s], we were told that scleroderma is a death sentence and there's no hope; now, that's changed."

### Many suspects, little proof

Since Curzio identified scleroderma, dozens of causes have been put forth but few have stood the test of time. Environmental factors such as organic solvents, asbestos, and even silicone breast implants have all been suspected triggers for the autoimmune reaction associated with scleroderma. However, the evidence for these factors has come from studies too small to be definitive; plenty of people get scleroderma without being exposed to any of these insults.

Fetal cells were another suspect. During pregnancy, such cells pass through the placental barrier and enter an expectant mother's circulation. Scientists found that these foreign cells could live for decades in a woman, and some theorized that the cells might trigger scleroderma. This theory could offer an explanation for one of scleroderma's puzzles: 80% of patients are women, most in their pospartum years. However, as more studies were done, some research suggested that fetal cells helped fight or prevent the disease in the mother, rather than cause it. The true role they play remains unresolved.

**Frozen fingers.** Scleroderma is often marked by stiff, hardened skin that severely limits movement in victims' joints.

CREDIT: AP PHOTO/*THE OAKLAND PRESS*/PAULA ARMAN

*10th International Workshop on Scleroderma Research, 2–6 August.

One solid scleroderma clue is the disease's link to genetics. Although the incidence in the U.S. general population is only about 14 people per million per year, the odds of a person developing the condition are more than 100 times greater if a family member does too, and more than 280 times greater if that member is your identical twin. Those rates indicate a genetic component to the disease, albeit a weak one because the great majority of family members or twins don't share the disease. "If you compare scleroderma to a traditional genetic disease, the genetic pattern in families is not that strong," says Xiaodong Zhou, a clinician who studies scleroderma genetics at the University of Texas Health Science Center in Houston. "But if you compare it to the [prevalence in] the general population, ... it's very high."

The Choctaw Nation of Oklahoma, a Native American population, has a much higher prevalence of scleroderma—roughly three times higher than the general population, which has led to several studies surveying their DNA. Researchers pinpointed several DNA markers around the gene for fibrillin-1 that correlate with the Choctaw scleroderma cases—and the protein's presence in connective tissue makes sense, given the disease's symptoms. Still, fibrillin's exact role in the condition remains murky. Researchers have failed to link the fibrillin gene to other populations of scleroderma patients.

Other genetic studies of scleroderma have pointed to the major histocompatibility complex, an array of genes that controls immune cell function, but "it's a common region for autoimmune disease," explains Zhou. "They've all been linked to that region."

More recently, Michael Whitfield, a geneticist with Dartmouth Medical School, has used genome-wide microarrays to screen all the gene activity within scleroderma skin and tissue samples. In July, Whitfield and colleagues reported in *PLoS ONE* that 17 out of 22 scleroderma patients had a genetic fingerprint, a distinct pattern of gene activity, differing from controls. Most of the overactive genes were the usual suspects for an auto-immune disorder—those involved in immune cell activation, including T, B, and macrophage cells—but others with altered activity were genes involved in fibrosis and collagen growth. Whitfield also found a cell proliferation signature—a group of cell-cycle genes that are expressed only when cells are dividing, which hints that scleroderma tissue has higher rates of DNA replication.

Whitfield says the most surprising outcome from the study is that even tissue from scleroderma patients that looks normal still has the distinctive genetic fingerprint of the disease. His group plans to repeat the experiment with a larger sample to see if it continues to hold true. If so, Whitfield hopes the multigene fingerprint could be turned into diagnostic or predictive tools for clinicians. "The limiting factor in terms of understanding scleroderma is getting large enough patient cohorts to do studies," notes Whitfield. "And it's the heterogeneity that's really plagued us, from the molecular level and from the genetic level."

> *"As medical students, we were told that scleroderma is a death sentence and there's no hope; now, that's changed."*
>
> —ALAN TYNDALL, UNIVERSITY OF BASEL

Whitfield says that his microarray approach isn't likely to yield one simple gene as an answer. "There's very likely to be multiple factors contributing to scleroderma," he says. "We're not going to find a single mutation. It's almost certainly going to be a combination."

### Treating the symptoms

Although figuring out the root of scleroderma remains a major research goal, the number-one priority has been to find treatments that keep the symptoms at bay, a quest that has led to a game of cat and mouse between drugs and the disease. The number-one killer of scleroderma patients used to be kidney failure. Twenty percent of patients would die in middle age as their kidneys' arteries became clogged and constricted with smooth muscle cells. However, in 1979, scientists found a class of drugs, angiotensin-converting enzyme (ACE) inhibitors, which relax the disease's stranglehold on the kidney. Harrison Farber, director of the Pulmonary Hypertension Center at BU, calls ACE-inhibitor therapy one of "the biggest breakthroughs in scleroderma," noting that people are no longer dying of renal failure.

Lungs then became the new battleground. Like the kidneys, the pulmonary arteries, the vessels that carry blood between the heart and the lungs, also tend to become occluded and constricted in scleroderma. But much to the frustration and puzzlement of doctors, ACE inhibitors don't help here. "Once people stopped dying of kidney failure, they now lived long enough to die from pulmonary problems," says Francesco Del Galdo, associate director of the Scleroderma Center at Jefferson University Hospitals in Philadelphia, Pennsylvania. One in seven scleroderma patients developed pulmonary hypertension, and it was inevitably deadly. By the late 1990s, however, researchers began employing a variety of drugs, including Viagra, which help to widen and relax the lung's arteries.

Although these treatments are touted as helping patients live longer, some clinicians remain unconvinced. Six different drugs have received approval from the U.S. Food and Drug Administration for treatment of lung problems in scleroderma, but all were largely tested using a simple approach: the 6-minute walk test. If a patient testing a new drug could complete this exercise with greater ease, the drug was considered to be effective. However, only one clinical trial has ever shown the drugs to improve a scleroderma patient's survival against a placebo. "These drugs can help the symptoms," says Lafyatis. "But it's not clear that it helps their mortality; ... some patients benefit from it and some don't."

Scleroderma poses a further deadly challenge: fibrosis. In severe cases, fibroblasts, the cells that create and maintain the extracellular matrix, seem to be irreversibly activated, inducing an unwanted scarring process. Chris Denton, an experimental rheumatologist at University College London Medical School,

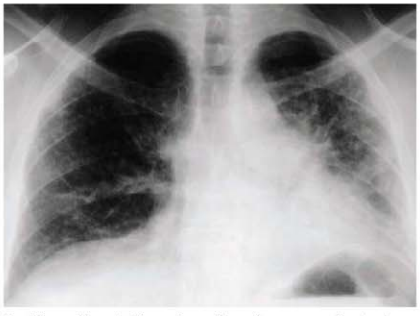

**Breathing problems.** In this x-ray image of lungs from a person with scleroderma, one lung (right) is clouded with fibrotic tissue, whereas the other is fairly untouched.

CREDIT: J. P. MAYBERRY ET AL., RADIOGRAPHICS 20, 1623 (2000)

notes that now "it's the fibrosis that causes the mortality of disease, because it's happening simultaneously in multiple organs." Yet the lungs remain the key battleground, as lung fibrosis can strike 70% of scleroderma patients, and scarring there leads to eventual suffocation.

Scientists at the Cambridge meeting agreed that eliminating the fibrosis problem should prevent scleroderma from being a killer and turn it into a more manageable chronic disease. How to thwart the process has been mostly a mystery, but there was new optimism at the conference. "We have a rich variety of potential molecular targets [for fibrosis], and for many of these, inhibitors are available and are being tested in clinical trials," says Oliver Distler, head of the scleroderma clinic at the University of Zurich, Switzerland.

Most of these inhibitors aim at a longtime suspect for fibrosis: TGF-β, a so-called cytokine with multifarious pathways. One track stimulates both collagen and scar-tissue formation, whereas other tracks stimulate cell death via apoptosis or cell differentiation. Researchers have found elevated levels of the receptors for TGF-β on fibroblasts from scleroderma patients, suggesting that the activated form of the protein plays a role in their dysfunction. (When TGF-β is initially secreted, it's bound by other molecules and inactive.) But what triggers the production and activation of TGF-β in scleroderma remains unknown.

Moreover, because TGF-β's stimulation of scar and collagen tissue is normal and necessary in many cases, completely disabling the cytokine pathway is not a good option for treating scleroderma. "If you can't do fibrosis, you're in big trouble," says Tyndall.

Scientists have therefore been teasing out how to selectively block the TGF-β route that elicits overactive scar formation. Some believe that targeting the upstream proteins that activate TGF-β may be the key to halting scleroderma's fibrosis while allowing normal wound healing to continue. One such TGF-β–inhibiting drug is Gleevec, which has previously earned fame for its successes treating leukemia and other cancers. In recent years, physicians have reported cures or near-cures of late-stage scleroderma patients after trying Gleevec, which has motivated a number of phase II clinical trials of the drug for the condition. Luke Evnin, chair of the board of directors at the Scleroderma Research Foundation in San Francisco, California, cautions that the results so far are by no means definitive. "In larger case series, it is not clear that [the drug] is broadly applicable," he says. "But still the enthusiasm from the initial cases persists."

CREDIT: © CORBIS

## PAUL KLEE, A TRAGIC METAMORPHOSIS

The famous modern artist Paul Klee is widely believed to have suffered from, and died of, scleroderma. Late in Klee's life, for example, the disease caused his fingers to curl so much he had trouble holding a paintbrush. "All his medical records were destroyed, so it's conjecture. But it's very hard to attribute [his symptoms] to anything else," says rheumatologist John Varga of Northwestern University in Chicago, Illinois, who in 2004 wrote a review of Klee's works in relation to scleroderma. Art experts believe the disease had a major impact on Klee, as his later works shifted from vibrant to darker colors and emphasized themes such as mortality and suffering (above, Klee's *Tragic Metamorphosis*, 1939). "His style and technique really did change and evolve," says Varga. In one late work, *Captive*, Klee painted a grotesque self-portrait that includes representations of cagelike bars. Scleroderma patients often say they feel "imprisoned within their own bodies," says Varga.

Many scleroderma scientists remain wary of overhyping Gleevec. "We had promising drugs 10 years ago that were very hopeful," says Distler. "But the clinical studies actually failed." Those drugs, he notes, were "rather unspecific immunosuppressive drugs." They had appeared to work in phase II studies, says Distler, but then failed in larger randomized controlled trials.

Tyndall believes that stem cell transplants could solve scleroderma's fibrosis and perhaps all its other symptoms, too. The approach mirrors a strategy used to treat leukemia: Stem cells from bone marrow that can give rise to new immune cells are taken out from a patient, and then physicians use drugs to purposely obliterate the patient's entire immune system, a strategy called immunoablation. After that, the preharvested stem cells are infused back into the patient, where they can create fresh bone marrow and, it is hoped, a new functioning immune system. Tyndall says some of his scleroderma patients went back to normal after receiving this aggressive immune rebooting. A multicenter randomized phase III trial with 150 patients is under way to confirm these findings.

Nonetheless, those at the conference in Cambridge seemed to reach a consensus that scleroderma would need more than just one solution. "No two scleroderma patients are alike. It's really amazing to me," says Farber. Each patient may need a tailor-made treatment: One requires an aggressive antifibrotic treatment whereas another demands an emphasis on fighting pulmonary hypertension, Farber and others suggested.

Still, Denton is increasingly optimistic. "I think we're in a stronger position now, because in the previous era, we were trying therapies with an unclear view of what the biology is," he says. "Now we're in an era where treatments are having an impact on outcome, … and we're also starting to understand the very complex biology that links the different processes in scleroderma."

–LAUREN CAHOON

# Skulls Show Dinos Blew Their Horns

Nothing gets a paleontologist's speculative juices flowing like a strange piece of anatomy. Case in point: lambeosaurs, duck-billed dinosaurs (hadrosaurs) whose skulls sported hollow, bony crests connected to the animals' noses. Scientists have argued that the weird headgear was good for fighting, snorkeling, smelling, cooling the brain, or signaling to other lambeosaurs with loud, resonant honks.

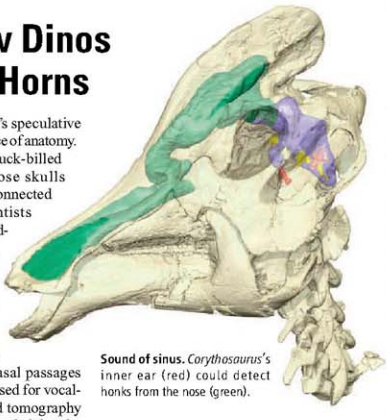

**Sound of sinus.** *Corythosaurus's* inner ear (red) could detect honks from the nose (green).

At the meeting, a group presented the most sophisticated evidence yet that the nasal passages within the crests were indeed used for vocalizing, not smelling. Computed tomography scans of lambeosaur skulls revealed that the brains weren't geared toward olfaction but that the inner ears were attuned to the frequencies the crests most likely produced. "Honking still survives" as a hypothesis, says David Weishampel of Johns Hopkins University in Baltimore, Maryland, who studied vocalization in the lambeosaur *Parasaurolophus* in the early 1980s.

At 10 meters long and weighing in at some 3 metric tons, lambeosaurs would have been some of the larger animals in the swampy floodplains of western North America, Asia, and Europe toward the end of the dinosaur era. They roamed around, mostly on their hind legs, grabbing vegetation with their toothless bills, then grinding it to a pulp with hundreds of small teeth in the back of their mouths. Fossil trackways suggest that flat-headed hadrosaurs lived in herds, and lambeosaurs may have, too.

Some early ideas about lambeosaur crests proved short-lived. The crests are too thin and brittle to have served as effective weapons, and the physics of breathing underwater through them turned out to be unworkable. Among the more plausible theories, vocalizing was first proposed in 1931 by a Swedish scientist who likened lambeosaurs to trumpeter swans. In the 1960s, paleontologist John Ostrom floated the ideas that the long, looping chambers inside the crests could have functioned as air-cooled radiators or heightened the animals' sense of smell. James Hopson of the University of Chicago in Illinois suggested in 1975 that the crest evolved its large size for visual display to attract mates.

David Evans of the Royal Ontario Museum in Toronto, Canada, studied the olfactory system of lambeosaurs and the nerves associated with it, looking at impressions of these nerve pathways that remain in skull bones. His findings, published in *Paleobiology* in January 2006, suggested that only a small part of the nasal cavity within the crest was used for smelling. But no one had actually looked at the entire brain of a lambeosaur. Working with Lawrence Witmer of Ohio University in Athens and others, Evans used computed tomography to scan the skulls of four species of lambeosaurids that lived about 75 million years ago.

The olfactory region turned out to make up less than 2% of the lambeosaurs' brains. In contrast, a crestless hadrosaur called *Edmontosaurus* had at least double that, whereas the predatory dinosaur *Tarbosaurus* devoted 9% of its brain to olfaction. "When you put it all together, the smell hypothesis can be rejected," Evans said.

Still, the crest does seem to be important. The elaborate nasal ductwork of the lambeosaurs points to a "strong selective pressure" for evolutionary adaptation, the team concludes. The inner ear, as revealed by the scans, suggests what advantage the odd organs might have offered. The clue is part of the cochlea called the basilar papilla. In living birds, studies have shown that its length correlates with the range of frequencies an animal can best hear. If the same relationship held in lambeosaurs, Evans and colleagues conclude, their optimal frequency in adults was 400 hertz, about the mid-range of a modern cornet. That's close to the frequencies an acoustic computer model has generated from the crest of *Parasaurolophus*. Hadrosaurs could have used their calls to attract mates, help keep the herd together, or warn one another of approaching predators, the researchers say. Other evidence from the skull suggests that hadrosaurs might have been particularly social, smart animals: Their cerebral hemispheres make up about 43% of the entire brain—more than in any group of dinosaurs except the small birdlike dromeosaurs, thought to be the brightest, most behaviorally complex ancient dinosaurs. The findings are in press at *The Anatomical Record*.

–ERIK STOKSTAD

# Two Legs Good

Our famed ancestor "Lucy" walked upright in the grasslands of Ethiopia 3.2 million years ago. But what of *her* ancestors? Researchers have glimpsed only bits and pieces of even older hominins, the group that includes humans and our ancestors. At the meeting, Bence Viola of the University of Vienna presented a single bone, the thighbone of an ancient australopithecine from Galili, Ethiopia, that may add an interesting piece to the puzzle of how Lucy's two-legged gait evolved. "It's a window into a time when key evolutionary changes are happening—it's exactly what you'd want," says J. Michael Plavcan of the University of Arkansas, Fayetteville, who was not involved in the work.

Although the femur was broken off at its lower end, its size suggests an owner slightly

**Making strides.** Horst Seidler (*left*) and Bence Viola (*right*) help study an early hominin thighbone.

CREDITS: (TOP TO BOTTOM) L. WITMER AND R. RIDGELY/OHIO UNIVERSITY; B. GINNER/UNIVERSITY OF VIENNA

larger than the roughly 1-meter-tall Lucy, Viola says. Argon-argon dates produced just a few weeks ago place the thighbone between 4.38 million and 3.92 million years ago—significantly earlier than the most ancient member of Lucy's species, *Australopithecus afarensis*, which dates to 3.6 million years ago.

In the view of Viola and his Vienna colleague Horst Seidler, the bone is more primitive than Lucy's femur and resembles that of a much earlier hominin, *Orrorin tugenensis*, thought to be about 6 million years old. They suspect that it came from *Au. anamensis*, a species that lived about 4 million years ago and is widely considered to be Lucy's ancestor.

Details of the femur's anatomy, such as a long neck of bone leading to a large femoral head (the "ball" of the hip's ball and socket joint), suggest that its owner—whatever its name—was bipedal, Viola said. But other clues imply that it may also have climbed trees, he added. For example, a thick layer of dense cortical bone is evenly distributed around the femoral neck. In upright walkers like us, that cortical bone is unevenly distributed. "Both *Orrorin* and this femur seem to show several traits which indicate bipedalism but also retain signs of arboreal behavior," Viola says. That suggests that our ancestors' move out of the trees was a long process.

But others aren't so sure that this single bone shows tree-climbing behavior. "It's not compelling enough to convince me of arboreality," says Yohannes Haile-Selassie of the Cleveland Museum of Natural History in Ohio. Carol Ward of the University of Missouri, Columbia, is more impressed: The cortical bone distribution is "pretty suggestive," she says. But she, too, would like to see more specimens, and the other end of the femur, to be sure. Stay tuned: Haile-Selassie's team is working on an unpublished partial hominid skeleton, also about 4 million years old, that may shed further light on how Lucy's ancestors walked (*Science*, 11 March 2005, p. 1545).

**–ELIZABETH CULOTTA**

## SNAPSHOTS FROM THE MEETING

**Up a tree?** The long hands, feet, and limbs of this fossil suggest it was a good climber.

**Earliest tree-climbers.** A 255-million-year-old creature called *Suminia getmanovi* caused a stir a few years ago when researchers examining its skull discovered it had the first known adaptations for highly efficient chewing of tough vegetation. Now a look at the rest of the skeleton reveals another record: the earliest evidence of living in trees. Jörg Fröbisch and Robert Reisz of the University of Toronto, Mississauga, in Canada studied a large block of stone that preserved 15 mostly complete skeletons. "This block provides a wealth of new information about *Suminia*," Fröbisch said at the meeting. The 50-centimeter-long animals had very long hands and feet—about 40% of the length of the limbs—and digits adapted for grasping. The new skeletons may be the most complete early therapsid (mammal-like reptile) yet found, so they could shed more light into the early evolution of the group, which flourished in the Permian and Triassic periods between 265 million and 225 million years ago. Kenneth Angielczyk of the Field Museum in Chicago, Illinois, notes that apart from a few burrowing species, most Permian therapsids were unspecialized four-legged herbivores. "The fact that [*Suminia*] was going in another direction is pretty cool," he says.

**Dinosaur-cruncher.** Any way you look at it, the extinct crocodilian *Deinosuchus* was a terror. Its 1.5-meter-long skull was double the length found in modern crocs, and the whole animal may have stretched more than 10 meters. To experts on the Late Cretaceous of North America, *Deinosuchus* practically screams "top predator." Now François Therrien of the Royal Tyrrell Museum of Palaeontology in Drumheller, Canada, and colleagues have buttressed that claim by estimating the strength of its bite. Taking five specimens from the United States, they compared the bending force of the jaw with that of the American alligator. The result: *Deinosuchus* could bite 13 times as powerfully as a modern alligator, nearly on a par with *Tyrannosaurus rex*. "Most assuredly *Deinosuchus* would have been a top predator of coastal environments," Therrien concluded. Paleontologist Hans-Dieter Sues of the Smithsonian's National Museum of Natural History in Washington, D.C., agrees. "Could it pull apart a hadrosaur? The answer was a definite yes."

**Steady on.** How much damage did that end-Cretaceous asteroid inflict, anyway? Researchers have long debated whether dinosaurs were already in decline before it hit, or whether they were struck down in their prime. A new analysis by Matthew Carrano of the Smithsonian's National Museum of Natural History in Washington, D.C., suggests the latter. Carrano took a close look at the scientific literature from North America, where the fossil record of Cretaceous dinosaurs is richest, and corrected for biases such as errors in classification and differences in how intensively paleontologists have searched for fossils in various places and times. The results showed that dinosaur diversity stayed steadily healthy through the late Cretaceous period, in North America at least. John Alroy of the University of California, Santa Barbara, sees the matter as settled. "It's the nail in the coffin" for the declining-dino scenario, he says.

**Acquired taste.** New skulls of juvenile *Diplodocus*, described at the meeting, suggest that young sauropod dinosaurs may have been pickier eaters than adults were. Stretching about 30 meters long, fully grown *Diplodocus*—massive four-legged plant eaters closely related to *Apatosaurus*—had remarkably square jaws crammed with narrow-crowned teeth in the front (see illustration). One idea is that these teeth helped them quickly crop vegetation to sate an appetite that presumably matched their enormous bulk.

**It's all good.** Square jaw may show *Diplodocus* adults had more varied tastes than their young did.

The new juvenile skulls look different. Their snouts are narrow and rounded, with a full mouthful of teeth. "We believe it records an important change in diet," John Whitlock, a Ph.D. student at the University of Michigan, Ann Arbor, told the audience. Whitlock and his adviser, Jeffrey Wilson, argue that the shape of the snout provides clues to the feeding behavior. A rounder snout correlates with more selective browsing, rather than indiscriminate noshing on vegetation.

Peter Dodson of the School of Veterinary Medicine at the University of Pennsylvania isn't convinced that the juvenile belongs to the same species as the known adults. But Kristi Curry-Rogers of Macalester College in St. Paul says that even if it doesn't, the new skull still shows that the genus *Diplodocus* was more varied and interesting than scientists had realized. "The fact that this juvenile with a rounded skull occurs in the midst of so many other square-snouted adults introduces a new view of what young members of this larger group looked like," she notes.

**–E.S.**

CREDITS (TOP TO BOTTOM): DIANE SCOTT; M. SKREPNICK AND L. WITMER/OHIO UNIVERSITY

Election special 676

Online electromagnetism 682

LETTERS | BOOKS | POLICY FORUM | EDUCATION FORUM | PERSPECTIVES

# LETTERS

*edited by Jennifer Sills*

## Informed Consent in Social Science

IN HIS PERSPECTIVE "*HOMO EXPERIMENTALIS* EVOLVES" (11 JULY, P. 207), J. A. LIST PROUDLY acknowledges that economists perform experiments on human subjects without notifying them: "[I]n a natural field experiment, the analyst manipulates experimental conditions in a natural manner, whereby the experimental subjects are unaware that they are participating in an experiment. This approach combines the most attractive elements of the laboratory and of naturally occurring data: randomization and realism." I know that psychologists tend to do the same thing. Yet this practice leads me to ask: Where has "informed consent" gone?

PIERRE COUTURE

Saint-Cyprien-de-Napierville, QC, Canada. E-mail: pa_couture@sympatico.ca

**Balancing act.** Social scientists must walk a fine line in determining when a study's potential for public good justifies a relaxation of informed consent requirements.

### Response

AS MY PERSPECTIVE MADE CLEAR, there are several types of field experiments. In some, subjects are made aware that they are taking part in an experiment and sign consent forms in the spirit of the guidelines of the Nuremberg code. There are, however, certain cases in which adhering to rigid ethical rules can affect the very issue that is being studied, such that it becomes quite difficult to conduct the research (*1*, *2*). For example, if one were interested in exploring whether, and to what extent, race or gender influences the prices that buyers pay for used cars, it would be difficult to measure accurately the degree of discrimination among used car dealers who know that they are taking part in an experiment.

For such purposes, it makes sense to consider executing a natural field experiment. This does not suggest that moral principles should be altogether abandoned in the pursuit of science. Quite the opposite: The researcher must weigh whether the research will inflict harm, gauge the extent to which the research benefits others, and determine whether experimental subjects chose the experimental environment of their own volition and are treated justly in the experiment. Local Research Ethics Committees and Institutional Review Boards in the United States serve an important role in monitoring such activities.

Consider the natural field experiment that was discussed in my 11 July Perspective. In this experiment, a coauthor and I worked with a national fundraiser to explore various methods that fundraisers might wish to implement to be able to provide more of the public good. During the research, we never learned the solicitees' names, solicitees received letters similar to the ones they were sent in the normal course of their lives, and they made charitable donation decisions in a natural manner. In the end, we learned something interesting about the economics of charity while doing no harm to the solicitees. Indeed, some might argue that these potential donors were better off because our methods induced more giving and therefore a higher provision of the public good. When the research makes participants better off, benefits society, and confers anonymity and just treatment to all subjects, the lack of informed consent seems defensible.

Ethical issues surrounding human experimentation are of utmost importance. Yet, the benefits and costs of informed consent should be carefully considered in each situation. Those cases in which there are minimal benefits of informed consent but large costs are prime candidates for relaxation of informed consent.

JOHN A. LIST

Department of Economics, University of Chicago, and NBER, Chicago, IL 60637, USA. E-mail: jlist@uchicago.edu

**References**

1. S. D. Levitt, J. A. List, *J. Econ. Persp.* **21**, 153 (2007).
2. R. Homan, *The Ethics of Social Research* (Longman, London, 1991).

## Viewing NASA's Mars Budget with Resignation

I WOULD LIKE TO CLARIFY SEVERAL POINTS IN the News of the Week story (26 September, p. 1754) by A. Lawler, "Rising costs could delay NASA's next mission to Mars and future launches."

When the National Research Council's Planetary Science Decadal Survey recommended the Mars Science Laboratory (MSL) mission for priority funding, it assigned a cost level of $650 million. This value, rather than $1.4 billion, is the true metric for seeing the deep damage that MSL's profligately overrunning cost—now likely to top $2.1 billion—has inflicted on NASA's Mars and wider planetary science budget.

Also, the story focused its overrun discussion on instrument costs. Although certainly part of the problem, instrument cost increases have been considerably smaller than overruns in the rest of MSL's budget, which was severely mismatched to the project's complexity from its inception. This mismatch sowed the most fundamental seeds of MSL's cost problems.

The article's end quote described NASA's Mars Sample Return (MSR) mission plan as "smoke and mirrors." Dis-

CREDIT: GETTY IMAGES


Putting the squeeze on polymers
689

Chromosome number and cancer
692

appointingly, MSR is becoming a mirage in the wake of MSL and other budget damage caused by numerous substantial Science Mission Directorate (SMD) cost overruns accepted in recent months. However, as evidenced by both internal NASA and external Office of Management and Budget scrutiny in 2007, NASA's MSR plan in the President's Fiscal Year 2009 budget did fit in SMD's future budget envelope. It could well have launched near 2020, had a strong emphasis on cost control been sustained as a priority.

Finally, there was no mention that a NASA independent review team found numerous development issues that called MSL's 2009 launch date into serious doubt almost a year ago. Nor did it describe that scenarios for dealing with MSL without causing such deep budgetary damage elsewhere were proposed by SMD but rejected at higher levels in early 2008. That, and the concurrent, forced disbanding of the MSL independent review team, precipitated my resignation as SMD Associate Administrator.

ALAN STERN

Clifton, VA 20124, USA. E-mail: astern2010@aol.com

## Food Insecurity's Dirty Secret

ATTEMPTS TO INCREASE CROP YIELDS IN SUB-Saharan Africa have failed repeatedly since the 1960s because soil quality has been ignored. The Green Revolution of the 1970s bypassed sub-Saharan Africa, and is stalling in the rice-wheat system of South Asia and elsewhere because of soil degradation, organic matter and nutrient depletion, and excessive withdrawal of ground water. Average yields of grain crops in sub-Saharan Africa have stagnated below 1 ton per hectare since the 1960s, with dire consequences on human well-being and ecosystem services. The problem of food insecurity, affecting 854 million people, is worsened by increases in the price of rice, wheat, and other food staples (*1*–*6*) and by global warming (*7*).

Proven soil management technologies, to be promoted in conjunction with improved varieties, include (i) no-till farming with mulch, cover crops, and complex rotations; (ii) water conservation, harvesting, and recycling with efficient irrigation including drip and furrow methods; and (iii) integrated nutrient management with compost, biochar, N fixation, and supplements of nano-enhanced and slow-release fertilizers. The yield potential of improved varieties can only be realized if grown following opti-

mal soils and agronomic management. Rather than giving handouts as emergency aids, resource-poor farmers must be compensated for ecosystem services (e.g., trading C credits) to promote technology adoption and soil restoration.

Food insecurity is exacerbated by emphasis on biofuels (*1*, *8*, *9*). We must establish energy plantations (*10*, *11*) (grasses, trees, algae, and cyanobacteria) using soils and waters that do not compete with food production. This energy can be used to provide modern cooking fuels to rural communities in sub-Saharan Africa and South Asia, in a way that will minimize health hazards, promote use of crop residues and dung as soil amendments, and mitigate the Asian soot cloud.

The strong relationship between soil degradation and survival of the past civilizations (*12*) cannot be ignored. If soils are not restored, crops will fail even if rains do not; hunger will perpetuate even with emphasis on biotechnology and genetically modified crops; civil strife and political instability will plague the developing world even with sermons on human rights and democratic ideals; and humanity will suffer even with great scientific strides. Political stability and global peace are threatened because of soil degradation, food insecurity, and desperation. The time to act is now.

RATTAN LAL

Carbon Management and Sequestration Center, School of Environment and Natural Resources, The Ohio State University, Columbus, OH 43210, USA. E-mail: lal.1@osu.edu

**References**

1. L. R. Brown, "Why ethanol production will drive world food prices even higher in 2008" (Earth Policy Institute, 24 January 2008).
2. Anonymous, *Economist* **387**, 32 (2008).
3. FAO, "Food Outlook 2007 Global Market Analysis" (FAO, Rome, 2007).
4. FAO, "The State of Food Insecurity in the World" (FAO, Rome, 2006).
5. FAO, "Food Balance Sheet 1961–2006" (FAO, Rome, 2007).
6. Anonymous, *Economist* **387**, 33 (2008).
7. W. R. Cline, "Global warming and agriculture: Impact estimates by country" (Peterson Institute, Washington, DC, 2007).
8. C. Hoyos, J. Blas, "West rethinks strategic threats," *Financial Times*, 22 June 2008.
9. J. S. Barbara, "The false promise of biofuels" (Special Report from the International Forum on Globalization and the Institute for Policy Studies, 2007); www.ifg.org/pdf/biofuels.pdf.
10. R. Lal, D. Pimental, *Soil Tillage Res.* **97**, 1 (2007).
11. R. Lal, *CSA News* **52**, 12 (2007).
12. J. Diamond, *Collapse: How Societies Choose to Fail or Succeed* (Viking, New York, 2005).

## CORRECTIONS AND CLARIFICATIONS

**ScienceScope:** "'Free' gets sold" (17 October, p. 359). Biomed Central had revenues, not profits, of €15 million last year.

**Special Section on Clinical Trials:** "Making clinical data widely available" by J. Kaiser (10 October, p. 217). The article misquoted NIH's Deborah Zarin about a proposal to include narrative summaries of trial data in ClinicalTrials.gov. Zarin did not suggest that NIH's posting of the narratives could be viewed as giving a drug "a stamp of approval." Rather, she said that posting them could be viewed as endorsing a specific interpretation.

**Table of Contents:** (5 September, p. 1261). The description of the Report "*Apobec3* encodes *Rfv3*, a gene influencing neutralizing antibody control of retrovirus infection" by M. L. Santiago *et al.* was incorrect. The sentence should read, "A resistance factor known to protect mice from retroviral infection is unexpectedly identified as *Apobec3*, a deoxycytidine deaminase."

**Letters:** "The case against the *CMJ*'s editors" by N. Čikeš (27 June, p. 1719). Čikeš stated that "the *CMJ*'s impact factor is around 0.8, and it has been declining." In fact, *CMJ*'s impact factor has had an increasing trend and

reached 1.174 in 2007, thus becoming the first Croatian scientific journal ever to achieve an impact factor greater than 1. Čikeš also failed to state that the decision of the School's Court of Honor against A. Marušić was officially abolished by the Ministry of Science, Education, and Sports (ruling UP/I-040-01/08-01/00001, no. 533-01-08-0001 from 28 January 2008).

**Books *et al.*:** "Hard facts about soft animals" by M. Glaubrecht (23 May, p. 1014). In the caption for the photographs on page 1015, *Falcidens halanychi* is erroneously identified as a solenogastre. It is actually a member of Caudofoveata, a different order of small, worm-shaped molluscs.

**Reports:** "Differential rescue of light- and food-entrainable circadian rhythms" by P. M. Fuller *et al.* (23 May, p. 1074). The following acknowledgment was omitted due to a misunderstanding: We thank C. Weitz and D. Knutti for the *Bmal1* gene construct used in our adeno-associated viral vector and for the description of its construction. In addition, the Supporting Online Material (SOM) contained several errors: In fig. S2, panels B and C were reversed; the legend for panel B described panel C, and the legend for panel C described panel B. In addition, fig. S3B contained an error, a result of mistakenly using an incorrect file to make the plot. The incorrect file was an incomplete working file obtained from the same animal and experiment as shown in Fig. 3B in the main text, but with an incorrect start time (which advanced the phase). Fig. S3D, in which the trace is derived from the data shown in fig. S3B, was also incorrect. A revised SOM file containing corrected versions of figs. S2 and S3 is available online.

**Books *et al.*:** "The golden weed, America's most deadly drug" by R. N. Proctor (4 May 2007, p. 692), book review of *The Cigarette Century* by Allan Brandt. The Books *et al.* editor failed to notice that Allan Brandt's acknowledgments note the substantial assistance of our reviewer, Robert N. Proctor—who provided "a constant sounding board" and "meticulously read and critiqued the complete manuscript."

## TECHNICAL COMMENT ABSTRACTS

### COMMENT ON "Differential Rescue of Light- and Food-Entrainable Circadian Rhythms"

**Ralph E. Mistlberger, Shin Yamazaki, Julie S. Pendergast, Glenn J. Landry, Toru Takumi, Wataru Nakamura**

Fuller *et al.* (Reports, 23 May 2008, p. 1074) reported that the dorsomedial hypothalamus contains a *Bmal1*-based oscillator that can drive food-entrained circadian rhythms. We report that mice bearing a null mutation of *Bmal1* exhibit normal food-anticipatory circadian rhythms. Lack of food anticipation in *Bmal1*$^{-/-}$ mice reported by Fuller *et al.* may reflect morbidity due to weight loss, thus raising questions about their conclusions.

Full text at www.sciencemag.org/cgi/content/full/322/5902/675a

### RESPONSE TO COMMENT ON "Differential Rescue of Light- and Food-Entrainable Circadian Rhythms"

**Patrick M. Fuller, Jun Lu, Clifford B. Saper**

The points raised by Mistlberger *et al.* arise from a shortcoming in their approach, namely, that they measure the response to food restriction by using food-seeking behavior, which is confounded by homeostatic inputs. We used unrelated circadian-driven physiological responses, and we stand by our finding that the dorsomedial nucleus of the hypothalamus contains a food-entrainable oscillator that is sufficient for entrainment of circadian rhythms of body temperature and locomotor activity.

Full text at www.sciencemag.org/cgi/content/full/322/5902/675b

## Letters to the Editor

Letters (~300 words) discuss material published in *Science* in the previous 3 months or issues of general interest. They can be submitted through the Web (www.submit2science.org) or by regular mail (1200 New York Ave., NW, Washington, DC 20005, USA). Letters are not acknowledged upon receipt, nor are authors generally consulted before publication. Whether published in full or in part, letters are subject to editing for clarity and space.

POLITICAL SCIENCE

# Why Rich States Aren't Republican

**Terry Nichols Clark and Christopher Graziul**

Many of us discuss elections, often with concepts like red and blue states. Andrew Gelman is a creative Columbia University statistician who joined with four of his former political science students to dig deeper. The most creative analyses in *Red State, Blue State, Rich State, Poor State* use Gelman's multilevel methods. But the technical background is nearly invisible: Here there are no equations and few numbers—rather, one finds dozens of revealing graphics, all of which are very clear.

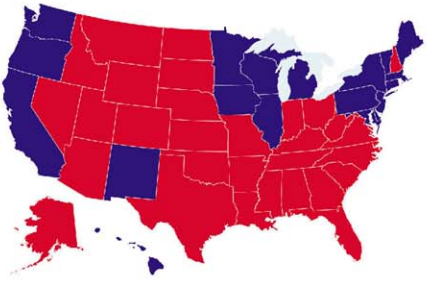

**The 2000 split.** Red states were carried by George Bush; blue states, by Al Gore.

The book is unusual in aiming to enlighten the general lay reader through a step-by-step analysis, not merely to engage in a debate with other political scientists. Through a clear and crisp writing style, it quotes and refutes many widespread views of journalists and political pundits, even as it builds on the political science literature.

Three main findings illustrate the authors' approach. First, rich individuals vote more Republican. Second, rich states (like Connecticut, with high average-income residents) vote more Democratic. These conclusions are contrasted with a third, very intriguing finding: In poor states like Mississippi, income strongly predicts Republican voting, whereas in rich states like Connecticut, the rich and poor differ little in their voting patterns. These results are illustrated through scatter plots and line charts showing income versus level of Republican voting for citizens. This alone may not seem novel, but by repeating the same analysis for different types of states, regions, and countries Gelman *et al.* produce surprisingly rich descriptions using just two variables, income and voting.

**Red State, Blue State, Rich State, Poor State**
Why Americans Vote the Way They Do

***by Andrew Gelman, David Park, Boris Shor, Joseph Bafumi, and Jeronimo Cortina***

Princeton University Press, Princeton, NJ, 2008. 247 pp. $27.95, £16.95. ISBN 9780691139272.

The three key ideas are refined by systematically adding other factors. Time: State voting differences have mostly emerged in the last 20 years. Religion: Surprisingly, church attendance seems more tied to voting Republican for the rich than for the poor. Class: State differences are stronger for upper-income persons. Race: A great deal of party-by-income voting may be due to race, especially in the South. Polarization: The parties have grown more deeply divided on issues since the 1960s.

The book's elegance comes first from the clarity of the income-party model but also from its methodology. By consistently repeating similar analyses that contrast state and individual effects, they refute the "ecological fallacy" of stereotyping individuals' behavior on the basis of data about where they live. For example, many have compared state income with state voting and falsely concluded that rich individuals vote more Democratic. The authors are able to quickly dispel this myth while simultaneously navigating the intricacies of relationships between income and voting.

So what is missing? Most obviously, little time is devoted to the complicating effect of social issues. Past work has shown that while income explains many fiscal preferences, education is more powerful for social issues like abortion, the environment, gender roles, and minority tolerance. When these several variables combine in party voting, the results are not always linear or elegant. Gelman *et al.* thus convey a view of income-based elites more than a view of citizens active in various issues. Income and presidential voting are hard to link neatly to such issue politics. The book continues an old tradition of class politics, despite decades of work stressing its decline [e.g., (*1*)]. The authors say almost nothing about political culture, although many analysts use culture to revise class-based models. Indeed, many argue that a new political culture is emerging built on combining social with income-related issues (e.g., David Brooks's bohemian-bourgeois or Bobos, who are fiscally conservative and socially liberal).

Or consider the culture wars debates, probed by Morris Fiorina (*2*) and Bill Bishop (*3*). These bring in a wide range of other variables and processes. Gelman *et al.* include many brief reviews of other subliteratures (like friends and neighbors) but do not use them seriously. They are especially critical of books by David Brooks (*4*) and Thomas Frank (*5*). Both Brooks and Frank stress how combining multiple dimensions (such as abortion and taxes) generates new results, but Gelman *et al.* mostly address each dimension separately, finessing the complex arguments. Or they present data on more complex points without joining them to their core model.

Unfortunately, although the authors recognize that their models have only some of the answers, they don't tell us how strong their models are. Others have shown that Gelman *et al.*'s variables explain some 10 to 20% of the variance in voting, which leaves at least 80% unexplained. Brooks and Bishop, two smart journalists, offer a richer interpretation, and Nelson Polsby and Aaron Wildavsky's classic text (*6*) provides a broader perspective.

The strength of *Red State, Blue State* is that Gelman *et al.* build a tight, parsimonious argument. Their work resembles mathematical model–building, sans equations. Extending the power of their methods by adding a few more critical processes would enrich the study of American politics. But even if too simplistic, this fun-to-read book may become a minor classic.

The reviewers are in the Department of Sociology, University of Chicago, 1126 East 59th Street, Chicago, IL 60637, USA. E-mail: tnclark@uchicago.edu

**References**

1. T. Clark, S. Lipset, Eds., *The Breakdown of Class Politics: A Debate on Post-Industrial Stratification* (Woodrow Wilson Center Press, Washington, DC, 2001).
2. M. P. Fiorina, *Culture War?: The Myth of a Polarized America* (Pearson, Longman, New York, 2005).
3. B. Bishop, *The Big Sort: Why the Clustering of Like-Minded America Is Tearing Us Apart* (Houghton Mifflin,

Boston, 2008).
4. D. Brooks, *Bobos in Paradise: The New Upper Class and How They Got There* (Simon and Schuster, New York, 2000).
5. T. Frank, *What's the Matter with Kansas? How Conservatives Won the Heart of America* (Metropolitan, New York, 2004).
6. N. W. Polsby, A. Wildavsky, D. A. Hopkins, *Presidential Elections: Strategies and Structures of American Politics* (Rowman and Littlefield, Lanham, MD, ed. 12, 2008).

10.1126/science.1166194

POLITICAL SCIENCE

# Can We Trust the Machines?

**Walter R. Mebane Jr.**

Since the 2000 U.S. presidential election, many have worked to increase voters' confidence that election results are fair and correct. One theme from 2000 was that the technology used to record votes—especially punchcard ballots—was deficient and needed to be replaced. The Help America Vote Act of 2002 provided federal funds for states to acquire electronic voting machines or optically scanned paper ballots. New controversy arose when computer scientists and others complained that the recommended technologies were far from being up to the task. The electronic technologies suffered from security weaknesses and production defects, and election officials often administered the new machines incompetently. Critics argued the machines lacked transparency, were unreliable, and were possibly subject to undetectable manipulation.

Michael Alvarez and Thad Hall belong to a group of political and computer scientists who after 2000 began the Caltech/MIT Voting Technology Project, intended to diagnose problems with current practices and to point the way to developing better ones. *Electronic Elections* summarizes insights they have gleaned from their extensive experience. The book is meant to instigate scientifically informed election administration. The authors argue for a comparative approach to risk management that considers the costs and benefits of alternative methods. Rather than consider how electronic voting technology performs in isolation, we should judge how it works in comparison to paper systems. The authors reject the position that voting reform is a high-risk activity to which we should apply the precautionary principle.

The authors' stance is evident when they argue that the idea of voting over the Internet has been unwarrantedly dismissed in the United States. They are particularly exercised about the U.S. Department of Defense's Secure Electronic Registration and Voting Experiment (SERVE), which was intended to determine whether using the Internet could facilitate voting by uniformed and overseas citizens. SERVE was canceled before being implemented in 2004, due to concerns by some experts that secure Internet voting was impossible. Alvarez and Hall point out that European countries were conducting similar voting experiments and that status quo methods involving mailing ballots are also insecure and fail to protect ballot secrecy. They see the critics' perspective as too narrow and note the loss of a chance to discover how well a set of methods works.

**Electronic Elections**
The Perils and Promises of Digital Democracy
*by R. Michael Alvarez and Thad E. Hall*
Princeton University Press, Princeton, NJ, 2008. 232 pp. $29.95, £17.95. ISBN 9780691125176.

In two early chapters, the authors discuss problems with paper voting and criticisms of electronic alternatives. They note that paper systems have been used in American elections for more than 100 years and have never been free of failures or fraud. They also review a variety of security concerns surrounding electronic voting, such as the profound flaws revealed in 2003 through studies of source code for Diebold touch-screen voting equipment. Their consideration of criticisms of electronic voting seems inadequate. Nowhere do Alvarez and Hall discuss the conflicts of interest others have identified in the fact that the vendors pay for the laboratories that validate their equipment. Nor do they mention the basic objection that it is technically not possible to verify what a computer system as complicated as a voting machine will do under all the conditions that may arise. Validation is currently not possible, and secrecy does not inspire trust.

Time has not been kind to electronic voting systems in the United States, and in important respects the book's coverage ends too early. Alvarez and Hall discuss developments through the end of 2006. During 2007, California's secretary of state assigned teams of experts to study the voting systems approved for use in the state. The teams reported that the security mechanisms were inadequate and that the systems "contain serious design flaws ... which attackers could exploit to affect election outcomes" (*1*). This year, Ohio's sec-

## BROWSINGS

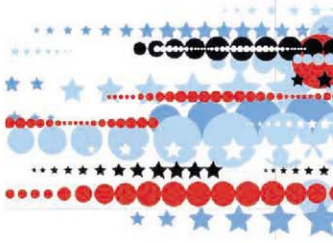

**Design for Democracy.** Ballot and Election Design. Marcia Lausen. University of Chicago Press and AIGA, Chicago, 2007. 186 pp. $65, £35. ISBN 9780226470467.
A group of graphics design specialists offer guidelines for improving the clarity of registration forms, signs, informational guides, administrative material, and ballots.

**Post-Broadcast Democracy.** How Media Choice Increases Inequality in Political Involvement and Polarizes Elections. Markus Prior. Cambridge University Press, Cambridge, 2007. 336 pp. Paper, $27.99, £16.99. ISBN 9780521675338.
Prior explores political consequences of the changes in patterns of news exposure produced by the rise of broadcast television, expansion of cable TV, and growth of the Internet. His data-packed yet lucid account documents shifts in important aspects such as political knowledge and interest, turnout, and voter partisanship.

**Bad for Democracy.** How the Presidency Undermines the Power of the People. Dana D. Nelson. University of Minnesota Press, Minneapolis, 2008. 271 pp. $24.95. ISBN 9780816656776.
People's unrealistic "expectations of what the president can and should do," Nelson claims, have fueled the continual expansion of the scope and power of the U.S. presidency. She argues that the trend must be reversed if citizens are to enjoy and practice the self-rule essential to democracy.

CREDIT: FROM *DESIGN FOR DEMOCRACY*/COURTESY UNIVERSITY OF CHICAGO PRESS

The reviewer is in the Department of Political Science and Department of Statistics, University of Michigan, Ann Arbor, MI 48109–1045, USA. E-mail: wmebane@umich.edu

retary of state ruled against the use of touch-screen systems (*2*). A defect in Diebold's system software that caused votes to be lost in several Ohio counties is present in source code used in machines in jurisdictions throughout the country (*3*, *4*).

Alvarez and Hall also consider the politics of election administration. They discuss the content of mass media coverage of voting technology along with survey evidence about public views of the topic. These aspects of *Electronic Elections* help flesh out the context for the scientific study and policy-making that Alvarez and Hall describe. The book offers a thoughtful early contribution to a new field of election science.

**References**

1. www.sos.ca.gov/elections/elections_vsr.htm.
2. www.sos.state.oh.us/SOS/elections/voterinformation/equipment/VotingSystemReviewFindings.aspx.
3. M. Niquette, "Voting machine glitch admitted," *Columbus Dispatch*, 22 August 2008.
4. www.mcclatchydc.com/100/story/50485.html.

10.1126/science.1165818

POLITICAL SCIENCE

# On Counterproductive Changes

**Michael Johnston**

Elections ought to be simple. Decide who is eligible to vote, put the options before them, tally up their choices, and then, by one set of electoral rules or another, declare the winners. But things do not always work out that way: vote totals are tampered with, equipment breaks down, and eligible electors are turned away while others vote early and often. Citizens in democracies around the world demand and, in the wake of electoral fiascos, often get aggressive rounds of clean election reform. But as Frederic Schaffer shows us in *The Hidden Costs of Clean Election Reform*, all too often the problems we see are the results of past reforms. Even more troubling, new measures frequently make matters worse.

Election reformers damage democracy with surprising frequency, producing what Schaffer—borrowing from medicine—terms "iatrogenic" (doctor-caused) harm, a useful initial metaphor even if it is used in overly literal ways in much of the book. In some cases damage is inadvertent: reform measures may be poorly thought out, create perverse incentives, or be starved of resources and support. In many other cases, however, devious political operatives march under the banner of reform, enacting and enforcing measures that suppress the vote, facilitate cheating, and alienate citizens from the electoral process itself.

**The Hidden Costs of Clean Election Reform**

*by Frederic Charles Schaffer*

Cornell University Press, Ithaca, NY, 2008. 263 pp. $35, £17.95. ISBN 9780801441158.

Schaffer (a research associate at MIT's Center for International Studies) has assembled an impressive database of recent clean election reforms in places ranging from Albania to Zimbabwe, many of which left democratic processes worse off than before. Lest we conclude that such countries' reformers are less skillful than ours, that database also includes 24 examples from various parts of the United States. In addition, Schaffer considers historical cases in detail: When, in 1852, France sought to prevent the practice of marking ballots (used to match voters with their choices), it ended up disallowing the votes of numerous citizens who did not understand the rules, who accidentally made additional marks, or who even wrote messages celebrating their choices. By 1881, rules against extraneous markings on ballots voided 3% of the national vote—a figure that rose to 20% in some districts. Schaffer also examines contemporary Taiwan, Venezuela, South Africa, and the Philippines in light of his own experiences in those countries.

Clean election reforms, Schaffer argues, come in three forms: controls on voter eligibility [e.g., who is entitled to vote or who has voted already (indicated by ink-stained fingers in many countries)]; voter insulation (e.g., the secret ballot or checks on vote-buying); and vote integrity (e.g., poll watchers from competing parties or automated vote tabulation). Schaffer's distinctive finding is that similar reform strategies can have quite different results, whereas differing mixes of reforms can produce similar outcomes in contrasting settings. Voter eligibility rules may protect the right to vote, but they can also keep opposition voters away from the polls. Voter insulation can stop vote-buying but may also inhibit persuasive processes essential to democracy. While vote-integrity measures can make for safe voting and swift reporting of results, they may also bring partisan interests and unproven technologies right into the polling place.

**A vote clearly cast.** The French use transparent ballot boxes, as in their presidential election.

CREDIT: RAMA/WIKIMEDIA COMMONS

The author attributes those outcomes to "the motives, knowledge, and capacities of the *actors* involved in crafting, implementing, or reacting to reforms." Those actors, in turn, fall into four categories: lawmakers; election officials and workers; candidates and backers; and civic educators—those charged with teaching citizenship. Reform is not a matter of choosing better ideas over riskier ones—and certainly not a choice between clean-but-exclusive elections versus open-but-risky ones. Rather, reforms have much more to do with who steers the changes, using what resources, and toward what goals. Accordingly, Schaffer devotes a full chapter to each of his four key groups.

The result is an illuminating, broadly comparative, and useful critique of clean election reforms. In one sense, the author might be open to the accusation of having examined the shortcomings of politics only to discover more politics, but any such critique would sell the book short. Although "reform" is a powerful word for friends of democracy, not everything called a reform is a good idea. Often the term covers up self-serving ideas: My bill intended to triple the pay of academicians across the country will—of course—be called the Higher Education Reform Act of 2008. Worse yet, "reform" slogans can be used to create a sense of crisis where none exists, as witness recent calls for "Social Security reform"

The reviewer is at the Department of Political Science, Colgate University, 13 Oak Drive, Hamilton, NY 13346, USA. E-mail: mjohnston@mail.colgate.edu

based on a misrepresentation of the purposes of the Social Security Trust Fund.

What would be better? In his concluding chapter, Remedies, Schaffer deploys an admirable amount of common sense. The problem, as noted, is not a lack of the right tools, but the need to put them in the right hands (motives, remember, are crucial) and to enable those entrusted with reform to act effectively. The goal is both to build capacity and to constrain partisanship. To that end, he identifies four paramount strategic ideas: "taking it slow," "keeping it simple," "making it transparent," and "forcing remedial action." Politics will not go away, nor should it: contending parties and interests should be able to understand, examine, and respond to new policies in ways that make it more difficult for anyone to bend reform to their own purposes. There will never be a clean elections "cookbook," there are no perfect or neutral political institutions, and technology (such as the electronic voting machines made by Diebold, a major Republican contributor, that are difficult to use and produce no paper record of voters' choices) is no cure-all. Instead, as Schaffer shows us, advocates of clean election reform must both be careful what they wish for and be selective in their choice of friends.

10.1126/science.1165805

POLITICAL SCIENCE

# The Power of Cross Pressures

**David A. M. Peterson**

Presidential campaigns influence voters to alter election outcomes, yet experts are unsure of the mechanism behind these influences. Politicians, consultants, and pundits emphasize the day-to-day changes in candidate activity. They look to the election outcome and assume that because the winning campaign was successful, it must have been the superior campaign. The outcome of the election is then ascribed to whatever specific tactics and events they focused on during the campaign. This perspective leads to the implicit assumption that voters are malleable and affected by the strategic choices of the candidates. It emphasizes the most trivial of campaign events as major influences on voters. The question then becomes which campaign tactic was more successful at swaying a majority of voters.

Academics offer a more circumspect perspective on the daily changes of a campaign. They demonstrate that the outcome of an election and the decisions of individual voters can be predicted before the campaign begins. Because the outcome is forecast without accounting for the campaign, the campaign must not have been crucial. According to this understanding, election campaigns inform voters and lead them to make predictable decisions based on the fundamentals: party, issue positions, and the economy. The question for political scientists becomes how the voters construct their vote choice based on these determinants and not how the campaigns change these determinants.

In their path-breaking *The Persuadable Voter: Wedge Issues in Presidential Campaigns*, D. Sunshine Hillygus and Todd G. Shields address the basic question of how much campaigns matter in two ways: First, they argue that the key to understanding how campaigns produce electoral outcomes is to determine how they influence individual voters. They start from the political science depiction of voters' attitudes as relatively resistant to campaigns. Campaigns do not fundamentally alter the balance of Republicans and Democrats or anti-abortion and pro-choice voters. Hillygus and Shields (political science professors at Harvard and the University of Arkansas, respectively) explain that campaigns influence voters by altering how much weight individuals place on party and what they know about the candidates' different policy positions. Second, the authors recognize that campaigns need to be understood as the interaction between voters and campaign organizations. Each makes decisions based on what they know about the other, and the connections between voters and candidates determine the choices of individual voters and the outcomes of elections.

**The Persuadable Voter**
Wedge Issues in Presidential Campaigns
*by D. Sunshine Hillygus and Todd G. Shields*
Princeton University Press, Princeton, NJ, 2008. 267 pp. $29.95, £17.95. ISBN 9780691133416.

The book advances the important point that although campaigns may not change a voter's predispositions, that does not mean that all such predispositions favor the same candidate. Instead, many voters are ambivalent because their partisanship and issue positions conflict. For example, there are a sizable number of pro-life Democrats and pro-choice Republicans. Campaigns can persuade these voters to favor one candidate over the other by altering the level of importance they place on their party and their issue positions.

The authors offer three interconnected reasons that this intersection of the two concepts drives election outcomes. First, there are a large number of potentially persuadable voters on any given issue. Hillygus and Shields examined 25 issues that dominated the 2004 campaign and found that, on average, a quarter of partisans disagree with their party on any issue. Second, campaigns sway these "cross-pressured" voters by shifting their priorities among the sources of this internal conflict. In 2004, for instance, Democrats' attempts to highlight stem cell research created cross pressures for many Republicans who, in opposition to their party's stance, favored federal funding for such research. Third, recent developments in information and communication technology allow candidates to carefully target voters of the opposite party based on these issues. Campaigns can now "micro-target" narrow appeals to small cross sections of voters.

The first and third of these reasons make up the heart of the book. The authors' novel approach to identifying both persuadable voters and effective micro-targeting techniques provides the most powerful evidence for their argument. They posit that given what we know about voters, not every campaign appeal will influence every voter. Instead, campaigns are effective because they can target their arguments to the predispositions of carefully selected voters. For example, campaigns can identify conflicted pro-guns Democrats or socially liberal Republicans and then tailor their appeals to tap these internal conflicts. Thus, the candidates who will win are the ones who can better exploit these internal divides of the other party's supporters while fending off the appeals for their own partisans.

Ultimately, Hillygus and Shields's theory and evidence extend beyond our understanding of campaigns and can be more broadly applied to American politics. Their theory can also explain historically important large shifts in the electorate. For example, they suggest that the cross pressures faced by racially conservative Democrats coupled with the Republican Party's appeals to racial conservatism created the steady transition of a solid Democratic South to a Republican stronghold. *The Persuadable Voter* reminds us that, overall, the outcome of elections and the face of politics hinge on the ability of parties, candidates, and voters to adapt to each other and to the changing nature of political appeals.

10.1126/science.1166146

The reviewer is in the Department of Political Science, Texas A&M University, College Station, TX 77843–4348, USA. E-mail: dave@polisci.tamu.edu

POLITICAL SCIENCE

# A Better Way to Choose?

Iain McLean

**An unfortunate consequence of approval voting?** The Burr-Hamilton duel.

CREDIT: BETTMANN/CORBIS

Steven Brams's opening sentence admits that "it may come as a surprise to some that there is a science of elections." But there is. It goes back hundreds of years; and most people—including, alas, many politicians and electoral system designers—are utterly ignorant of it. This book would be a good place to start. Brams (a professor at New York University) has been known for many years as a quirky but heavyweight mathematical political scientist. With colleagues, he has pioneered two main areas. One is approval voting; the other is fair division. He brings them together in *Mathematics and Democracy*, which chains together papers written with several coauthors but has more unity than most such collections.

The world of social choice has been divided for 200 years between the Condorcet and Borda principles, named after their proponents, who were both active in the French Academy of Sciences just before the Revolution. These principles would have led to elections of different academicians—something academicians care about. By the Condorcet principle, we should choose the candidate who beats all others in exhaustive pairwise comparisons. The Borda principle chooses the candidate who on average scores highest. Both criteria sound reasonable, but they may yield different rankings and a Condorcet winner may not exist. (In that case, no matter which candidate is ranked highest, another would have won a simple majority vote against that candidate.)

**Mathematics and Democracy**
Designing Better Voting and Fair-Division Procedures
*by Steven J. Brams*
Princeton University Press, Princeton, NJ, 2008. 389 pp. Paper, $27.95, £16.95. ISBN 9780691133218.

The Condorcet and Borda rules ask each voter to supply a full ranking (of preference or indifference) among all the candidates. So do proportional representation electoral systems. Approval voting asks for less. With it, each voter partitions the set of candidates into "approved" and "not approved" groups. The candidate(s) with the most approvals is (are) elected. Approval voting may be used to fill one or more seats. It has been adopted, at Brams's urging, by several professional societies in mathematics and statistics—but not by the American Political Science Association.

Approval voting does not throw away as much information as the U.S., Canadian, or British electoral systems, which merely ask voters to select one winner and elect the modal choice. (The United States adds the distorting mirror of the Electoral College for the presidency.) But it uses less information than either Condorcet or Borda. So why has it any claim?

Like Borda, it may promote broadly acceptable candidates against those intensely liked by some and intensely disliked by others. However, Borda is flagrantly manipulable (its inventor said "my scheme is only for honest men"), and approval voting is not. In addition, approval voting is likely to choose a Condorcet winner if one exists.

However, approval voting is not for every election. As Brams admits in a footnote, something like it was initially used under the U.S. Constitution to select both the president and vice president. In 1800, after extensive manipulation by sophisticated voters, it elected the very odd couple of Thomas Jefferson and Aaron Burr. In 1804, Burr became the only serving vice president before Dick Cheney to shoot another politician (Alexander Hamilton, who died of his wounds). The same year, the Twelfth Amendment abolished the approval voting–like procedure and substituted the one still used.

The book explores several contexts in which approval voting and its cousins may be useful. It is safe in scientific societies but may lead to odd results in mass elections unless designed very carefully. Mathematically (but not politically) simpler steps like abolishing the Electoral College should probably come first.

Fair division starts with the famous cake-cutting protocol: you cut, I choose. For two quarreling siblings, this produces an envy-free distribution. For more than two parties, the math is surprisingly difficult. Brams has contributed to the underlying mathematical analyses; in the book, he discusses several practical applications. One is to allocate portfolios (ministries) in a coalition government. This is required in Northern Ireland, where the designers of the constitution assumed that the parties would always quarrel, as they have been quarreling since about 1641. In Northern Ireland, parties choose portfolios in an order determined by the number of seats they hold. There are two main algorithms. The Jefferson rule (yes, that Jefferson) weights the outcome in favor of large parties. The (Daniel) Webster rule is unbiased between large and small. Northern Ireland uses Jefferson. Probably almost nobody there knows that it is the Jefferson

The reviewer is in the Department of Politics and International Relations and at Nuffield College, Oxford OX1 1NF, UK. E-mail: iain.mclean@nuffield.ox.ac.uk

rule. The first and deputy first ministers of Northern Ireland, among others, should read Brams's book.

King Solomon introduced game theory to dividing indivisible babies. Brams has developed it. Another practical application is to dividing assets after a divorce (of people, companies, or Czechoslovakia). In this case, the goods are often heterogeneous. One party values the sports car more than the other, who values the garden more than the first. For both heterogeneous and homogeneous goods, Brams has proposed practical algorithms, which are available to divorce lawyers and the Middle East Quartet.

The image on the cover of *Mathematics and Democracy* shows four people pulling on two ropes. If they all pull, the knot will jam. The book's contents show, on the contrary, that sometimes mathematics and game theory can unjam the problems of voting.

10.1126/science.1165974

POLITICAL SCIENCE

# Elective Inequality

**Robert Grafstein**

In the 1960s, George Wallace inveighed against both the Democrats and the Republicans, declaring "there ain't a dime's worth of difference between them." Although a dime is worth a lot less now, Wallace's charge still resonates. Ralph Nader's similar message, for example, may have cost Al Gore the presidency in 2000. In *Unequal Democracy*, Larry Bartels (a distinguished political scientist at Princeton University) forcefully argues that, in fact, many dimes separate the Democrats and Republicans: Democrats substantially reduce income inequality, and Republicans substantially increase it. Put another way, inequality in the United States is not merely an economic phenomenon but a political-economic phenomenon.

Given that a majority of the American electorate have below-average incomes, why is this inequality tolerated? Part of the answer, according to Bartels, is that the association between Democrats and civil rights realigned the South. More than racial politics, however, the public's ignorance and myopia are key ingredients in Republican ballot box success. Democracy is working poorly in the United States not only, Bartels argues, because Republicans work against the material interests of a majority of the voters and political elites are more responsive to higher-income groups but also because the majority is complicit in its own political fleecing.

A short review cannot convey the rich variety of arguments and data Bartels deploys in making his case. Some of his analysis focuses on broadly characterized partisan differences, some on high-profile examples such as the politics of the minimum wage and the estate tax. He will have done a considerable service if the next time we start thinking about economics we also think about politics.

**Unequal Democracy**
The Political Economy of the New Gilded Age
*by Larry M. Bartels*
Russell Sage Foundation, New York, and Princeton University Press, Princeton, NJ, 2008. 341 pp. $29.95, £17.95. ISBN 9780691136639.

But we should not stop thinking about economics. What is the mechanism by which the parties affect inequality? Bartels, as he acknowledges, does not fully explore this important and difficult question. He does argue that the parties have an impact on after-tax income distributions and the real value of the minimum wage. His key systematic explanation for pre-tax differences is the idea that Democrats are more likely to favor growth at the expense of inflation, and growth has the greatest proportional impact on those at the bottom of the economic ladder.

Governments stimulate growth through monetary and fiscal policy. There is widespread agreement that monetary policy can improve growth only in the short run. Persistent use of this lever will be ineffective or worse. Long-run economic growth is determined by productivity, so economic policies having an impact during the life of an administration will mostly produce fluctuations around the overall trend in growth. True, Democrats may promote higher productivity growth with education spending (but maybe not policy), investment in research, and spending on infrastructure, just as Republican tax policy may improve long-run growth with a positive impact not necessarily reflected in income distribution tables. But it is an open question whether these economic results register within the life of the responsible administration, which is essentially where Bartels's political accounting focuses.

A difficulty with this part of Bartels's argument, then, is that too often it amounts to atheoretical political accounting, albeit accounting buttressed with sophisticated and extensive statistical analysis. Thus, he calculates that there is an extremely small probability (0.006) of getting by chance the United States' historical pattern—four out of five Democratic administrations with decreased inequality, six out of six Republican administrations with increased inequality. But even if voters use his particular statistical approach, they would be mistaken to infer that the conditional probability of reduced inequality given a Democrat is correspondingly high. More important, the underlying statistical model is off-base. Although inequality can be mitigated, the model seems to imply that if the United States consistently elected Democrats, it would consistently have above-trend growth and never-ending reductions in inequality (an idea implicitly tempered by empirical estimates Bartels offers elsewhere in the book).

Bartels tries to discredit the idea that partisan effects are deviations from trend and thereby tries to downplay the role of economic interactions across administrations. He does so by claiming that Democrats and Republicans are not elected as antidotes to one another, because changes in the direction of inequality are smaller after the White House changes hands. But surely the degree of inequality is not chosen unilaterally: reversals are conditioned on the required amount of adjustment. Inequality reduction under Johnson was large, for instance, but the succeeding Nixon administration faced the inflationary consequences. Indeed, some of the literature Bartels cites (in his discussion of macroeconomic performance and income growth) actually argues that Democratic economic "success" hinges on the existence of a viable Republican opposition.

In any case, myopia and ignorance are not particularly deep explanations for the electorate's willingness to vote against its apparent economic interest. And sometimes the ignorance charge boomerangs. For example, pace Bartels, the estate tax does represent double taxation to the extent that after-tax income originally funded the investments making up the relevant estates. In further defense of voters, Bartels shows that social issues do not create as strong a headwind against class-based voting as is often assumed and that lower-income voters do tend to vote Democratic while upper-income voters do tend to vote Republican. *Unequal Democracy* offers an important case for why this might be.

10.1126/science.1166147

The reviewer is at the Department of Political Science, Baldwin Hall, University of Georgia, Athens, GA 30602, USA. E-mail: bobgraf@uga.edu

PHYSICS

# PhET: Simulations That Enhance Learning

A library of interactive computer simulations aids physics instruction worldwide.

Carl E. Wieman,[1] Wendy K. Adams,[2]* Katherine K. Perkins[2]

Research on learning shows that students learn better when they construct their own understanding of scientific ideas within the framework of their existing knowledge (*1*). To accomplish this process, students must be motivated to actively engage with the content and must be able to learn from that engagement. Interactive computer simulations can meet both of these needs. A growing body of research analyzes their design and use (*2*, *3*). Here, we summarize some of the research of the Physics Education Technology (PhET) project, particularly that related to simulations and student motivation.

We find that an important element of educationally effective simulations is that students view these simulations much as scientists view their research experiments (*3*). The scientist approaches research as an enjoyable opportunity to explore basic concepts, as well as to challenge, correct, and add to his or her understanding of how the world works. Similarly, the student usually finds exploring the simulations fun and, through this exploration, discovers new ideas about the science. A well-designed simulation focuses the student's attention on the basic scientific concepts. When something unexpected happens, the student questions her understanding and changes parameters in the simulation to explore and improve her understanding—approaches similar to those taken by a scientist working with an experiment. This behavior is in contrast to the way students approach hands-on experiments typically used in classes. Students often think that their goal with such experiments is to reproduce a preordained result as fast as possible, without making a mistake.

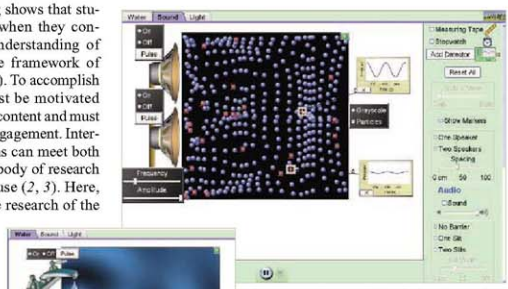


**"Wave Interference" simulation.** The student can investigate water waves (inset), sound waves (panel shown), and light waves.

Many factors of simulations contribute to this contrast. Identifying these factors is important for effective design and use of educational simulations and could help improve typical in-class experiments.

The PhET project (http://phet.colorado.edu) has developed more than 80 interactive simulations. These cover various topics in physics and real-world applications, such as the greenhouse effect and lasers. There are 16 simulations on chemistry topics, as well as several simulations for math, biology, and earth science. PhET simulations run through standard Web browsers and they can be integrated into a lecture, used with laboratories or as homework assignments, or used as informal resources. A PhET simulation requires several months to create, has 10,000 to 20,000 lines of code, and is tested through a series of student interviews. These simulations are used worldwide and at all levels—from grade school through upper-level university courses.

The "Wave Interference" simulation (see figure above) illustrates common PhET simulation features: (i) familiar elements (audio speakers and faucets) to build real-world connections; (ii) visual representations to show the invisible (the motion of air molecules in a sound wave); (iii) multiple representations to support deeper understanding (pressure differences visualized by density of air molecules, by light and dark shading on the gray-scale view, and by the pressure versus time graph); (iv) multiple directly manipulated variables (sliders controlling frequency and amplitude of the wave, as well as choice of number and spacing of the sources); (v) instruments for quantitative measurements and analysis (measuring tape, clock, and pressure meter); (vi) animated graphics tested to ensure correct interpretation; and (vii) distortion and simplification of reality to enhance educational effectiveness.

In PhET simulations, the visual display and direct interaction help answer students' questions and develop their understanding. Animated graphics are used to convey how scientists visualize certain phenomena such as electrons, fields, and graphs (see figure, page 683). Interacting with the simulation helps users develop their own mental models and understanding of the science. This is particularly helpful for students of quantum mechanics (*4*).

Research by the PhET project on design and use of simulations in a variety of educational settings (*5*) generated the following findings. Students doing a 2-hour exercise using the "Circuit Construction Kit" simulation in a one-semester course demonstrated higher mastery of the concepts of current and voltage on the final exam than students who did a parallel laboratory exercise with real electrical equipment (*6*). In a quantum mechanics course using a curriculum based on the "Photoelectric Effect" simulation, ~80% of the students demonstrated mastery of the concepts, whereas only 20% did so in a course using traditional instruction (*4*). When used as a lecture demonstration, the "Wave on a String" simulation resulted in

[1]Science Education Initiative and Department of Physics & Astronomy, University of British Columbia, Vancouver, BC V6T1Z3, Canada. [2]Department of Physics, University of Colorado, Boulder, CO 80309, USA.

*Author for correspondence. E-mail: wendy.adams@colorado.edu

greater conceptual learning than did the standard demonstration (*2*).

We have also conducted more than 250 interviews of individual students using PhET simulations in a think-aloud format. These interviews reveal how and why students interact with simulations and how this interaction leads to learning (*7, 8*). First, students find the simulations to be fun and intellectually engaging. Students (and teachers) will spontaneously play for hours with some simulations in educationally productive ways. We have identified a number of characteristics that make a simulation this engaging, many of which are what make video games engaging (*9*). These include (i) dynamic visual environments that are directly controlled by the user, (ii) challenges that are neither too hard nor too easy, and (iii) enough visual complexity to create curiosity without being overwhelming. Items (ii) and (iii) are best developed through iteration and testing with students.

We find that students are not able to make sense of the science in the simulation just from watching. They must interact actively with the simulation. Most of the learning occurs when the student is asking herself questions that guide her exploration of the simulation and her discovery of the answers. When students engage in such self-driven exploration, they learn better. For example, nonscience students with no prior knowledge of physics are able to provide quite good explanations of an electromagnetic wave after less than an hour playing with the "Radio Waves" simulation. (Even physics majors have a hard time explaining electromagnetic waves after a year of physics.)

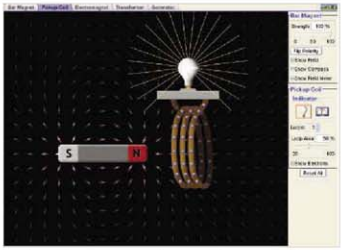


**Faraday Laboratory.** In a series of panels, students explore bar magnets and electromagnets, induced currents, transformers, and, finally, hydroelectric power generation.

This sort of self-driven exploration is very similar to what a scientist does with an experiment. It is the students' perceptions of the simulations that encourage them to explore in a similar manner. Students have little fear of breaking the simulations or hurting themselves, and they trust the simulations to be correct. Some learning goals are not addressed through the simulations, such as operating complex laboratory equipment (*3*).

In the study comparing the use of "Circuit Construction Kit" with equivalent real equipment (*5*), students were observed to do more spontaneous experiments with the simulation than with the corresponding real electrical equipment. Groups using the real equipment frequently stopped to ask questions of the Teaching Assistant (TA) that indicated concerns over hurting themselves or breaking the equipment. The simulation groups rarely asked questions of the TA and were constantly discussing within their peer groups and trying various circuit configurations to test their ideas. In another study, we used the simulations "Moving Man," "Projectile Motion," and "Energy Skate Park" to supplement the use of laboratory equipment. Students expressed a strong preference for simulations over the real equipment. They repeatedly commented that it was easier to see what was happening with the simulations and that they were more fun than the real equipment. In contrast, unexpected results with the real equipment were commonly blamed on human error or defective equipment, and there was very little exploration. We heard numerous comments about how it was nice that the simulations were always correct and they (the students) could not break them, as they could the real equipment (*10*).

As scientists, we perceive our experiments through an "expert filter" arising from our extensive experience and knowledge, and this perception allows us to see our experiment much the way these students perceive PhET simulations. As scientists, we recognize the important aspects of the apparatus and ignore the trivial, so it is neither overwhelmingly complex nor frightening. We perceive challenges that engage us to carry out exploration and discovery.

A good simulation provides the student with the equivalent of training wheels on a bicycle, effectively substituting the constraints and display of the simulation for expertise. This support allows students to carry out exploration and learning that is cognitively similar to that of a scientist, something they do not have the experience or motivation to do with most real equipment in physics. With real equipment, the numerous complex unknowns are mysterious, uncontrollable, and threatening. Without an "expert filter," every detail is seen as equally important. For example, we have seen students in electric circuit laboratories spend considerable time worrying about the significance of the (irrelevant) color of plastic insulation on the wires. We also see in simulation testing how rapidly expert-like understanding can change a person's perception. With the "Radio Waves" simulation, if students are initially faced with the full-field view, they are overwhelmed. They find the simulation unpleasant, and they are reluctant to interact with it. However, if a student begins with the standard simple start-up panel, they will readily explore and develop an understanding so that, when they later encounter the full-field view, they understand it and actually prefer it. Simulations can therefore be designed to introduce students to increasing levels of complexity and messiness, which may be an effective and engaging way to prepare students for real scientific research.

Carefully developed and tested educational simulations can be engaging and effective. They encourage authentic and productive exploration of scientific phenomena, and provide credible animated models that usefully guide students' thinking.

**References and Notes:**

1. J. Bransford, A. Brown, R. Cocking, Eds., *How People Learn: Brain, Mind, Experience, and School* (National Academy Press, Washington, DC, 2000).
2. K. K. Perkins *et al.*, *Phys. Teach.* **44**, 18 (2006).
3. See supporting material available on *Science* Online for additional information.
4. S. B. McKagan *et al.*, *Am. J. Phys.* **76**, 406 (2008).
5. All research papers by the PhET team can be found at: http://phet.colorado.edu/new/research/index.php.
6. N. D. Finkelstein *et al.*, *Phys. Rev. Spec. Top. Phys. Educ. Res.* **1**, 010103 (2005).
7. W. K. Adams *et al.*, *J. Interact. Learn. Res.* **19**, 397 (2008).
8. W. K. Adams *et al.*, *J. Interact. Learn. Res.* **19**, 551 (2008).
9. T. Malone, *Cogn. Sci.* **5**, 333 (1981).
10. Student perception of the accuracy of simulations is a complex topic that is discussed in the supporting material.
11. The PhET work has been supported by the NSF, the William and Flora Hewlett Foundation, Microsoft, the University of Colorado, the Kavli Operating Institute, and C. Wieman and S. Gilbert. This work represents the valuable contributions of the entire PhET Team.

**Supporting Online Material**
www.sciencemag.org/cgi/content/full/322/5902/682/DC1

10.1126/science.1161948

UNDERGRADUATE RESEARCH

# Genomics Education Partnership

D. Lopatto,[1]* C. Alvarez,[2] D. Barnard,[3] C. Chandrasekaran,[4] H.-M. Chung,[5] C. Du,[6] T. Eckdahl,[7] A. L. Goodman,[8] C. Hauser,[9] C. J. Jones,[10] O. R. Kopp,[11] G. A. Kuleck,[12] G. McNeil,[13] R. Morris,[14] J. L. Myka,[15] A. Nagengast,[14] P. J. Overvoorde,[16] J. L. Poet,[17] K. Reed,[18] G. Regisford,[19] D. Revie,[20] A. Rosenwald,[21] K. Saville,[22] M. Shaw,[23] G. R. Skuse,[24] C. Smith,[25] M. Smith,[26] M. Spratt,[27] J. Stamm,[28] J. S. Thompson,[29] B. A. Wilson,[30] C. Witkowski,[31] J. Youngblom,[32] W. Leung,[33] C. D. Shaffer,[33] J. Buhler,[33] E. Mardis,[33] S. C. R. Elgin[33]*

The Genomics Education Partnership offers an inclusive model for undergraduate research experiences, with students pooling their work to contribute to international databases.

Teaching students to think as scientists do has traditionally been accomplished by immersing undergraduates in a full-time summer research program, an experience that enhances professional development and provides career clarification (*1*, *2*). We believe that conducting research is the best way to learn how knowledge is defined and created in a field. Furthermore, students acquire a deeper understanding of fundamental concepts as they apply what they have learned to accomplish defined research goals. Undergraduate research experiences can sustain student interest in a science career, providing an opportunity to work collaboratively with colleagues while making novel contributions to the community (*1*).

Most undergraduates begin their research with mentoring by a faculty member, graduate student, or postdoctoral student (postdoc) during a summer spent in the laboratory. This approach, while usually successful, excludes many students who do not have the summer free or funded. Other barriers include limited funding and facilities, as well as a lack of experienced mentors (*1*, *3*). Thus, we must incorporate student research experiences into our regular academic-year curriculum to make such experiences more broadly available. Our experiences as founding members of the Genomics Education Partnership (GEP) encourage us to believe that a curriculum in genomics can train students to think like scientists (*4*).

### Genomics for Undergraduates

Genomics is an attractive area for student-scientist partnerships. First, genomics represents an exciting advance in the life sciences. With genomics, we can analyze not only one gene, but many genes, and can address questions ranging from patterns of gene expression to evolution of a species. Second, the teaching and research materials can be obtained for little or no cost: DNA sequences and microarray results are freely available on the Web (*5*, *6*). Third, genomics research projects can range from simple to complex, which allows engaging in them to match a variety of academic calendars.

Mindful of these advantages, a number of faculty groups and institutions have launched projects to bring genomics into the undergraduate curriculum. These range from primarily utilizing computer-based resources for annotation and analysis to having a major wet-laboratory focus (*7*, *8*). Two major projects engage students in analyzing genomes from phage and from bacteria or archaea (*9*, *10*) (see supporting online text). GEP was formed in 2006 as a collaboration between faculty from various institutions and the Biology Department and Genome Sequencing Center at Washington University in Saint Louis. The group currently consists of over 40 faculty members who teach undergraduate courses in biology, statistics, mathematics, and computer science at a variety of institutions, including research universities, master's degree–granting comprehensive universities, and private baccalaureate-granting colleges (*4*). The goal of the GEP is to provide opportunities for undergraduate students to participate in original research

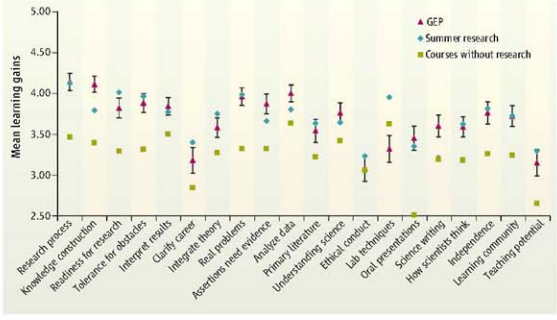


**Student ratings of learning gains.** Mean learning gains for common survey items on the SURE, CURE, and GEP surveys. The SURE survey data represent 1973 undergraduate summer research experiences ("Summer research" data points). The CURE survey data represent 560 student surveys from science courses that did not include a research-like experience "Courses without research" data points). The GEP survey data represent 308 students in GEP courses (SOM). Error bars represent 2 SEM.

[1]Grinnell College, Grinnell, IA. [2]Longwood University, Farmville, VA. [3]Worcester State College, Worcester MA. [4]Texas Wesleyan University, Fort Worth, TX. [5]University of West Florida, Pensacola, FL. [6]Montclair State University, Montclair, NJ. [7]Missouri Western State University, St. Joseph, MO. [8]California Polytechnic State University–San Luis Obispo, CA. [9]St. Edward's University, Austin, TX. [10]Moravian College, Bethlehem, PA. [11]Utah Valley University, Orem UT. [12]Loyola Marymount University, Los Angeles, CA. [13]York College, The City University of New York, Jamaica, NY. [14]Widener University, Chester, PA. [15]Galen College of Nursing, Cincinnati, OH. [16]Macalester College, St. Paul, MN. [17]Missouri Western State University, St. Joseph, MO. [18]Austin College, Sherman, TX. [19]Prairie View A&M University, Prairie View, TX. [20]California Lutheran University, Thousand Oaks, CA. [21]Georgetown University, Washington, DC. [22]Albion College, Albion, MI. [23]New Mexico Highlands University, Las Vegas, NM. [24]Rochester Institute of Technology, Rochester, NY. [25]San Francisco State University, San Francisco, CA. [26]North Carolina Agricultural & Technical State University, Greensboro, NC. [27]William Woods University, Fulton, MO. [28]University of Evansville, Evansville, IN. [29]Denison University, Granville, OH. [30]Jackson State University, Jackson, MS. [31]Missouri State University, Springfield, MO. [32]California State University–Stanislaus, Turlock, CA. [33]Washington University in St. Louis, St. Louis, MO. (For complete addresses, see supporting online material.)

*To whom correspondence should be addressed. E-mail: lopatto@grinnell.edu (D.L.); selgin@biology.wustl.edu (S.C.R.E.).

experiences within the framework of course curricula. The GEP pools student efforts across institutions to improve DNA sequence quality and to generate hand-curated gene models. Developing a coordinated research effort allows us to tackle large projects together and to make work in eukaryotes accessible. The first project undertaken by GEP members was sequence improvement and annotation of the dot chromosomes of several *Drosophila* species. The distal 1.2 megabases of this unusual small chromosome are of interest because the domain appears to be heterochromatic, a packaging state normally associated with gene silencing, but it has the same gene density of more transcriptionally active euchromatic regions (*11*). Because of the high density of repetitious elements, improving the sequence to verify the assembly, close gaps, and raise the quality estimate to 1 error in 1000 bases provides greater credibility to the analysis. Annotation then follows, with students generating the most plausible gene models based on available evidence, and then defending their models (*4*). (See supporting online text for a more detailed description.)

Economies in mentoring can be realized because the students are all using similar tools and strategies as they work independently on a specific region. The amount of sequence assigned to a student can be adjusted according to the available time. During a typical semester laboratory course, one student can improve and annotate 40 kb of *Drosophila* DNA. By organizing the raw data into 40-kb packages that can be "claimed" from a Web site, the GEP can undertake fairly large projects for sequence improvement and annotation.

Participating course instructors integrate this research into their courses using a variety of formats. Results from the individual students are then checked and pooled at Washington University to create the final dot chromosome assembly that is used to generate a variety of statistics documenting the nature of the chromosome and the genes present. Comparing dot chromosomes of several *Drosophila* species allows us to address issues of chromosome evolution.

### Assessment and Sustainability

Students know that their work will be used for a scientific publication and deposited in a public database for other scientists to build from. Sequence data are submitted to GenBank, and annotation results to FlyBase. One scientific paper has been published based on student work (*12*); contributing students are coauthors. We anticipate an accumulation of publications and database contributions with time. The significance of this is illustrated by some of the comments from students and teaching assistants (TAs) (table S1).

Students completed a postcourse survey of their perceptions. This survey, a variation of the Classroom Undergraduate Research Experiences survey (CURE) (*4*), parallels one evaluating summer undergraduate research experiences (SURE) (*1*, *13*). GEP students report learning and professional gains similar to those reported by students who have spent a summer in the laboratory (see the figure on page 684 and table S2). High ratings from GEP students on "knowledge construction," "assertions need evidence," "analyze data," and "science writing" are similar to other research-like experiences (*14*, *15*). From the perspective of students, the GEP course experience is more like summer research than like a standard science course without research. As the GEP matures, more assessment protocols are being added. Currently, the faculty are devising content tests for annotation and finishing. The GCAT has reported that students in that program make significant gains in comprehension of topics in functional genomics and show increased interest in research (*16*).

Research opportunities in genomics are likely to increase. There are now 11 sequenced *Drosophila* species in addition to *D. melanogaster*, the commonly used laboratory species (*17*). By choosing regions of biological interest, so that the results contribute to research papers, as well as to the databases, much can be accomplished by a student-scientist partnership that otherwise might be difficult to attain.

We invite scientists to consider what might be accomplished by a distributed community of undergraduate scientists collaborating on a particular set of genes or genomes. At present, the GEP has over 40 members, and membership is growing (*4*). GEP faculty and their (usually undergraduate) TAs come to Washington University for a 1-week workshop to learn the relevant software and to discuss pedagogical issues. As the program develops at an institution, the previous year's students can be recruited as the next year's TAs. This strategy fosters sustainability and allows class size to grow. Efficient implementation favors one experienced person (the TA or faculty member) for every six or seven novices to provide support for students learning to use software and to evaluate data. Although most institutions already maintain computer laboratories, which minimizes start-up costs, training for faculty and TAs is essential. Faculty and project leaders must agree on a common rubric for sequence improvement and annotation goals and on a common reporting mechanism. Good on-site information technology support is important, but the basic strategy is very portable. The opportunity to teach about genes, genomes, and the flow of biological information using this hands-on approach provides entry into a rich domain of data. We have found that involving undergraduates in a genomics research project is a rewarding way for faculty to teach and for undergraduates to learn.

### References and Notes


1. D. Lopatto, *CBE Life Sci. Educ.* **6**, 297 (2007).
2. E. Seymour *et al.*, *Sci. Educ.* **88**, 493 (2004).
3. S. H. Russell, in *Creating Effective Undergraduate Research Programs in Science*, R. Taraban, R. L. Blandon, Eds. (Teachers College Press, New York, 2008), pp. 53–80.
4. Genomics Education Partnership (http://gep.wustl.edu). This site includes the list of member institutions and a facsimile of the GEP assessment instrument.
5. Summary of Principles Agreed at the First International Strategy Meeting on Human Genome Sequencing, www.ornl.gov/sci/techresources/Human_Genome/research/bermuda.shtml#1.
6. *Sharing Data from Large-Scale Biological Research Projects: A System of Tripartite Responsibility*, report of a meeting organized by the Wellcome Trust, Fort Lauderdale, FL, 14 and 15 January 2003; www.genome.gov/Pages/Research/WellcomeReport0303.pdf.
7. For examples, see this reference and (*8*); *Teaching Big Science at Small Colleges*, http://serc.carleton.edu/genomics/index.html.
8. *Genome Consortium for Active Teaching* (GCAT) introduces students to microarray experiments; www.bio.davidson.edu/projects/gcat/gcat.html.
9. The Science Education Alliance of HHMI works on phage, www.hhmi.org/grants/sea/.
10. The DOE Joint Genome Institute sponsors work on bacteria, www.jgi.doe.gov/education/genomeannotation.html.
11. N. C. Riddle, S. C. R. Elgin, *Chromosome Res.* **14**, 405 (2006).
12. E. E. Slawson *et al.*, *Genome Biol.* **7**, R15 (2006).
13. D. Lopatto, in *Creating Effective Undergraduate Research Programs in Science*, R. Taraban, R. L. Blandon, Eds. (Teachers College Press, New York, 2008), pp. 112–132.
14. L. A. Denofrio *et al.*, *Science* **318**, 1872 (2007).
15. C. Trosset *et al.*, in *Creating Effective Undergraduate Research Programs in Science*, R. Taraban, R. L. Blandon, Eds. (Teachers College Press, New York, 2008), pp. 33–49.
16. A. M. Campbell *et al.*, *CBE-Life Sci. Educ.* **6**, 109 (2007).
17. A. Stark *et al.*, *Nature* 450, 219 (2007).


18. We thank F. Thuet (Washington University) for management of the GEP CURE assessment Web site; L. Crosby and W. Gelbart of FlyBase (Harvard University); the staff of the Washington University Genome Sequencing Center for assistance; and the Howard Hughes Medical Institute for financial support (grant 52005790 to S.C.R.E., HHMI Professor).


Supporting Online Material
www.sciencemag.org/cgi/content/full/322/5902/684/DC1

10.1126/science.1165351

GEOPHYSICS

# Assessing Ground Shaking

Monitoring and modeling the complex interaction of seismic waves with soils is critical for mitigating earthquake risks.

Daniel R. H. O'Connell

When engineers design structures to withstand earthquakes, they rely on ground-shaking prediction models (*1*). These models must account for the different ways in which the seismic energy radiated from the rupture of a fault propagates through the subsurface rock and the overriding soil (see the figure, panel A). These models are based on ground-shaking data recorded at surface and at depth in underlying rock and soil (*2*–*5*). Such data are collected by the Kyoshin Network, or Kik-net, in Japan (*6*). On page 727 of this issue, Aoi *et al.* (*7*) analyze ground motions recorded by Kik-net during the 2008 magnitude 6.9 Iwate-Miyagi earthquake. One soil-surface site recorded a vertical acceleration of 3.8*g* (gravity), which was unprecedented both in its magnitude and because the peak vertical acceleration vastly exceeded the peak horizontal acceleration. Aoi *et al.* present a plausible mechanism that accounts for this exceptional behavior that illustrates some of the outstanding challenges in modeling surface motion caused by earthquakes.

Seismic wave propagation is complex because although rock layers respond linearly to changes in input shaking amplitudes, shallow soils can nonlinearly amplify seismic waves as a function of seismic wave amplitude, particularly near the surface, and typically reduce the amplitudes of high-frequency accelerations (*2*, *3*, *8*, *9*).

Ground-motion observations obtained solely at the surface do not uniquely constrain models of surface motion (*2*–*5*), so specialized recording networks have been created. The 660 stations of Kik-net record accelerations in three orthogonal directions, both at the surface and in boreholes at the depths required to reach competent rock. These data generally show that soil acts as a damper that reduces amplification of horizontal and vertical motions. Laboratory testing of most soils shows that, at the low confining pressures typical of shallow soils, increasing shear strains will decrease soil shear stiffness and increase anelastic damping of seismic waves (*10*–*12*). What this means in the field is that at many soil sites the ground does not shake as hard or as long during large earthquakes as would be suggested by ground shaking produced by small earthquakes (*3*, *8*, *9*, *13*).

Exceptions are known, however. Fluid-saturated soil can exhibit high-frequency horizontal acceleration spikes (0.4 to 0.8*g*), associated with transient periods when the soil dilates and pore pressure decreases, that can increase ground-shaking durations and high-frequency amplification (*2*, *14*). The horizontal borehole and surface motions reported in Aoi *et al.* are generally consistent with the soil reducing surface horizontal accelerations at high frequencies, as is widely observed at soil sites (*3*, *8*, *9*, *13*). However, the surface vertical peak acceleration exceeded 3.8*g*, exceeding the maximum expected amplification, based on the site velocity profile between the borehole and the surface accelerometers, and known linear or nonlinear theories of soil behavior. Further, the largest upward accelerations at the surface were more than twice that of the largest downward accelerations.

Aoi *et al.* propose a conceptual model for this asymmetry. Their model uses a loose soil with nearly zero confining pressure near the surface. The soil particles that were transported upward separate under large downward acceleration, and in this quasi free-fall state, the accelerations at the surface only modestly exceed gravity. When the particles rebound, large upward accelerations compact the soil and produce much larger upward accelerations. Aoi *et al.* report three cases of these anomalous large vertical acceleration amplifications in a search of 200,000 strong motion recordings. At least one example from a site in North America may also exist (*15*). Another candidate physical mechanism that could produce these vertical accelerations would be the development of transient force chains in a granular material, which are regions that temporarily become stiffer, in response to strong horizontal shear strains (*16*, *17*). A quantitative physical understanding of these anomalous large vertical accelerations will require more detailed investigations of the sites' material properties to determine the conditions and processes that produce them.

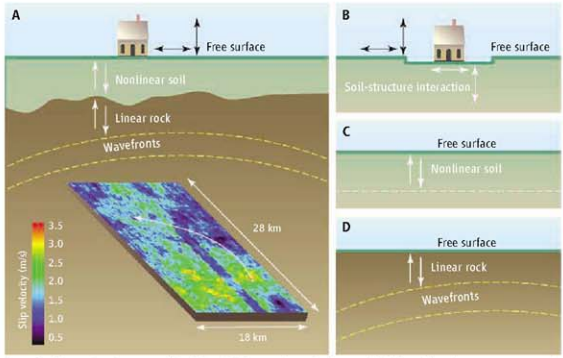


**From fault rupture to ground shaking. (A)** A complex seismic wave field is radiated as rupture proceeds across a fault. At the bottom, the color-coded slip-velocity distribution (in meters per second) estimated for the 1994 moment magnitude 6.7 Northridge earthquake illustrates this complexity. Fault rupture began at the hypocenter (base of white arrow), and the white arrow points toward the last part of the fault to rupture. At the top, ground motions at the surface result from complex linear and nonlinear interactions between waves propagating upward from the fault, waves reflected downward from the surface, and waves scattered by heterogeneity within the crust. **(B to D)** The substructure approach used in engineering analyses of buildings is illustrated by three separate and isolated analyses, which can adequately approximate the actual ground shaking at the base of the structure if nonlinear soil amplification responses vary smoothly as a function of amplitude.

William Lettis & Associates, Inc., Golden, CO 80401, USA. E-mail: oconnell@lettis.com

These observations of nonlinear wave propagation need to be modeled successfully in order to have practical engineering implications. Currently, the integrated physical processes of earthquake rupture and wave propagation are separated into simpler substructure analyses. To make the computations feasible, empirical ground-motion prediction equations (*18*) or the large-scale physics of earthquake rupture and wave propagation are used to obtain linear free-surface ground shaking (*1*, *19*, *20*) that omits the soil component (see the figure, panel D). The linear ground motions are then used as inputs to calculate surface and embedded motions in a model that accounts for nonlinear soil responses (see the figure, panel C). Finally, the ground-motion outputs are used to conduct soil-structure interaction (SSI) analyses (*21*) that include both the foundation and the engineered structure (see the figure, panel B).

It is not clear that the anomalous large vertical accelerations observed by Aoi *et al.* could occur in the foundation of a structure at a site that has been compacted and had a foundation emplaced, particularly because large structures impose considerable confining pressures on a soil. Specifically, can these new large accelerations occur at the foundation level of buildings and critical structures?

Answers to this question will require a much larger-scale deployment of strong motion sensors at the foundation level of buildings. In this regard, the volunteer-based Quake-Catcher Network (QCN) links triaxial accelerometers internal to many laptops and low-cost USB-port accelerometers connected to desktops to a network of servers (*22*, *23*). The USB sensors are typically set to record up to 2*g*, but can record up to 6*g* with reduced resolution. Currently, the network has roughly 500 users globally, but within the next 6 to 9 months 1100 USB sensors will be installed in schools, firehouses, and community buildings. The QCN could record many thousands of ground motions at the foundation level of buildings from a single earthquake, vastly exceeding the scope of single-earthquake ground-motion recordings that have been obtained to date. The data obtained will provide valuable constraints on the practical limits on ground-shaking amplitudes imposed on buildings and critical structures, an issue that is currently far from resolved (*24*, *25*).

**References and Notes**


1. A. D. Frankel, *Science* **283**, 2032 (1999).
2. L. F. Bonilla *et al.*, *Bull. Seismol. Soc. Am.* **95**, 2373 (2005).
3. E. H. Field *et al.*, *J. Geophys. Res.* **103**, 26869 (1998).
4. D. R. H. O'Connell, *Science* **283**, 2045 (1999).
5. S. Hartzell *et al.*, *Bull. Seismol. Soc. Am.* **95**, 614 (2005).
6. H. Fujiwara *et al.*, *Technical Note of the National Research Institute for Earth Science and Disaster Prevention* **264**, 91 (2005).
7. S. Aoi, T. Kunugi, H. Fujiwara, *Science* **322**, 727 (2008).
8. H. B. Seed, I. M. Idriss, *Bull. Seismol. Soc. Am.* **60**, 125 (1970).
9. I. A. Beresnev *et al.*, *Bull. Seismol. Soc. Am.* **85**, 496 (1995).
10. B. O. Hardin, V. P. Drnevich, *J. Soil Mech. Found. Div. ASCE* **98**, 603 (1972).
11. B. O. Hardin, V. P. Drnevich, *J. Soil Mech. Found. Div. ASCE* **98**, 667 (1972).
12. M. Vucetic, *Can. Geotech. J.* **27**, 29 (1990).
13. I. A. Beresnev *et al.*, *Bull. Seismol. Soc. Am.* **92**, 3152 (2002).
14. S. Iai *et al.*, *Soils Found.* **35**, 115 (1995).
15. D. H. Weichert *et al.*, *Bull. Seismol. Soc. Am.* **76**, 1473 (1986).
16. D. Howell *et al.*, *Phys. Rev. Lett.* **82**, 5241 (1999).
17. Animations are available online at www.phy.duke.edu/~dhowell/research.html.
18. Next Generation of Ground-Motion Attenuation Models, *Earthquake Spectra* **24**, 1, (2008).
19. S. Hartzell *et al.*, *Bull. Seismol. Soc. Am.* **92**, 831 (2005).
20. Southern California Earthquake Center (SCEC) PetaSHA/PetaShake Project, http://scecdata.usc.edu/petasha.
21. C. B. Crouse, J. C. Ramirez, *Bull. Seismol. Soc. Am.* **923**, 546 (2003).
22. E. S. Cochran *et al.*, *SCEC Ann. Meet. Proc. Abs.* **18**, 85 (2008).
23. For more information on QCN, see qcn.stanford.edu.
24. T. C. Hanks *et al.*, in *Directions in Strong Motion Instrumentation*, P. Gülkan, J. G. Anderson, Eds., (Springer Netherlands, Dorcrecht, 2005), vol. 58, pp. 55–59.
25. 2008 SCEC Étreme Ground Motion Workshop http://scec.org/meetings/2008am/exgmworkshop.html


26. Research supported by USGS award no. 08HQGR0068.

10.1126/science.1166149


CLIMATE CHANGE

# Whither Hurricane Activity?


**Gabriel A. Vecchi,[1] Kyle L. Swanson,[2] Brian J. Soden[3]**



Alternative interpretations of the relationship between sea surface temperature and hurricane activity imply vastly different future Atlantic hurricane activity.


A key question in the study of near-term climate change is whether there is a causal connection between warming tropical sea surface temperatures (SSTs) and Atlantic hurricane activity (*1*–*3*). Such a connection would imply that the marked increase in Atlantic hurricane activity since the early 1990s is a harbinger of larger changes to come and that part of that increase could be attributed to human actions (*3*). However, the increase could also be a result of the warming of the Atlantic relative to other ocean basins (*4*), which is not expected to continue in the long term (*5*). On current evidence, can we decide which interpretation is likely to be correct?

To appreciate the problem, consider the observed relation between hurricane activity [power dissipation index (PDI)] (*6*) and SST in the main development region of Atlantic hurricanes (hereafter "absolute SST"). Between 1946 and 2007, this relation can be defined by a simple linear regression between the two quantities (see Supporting Online Material). This observed relation can be extrapolated into the 21st century using absolute SSTs calculated from global climate model projections (see the figure, top panel) (*7*). By 2100, the model projections' lower bound on 5-year averaged Atlantic hurricane activity is comparable to the PDI level of 2005, when four major hurricanes (sustained winds of over 100 knots) struck the continental United States, causing more than $100 billion in damage. The upper bound of the projected 5-year average exceeds 2005 levels by more than a factor of two. This is a sobering outlook that, combined with rising sea levels, would have dramatic implications for residents of regions impacted by Atlantic hurricanes.

However, there is an alternate future, equally consistent with observed links between SST and Atlantic hurricane activity. Observational relationships (*4*), theories that provide an upper limit to hurricane intensity (*5*), and high-resolution model studies (*8*) suggest that it is the SST in the tropical Atlantic main development region relative to the tropical mean SST that controls fluctuations in Atlantic hurricane activity. Between 1946 and 2007, this "relative SST" (see the figure, bottom panel) is as well correlated with Atlantic hurricane activity as the absolute SST. However, relative SST does not experience a substantial


[1]NOAA/Geophysical Fluid Dynamics Laboratory, Princeton, NJ 08542, USA. E-mail: gabriel.a.vecchi@noaa.gov [2]Atmospheric Sciences Group, Department of Mathematical Sciences, University of Wisconsin–Milwaukee, Milwaukee, WI 53201, USA. [3]Rosentiel School of Marine and Atmospheric Science, University of Miami, Miami, FL 33149, USA.

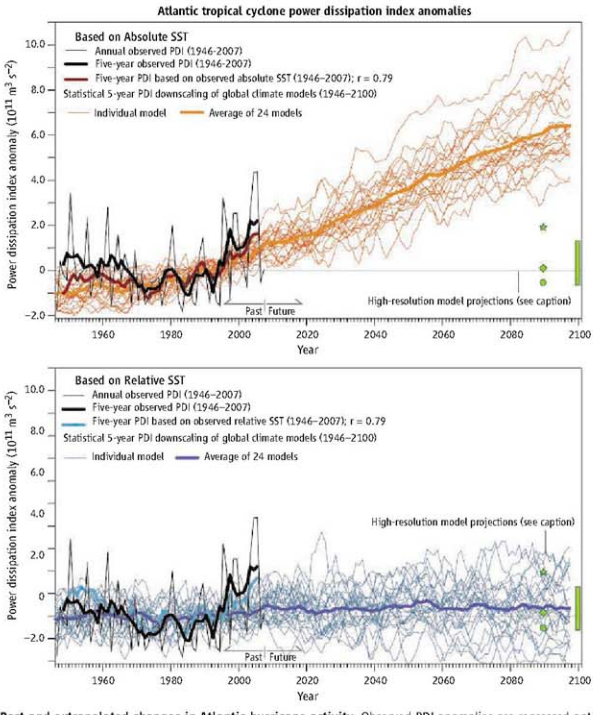


**Past and extrapolated changes in Atlantic hurricane activity.** Observed PDI anomalies are regressed onto observed absolute and relative SST over the period from 1946 to 2007, and these regression models are used to build estimates of PDI from output of global climate models for historical and future conditions. Anomalies are shown relative to the 1981 to 2000 average ($2.13 \times 10^{11}$ m$^3$ s$^{-2}$). The green bar denotes the approximate range of PDI anomaly predicted by the statistical/dynamical calculations of (*12*). The other green symbols denote the approximate values suggested by high-resolution dynamical models: circle (*8*), star (*13*), and diamond (*15*). SST indices are computed over the region 70°W-20°W, 7.5°N-22.5°N, and the zero-line indicates the average over the period from 1981 to 2000. See Supporting Online Material for details.

trend in 21st-century projections. Hence, a future where relative SST controls Atlantic hurricane activity is a future similar to the recent past, with periods of higher and lower hurricane activity relative to present-day conditions due to natural climate variability, but with little long-term trend.

From the perspective of correlation and inferred causality, this analysis suggests that we are presently at an impasse. Additional empirical studies are unlikely to resolve this conflict in the near future: Many years of data will be required to reject one hypothesis in favor of the other, and the climate model projections of hurricane activity using the two statistical models do not diverge completely until the mid-2020s. Thus, it is both necessary and desirable to appeal to nonempirical evidence to evaluate which future is more likely.

Physical arguments suggest that hurricane activity depends partly on atmospheric instability (*2*), which increases with local warming but is not determined by Atlantic SSTs alone (*5*). Warming of remote ocean basins warms the upper troposphere and stabilizes the atmosphere (*5*). Furthermore, relative Atlantic SST warming is associated with atmospheric circulation changes that make the environment more favorable to hurricane development and intensification (*9–11*).

Further evidence comes from high-resolution dynamical techniques that attempt to represent the finer spatial and temporal scales essential to hurricanes, which century-scale global climate models cannot capture due to computational constraints. High-resolution dynamical calculations under climate change scenarios (*8*, *12–14*) (green symbols in the figure) are consistent with the dominance of relative SSTs as a control on hurricane activity. Even the dynamical simulation showing the most marked increase in Atlantic hurricane activity under climate change (*13*) is within the projected range for relative SST but outside the projected range for absolute SST.

Whether the physical connections between hurricane activity and SST are more accurately captured by absolute or relative SST also has fundamental implications for our interpretation of the past. If the correlation of activity with absolute SST represents a causal relation, then at least part of the recent increase in activity in the Atlantic can be connected to tropical Atlantic warming driven by human-induced increases in greenhouse gases and, possibly, recent reductions in Atlantic aerosol loading (*3*, *15*, *16*). In contrast, if relative SST contains the causal link, an attribution of the recent increase in hurricane activity to human activities is not appropriate, because the recent changes in relative SST in the Atlantic are not yet distinct from natural climate variability.

We stand on the cusp of potentially large changes to Atlantic hurricane activity. The issue is not whether SST is a predictor of this activity but how it is a predictor. Given the evidence suggesting that relative SST controls hurricane activity, efforts to link changes in hurricane activity to absolute SST must not be based solely on statistical relationships but must also offer alternative theories and models that can be used to test the physical arguments underlying this premise. In either case, continuing to move beyond empirical statistical relationships into a fuller, dynamically based

understanding of the tropical atmosphere must be of the highest priority, including assessing and improving the quality of regional SST projections in global climate models.


**References and Notes**

1. C. D. Hoyos, P. A. Agudelo, P. J. Webster, J. A. Curry, *Science* **312**, 94 (2006).
2. K. Emanuel, *J. Climate* **20**, 5497 (2007).
3. U.S. Climate Change Science Program, *Weather and Climate Extremes in a Changing Climate*, T. R. Karl *et al.*, Eds. (Department of Commerce, NOAA's National Climatic Data Center, Washington, DC, 2008).
4. K. L. Swanson, *Geochem. Geophys. Geosys.* **9**, Q04V01; 10.1029/2007GC001844 (2008).
5. G. A. Vecchi, B. J. Soden, *Nature* **450**, 1066 (2007).
6. PDI is the cube of the instantaneous tropical cyclone wind speed integrated over the life of all storms in a given season; more intense and frequent basinwide hurricane activity lead to higher PDI values.
7. We use 24 different global climate models run in support of the Intergovernmental Panel on Climate Change Fourth Assessment Report (IPCC-AR4) (17). See Supporting Online Material for details.
8. T. R. Knutson *et al.*, *Nature Geosci.* **1**, 359 (2008).
9. R. Zhang, T. L. Delworth, *Geophys. Res. Lett.* **33**, L17712 (2006).
10. D. J. Vimont, J. P. Kossin, *Geophys. Res. Lett.* **34**, L07709 (2007).
11. M. Latif, N. Keenlyside, J. Bader, *Geophys. Res. Lett.* **34**, L01710 (2007).
12. K. A. Emanuel, R. Sundararajan, J. Williams, *Bull. Am. Met. Soc.* **89**, 347 (2008).
13. K. Oouchi *et al.*, *J. Met. Soc. Japan* **84**, 259 (2006).
14. L. Bengtsson *et al.*, *Tellus* **59A**, 539 (2007).
15. B. Santer *et al.*, *Proc. Natl. Acad. Sci. U.S.A.*; 10.1073/pnas.0602861103 (2008).
16. T. R. Knutson *et al.*, *J. Climate* **19**, 1624 (2006).
17. G. A. Meehl *et al.*, *Bull. Am. Meteorol. Soc.* **88**, 1549 (2007).



18. We are grateful for comments from T. Delworth, I. Held, S. Ilcane, A. Johansson, T. Knutson, D. E. Harrison, and M. Vecchi. This work was partly supported by NOAA/OGP.


**Supporting Online Material**

www.sciencemag.org/cgi/content/full/322/5902/687/DC1
Materials and Methods
SOM Text
Figs. S1 to S8
References

10.1126/science.1164396

MATERIALS SCIENCE

# Nanoscale Polymer Processing

The established rules for fabricating plastics now require a rethink as feature sizes of the products head toward the nanoscale.

**Christopher L. Soles[1] and Yifu Ding[2]**

It is difficult to find a manufactured object that does not contain at least some polymeric (plastic) components. This ubiquity reflects the ease with which polymers can be formed into arbitrary shapes through processes that induce flow of a viscous polymer melt into the cavity of a mold or die. The equations that quantify the rheological response of viscous polymer melts under large-scale deformations have been developed over the past 60 years, providing the paradigms by which forming processes are optimized to produce well-controlled, high-quality, robust polymeric parts (*1*). These paradigms, however, are poised to change as polymer processing approaches the nanoscale. On page 720 of this issue, Rowland *et al.* present evidence suggesting that the relationships that govern the viscous flow of polymers in highly confined geometries are dramatically different from those of the bulk (*2*).

Nanoimprint lithography (NIL) can be used to manufacture polymeric features with dimensions of 10 nm or smaller (*3*). The thermal embossing form of NIL relies on a melt squeeze-flow process to transform a smooth polymer film into a patterned surface. Nanoscale features that have been etched into silicon, quartz, or some other hard template material can be inexpensively replicated by stamping the template into a thin polymeric film. Even roll-to-roll NIL tools capable of continuous, high-throughput patterning are now available (*4*). However, optimizing such NIL processes will require knowledge of the rheological response of the polymer being squeezed into a nanoscale cavity, as well as the effect of this response on the properties of the imprinted structure (*5*).

The large-strain deformation properties of a polymer melt are dominated by the topological entanglement of the transient network established by the sea of interpenetrating polymer coils (see the figure). The volume pervaded by a single molecule (proportional to $R_g^3$, where $R_g$ is the radius of gyration of a single coil) is nearly an order of magnitude larger than the sum of the hard-core volumes of the atoms that constitute the macromolecular chain. The degree of interpenetration or entanglement between neighboring coils is determined by the pervaded volume of a single macromolecular coil and the packing density of the individual chain segments. The large-scale rheological response of a polymer melt is then determined by the response of this entangled network to an applied load. Both the pervaded volume and the extent of entanglement increase with molecular mass, thereby making the flow of the high-molecular-mass melts more viscous. The rheological consequences of squeezing a polymer into a cavity or dimension that is smaller than the pervaded volume of the molecule itself are not obvious.

Because quantitative rheological measurements in NIL are complicated, Rowland *et al.* designed a simplified method that mimics the large-strain deformation fields encountered. An instrumented indenter records the force and displacement as a well-defined flat punch

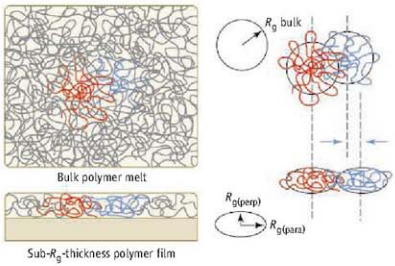


**Processing polymers. (Upper left)** A sea of interpenetrating macromolecular coils in a polymer melt. **(Right)** An arbitrary pair of nearest-neighbor coils, highlighted in red and blue, is lifted from the melt to illustrate their radius of gyration ($R_g$) and the fact that interpenetration or entanglement between the coils exists; the separation between the centers of mass between the two coils is less than $2R_g$. **(Lower left)** For thin films with total thickness below $R_g$, the coils do not appear to spread laterally, and $R_{g(para)} \approx R_g > R_{g(perp)}$. This implies that the interpenetration of the coils decreases, and as argued by Rowland *et al.*, suggests a loss of entanglement and a decreased resistance to flow in a thin-film polymer melt.

[1]Polymers Division, National Institute of Standards and Technology, Gaithersburg, MD 20899, USA. [2]Department of Mechanical Engineering, University of Colorado, Boulder, CO 80309, USA. E-mail: csoles@nist.gov

is pressed into a polymer film. The films are monodispersed polystyrenes with average molecular masses of 9000 kD, 900 kD, and 44 kD, with corresponding $R_g$ values of approximately 84 nm, 26 nm, and 6 nm, respectively, in the bulk melt state ($R_g$ scales with the square root of molecular mass). The film thickness, $h$, is varied from 170 nm to 36 nm, becoming thinner than the $R_g$ of the highest-molecular-mass polystyrenes. The authors argue that the rheological response where the thickness of the film is strongly confining relative to the diameter of the molecule is relevant to an NIL imprint where the mold cavity is smaller than the $R_g$ of the polymer.

The results are striking. For thick films ($h >> R_g$), the resistance to the large-strain deformation of the polymer melt increases substantially with the molecular mass of the polystyrene, consistent with the bulk viscosity. However, when the film thickness is smaller than the radius of gyration, both the contact modulus (the resistance to small-scale elastic deformation) and the forming stress (the load required to induce large-scale plastic deformation) are strongly reduced. For the polystyrene with the highest molecular mass (9000 kD) in the 36-nm film, which is approximately one-half the bulk $R_g$, both the forming stress and large-strain deformation resistance are smaller than for the lowest-molecular-mass polystyrene (44 kD) of the same thickness. This thickness is still about 6 times the bulk $R_g$ for the 44-kD polystyrene and is therefore presumably less confined.

Why such a dramatic reduction of the forming stress and flow resistance in high-molecular-mass polymers relative to the bulk viscosity? The large-strain properties of polymers are dominated by the topological entanglements of the transient network established by the interpenetrating polymer coils (*6*). For chains at surfaces, at interfaces, and in thin films, it has been suggested that the interface acts as a reflecting plane. The polymer coil is not allowed to cross the boundary, so it must "reflect" and remain within the confines of the interface (*7*–*9*). Small-angle neutron scattering measurements on thin polymer films have shown that the $R_g$ in the plane of the film is unaffected by thin-film confinement (*10*). This means that when the film thickness decreases and starts to compress the coil in the vertical direction, the polymer does not respond by spreading laterally in-plane (see the figure). Rather, the chain folds back on itself at the film interface, resulting in the chain segment's nearest neighbors belonging to the same chain, thus decreasing the degree of coil-coil interpenetration (*11*).

These arguments are provocative given the strong correlation between entanglement and melt rheology. A loss of entanglement would seem to facilitate flow in polymer thin films. Although this has been very difficult to prove, the experimental results of Rowland *et al.* provide some of the strongest evidence to date to support this argument. Si and co-workers (*12*) used tensile deformation measurement of glassy polystyrene to deduce a loss of entanglement in thin polymer films, which seems to support the reports of facilitated flow here. However, there are also compelling reports from bubble inflation (*13*) and surface force (*14*) measurements of polymer melts "stiffening" in very thin films. How this problem unravels is not only a scientifically intriguing question, but is also of technical relevance as manufacturing processes such as NIL evolve to fabricate nanoscale features from relatively gigantic molecules.


**References**

1. J. D. Ferry, *Viscoelastic Properties of Polymers* (Wiley, New York, ed. 3, 1980).
2. H. D. Rowland, W. P. King, J. B. Pethica, G. L. W. Cross, *Science* **322**, 720 (2008); published online 2 October 2008 (10.1126/science.1157945).
3. S. Y. Chou, P. R. Krauss, P. J. Renstrom, *Science* **272**, 85 (1996).
4. S. H. Ahn, L. J. Guo, *Adv. Mater.* **20**, 2044 (2008).
5. Y. F. Ding *et al.*, *Adv. Mater.* **19**, 1377 (2007).
6. M. S. Green, A. V. Tobolsky, *J. Chem. Phys.* **14**, 80 (1946).
7. E. A. DiMarzio, *J. Chem. Phys.* **42**, 2101 (1965).
8. H. R. Brown, T. P. Russell, *Macromolecules* **29**, 798 (1996).
9. L. J. Fetters, D. J. Lohse, D. Richter, T. A. Witten, A. Zirkel, *Macromolecules* **27**, 4639 (1994).
10. R. L. Jones, S. K. Kumar, D. L. Ho, R. M. Briber, T. P. Russell, *Nature* **400**, 146 (1999).
11. P. G. de Gennes, *Scaling Concepts in Polymer Physics* (Cornell Univ. Press, Ithaca, NY, 1979).
12. L. Si, M. V. Massa, K. Dalnoki-Veress, H. R. Brown, R. A. L. Jones, *Phys. Rev. Lett.* **94**, 4 (2005).
13. R. A. O'Connell, G. B. McKenna, *Science* **307**, 1760 (2005).
14. H. W. Hu, S. Granick, *Science* **258**, 1339 (1992).


10.1126/science.1165174

ECOLOGY

# Physiology and Climate Change

Studies of physiological mechanisms are needed to predict climate effects on ecosystems at species and community levels.

**Hans O. Pörtner[1] and Anthony P. Farrell[2]**

Ongoing ecosystem changes in response to climate change include poleward or altitudinal shifts in geographical distribution (*1*–*3*), population collapses or local extinctions (*4*), failure of large-scale animal migrations (*5*), changes in the seasonal timing of biological events (*6*), and changes in food availability and food web structure. These changes are largely driven by environmental temperature (*1*, *7*). Examples from aquatic animal communities show that study of physiological mechanisms can help to elucidate these ecosystem changes and to project future ecological trends.

All organisms live within a limited range of body temperatures, due to optimized structural and kinetic coordination of molecular, cellular, and systemic processes. Functional constraints result at temperature extremes. Increasing complexity causes narrower thermal windows for whole-organism functions than for cells and molecules, and for animals and plants than for unicellular organisms (*8*). Direct effects of climatic warming can be understood through fatal decrements in an organism's performance in growth, reproduction, foraging, immune competence, behaviors and competitiveness. Performance in animals is supported by aerobic scope, the increase in oxygen consumption rate from resting to maximal (*9*). Performance falls below its optimum during cooling and warming. At both upper and lower pejus temperatures, performance decrements result as the limiting capacity for oxygen supply causes hypoxemia (*4*, *8*) (see the figure, left). Beyond low and high critical temperatures, only a passive, anaerobic existence is possible. Fish rarely exploit this anaerobic range, but invertebrates inhabiting the highly variable intertidal environment use metabolic depression, anaerobic energy production, and stress protection mechanisms to provide short- to medium-term tolerance of extreme temperatures.

Thermal windows likely evolved to be as narrow as possible to minimize maintenance costs, resulting in functional differences, between species and subspecies in various climate zones (*10*–*12*) and even between populations of a species (*13*); for example, the

[1]Animal Ecophysiology, Alfred-Wegener-Institute for Polar and Marine Research, 27515 Bremerhaven, Germany. E-mail: hans.poertner@awi.de [2]Department of Zoology and Faculty of Land and Food Systems, University of British Columbia, Vancouver, V6T 1Z4 Canada.

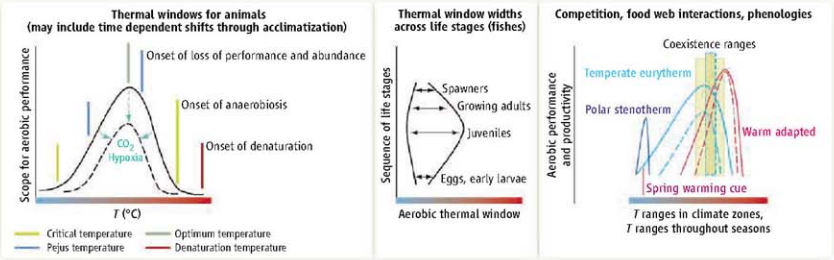


**Temperature effects on aquatic animals.** The thermal windows of aerobic performance (**left**) display optima and limitations by pejus (pejus means "turning worse"), critical, and denaturation temperatures, when tolerance becomes increasingly passive and time-limited. Seasonal acclimatization involves a limited shift or reshaping of the window by mechanisms that adjust functional capacity, endurance, or protection (*4*). Positions and widths of windows on the temperature scale shift with life stage (**middle**). Acclimatized windows are narrow in stenothermal species, or wide in eurytherms, reflecting adaptation to climate zones. Windows still differ for species whose biogeographies overlap in the same ecosystem (**right**, examples arbitrary). Warming cues start seasonal processes earlier (shifting phenology), causing potential mismatch with processes timed according to constant cues (light). Synergistic stressors like ocean acidification (by $CO_2$) and hypoxia narrow thermal windows according to species-specific sensitivities (broken lines), modulating biogeographies, coexistence ranges, and other interactions further.

optimal and critical temperatures differ by 2° to 3°C between two sockeye salmon populations from the Fraser River in British Columbia, Canada (*5*).

Long-term fisheries data revealing climate impacts on fish stocks have often been related to food web effects. However, they can also involve direct warming impacts on individual species, linked to thermal windows. For example, in the German Wadden Sea, growth and abundance of a nonmigratory eelpout decreased when summer maximum temperatures surpassed the upper pejus temperature, with larger individuals affected first (*4*). In the Japan Sea, different thermal windows between sardines and anchovies for individual growth, gamete production and quality, and spawning activity caused a regime shift to anchovies in the late 1990s (*14*, *15*). In the Fraser and Columbia River systems, warming has often delayed spawning migrations of nonfeeding Pacific salmon, potentially causing loss of fitness (*16*). Cardiac collapse above the critical temperature likely brought on swimming failure and mortality among Fraser River sockeye in 2004 (*5*).

The ongoing northward shifts of North Sea Atlantic cod stocks likely involve both direct effects on cod and indirect food web effects. Clear correlation of these shifts with winter warming indicates greatest sensitivity of the fishes during their winter reproductive period (*1*). One reason may be that the oxygen demand of a 20% gonadal mass (*17*) disadvantages mature females by narrowing their thermal window (see the figure, middle). Also, the enhanced reproductive capacity of large body size reduces optimal temperatures for growth and increases heat sensitivity (*13*). Furthermore, thermal windows for growing larval fish, which might be as narrow as those of reproducing adults, may also reflect limited oxygen supply, when the developing ventilation and circulatory systems take over from simple diffusion across the body surface.

An indirect effect of warming is implied in the shifted community composition in the Southern North Sea from larger to smaller zooplankton prey (*18*), reducing the food available to juvenile cod. This shift likely reflects different thermal windows for these copepod species as well as for cod and their prey, given that oxygen-limited thermal tolerance was recently confirmed for small zooplankter (*19*). Such differences between windows may, in general, underpin changes in species interactions and cause shifts in spatial or temporal overlap (see the figure, right).

Further ecosystem-level responses to climate change include shifts in the seasonal timing of recurring processes (*20*). Earlier seasonal development of zooplankton or its grazing later in the year may no longer match the timing of phytoplankton blooms (*6*). Climate could elicit such shifts when warming cues enter or leave thermal windows earlier in the year (see the figure, right). As other cues like seasonal light conditions remain constant, this may cause previously matched species interactions to go out of phase; food availability may change.

Extending the principle of specialization on differing thermal windows to interacting species can help explain changing biogeographies, community composition, and food web structures. These changes mostly set in at the borders of current distributions, where species operate at the limits of their thermal windows; acclimatization mechanisms fail to maintain performance and shift thermal limits further. Such trends can be compensated for by evolutionary selection for adequate genotypes. However, such adaptation may be too slow for long-lived species. Climate change will thus differentially favor species with wide thermal windows, short generation times, and a range of genotypes among its populations.

Carbon dioxide, hypoxia, salinity change, and eutrophication contribute to ecosystem responses to climate change (*21*). Key to setting sensitivity to ocean acidification are the mechanisms and efficiency of systemic acid-base regulation (*22*). Such specific effects of each stressor will reduce whole-organism performance, especially at extreme temperatures, thereby narrowing thermal windows and reducing biogeographical ranges. Studies of ecosystem consequences of stressors like ocean acidification through carbon dioxide should thus consider effects on thermally limited oxygen supply. The principles elaborated here may also be applicable to organisms other than animals and to both aquatic and terrestrial ecosystems (*23*).

**References**

1. A. L. Perry, P. J. Low, J. R. Ellis, J. D. Reynolds, *Science* **308**, 1912 (2005).
2. K. Brander *et al.*, *ICES Mar. Sci. Symp.* **219**, 261 (2003).
3. J. M. Grebmeier *et al.*, *Science* **311**, 1461 (2006).
4. H. O. Pörtner, R. Knust, *Science* **315**, 95 (2007).

5. A. P. Farrell *et al.*, *Physiol. Biochem. Zool.* **81**, 697 (2008).
6. K. H. Wiltshire, B. F. J. Manly, *Helgol. Mar. Res.* **58**, 269 (2004).
7. C. Rosenzweig *et al.*, *Nature* **453**, 353 (2008).
8. H. O. Pörtner, *Comp. Biochem. Physiol.* **132 A**, 739 (2002).
9. J. R. Brett, *Am. Zool.* **11**, 99 (1971).
10. H. O. Pörtner, *Deep Sea Res. II* **53**, 1071 (2006).
11. N. A. Fangue, M. Hofmeister, P. M. Schulte., *J. Exp. Biol.* **209**, 2859 (2006).
12. J. H. Stillman, *Science* **301**, 65 (2003).
13. H. O. Pörtner *et al.*, *Climate Res.* **37**, 253 (2008).
14. A. Takasuka, Y. Oozeki, I. Aoki, *Can. J. Fish. Aquat. Sci.* **64**, 768 (2007).
15. A. Takasuka, Y. Oozeki, H. Kubota, *Mar. Ecol. Prog. Ser.* **360**, 211 (2008).
16. T. M. Gorries *et al.*, *Trans. Am. Fish. Soc.* **135**, 408 (2006).
17. R. Dahle, G. L. Taranger , Ø. Karlsen, O. S. Kjesbu, B. Norberg, *Comp. Biochem. Physiol.* **136 A**, 641 (2003).
18. P. Helaouët, G. Beaugrand, *Mar. Ecol. Progr. Ser.* **345**, 147 (2007).
19. O. Pinkhaus *et al.*, *Freshw. Biol.* **52**, 1537 (2007).
20. M. Winder, D. B. Schindler, *Ecology* **85**, 2100 (2004).
21. J. M Guinotte, V. J. Fabry, *Ann. N.Y. Acad. Sci.* **1134**, 320 (2008).
22. H. O. Pörtner, M. Langenbuch, B. Michaelidis, *J. Geophys. Res.* **110**, C09S10, 10.1029/2004JC002561 (2005).
23. J. J. Tewksbury, R. B. Huey, C. A. Deutsch, *Science* **320**, 1296 (2008).


10.1126/science.1163156

CANCER

# Aneuploidy Advantages?

The gain or loss of specific chromosomes can determine whether a cell becomes tumorigenic.

**Eva Hernando**

The role of aneuploidy—the presence of an abnormal number of chromosomes—in cancer has been at the center of debate for almost a century. Although aneuploidy is a hallmark of most tumor cells, whether it is a cause or a consequence of the malignant transformation (oncogenesis) has not been clear. In 1914, German biologist Theodor Boveri postulated that aneuploidy arising from altered cell division (mitosis) might lead to oncogenesis. However, recent studies with genetically modified organisms have kept the issue open to argument. Certain defects in chromosome segregation during mitosis that lead to aneuploidy can either promote (*1*, *2*) or inhibit tumor formation (*2*, *3*), or even have no effect at all (*4*). On page 703 in this issue, Williams *et al.* (*5*) provide an interesting twist, by showing that harboring an extra chromosome may or may not drive a mammalian cell into oncogenesis, depending on the chromosome itself and on the state of the cell.

Earlier studies reported the deleterious effects of aneuploidy during human development (causing miscarriages) and in adulthood (underlying mental retardation). The findings of Williams *et al.* are compatible with this view, showing that having an abnormal number of chromosomes is initially disadvantageous for mammalian cells. The authors cultured mouse cells that were engineered to express a specific additional chromosome (trisomy). These cell lines had decreased rates of proliferation, and increased cell size and metabolic rates, all conditions that reduce cell fitness. However, in some cases, these limitations could be overcome. The ability of a cell line to proliferate indefinitely in culture (immortalization) depended on the identity of the extra chromosome. Certain chromosome gains accelerated the attainment of immortalization, whereas others delayed or impaired it.

To what extent do these in vitro results reproduce the survival pressure that somatic cells undergo in vivo, and their capacity to adapt to stressful conditions? The mouse embryonic fibroblasts used by Williams *et al.* have higher spontaneous immortalization rates than other primary mouse or human cells in culture. Do the effects of aneuploidy in these fibroblasts occur in other cell types from which most common tumors arise? Also, the elegant strategy of chromosomal translocation used by the authors to simulate increased chromosome numbers may not strictly represent all forms of aneuploidy, nor fully recapitulate, from a structural standpoint, the gain or loss of individual chromosomes.

In any case, Williams *et al.* propose that certain gains or losses of specific chromosomes are more compatible with cell viability than others, thus explaining the variable effects of chromosome gains observed in the mouse cells. Thus, in a normal cellular context—that is, in the absence of mutations that predispose a cell for transformation—aneuploidy alone seems an unlikely driver of oncogenesis. But in a procancerous context, aneuploidy could promote malignant cell transformation. This hypothesis could be tested by introducing aneuploidy in immortalized (not yet transformed) cell lines.

What are the advantages conferred by aneuploidy in a permissive context? Although initially less proliferative, aneuploid cells are inherently unstable, and thus endowed with increased genomic instability and mutational rate. This may lead them to acquire the hallmarks of cancer, such as resistance to cell

Department of Pathology, New York University School of Medicine, New York, NY 10016, USA. E-mail: eva.hernando@med.nyu.edu

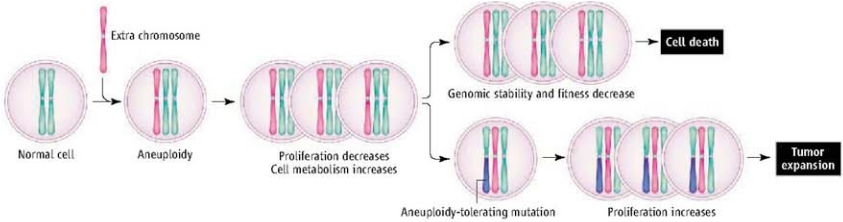


**Gains and losses.** According to the aneuploidy model of Williams *et al.*, an abnormal chromosome number may be costly to cell fitness. However, if mutations arise that allow the cell to adapt to cellular imbalances caused by the abnormal chromosome content, cells may eventually form tumors.

death and enhanced migration (and increased metastastic potential). Thus, what may be disadvantageous in the initial phases of transformation could later become beneficial, permitting a switch from a "slow phase" (during which mutations occur in genes involved in fitness and proliferation control) to an "expansive phase." Thus, aneuploidy could force a bottleneck [or Darwinian selection (*6*)], from which only a selection of superfit cells—those able to adapt and survive—will accumulate more mutations and emerge reinforced against cell death, and with enhanced proliferative and migratory capacities. A corollary of this model is that loosening the adaptation mechanisms acquired in response to aneuploidy could restore tumor cells' vulnerability, thereby representing an attractive therapeutic target. The question is whether this process will be reversible at advanced stages, or whether the accumulation of compensatory mutations will have shielded this tumor Achilles' heel.

A number of models can thus be envisioned for the role of aneuploidy in neoplastic transformation, which are not mutually exclusive and can coexist in specific cellular contexts. As proposed by Williams *et al.*, aneuploidy in most normal cells can repress cell proliferation, reduce cellular fitness, and suppress tumorigenesis (see the figure). In a small subset of cells, however, aneuploidy may trigger a cellular "imbalance" that increases the mutation rate, gene amplification, and/or genomic instability. Aneuploidy unbalances the expression of numerous proteins, which may be involved in DNA synthesis and repair, and chromosome segregation. Subsequent aneuploidy-tolerating mutations would lead to tumor cells with increased proliferative capacity. A second model proposes that aneuploidy can promote transformation when cells enter a "tolerant" state. Incorporation of aneuploidy in cells that already have altered proliferation and a permissive context could stimulate genomic instability and promote cellular transformation. A third model considers aneuploidy as the driving force of mutation and transformation, causing cellular imbalances that increase the rate of mutation and gene amplification. Specific mutations will confer a selective advantage (such as enhanced proliferative capacity). A fourth model sees aneuploidy as a by-product of cellular transformation, which may further promote tumor progression. Specific mutations in oncogenes or genes encoding tumor suppressor proteins would increase cell proliferation and survival, but also may affect chromosome integrity and segregation, producing aneuploidy. This, in turn, could fuel additional genomic instability and mutation rate, accelerating tumor progression.

The work of Williams *et al.* contributes to the notion that tumorigenesis is an integrative process to which aneuploidy by itself has a rather debilitating contribution. But it seems that tumor cells may be operating under Friedrich Nietzsche's general premise that what doesn't kill them (aneuploidy) may make them stronger.

**References**


1. R. Sotillo *et al.*, *Cancer Cell* **11**, 9 (2007).
2. B. A. Weaver *et al.*, *Cancer Cell* **11**, 25 (2007).
3. T. E. Sussan *et al.*, *Nature* **451**, 73 (2008).
4. D. J. Baker *et al.*, *Nat. Genet.* **36**, 744 (2004).
5. B. R. Williams *et al.*, *Science* **322**, 703 (2008).
6. D. P. Cahill *et al.*, *Trends Cell Biol.* **9**, M57 (1999).


10.1126/science.1166151

NEUROSCIENCE

# A New Glance at Glia

Glial cells assist sensory neurons to perceive and respond to stimuli by improving the signal-to-noise ratio.

**Andreas Reichenbach and Thomas Pannicke**

The term neuroglia ("nerve glue") was introduced 150 years ago by German pathologist Rudolf Virchow, who searched for a connective tissue of the central nervous system. Accordingly, glial cells were considered as mere support for neurons, and little was known about their functional roles until the 1980s. Since then, a wealth of data indicate a wide range of glial functions, including optimizing environmental conditions for neuronal function. Close morphological association of glial processes with neuron-neuron connections (synapses), and the physiological responses of glia to neuronal activity (*1*), suggested an active role for glia in the transmission of chemical signals at synapses. This raised the idea of a tripartite synapse (*2*), but evidence based on the ablation of glial cells in an organism has been difficult to acquire, given that neurons die in the absence of glia in most animal models. On page 744 of this issue, Bacaj *et al.* (*3*) demonstrate that neurons in the major sensory organ of the nematode *Caenorhabditis elegans* survive the elimination of glia but display functional deficits.

*C. elegans* is often used as a model organism because the number of its somatic cells is constant. Of its 959 cells, 358 belong to the nervous system, of which 50 are glial cells associated with sensory organs. Because of the determined cell fate, the development of certain cells can be prevented by ablating their respective precursors. An important breakthrough in glia research was the demonstration that in this model organism, a certain type of neuron-ensheathing glial cell is not required for neuronal survival (*4*).

Bacaj *et al.* show that lack of glia results in altered neuronal morphology, sensory deficits, and ultimately modified organism behavior. In particular, with the exception of one type of neuron (AWB), all of the glia-deprived sensory neurons partially (AWC, AWA) or totally (ASE, ASH, ADL) lost sensitivity for their stimuli. The organism's thermophilic behavior observed after glia ablation may also be explained by an increased threshold of thermosensation by the AFD neuron. Most intriguingly, the ASH neuron lost its $Ca^{2+}$ response to high osmotic conditions (as well as its ability to trigger an avoidance reaction) despite normal protein expression. One of the identified glial transmembrane proteins, a KCl cotransporter, may be involved in glial contribution to osmosensitivity of the ASH neuron (*3*), perhaps by maintaining a local normal osmotic "standard" against which environmental changes can be detected. These observations support the view that in *C. elegans* sensory organs, glial cells may be required for the selection, processing, and even transduction of adequate stimuli for their adjacent neurons.

In more general terms, these studies (*3*, *4*) help to clarify the role of glial cells in metazoa with different degrees of complexity. In small "primitive" animals such as polyps, single sensory and ganglion neurons are scattered throughout the tissue, without any associated glia-like cells; this can be thought of as the

Paul Flechsig Institute of Brain Research, Leipzig University, Jahnallee 59, D-04109 Leipzig, Germany. E-mail: reia@medizin.uni-leipzig.de

single-cell stage of nervous system complexity (see the figure). Obviously, these single neurons do not require glial cells to differentiate, function, or survive. The evolution of larger and more complex animals (such as *C. elegans*) resulted in the development of specialized sensory organs and of groups of loosely associated ganglion neurons—the oligocellular stage of nervous system complexity. Such sensory organs usually contain glia-like cells as well, but ganglion neurons are touched, at best, by a glial cell process. The new data of Bacaj *et al.* allow us to speculate that these "ancestral" sensory glial cells are primarily required to increase the sensitivity and/or specificity of the sensory neurons, whereas all neurons remain apparently independent of glia with respect to their metabolism and survival. This situation can still be observed in oligocellular mechanoreceptive organs in the skin or cuticle of insects and vertebrates (*5*).

More complex animals develop large, sophisticated sensory organs and nervous centers (brains), with a multicellular level of nervous system complexity. The sensory epithelia in such organs consist of a mixture of neurons and glia-like cells; this level of complexity exists even in some specialized cnidarians (*6*). As exemplified by the vertebrate retina, glial (Müller) cells support the receptive functions of neurons—for example, by guiding light toward photoreceptive neurons (*7*). However, in such complex multicellular sensory organs, glial cells delegate some of their sensory support functions to other structures. Thus, in the retina, a major part of stimulus selection and processing is passed on to "offshore" structures, such as the cornea, iris, and lens of the eye. In some retinae, one Müller cell may be responsible for up to 30 photoreceptors (*8*). Consequently, this reduces the number of glial cells per sensory neuron (although there are exceptions to this ratio, such as the mammalian inner ear), whereas in oligocellular sensory organs, glia-like cells may outnumber neurons. However, in multicellular sensory organs, glial cells become absolutely essential for neuron survival; if Müller cell death is induced, the entire neural retina soon degenerates (*9*).

Similarly, when many neurons accumulate in ganglia or even in brains, the perisynaptic glia becomes essential for synaptic transmission (*2*), which, as argued by Bacaj *et al.*, is the case for chemosensation by the postsynaptic neuron. In addition, glial cells are crucial for the metabolism and survival of the neurons, as implied by the finding of neuronal damage after glial depletion in mammalian hepatic encephalopathy (*10*). Generally, a

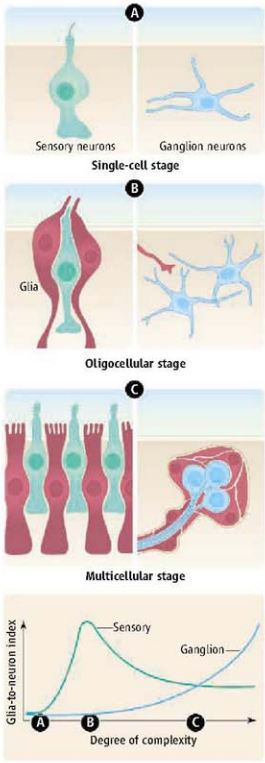


**Glia, by complexity.** A schematic survey of the differentiation stages of sensory (green) and ganglion (blue) neurons and glial cells (red). The numerical relation between glial and neuronal cells (glia-to-neuron index) is shown over the three stages of increasing nervous system complexity.

multiplication of the number of glial cells per neuron occurs with increasing brain size (*8*).

What are the ancestral roles of glia (*11*) and what causes their different involvement among the three stages of nervous system complexity? The step from the single-neuron stage, which lacks glia, to the functionally associated neurons and glia-like cells of an oligocellular-stage sensory organ may have been triggered by the need for more sensitive and/or specific perception of environmental stimuli, forcing the development of accessory "sensory" glia-like cells as the most ancestral glia type. For example, the primary glial function of improving the signal-to-noise ratio of perception appears to involve homeostasis of the extracellular milieu during chemo- and osmosensation (*3*). Once established, these homeostatic glial functions may have been used to assist synaptic transmission (as well as fast axonal signal transport and other neuronal tasks) (*11*, *12*).

The step from the oligocellular stage to more complex neural tissues may have solved an additional quantitative problem—the dense crowding of neurons in large sensory epithelia or ganglia (or brains). Both types of tissues are typically encapsulated against their non-neural environment, usually involving a blood-brain barrier to which glial cells contribute (*12*, *13*). The insulated, highly active neurons depend on nutrient delivery and clearance of waste products. Thus, the need for extracellular homeostasis in an extended sense may have been the driving force for the ubiquitous appearance and further multiplication (*8*) of glia in complex animals. Eventually, the homeostatic functions of glia may have been the basis for their currently evaluated "more exciting roles" including direct involvement in neuronal information processing, both by controlled modification of these functions (*14*) and by their further elaboration into mechanisms such as gliotransmitter release (*2*).

**References and Notes**

1. J. Grosche *et al.*, *Nat. Neurosci.* **2**, 139 (1999).
2. A. Araque, V. Parpura, R. P. Sanzgiri, P. G. Haydon, *Trends Neurosci.* **22**, 208 (1999).
3. T. Bacaj, M. Tevlin, Y. Lu, S. Shaham, *Science* **322**, 744 (2008).
4. S. Yoshimura, J. I. Murray, Y. Lu, R. H. Waterston, S. Shaham, *Development* **135**, 2263 (2008).
5. A. Reichenbach, A. Derouiche, J. Grosche, M. Hanani, in *Glial Neuronal Signaling*, G. I. Hatton, V. Parpura, Eds. (Kluwer, Dordrecht, Netherlands, 2004), pp. 53–97.
6. V. J. Martin, *Can. J. Zool.* **80**, 1703 (2002).
7. K. Franze *et al.*, *Proc. Natl. Acad. Sci. U.S.A.* **104**, 8287 (2007).
8. A. Reichenbach, *Glia* **2**, 71 (1989).
9. M. Dubois-Dauphin *et al.*, *Neuroscience* **95**, 9 (2000).
10. M. D. Norenberg, J. T. Neary, A. S. Bender, R. S. Dombro, *Prog. Brain Res.* **94**, 261 (1992).
11. M. G. Heiman, S. Shaham, *Neuron Glia Biol.* **3**, 55 (2007).
12. R. J. Parker, V. J. Auld, *Semin. Cell Dev. Biol.* **17**, 66 (2006).
13. H. Wolburg, S. Noell, A. Mack, K. Wolburg-Buchholz, P. Fallier-Becker, *Cell Tissue Res.* 10.1007/s00441-008-0658-9 (2008).
14. S. H. R. Oliet, R. Piet, D. A. Poulain, *Science* **292**, 923 (2001).
15. We thank J. Grosche for help on the graphics, and A. Bringmann, B. Altenheim, and V. J. Martin for helpful discussions.

10.1126/science.1166197

RETROSPECTIVE

# George E. Palade (1912–2008)

A pioneer of modern cell biology used cell fractionation and electron microscopy to describe subcellular structures.

**Randy W. Schekman**

The birth of modern cell biology can be traced to the pioneering work of George Palade, who developed the tools of cell fractionation and thin section electron microscopy to visualize the intricate network of membranes comprising the secretory pathway. By a curious coincidence, the next generation of tools to visualize cells and their constituents in real time—green fluorescent protein and its derivatives—was celebrated with a Nobel Prize in Chemistry on the day after Palade died on 7 October 2008.

George Emil Palade was born in Jassy, Romania, in 1912. His father was a philosophy professor and his mother was a teacher, but Palade developed an interest in biomedicine and specialized in anatomy during his medical training at the University of Bucharest. After serving in the medical corps of the Romanian Army during World War II, he traveled to the United States in 1946 to begin his research career at New York University. Working through the 1940s and 1950s with Albert Claude and Keith Porter at what is now Rockefeller University, Palade focused on membranes of the endoplasmic reticulum (ER) and elucidated the basis of protein synthesis and secretion.

Palade's work in the 1950s established the ribosome as the seat of protein synthesis in the cytoplasm. In the 1950s and 1960s, he teamed with Philip Siekevitz and then with Lewis Greene, Colvin Redman, David Sabatini, and Yutaka Tashiro to demonstrate that the dense membranes isolated by Claude represented fragments of ER with bound ribosomes. In critical experiments conducted first by Palade and then by Sabatini, the role of the ribosome in secretory protein synthesis was established, leading to the proposal that nascent polypeptide chains are vectorially discharged across the ER membrane and into the lumen. This work inspired Günter Blobel (another one of Palade's protégés), who won the 1999 Nobel Prize for his work on the signal hypothesis.

At the same time, Palade teamed with Lucien Caro and James Jamieson to develop an autoradiographic technique using the electron microscope to trace the fate of secretory proteins en route to the cell surface. The team achieved nearly quantitative incorporation of radioactive amino acids into secretory proteins within cells of pancreatic tissue slices, and perfected an autoradiographic method to visualize the localization of the radioactive proteins in fixed and sectioned tissues. A 5-minute pulse of $^{14}$C-labeled amino acids was incorporated in the region of the ER membrane in the basal half of the cell. Subsequent incubation of tissues in non-radioactive amino acids revealed sequential movement of grain tracks to the Golgi membrane area and then to the secretory granule region, followed by discharge at the apical cell surface. These "pulse-chase" observations are so tightly woven into the fabric of cell biology that it is hard to remember a time when the interrelations of secretory organelles were far from certain. Indeed, the very existence of the Golgi in the secretory pathway was questioned from the moment it was first visualized by Camillo Golgi in 1898, until Palade, Caro, and Jamieson showed that it mediated protein traffic.

Palade's rich career touched on many aspects of membrane morphology, ranging from the structures of the neuronal synapse, mitochondria, and chloroplast envelope, to the mechanism of capillary permeability (along with Marilyn Farquhar and Nicolae and Maia Simionescu, among others). However, it was his work on membrane biogenesis, which characterized membrane assembly as an expansion of a preexisting organelle (and not de novo), and identification of "transport carriers" in mediating the flow of material along the secretory pathway, that remain as fundamental contributions to the foundation of cell biology. His mastery of electron microscopy—the thin section micrographs he took remain strikingly beautiful even decades later—is unsurpassed. For his achievements, he shared the 1974 Nobel Prize in Physiology and Medicine with Claude and Christian de Duve.

Palade was often called upon to deliver the concluding lecture at major symposia. I recall a meeting in Strasbourg where the talks were in English, but Palade delivered his in French, and could have done so in several other languages, including Latin. I'll also not forget his remarks at a 1995 Cold Spring Harbor Symposium, where at the tender age of 83, he mused that according to 17th century French literature, Cid Campeador, hero of the Spanish wars against the Moors, returned to court after a fierce and long battle—"long, but not as long as this symposium," as Palade put it—to tell his king that the battle ended because there were no fighters left. As the days of the symposium wore on, Palade hoped that by the time he was scheduled to speak, the conference would be finished because there would no longer be "combatants" left to listen, and his presentation would no longer be called for!

Palade enriched the field he helped create through his efforts to establish modern cell biology as a discipline equal in importance to genetics, molecular biology, and biochemistry. He helped found the influential American Society for Cell Biology and the *Journal of Cell Biology* and was the inaugural Editor-in-Chief of the *Annual Review of Cell and Developmental Biology*. He not only created a new Department of Cell Biology at Yale Medical School, but well into his ninth decade, he was founding Dean of scientific affairs at University of California at San Diego (UCSD) School of Medicine.

Palade had a direct role in so many young careers. In fact, he encouraged Peter Novick, one of my first graduate students, to examine the first yeast secretion mutant by thin section electron microscopy. Having also been at Yale as faculty members in Palade's department, Peter and his wife Susan Ferro-Novick just moved to UCSD where Peter is the first holder of the Palade Chair.

Palade will be remembered as a kind and generous mentor, colleague, and family man. Above all, his scholarship remains as a legacy to future generations of cell biologists.

10.1126/science.1167174

Department of Molecular and Cell Biology, University of California, Berkeley, CA 94720, USA. E-mail: schekman@berkeley.edu

AAAS ARCTIC DIVISION

# Scientists Link Climate, Energy to Growing Arctic "Food Insecurity"

**FAIRBANKS, Alaska**—For generations, caribou have been central to the diet and culture of the Naskapi people who live on the tundra of northeastern Canada. But when researcher Archana Bali visited last summer, they told her that warming weather and increased mining have driven the caribou so far off of old migration routes that their meat staple is in short supply.

According to researchers at the recent annual meeting of the AAAS Arctic Division, the Naskapi's struggle reflects a broader pattern: Unpredictable weather, shrinking sea ice, and soaring fuel costs are making hunting and fishing more difficult for people long accustomed to living off the land. As a result, food supplies in many Far North communities are increasingly at risk.

"I've worked with people, both in the interior and on the coast, who say, 'I don't have the money to put fuel in my boat to go searching for food,'" said Philip Loring, an anthropologist at the University of Alaska-Fairbanks (UAF). "I'm talking to people who say: 'I'm worried about having enough food for the winter.'"

Added anthropologist S. Craig Gerlach: "Climate change, food shortages—all these things we said were going to happen by 2050 or 2070, they're happening now."

Gerlach just finished a year-long term as president of the AAAS Arctic Division, and he worked with Executive Director Lawrence K. Duffy, interim dean of the UAF Graduate School, to organize the division's 59th annual meeting. Under the theme "Growing Sustainability Science in the North," it brought more than 170 researchers, educators, students, and native Alaskan leaders to Fairbanks from 15 to 17 September.

In the midst of the meeting came news that Arctic sea ice in the summer of 2008 had shrunk to the second smallest size on record. That underscored the researchers' often dramatic reports on changes under way in the Far North climate and in land and marine ecosystems—and how those changes are affecting human communities.

Loring organized a half-day symposium on the future of northern food systems, but food security was a recurring theme throughout the meeting. Problems are manifest not only in food shortages, he said, but in the rising incidence of diabetes and cancer that are linked to modern, processed foods.

**Changing nature.** Elizabeth Nibgorsi is a hunter from Canada's Nunavut territory. Northern "caribou people" say changing weather and new development are threatening their food supplies.

Bali, working toward a Ph.D. degree in wildlife biology and natural resource management at UAF, visited six communities in northern Alaska and Canada this summer and found them preoccupied with food security and environmental changes. In northern Quebec Province, the Naskapi said they'd sent hunters far out into the tundra for caribou. The trip was expensive, and the harvest limited. "Following local traditions, the elders and single mothers received the harvested caribou first," she said. "There wasn't much for others."

Ecologist Bruce Forbes, based at Finland's Arctic Centre, University of Lapland, has found that oil and gas development on Russia's Yamal Peninsula appears to be harming food supplies for the Nenets, a nomadic reindeer-herding people. New roads and pipelines create barriers to migration. Stress on tundra pastures has altered the quantity and quality of reindeer forage; road dust has reduced the cloudberries consumed by the Nenets.

In Alaska, record rains this summer caused damaging floods. Floods and high gas prices are disrupting subsistence hunting and fishing out in the Bush. Over the past decade, the cost of food, fuel, and other supplies has risen more than 90% in remote Athabascan villages on the upper Yukon River, Gerlach said, and a droopy bunch of broccoli can now cost $12 or more in stores there. This fall, schools in Alaska's urban areas are reporting a surge in new students, apparently because families are migrating from the villages.

But people of the Arctic are resilient—over thousands of years, they've had to adapt to survive. Alaskan cities and towns from Juneau to Fort Yukon, on the Arctic Circle, have started community gardens. In August, Sitka became the latest municipality to host a farmers' market.

Scientists and local residents have teamed to develop new food sources and improve nutrition. Gerlach said that he and his colleagues have offered scientific advice to the Athabascans as they experiment with village gardens, sustainable forestry, and biofuels.

"The Athabascan people are right out there on the edge," he said. "They have no word for sustainability, but they do have a word for self-reliance—it's self-reliance they're interested in, strong and healthy communities."

*Learn more about the four AAAS regional divisions at www.aaas.org/go/divisions/.*

ANNUAL MEETING

## AAAS Council Reminder

The next meeting of the AAAS Council will take place during the AAAS Annual Meeting and will begin at 9:00 a.m. on 15 February 2009 in Chicago, Illinois, in the Plaza Ballroom of the Hyatt Regency Chicago Hotel.

Individuals or organizations wishing to present proposals or resolutions for possible consideration by the Council should submit them in written form to AAAS Chief Executive Officer Alan Leshner by 21 November 2008. This will allow time for them to be considered by the Committee on Council Affairs at their winter meeting.

Items should be consistent with AAAS's objectives and be appropriate for consideration by the council. Resolutions should be in the traditional format, beginning with "Whereas" statements and ending with "Therefore be it resolved."

Late proposals or resolutions delivered to the AAAS Chief Executive Officer in advance of the February 2009 Open Hearing of the Committee on Council Affairs will be considered, provided that they deal with urgent matters and are accompanied by a written explanation of why they were not submitted by the November deadline. The Committee on Council Affairs will hold its open hearing at 2:30 p.m. on 14 February 2009 in the State Room of the Fairmont Chicago.

Summaries of the council meeting agenda will be available during the annual meeting at both the AAAS information desk and in the AAAS headquarters office. A copy of the full agenda will also be available for inspection in the headquarters office in the Hyatt Regency Chicago.

PHOTO CREDIT: ARCHANA BALI

# Structural Insights into a Circadian Oscillator

Carl Hirschie Johnson,[1]* Martin Egli,[2] Phoebe L. Stewart[3]

An endogenous circadian system in cyanobacteria exerts pervasive control over cellular processes, including global gene expression. Indeed, the entire chromosome undergoes daily cycles of topological changes and compaction. The biochemical machinery underlying a circadian oscillator can be reconstituted in vitro with just three cyanobacterial proteins, KaiA, KaiB, and KaiC. These proteins interact to promote conformational changes and phosphorylation events that determine the phase of the in vitro oscillation. The high-resolution structures of these proteins suggest a ratcheting mechanism by which the KaiABC oscillator ticks unidirectionally. This posttranslational oscillator may interact with transcriptional and translational feedback loops to generate the emergent circadian behavior in vivo. The conjunction of structural, biophysical, and biochemical approaches to this system reveals molecular mechanisms of biological timekeeping.

Many biological processes undergo daily (circadian) rhythms that are dictated by self-sustained biochemical oscillators. These circadian clock systems generate a precise period of ~24 hours in constant conditions (constant light and temperature) that is nearly invariant at different temperatures (temperature compensation) (*1*). Circadian clocks also show entrainment to day and night, predominantly mediated by the daily light/dark cycle, so that the endogenous biological clock is phased appropriately to the environmental cycle (*2*). These properties, especially the period's long time constant and temperature compensation, are difficult to explain biochemically. Full understanding of these unusual oscillators will require knowledge of the structures, functions, and interactions of their molecular components.

### Pervasive Circadian Rhythms in a Bacterium

We study the components of the biological clock in the prokaryotic cyanobacterium *Synechococcus elongatus*, which programs many processes to conform optimally to the daily cycle, including photosynthesis, nitrogen fixation, and gene expression (*1–3*). Competition assays among different strains of *S. elongatus* rigorously demonstrated that this clock system significantly enhanced the fitness of the cells in rhythmic environments, but not in nonselective constant environments (*3*). The first circadian rhythm measured in *S. elongatus* was that of *psbAI* promoter activity as assayed by a luciferase reporter in populations of cells (*4*). More recently, a tour de force imaging study visualized the rhythm of luminescence from single bacterial cells (Fig. 1, A and B) (*5*). That study also demonstrated that as single cells divide, the daughter cells maintain the circadian phase of the mother cell (Fig. 1B). Therefore, the circadian clock in cyanobacteria is not perturbed by cell division. That result confirmed studies in populations of cells that showed that the circadian clock ticks away with a period of ~24 hours in cells that are dividing with average doubling times of 6 to 10 hours (*6–8*). Conversely, the circadian clock gates cell division so that there are some times of the day/night cycle when the cells grow without dividing (*6*). Therefore, two independent timing circuits coexist in this unicellular bacterium; the circadian pacemaker provides a checkpoint for the cell-division cycle, but there is no feedback of the cell-division timing circuit upon the circadian clock (*8*).

Although it was the *psbAI* promoter that was initially found to be robustly rhythmic in *S. elongatus* (*4*), further investigation of transcriptional control discovered that essentially all promoters were modulated by the circadian clock (*9*). Even a heterologous promoter from *Escherichia coli* is transcribed rhythmically when inserted ectopically into the cyanobacterial chromosome (*10*). Those observations have now been linked with the discovery that the topology of the entire cyanobacterial chromosome is under the control of this circadian program. The *S. elongatus* chromosome undergoes robust oscillations of compaction and decompaction that can be visualized with DNA-binding dyes (Fig. 1C) (*11*). Moreover, the superhelical status of DNA experiences correlative circadian oscillations (Fig. 1D) (*12*). Such large-scale changes in chromosomal structure and torsion are likely to modulate transcriptional rates. It is therefore possible that rhythmic gene-expression patterns are mediated by daily changes in the topology of the chromosome. From this perspective, the cyanobacterial chromosome might be envisioned as an oscillating nucleoid, or "oscilloid," that regulates all promoters—including heterologous promoters—by torsion-sensitive transcription (*12*). Gene expression in cyanobacteria is also regulated in a circadian fashion by the putative transcriptional factor RpaA; rhythmic gene expression is attenuated when the *rpaA* gene is deleted (*2*, *13*). The phosphorylation status of RpaA is regulated by the two-component system kinase SasA, whose phosphorylation is controlled in turn by the KaiABC oscillator that is described in the next paragraph (*13*). These results support an alternative model in which the SasA/RpaA two-component system mediates signals from the KaiABC oscillator to drive genome-wide transcription rhythms. Although the oscilloid and the SasA/RpaA models appear to be mutually exclusive, an analysis of stochastic gene expression in cyanobacteria (*14*) supports regulation both locally (by DNA topology, for example) and comprehensively (by trans factors such as RpaA).

### Cogs and Gears: The Kai Proteins

The clockwork mechanism that controls these global rhythms of transcription, chromosomal topology, and cell division is composed of three essential proteins—KaiA, KaiB, and KaiC—which were identified in 1998 (*15*). Their three-dimensional structures, which became available in 2004 (*16–21*), are the only full-length structures of core circadian clock proteins that have been determined. KaiA is a dimer of intertwined monomers, KaiB has a thioredoxin-like fold and forms dimers and tetramers, and KaiC is a "double-doughnut" hexamer (fig. S1). The structure of KaiC revealed a two-domain fold (N-terminal CI and C-terminal CII lobes) in the monomer and six adenosine 5′-triphosphate (ATP) molecules bound between subunits in both the CI and the CII rings (Fig. 2A). ATP binding within CI serves to stabilize the CI ring that forms the hexamer even in the absence of CII domains (*16*). When the three Kai proteins are combined together with ATP in a test tube, a molecular oscillator is reconstituted (Fig. 1E) (*22*). This in vitro oscillator perpetuates a ~24-hour cycle for at least 10 days (*23*), with KaiC alternating between a hypophosphorylated and a hyperphosphorylated state. KaiC is phosphorylated at serine 431 (S431) and threonine 432 (T432) residues in the CII half (*24*, *25*) (Fig. 3, A and B), whereas the CI ring appears devoid of phosphorylation sites. Phosphorylation of CII residues occurs across the subunit-subunit interface, because S431 and T432 are closest to an ATP molecule that is held by the P loop of the adjacent subunit (Fig. 3A).

KaiC is both an autokinase and an autophosphatase (*26–28*) that rhythmically hydrolyzes 15 ATP molecules per subunit during a complete in vitro cycle (*29*). Because only two ATP molecules are needed to phosphorylate S431 and T432, the consumption of the extra ATP molecules may be used to drive conformational changes within KaiC, including monomer exchange (*23*, *30*, *31*). KaiA promotes the formation of the KaiC hyper-

[1]Department of Biological Sciences, Box 35-1634, Vanderbilt University, Nashville, TN 37235–1634, USA. [2]Department of Biochemistry, Vanderbilt University, Nashville, TN 37235–0146, USA. [3]Department of Molecular Physiology and Biophysics, Vanderbilt University, Nashville, TN 37235–0615, USA.

*To whom correspondence should be addressed. E-mail: carl.h.johnson@vanderbilt.edu

phosphorylated state, whereas KaiB antagonizes the actions of KaiA and promotes a return to the hypophosphorylated state. Structural and biophysical studies have enhanced our understanding of the KaiA•KaiC complex (Fig. 2) (*32*, *33*) and the KaiB•KaiC complex (Fig. 3, C and D) (*34*), as well as quantified the relative levels of KaiC versus KaiA•KaiC versus KaiB•KaiC versus KaiA•KaiB•KaiC complexes formed during the in vitro reaction cycle (*30*, *31*). In addition, the KaiC phosphorylation cycle comprises four consecutive steps: (i) T432 phosphorylation, (ii) S431 phosphorylation, (iii) T432 dephosphorylation, and (iv) S431 dephosphorylation (*28*, *35*). This information provides the framework for a reanalysis of the Kai protein structures, suggesting how the in vitro clock might work.

### KaiC Interacts with KaiA and KaiB

KaiA binds repeatedly and rapidly to KaiC during the phosphorylation phase (*30*) and enhances KaiC's autokinase activity. Moreover, a single KaiA dimer appears to be sufficient to up-regulate phosphorylation of a KaiC hexamer to saturated levels (*36*). This is consistent with the higher abundance of KaiC in vivo relative to KaiA (*37*). What is the structural basis of KaiA's function? KaiA binds to the KaiC CII lobe C-terminal tail (*32*). This binding interaction requires concomitant unfolding of an S-shaped loop in the contacted KaiC subunit. We hypothesize that KaiA pulls the S-shaped loop out of the central channel of the KaiC hexameric barrel (Fig. 2). In the KaiC crystal structure, the loop residues (amino acids 485 to 497) are engaged in hydrogen bonding interactions across subunits at the periphery of the channel (Fig. 2B) (*21*). Disrupting the fold of the S-shaped loop of a single subunit might weaken the interface between adjacent CII lobes and promote conformational changes within the CII ring that support phosphorylation at T432 and S431 (*38*). A three-dimensional electron microscopy (EM) structure of the KaiA•KaiC complex reveals that KaiA is connected to the hexameric barrel of KaiC via a flexible linker (*33*). The

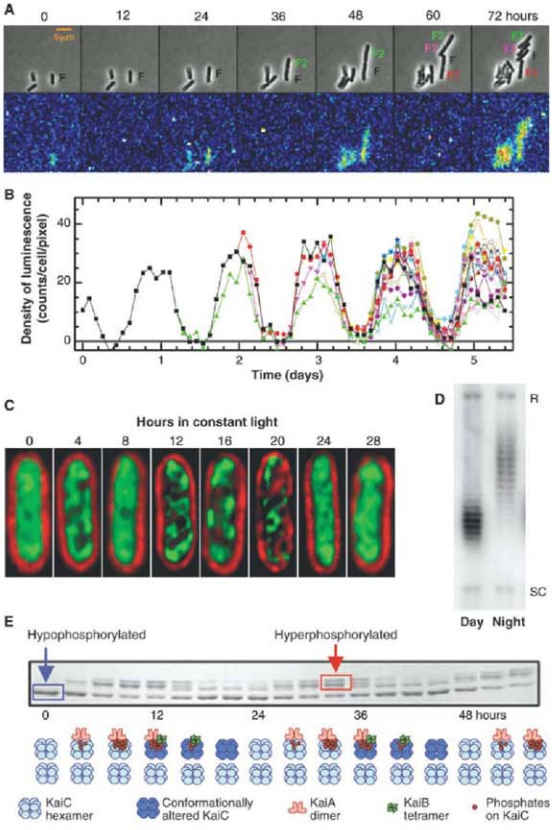


**Fig. 1.** Rhythms in cyanobacteria from cells to molecules. (**A** and **B**) Circadian rhythms of bioluminescence in single cyanobacterial cells. (A) Micrographs of cyanobacterial cells at different times in constant light conditions. (Upper) Brightfield images showing growth and cell division as a function of approximate circadian time; (lower) luminescence emanating from these cells (the luminescence reporter was the *psbAI* promoter driving expression of bacterial luciferase, *luxAB*). (B) Quantification of bioluminescence from a single cell as it divides into multiple cells as a function of time in constant light. Starting at day 1.5, there are two differently colored traces as a result of cell division; the next division occurs at day 2.0, and so on [(A) and (B) are courtesy of I. Mihalcescu, reprinted with permission from (*5*)]. (**C**) Circadian rhythm of chromosomal compaction as visualized by a fluorescent DNA-binding dye (green) (red indicates chlorophyll autofluorescence). The chromosome is more compacted in the subjective night (hours 12 to 20) and less compacted in the subjective day (hours 0 to 8, 24 to 28) [(C) is courtesy of S. Williams, reprinted with permission from (*11*)]. (**D**) Chromosomal topology shows a circadian rhythm as assayed by supercoiling of an endogenous plasmid. Topoisomers of the plasmid are more relaxed (R) in the subjective night and are more supercoiled (SC) in the subjective day (*12*). (**E**) (Upper) KaiC phosphorylation in the oscillating in vitro reaction is shown by SDS-PAGE; upper bands are hyperphosphorylated KaiC, and lower band is hypophosphorylated KaiC. (Lower) The predominant species of complexes of KaiA, KaiB, and KaiC that form during the in vitro oscillation; hypophosphorylated and uncomplexed KaiC hexamers (lower row) are present at all phases, but KaiC in complexes with KaiA and/or KaiB forms rhythmically in concert with changes in KaiC's phosphorylation status (upper line, only the predominant complex is shown). Light blue KaiC hexamers are in the phosphorylating phase before monomer exchange, while dark blue KaiC hexamers are those undergoing dephosphorylation and monomer exchange.

EM structure also suggests that a transient interaction may occur between the apical loop of KaiA and the ATP-binding cleft of KaiC. Thus, the action of KaiA might be to promote conformational flexibility of the KaiCII ring by disrupting the S-shaped loop hydrogen bond network (Fig. 2, C to E) or alternatively, to enhance the residence time of ATP by covering the ATP-binding cleft. Therefore, these interactions of KaiA with KaiC could promote the hyperphosphorylation of KaiC by enhancing its rate of autophosphorylation and/or its ATP residence time.

The binding mode of KaiB to KaiC differs fundamentally from that of KaiA. Unlike KaiA, which is associated with KaiC during the entire phosphorylation cycle, KaiB preferentially binds to the phosphorylated form of the hexamer (*28*, *30*, *31*, *35*). Structural analyses combining cryo- and negative-stain EM, x-ray crystallography, native polyacrylamide gel electrophoresis (PAGE), and fluorescence methods revealed that KaiB dimers bind to the CII ring (Fig. 3C) (*34*). Instead of interacting with C-terminal KaiC tails, KaiB dimers form a third layer on top of CII without obscuring the central channel. This arrangement has important consequences for KaiA; although still tethered to the C-terminal CII peptide, KaiA is unable to approach the ATP-binding clefts (Fig. 3D). Thus, the EM structure offers a plausible model for KaiB's antagonism to KaiA. In addition to sequestering KaiA, KaiB may use its conserved, negatively charged C-terminal tail to weaken subunit interactions at the CII side of the KaiC hexamer and to destabilize or displace ATP. Notably, the EM structure of the KaiB•KaiC complex showed no density for the folded S loops, suggesting that they are pulled out of the central channel of the KaiC hexameric barrel when KaiB is bound.

### Why Biological Time Does Not Run Backward

The KaiC crystal structure exhibited double phosphorylation at T432 and S431 in four of the six subunits (*21*, *24*). In the remaining two subunits, only T432 was phosphorylated (Fig. 3A). The T432 side-chain oxygen atoms are closer on average to the ATP γ-phosphate (7.3 Å) than the S431 side-chain oxygen atoms (8.4 Å); however, neither side chain is in an optimal position for phosphotransfer. This is not surprising because phosphorylated subunits represent the kinase product state and the phosphorylated side chains have presumably moved away from ATP to avoid unfavorable electrostatic interactions. The crystal structure shows a subtle 1 to 2 Å variation in the distances between phosphorylation sites and ATP γ-phosphates, suggesting that the CII domains have a tendency to flex. Phosphorylation of T432 results in stabilizing interactions between adjacent CII domains (Fig. 3E and fig. S2) (*24*). The phosphate group is engaged in multiple hydrogen bonds to arginine and serine residues, suggesting that local conformational fluctuations will be more limited after the initial phosphate transfer. If S431 is phosphorylated by a pathway similar to that resulting in T432 phosphorylation, the stabilizing intersubunit interactions formed by P-T432 would have to be broken in order to bring S431 in an optimal position for phospho-transfer from ATP. In a potential alternative mechanism for S431 phosphorylation, S431 could receive a phosphate from P-T432, followed by immediate rephosphorylation of T432. This alternative mechanism would explain the strict order of phosphorylation events (T432 first and S431 second) and is consistent with the structural data.

Once phosphorylated, S431 can engage in additional hydrogen bonding interactions with amino acids in the same subunit (Fig. 3F and fig. S3). Among the interacting residues is T426, whose mutation to Ala abolishes clock function (*24*). The configuration observed in the crystal structure for the T432 and S431 phosphate groups of chain f is particularly interesting in that it shows the two phosphate groups in van der Waals contact and stabilized by an interacting arginine (R393; Fig. 3G). This provides structural evidence that T432 and S431 can, in principle, get close enough to each other to allow for a phosphate transfer. Another structural observation supporting the alternative mechanism is that in the two subunits exhibiting phosphorylation only at T432 (chains c and d; Fig. 3A), the side-chain oxygen atom of S431 lies closer to the phosphate of P-T432 (7.0 Å) than to the γ-phosphate of ATP (8.4 Å). However, the observation that the T432E mutant protein can still be phosphorylated at S431 (*28*) indicates that phospho-transfer to S431 can occur directly from ATP. Overall, the structural information on the phosphorylation events at the KaiCII subunit interfaces and the inter- and intra-subunit interactions formed by the phosphorylated residues indicates that the number of hydrogen bonds increases as first T432 and subsequently S431 is phosphorylated. This progressive increase in molecular interaction would make the reverse reactions unfavorable, causing a built-in ratcheting mechanism that drives the KaiC oscillator unidirectionally.

We envision that a conformational change is then required to drive KaiC forward to the phosphatase state and achieve dephosphorylation first of T432 and then of S431 in all six subunits. Sequential dephosphorylation in this order has been observed in biochemical assays (*28*, *35*). Interaction of KaiB with KaiC facilitates the formation of the phosphatase state. Unlike KaiA, which has similar affinities for various forms of KaiC (*30*), KaiB binds preferentially to the hyperphosphorylated form of KaiC (specifically, P-S431) (*28*, *35*). KaiC can thus be either a kinase or a phosphatase; at present, only the kinase state has been captured in a high-resolution crystal structure. Some of the outstanding questions for further research on the biochemistry of these key reactions include understanding the mechanism of monomer exchange, the configuration of KaiC in the unphosphorylated state, and the means by which KaiC can dephosphorylate.

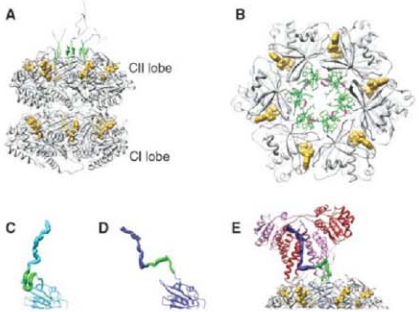


**Fig. 2.** KaiA-KaiC interaction. **(A)** The crystal structure of the KaiC hexamer shows a double doughnut shape formed by two lobes per subunit [Protein Data Bank (PDB) ID 2GBL]. The S-shaped loops (amino acids 485 to 497) (green) dip into the central channel of the hexameric barrel. The flexible C-terminal residues (amino acids 498 to 519) extend from the CII end of the hexamer. Some of the C-terminal tails are shorter than others because this region is partly disordered and only two chains have been completely traced out to the C-terminal S519 residue. ATP (gold) is bound between subunits in both the lower CI ring and the upper CII ring. **(B)** The six S-shaped loops (green stick representation) interact via a hydrogen bond network. Hydrogen bonds are shown in magenta and the view is perpendicular to (A) as seen from the CII side. **(C)** The CII end of one KaiC monomer as in the crystal structure with the S-shaped loop in green. **(D)** The CII end of one KaiC monomer as proposed to interact with KaiA, with the S-shaped loop pulled out (*33*). In (C) and (D), the S-shaped loop and C-terminal tail are shown as a wide ribbon. **(E)** Model of the KaiA-KaiC interaction based on combined structural information from x-ray crystallography, nuclear magnetic resonance, and three-dimensional EM (*33*). One S-shaped loop (green) is shown pulled out of the KaiC hexameric barrel. For clarity, the S-shaped loop and C-terminal residues are shown for only one of the six KaiC subunits. The KaiA dimer is shown in red and purple.

### How Does This in Vitro Clockwork Tick?

The unexpected demonstration that KaiC's phosphorylation status continued to cycle when the three Kai

proteins are combined in a test tube and ATP was added to provide energy (Fig. 1E) (*22*) shows that circadian oscillations are not absolutely dependent upon transcriptional and/or translational feedback (*22*, *27*, *39*, *40*). The in vitro rhythm, KaiC's dephosphorylation rate, and KaiC's ATP hydrolytic activity are all temperature compensated (*22*, *29*, *40*); that is, a temperature compensation mechanism is intrinsic to the characteristics of the three Kai proteins and the nature of their interactions. How this is accomplished is an important unresolved question for the cyanobacterial system and for circadian clocks in general (*22*, *29*, *40*).

The availability of the in vitro system for analyzing the molecular nature of a circadian clockwork allows biophysical, biochemical, and structural analyses that were previously impossible. EM, chromatography, and native gel electrophoresis techniques have been applied to quantify the time-dependent formation of complexes among the Kai proteins (*30*, *31*). KaiC exists in all possible combinations with KaiA and KaiB throughout the in vitro oscillation: free KaiC hexamers, KaiA•KaiC complexes, KaiB•KaiC complexes, and KaiA•KaiB•KaiC complexes (Fig. 1E). The proportions of these complexes vary in a phase-dependent manner: Free KaiC hexamers predominate at all phases; ~10% of KaiC hexamers appear as KaiA•KaiC complexes at all phases; and KaiB•KaiC and KaiA•KaiB•KaiC complexes are clearly rhythmic, becoming most common in the KaiC dephosphorylation phase (Fig. 1E) (*30*, *31*). Therefore, during the in vitro oscillation, KaiC is undergoing rhythmic changes in conformation, phosphorylation status, and interactions with KaiA and KaiB. As structural studies have indicated, changes in the KaiC phosphorylation/dephosphorylation status correlate with conformational changes in KaiC. The central core of the oscillator is probably the rhythm of changes in KaiC conformation that modulate interactions with KaiA and KaiB and influence the activity of transduction factors such as SasA and RpaA (*13*, *30*, *31*), whereas the role of the KaiC phosphorylation/dephosphorylation is to facilitate the changes of KaiC conformation that mediate these interactions.

Maintenance of a high-amplitude oscillation in the face of noise is a crucial characteristic of any circadian oscillator (*5*). In the case of the in vitro oscillator, KaiC monomers exchange among the hexamers, a process that synchronizes the phosphorylation status of the individual hexamers in the population of hexamers (Fig. 4) (*23*, *30*, *31*). Consequently, although cyanobacterial cells in populations are autonomous oscillators that do not communicate phase information intercellularly (*5*), communication among KaiC hexamers via monomer exchange maintains a high-amplitude rhythm inside the cell (*23*, *31*). Therefore, the posttranslational cyanobacterial clockwork is composed of biochemical reactions such as phosphorylation, ATP hydrolysis, monomer exchange, and conformational changes among thousands of molecules per cell (~10,000 KaiC monomers per cell) (*37*), permitting robust oscillations of high precision and synchrony.

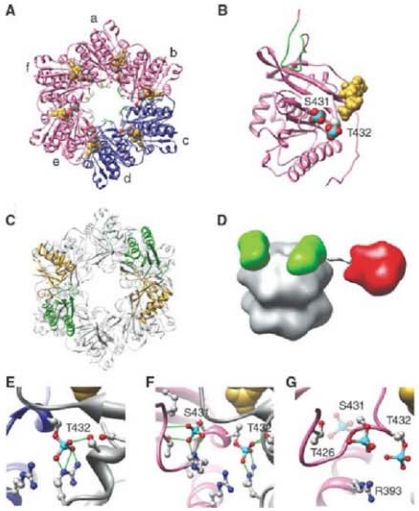


**Fig. 3.** Structural stabilization mediated by phosphorylation and KaiB-KaiC interaction. **(A)** Ring of CII lobes from the KaiC crystal structure. Four subunits, chains a, b, e, and f (pink), are doubly phosphorylated at S431 and T432. Two subunits, chains c and d (blue), are singly phosphorylated at T432. The side chains of S431 and T432 are shown in space-filling representation and are colored by element with phosphorus atoms in cyan and oxygen atoms in red. ATP (gold) is bound between the CII lobes. **(B)** CII lobe of a doubly phosphorylated KaiC monomer (chain a) with the S-shaped loop in green. The view is perpendicular to (A). **(C)** Model of the KaiB•KaiC interaction based on combined structural information from x-ray crystallography and three-dimensional EM (*34*) with KaiB dimers in green and gold. **(D)** Model of the KaiA•KaiB•KaiC interaction with KaiA (red) and KaiB (green) dimers in orientations resembling those in the class IV KaiABC particle images from negative-stain EM [see figure 1D in (*31*)]. **(E)** Hydrogen bonds (green) formed by the phosphate group of T432 in chain c (blue). **(F)** Hydrogen bonds formed by the phosphate groups of S431 and T432 in chain b (pink). In (E) and (F), the neighboring chain is shown in gray. See figs. S2 and S3 for the hydrogen bonds formed by the additional phosphate groups in chains a to f. **(G)** In chain f, the phosphate group of S431 is leaning toward T432, rather than toward T426 as in chains a, b, and e. The position of the S431 phosphate group in chain e is shown in a faint representation. The phosphate groups of both S431 and T432 in chain f are stabilized by electrostatic interactions with R393.

### From Test Tube to Cell; Embedding the KaiABC Oscillator Within a Transcription and Translation Feedback Loop

What is the role of the post-translational KaiABC oscillator in the overall cellular program (Fig. 4)? There is a rhythm of KaiC phosphorylation in vivo that continues in the absence of transcription or translation, but there are also rhythms of KaiB and KaiC abundance in metabolically active cells that have been interpreted in terms of a transcription and translation feedback loop (TTFL) (*40*, *41*). Perhaps the rhythms of KaiC phosphorylation and abundance are complementary processes that can oscillate independently or can interact to generate a more robust overall program (*42*). Early evidence for a core TTFL oscillator in cyanobacteria was partly based on experiments in which KaiC abundance was experimentally manipulated in vivo; KaiC expression from an inducible promoter reset the cellular clock in a phase-dependent manner (*15*, *41*). Although the most direct impact of KaiC expression is upon abundance, such expression could also perturb the phosphorylation oscillator; flooding KaiC pools with newly synthesized and therefore unphosphorylated KaiC would be expected to alter the phosphorylation ratio of the KaiC pool. If the new synthesis of KaiC occurs at a phase when hexamers are predominantly hypophosphorylated, the oscillation of KaiC phosphorylation would be reinforced (enhanced amplitude). By contrast, new synthesis of unphosphorylated KaiC when hexamers are predominantly hyperphosphorylated would lead to an overall decrease in the KaiC phosphorylation status, thereby altering the phase of the KaiABC oscillator (phase shift) and/or reducing its amplitude. Therefore, the posttranslational oscillator (PTO) may regulate the timing of transcription and translation to occur in an optimal phase to enhance robustness of the larger oscillating system (Fig. 4). In this scenario, the PTO is embedded in a TTFL; the PTO may most directly determine the dynamics of the circadian system, but the TTFL provides a secondary feedback loop that aids robustness.

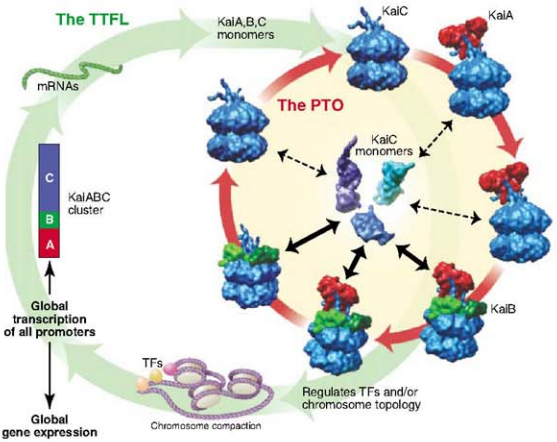


**Fig. 4.** A self-sustained posttranslational oscillator (PTO) embedded within a transcription and translation feedback loop (TTFL). The posttranslational KaiABC oscillator (cycle connected by red arrows) is determined by phosphorylation of KaiC (blue hexamers) as regulated by interactions with KaiA (red dimers) and KaiB (green tetramers). Robustness is maintained by synchronization of KaiC hexameric status via exchange of KaiC monomers (*23*, *30*, *31*). Monomer exchange is depicted in the center of the PTO by KaiC monomers exchanging among KaiC hexamers; phase-dependent changes in the rate of monomer exchange are indicated by the thickness of the double-headed black arrows. New synthesis of KaiC feeds into the KaiABC oscillator as nonphosphorylated hexamers or as monomers that exchange into preexisting hexamers. The PTO brings KaiC to a state that regulates chromosome topology and/or transcriptional factors ("TFs") to control global transcription of all promoters (including those driving expression of the essential clock genes *kaiA*, *kaiB*, and *kaiC*).

What are the potential benefits of a biochemical (PTO) oscillator embedded within a genetic (TTFL) oscillator? A core oscillator that is composed of biochemical reactions among thousands of molecules per cell should be more robust in the face of metabolic noise than one founded on transcriptional activity. This is particularly true for cells that must maintain precise timekeeping during cell division, when the ratio of DNA to transcriptional factors can change during replication and where DNA can become less accessible when chromosomes condense in preparation for division. The advantage provided by a biochemical oscillator such as KaiABC is that this posttranslational system would be less susceptible to the influences of cell division (*5*–*8*) or major changes in metabolic rate (*40*, *41*) than one based on transcriptional and translational rates. Although eukaryotic circadian genes are not homologous to *kaiABC* sequences, the proteins they encode also undergo circadian rhythms of abundance and phosphorylation (*1*, *43*, *44*). The benefit of a clockwork that is imperturbable even when buffeted by the massive intracellular changes of cell division could have provided an evolutionary driving force for convergent circadian clock mechanisms among diverse organisms.

We now recognize KaiABC as a dynamically oscillating nanomachine that has evolved to precess unidirectionally and robustly. The challenges ahead are to delve deeper into the molecular nature of its temperature compensation, to examine the place of the PTO in the larger cellular program, and to discover if the clocks in our own cells have attributes that are similar to those of bacteria.

### References and Notes


1. J. C. Dunlap, J. J. Loros, P. J. DeCoursey, Eds., *Chronobiology: Biological Timekeeping* (Sinauer, Sunderland, MA, 2004).
2. S. R. Mackey, S. S. Golden, *Trends Microbiol.* **15**, 381 (2007).
3. C. H. Johnson, in *Methods in Enzymology*, M. W. Young, Ed. (Academic Press, New York, 2005), vol. 393, pp. 818–837.
4. T. Kondo *et al.*, *Proc. Natl. Acad. Sci. U.S.A.* **90**, 5672 (1993).
5. I. Mihalcescu, W. Hsing, S. Leibler, *Nature* **430**, 81 (2004).
6. T. Mori, B. Binder, C. H. Johnson, *Proc. Natl. Acad. Sci. U.S.A.* **93**, 10183 (1996).
7. T. Kondo *et al.*, *Science* **275**, 224 (1997).
8. T. Mori, C. H. Johnson, *J. Bacteriol.* **183**, 2439 (2001).
9. Y. Liu *et al.*, *Genes Dev.* **9**, 1469 (1995).
10. M. Katayama, N. F. Tsinoremas, T. Kondo, S. S. Golden, *J. Bacteriol.* **181**, 3516 (1999).
11. R. M. Smith, S. B. Williams, *Proc. Natl. Acad. Sci. U.S.A.* **103**, 8564 (2006).
12. M. A. Woelfle, Y. Xu, X. Qin, C. H. Johnson, *Proc. Natl. Acad. Sci. U.S.A.* **104**, 18819 (2007).
13. N. Takai *et al.*, *Proc. Natl. Acad. Sci. U.S.A.* **103**, 12109 (2006).
14. J. R. Chabot, J. M. Pedraza, P. Luitel, A. van Oudenaarden, *Nature* **450**, 1249 (2007).
15. M. Ishiura *et al.*, *Science* **281**, 1519 (1998).
16. M. Egli, R. Pattanayek, S. Pattanayek, in *Models, Mysteries and Magic of Molecules*, J. C. A. Boeyens, J. F. Ogilvie, Eds. (Springer, Dordrecht, Netherlands, 2007), pp. 283–299.
17. S. Ye, I. Vakonakis, T. R. Ioerger, A. C. LiWang, J. C. Sacchettini, *J. Biol. Chem.* **279**, 20511 (2004).
18. K. Hitomi, T. Oyama, S. Han, A. S. Arvai, E. D. Getzoff, *J. Biol. Chem.* **280**, 19127 (2005).
19. R. G. Garces, N. Wu, W. Gillon, E. F. Pai, *EMBO J.* **23**, 1688 (2004).
20. I. Vakonakis *et al.*, *Proc. Natl. Acad. Sci. U.S.A.* **101**, 1479 (2004).
21. R. Pattanayek *et al.*, *Mol. Cell* **15**, 375 (2004).
22. M. Nakajima *et al.*, *Science* **308**, 414 (2005).
23. H. Ito *et al.*, *Nat. Struct. Mol. Biol.* **14**, 1084 (2007).
24. Y. Xu *et al.*, *Proc. Natl. Acad. Sci. U.S.A.* **101**, 13933 (2004).
25. T. Nishiwaki *et al.*, *Proc. Natl. Acad. Sci. U.S.A.* **101**, 13927 (2004).
26. H. Iwasaki, T. Nishiwaki, Y. Kitayama, M. Nakajima, T. Kondo, *Proc. Natl. Acad. Sci. U.S.A.* **99**, 15788 (2002).
27. Y. Xu, T. Mori, C. H. Johnson, *EMBO J.* **22**, 2117 (2003).
28. T. Nishiwaki *et al.*, *EMBO J.* **26**, 4029 (2007).
29. K. Terauchi *et al.*, *Proc. Natl. Acad. Sci. U.S.A.* **104**, 16377 (2007).
30. H. Kageyama *et al.*, *Mol. Cell* **23**, 161 (2006).
31. T. Mori *et al.*, *PLoS Biol.* **5**, e93 (2007).
32. I. Vakonakis, A. C. LiWang, *Proc. Natl. Acad. Sci. U.S.A.* **101**, 10925 (2004).
33. R. Pattanayek *et al.*, *EMBO J.* **25**, 2017 (2006).
34. R. Pattanayek *et al.*, *EMBO J.* **27**, 1767 (2008).
35. M. J. Rust, J. S. Markson, W. S. Lane, D. S. Fisher, E. K. O'Shea, *Science* **318**, 809 (2007).
36. F. Hayashi *et al.*, *Biochem. Biophys. Res. Commun.* **316**, 195 (2004).
37. Y. Kitayama, H. Iwasaki, T. Nishiwaki, T. Kondo, *EMBO J.* **22**, 2127 (2003).
38. Y. I. Kim, G. Dong, C. W. Carruthers, S. S. Golden, A. LiWang, *Proc. Natl. Acad. Sci. U.S.A.* **105**, 12825 (2008).
39. Y. Nakahira *et al.*, *Proc. Natl. Acad. Sci. U.S.A.* **101**, 881 (2004).
40. J. Tomita, M. Nakajima, T. Kondo, H. Iwasaki, *Science* **307**, 251 (2005).
41. Y. Xu, T. Mori, C. H. Johnson, *EMBO J.* **19**, 3349 (2000).
42. Y. Kitayama, T. Nishiwaki, K. Terauchi, T. Kondo, *Genes Dev.* **22**, 1513 (2008).
43. G. Huang *et al.*, *Genes Dev.* **21**, 3283 (2007).
44. M. Gallego, D. M. Virshup, *Nat. Rev. Mol. Cell Biol.* **8**, 139 (2007).


45. We thank our colleagues and coauthors at Vanderbilt University, especially M. Byrne, T. Mori, X. Qin, R. Pattanayek, S. Pattanayek, D. Williams, M. Woelfle, and Y. Xu. We also thank T. Kondo, S. Golden, M. Ishiura, and their laboratory members whose seminal contributions continue to make the study of cyanobacterial clocks fascinating. Supported by funds from the NIH, specifically the National Institute of General Medical Sciences (grant GM067152 to C.H.J. and grant GM073845 to M.E.). Additional support from the NIH (grant F32 GM71276 to D. R. Williams in the Stewart laboratory) is gratefully acknowledged.


### Supporting Online Material

www.sciencemag.org/cgi/content/full/322/5902/697/DC1
Figs. S1 to S3
References

10.1126/science.1150451

# *Wolbachia* and Virus Protection in Insects

Lauren M. Hedges, Jeremy C. Brownlie, Scott L. O'Neill, Karyn N. Johnson*

*Wolbachia pipientis* are maternally transmitted, Gram-negative, obligate intracellular bacteria found in filarial nematodes, crustaceans, arachnids, and at least 20% of all insect species. Many *Wolbachia* bacteria increase their prevalence in populations by manipulating host reproductive systems (*1*). Insects are also commonly infected with viruses, and, considering the shared intracellular location, it is possible that *Wolbachia* may influence the outcome of virus infection in an insect host.

*Drosophila melanogaster* is commonly infected with *Wolbachia* and is a powerful model for studying host-pathogen interactions and antiviral responses (*2*). *Drosophila C virus* (DCV), a member of the *Dicistroviridae* family, is a natural pathogen of *D. melanogaster* and is found in 30 to 40% of both laboratory and wild-caught populations (*3*, *4*). Infection of adult *Drosophila* with DCV by injection can result in 100% mortality within 3 to 4 days. Although variation in susceptibility of fly strains to DCV-induced mortality has been recorded (*3*), the underlying basis for this variation has not been determined.

We compared the survival of flies infected with DCV in the presence or the absence of *Wolbachia* infection (Fig. 1 and fig. S1) (*5*). In flies from the standard laboratory strain, Oregon RC, *Wolbachia* infection delayed DCV-induced mortality compared with Oregon RC flies cured of *Wolbachia* infection (Fig. 1A). The delay in mortality corresponded with a delay in virus accumulation in *Wolbachia*-infected flies (fig. S2). The experiment was repeated with the fly strain $w^{1118}$ with similar results observed (Fig. 1B). The survival curves of Oregon RC and $w^{1118}$ *Wolbachia*-free flies were similar to those of two wild-type laboratory populations (Champetières and Oregon R) that are naturally uninfected with *Wolbachia* (compare Fig. 1, A and B, with fig. S1). Oregon RC and $w^{1118}$ flies are infected with two closely related strains of *Wolbachia*, *w*MelCS and *w*MelPop, respectively (*6*). These results indicate that these strains of *Wolbachia*, in different genetic backgrounds of *Drosophila*, have an antiviral effect.

Two further viruses were tested with use of the survival bioassay: *cricket paralysis virus* (CrPV; *Dicistroviridae*), a natural *Drosophila* pathogen, and *Flock House virus* (FHV; *Nodaviridae*). The latter is unrelated to DCV and CrPV and is pathogenic in adult flies (*7*), although natural infections have not been reported. Like DCV, both CrPV and FHV induce rapid mortality when injected into adult *Drosophila*. All Oregon RC flies infected with *Wolbachia* and CrPV died within 17 days postinfection (Fig. 1C). In contrast, the *Wolbachia*-free Oregon RC flies died within 7 days of infection. Similarly, *Wolbachia*-free flies challenged with FHV died within 8 days of infection, whereas 26 days postinfection only 35% of the *Wolbachia*-infected flies had succumbed to FHV-induced mortality (Fig. 1D). These results indicate that the antiviral effect observed in *Wolbachia*-infected *Drosophila* functions to protect flies from diverse RNA viruses.

Typically *Wolbachia* manipulate host reproductive systems to increase the number of infected hosts within a population. However, *Wolbachia* strains that infect *D. melanogaster* do not induce these parasitic traits under field conditions at levels sufficient to invade host populations (*8*). Theory predicts that in the absence of strong reproductive parasitism *Wolbachia* should confer a fitness benefit to the host, but for *D. melanogaster* no such benefit has been identified in nature (*8*). Because both DCV and *Wolbachia* are common in wild *Drosophila* populations, the association of *Wolbachia* with a robust antiviral effect may confer a positive selective advantage to flies. If generalized, the antiviral protection associated with *Wolbachia* infection might be exploited in future strategies to reduce insect-transmitted diseases.

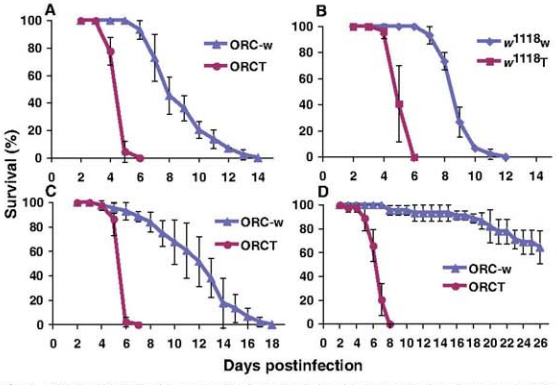


**Fig. 1.** Infection with *Wolbachia* protects flies from virus-induced mortality. The data shown represent the mean of triplicates, and the bars indicate standard error. The survival curves were significantly different for *Wolbachia* infected versus uninfected flies (Kaplan-Meier analysis, $P < 0.0001$ in each case). **(A)** Comparison of the survival of *Wolbachia*-infected (ORC-w) and uninfected Oregon RC (ORCT) flies after challenge with DCV. **(B)** Comparison of the survival of *Wolbachia*-infected (w) and uninfected (T) $w^{1118}$ flies after challenge with DCV. **(C)** Comparison of the survival of *Wolbachia*-infected (ORC-w) and uninfected Oregon RC (ORCT) flies after challenge with CrPV. **(D)** Comparison of the survival of *Wolbachia*-infected (ORC-w) and uninfected Oregon RC (ORCT) flies after challenge with FHV.


**References and Notes**

1. S. L. O'Neill, A. A. Hoffmann, J. H. Werren, *Influential Passengers: Inherited Microorganisms and Arthropod Reproduction* (Oxford Univ. Press, Oxford, 1997).
2. S. Cherry, N. Silverman, *Nat. Immunol.* **7**, 911 (2006).
3. G. Brun, N. Plus, in *The Genetics and Biology of Drosophila*, M. Ashburner, T. F. R. Wright, Eds. (Academic Press, New York, 1980), vol. 2D, pp. 625–702.
4. K. N. Johnson, P. D. Christian, *J. Gen. Virol.* **79**, 191 (1998).
5. Materials and methods are available as supporting material on *Science* Online.
6. M. Riegler, M. Sidhu, W. J. Miller, S. L. O'Neill, *Curr. Biol.* **15**, 1428 (2005).
7. X. H. Wang *et al.*, *Science* **312**, 452 (2006); published online 22 March 2006 (10.1126/science.1125694).
8. A. A. Hoffmann, M. Hercus, H. Dagher, *Genetics* **148**, 221 (1998).


9. We thank M. Riegler for advice and E. McGraw and F. Pringle for critical reading of the manuscript. This work was supported by funding from The University of Queensland, Australian Research Council, and the Foundation for the National Institutes of Health through the Grand Challenges in Global Health Initiative.


**Supporting Online Material**

www.sciencemag.org/cgi/content/full/322/5902/702/DC1
Materials and Methods
Figs. S1 and S2


26 June 2008; accepted 29 August 2008
10.1126/science.1162418



School of Integrative Biology, The University of Queensland, Brisbane 4072, Australia.

*To whom correspondence should be addressed. E-mail: karynj@uq.edu.au

# Aneuploidy Affects Proliferation and Spontaneous Immortalization in Mammalian Cells

Bret R. Williams,[1,2] Vineet R. Prabhu,[1] Karen E. Hunter,[1,2]* Christina M. Glazier,[1,2] Charles A. Whittaker,[1] David E. Housman,[1] Angelika Amon[1,2]†

Aneuploidy, an incorrect number of chromosomes, is the leading cause of miscarriages and mental retardation in humans and is a hallmark of cancer. We examined the effects of aneuploidy on primary mouse cells by generating a series of cell lines that carry an extra copy of one of four mouse chromosomes. In all four trisomic lines, proliferation was impaired and metabolic properties were altered. Immortalization, the acquisition of the ability to proliferate indefinitely, was also affected by the presence of an additional copy of certain chromosomes. Our data indicate that aneuploidy decreases not only organismal but also cellular fitness and elicits traits that are shared between different aneuploid cells.

Numerical alterations in an organism's karyotype, a condition known as aneuploidy, is associated with developmental abnormalities in all species examined to date. Studies in budding yeast (*1*), fission yeast (*2*, *3*), *Drosophila* (*4*), maize (*5*), rice (*6*), and mice (*7*, *8*) showed that aneuploidy interferes with organismal fitness and development. In humans as well, aneuploidy is detrimental, representing the major cause of mental retardation and miscarriages (*9*, *10*). However, aneuploidy is also a characteristic of the disease of uncontrolled proliferation, cancer. This raises the question: If aneuploidy is so deleterious, why are most solid tumors aneuploid? We thus examined the consequences of aneuploidy on cell proliferation and physiology by generating four primary mouse cell lines that carry an additional chromosome. Aneuploidy was detrimental at the cellular level, causing a slowing of cell proliferation and changes in cellular metabolism. We speculate that tumor development requires the acquisition of aneuploidy-tolerating mutations and propose that the mechanisms that elicit the traits shared by aneuploid cells are ideal targets for cancer therapeutics.

**Generation of mouse embryonic fibroblasts trisomic for chromosome 1, 13, 16, or 19.** To determine the effects of an additional chromosome on murine-cell physiology, we generated mouse embryonic fibroblast (MEF) lines that carried an additional chromosome (trisomic MEFs). We used a breeding scheme to obtain trisomic (Ts) embryos (fig. S1) (*10*). Mice that were homozygous for a Robertsonian translocation [for example, a fusion between chromosomes 6 and 16 (strain A)] were crossed with a strain homozygous for a second Robertsonian translocation [for example, between chromosomes 16 and 17 (strain B)]. From this cross, male offspring were selected that carried both Robertsonian translocations (compound heterozygotes) and mated to wild-type mice lacking any Robertsonian translocation. Between 7 to 40% of the resulting progeny [the exact percentage depended on the strain background, stage of embryogenesis analyzed, and identity of the translocation chromosome (*8*)] were trisomic for the chromosome common to the two Robertsonian translocations because of a meiotic nondisjunction event in the male germline.

With the exception of mice trisomic for chromosome (Chr) 19 (Ts19), of which a small percentage of embryos developed to term and survived for a short period of time, trisomic embryos died in utero. However, many of these embryos developed past embryonic day 10.5, allowing for the generation of MEF lines (*7*). We used mice that carried different combinations of Robertsonian translocations to generate embryos trisomic for chromosome 1, 13, 16, or 19. We chose these four chromosomes because they cover a large portion of the size and coding spectrum of mouse chromosomes [Chr1, 197 mega–base pairs (Mbp) and 1228 genes; Chr13, 120 Mbp and 843 genes; Chr16, 98 Mbp and 678 genes; Chr19, 61 Mbp and 734 genes] (*11*).

Initially, trisomic embryos were identified by their distinctive morphology. They developed more slowly than their euploid littermates and many exhibited nuchal edema and other developmental abnormalities (Fig. 1A) (*7*). To verify that the embryos were indeed trisomic for a particular chromosome, we counted the number of chromosome arms in preparations of spread metaphase chromosomes from early-passage (≤2 passages) MEF cultures generated from the trisomic embryos (*12*). We also used spectral karyotype analysis (SKY), which identifies each chromosome by a unique fluorescent color, to confirm that the cell lines generated were trisomic for a single specific chromosome and that other changes in chromosomal composition had not occurred, at least during the early stages of cell culture (Fig. 1B).

**Gene expression from the additional chromosomes is proportional to gene copy number.** The presence and consequence of an additional chromosome in MEFs was further determined by a genomewide transcript-expression analysis. Total RNA was isolated from passage 2 cultures (*12*). Overall, gene expression changed according to gene copy number, with expression of genes present on Chr16 increasing by on average 152% in cells trisomic for this chromosome ($n = 3$ independent cell lines) (Fig. 1C and table S1). The expression of genes on Chr13 increased on average 146% in Ts13 cell lines ($n = 4$ independent cell lines), the expression of genes on Chr1 increased an average of 155% in a Ts1 cell line ($n = 1$ cell line), and the expression of genes on Chr19 increased on average 151% in a single Ts19 cell line ($P \leq 10^{-74}$ for all cell lines, Student's $t$ test) (Fig. 1C and table S1). The approximate 150% increase in gene expression of genes present on the trisomic chromosome indicates that the genes present on the additional chromosome are transcribed, which is consistent with expression profiles obtained from patients with Down syndrome (*13*). Comparison of the expression patterns of the different trisomic cell lines did not reveal genes that showed increased or decreased expression in all four different trisomic MEFs (tables S1 and S2), which suggests that a gene-expression pattern common to all aneuploid cell lines does not exist. We conclude that the majority of the genes present on the additional chromosome are expressed. Thus, dosage compensation at the transcriptional level does not occur in these cells.

**Proliferation defects of aneuploid cells.** We next examined the ability of trisomic MEFs to proliferate in culture. We used four independent cell lines trisomic for either Chr13, Chr16, or Chr19 and three independent cell lines trisomic for Chr1. These trisomic cell lines were compared with cell lines derived from euploid littermates, which, because of the breeding scheme, carried a single Robertsonian translocation.

We seeded MEFs, kept for a short time in culture (we used MEFs at passage 3 to ensure that both the euploid and trisomic cells were karyotypically consistent with those of the embryo) on multiple plates, and the number of cells present in the wells was counted for 7 or 9 days. In these accumulation assays, the medium was changed every other day (figs. S2A and S3A) or cells were kept in the same medium for the entire experiment (Fig. 2A and fig. S3B) (*12*). In both fed and unfed euploid cultures, cell

[1]David H. Koch Institute for Integrative Cancer Research, Massachusetts Institute of Technology (MIT), Cambridge, MA 02139, USA. [2]Howard Hughes Medical Institute, MIT, E17-233, 40 Ames Street, Cambridge, MA 02139, USA.

*Present address: Gerstner Sloan-Kettering Graduate School of Biomedical Sciences, Memorial Sloan-Kettering Cancer Center, 1275 York Avenue, New York, NY 10065, USA.

†To whom correspondence should be addressed. E-mail: angelika@mit.edu

number increased during the first 5 to 7 days and then remained constant thereafter. The trisomic cell lines behaved similarly to the wild-type cells over the first two days of the experiment. However, after the initial two days, proliferation of the trisomic cells decreased as compared with that of euploid controls. The decrease in proliferative capacity was severe in Ts1 and Ts13 cells but less dramatic and more variable though still statistically significant in Ts16 and Ts19 cells (Figs. 2A and 3D and figs. S2A; S3, A and B; and S4A). Thus, the presence of an additional chromosome inhibits cell proliferation in culture. This reduced proliferation appears to be more pronounced as the size of the additional chromosome increases.

The trisomic cell lines analyzed carried two Robertsonian translocations (Fig. 1B and fig S1). To test the possibility that the Robertsonian translocations rather than the presence of an extra chromosome caused the proliferation defect, we analyzed euploid cell lines that harbored 0, 1, or 2 Robertsonian translocations. The presence of Robertsonian chromosomes did not affect cell proliferation regardless of whether the medium was changed or not (fig. S5A). We conclude that the presence of an additional chromosome, not the chromosomal fusion, reduced cell proliferation.

**Cell volume is increased in trisomic cells.** During the establishment of MEF cultures, we observed that the average size of trisomic cells was increased (*12*). This was not caused by an increase in the breadth of the size distribution but was due to a shift in the distribution of the cell size toward a larger average size (Figs. 2, B and C, and 3D and figs. S2, B and C; S3, C and D; and S4B). The increase in cell volume was readily detectable by passage 3, the beginning of the proliferation experiment, in all trisomic lines, and persisted and sometimes even increased during the course of the experiment (Fig. 2B and figs. S2B and S3C). As observed in the cell proliferation analysis, the increase in cell volume was more pronounced in cells carrying an extra copy of the larger chromosomes (Ts1 and Ts13 cells) and was less dramatic and variable but nevertheless statistically significant in cells carrying an extra copy of the smaller chromosomes 16 or 19 (Figs. 2C and 3D and figs. S2B, S3C, and S4B). Analysis of euploid cells with 0, 1, or 2 Robertsonian translocations showed that this increase in cell volume was not due to the presence of fusion chromosomes but to the presence of the additional chromosome (fig. S5B).

Because proliferation of primary MEFs is inhibited when the cells come into close contact with one another (*14*), the increased size of trisomic MEFs raised the possibility that the lower cell number observed in these cultures resulted from earlier contact inhibition rather than a decreased ability to proliferate. To test this possibility, we calculated the cumulative cell volume (CCV) by multiplying the cell number by the average cell volume. If a larger cell size and thus earlier contact inhibition was responsible for the decreased cell number in trisomic cultures, the CCV should be the same in wild-type and trisomic cell lines. This was not the case. Trisomic cell lines produced less CCV than euploid controls. This defect was pronounced in cell cultures trisomic for Chr1 or Chr13, more subtle and variable but nevertheless statistically significant in cell cultures trisomic for Chr16, and not detectable in cells trisomic for Chr19 (Figs. 2D and 3D and figs. S2D, S3E, and S4C). Our results indicate that the CCV of cultures trisomic for chromosome 1, 13, or 16 is less than that of euploid controls. Analysis of euploid cells with 0, 1, or 2 Robertsonian translocations showed that this decrease in CCV was not due to the presence of fusion chromosomes but to the presence of the additional chromosome (fig. S5C). We conclude that the reduced cell accumulation in trisomic

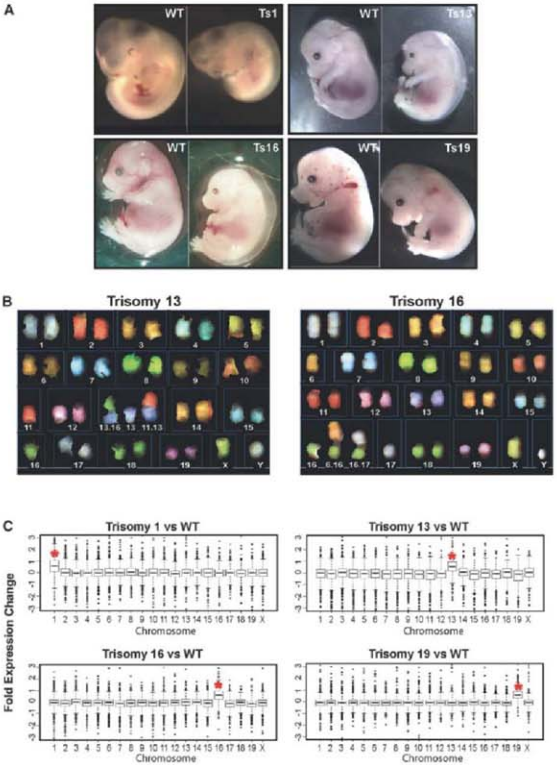


**Fig. 1.** Generation of trisomic embryos and MEF cell lines. **(A)** Ts embryos were recovered by timed matings. The trisomy 1 (Ts1) embryo was recovered at 10.5 days after coitus. Ts13, Ts16, and Ts19 embryos were recovered at 14.5 or 15.5 after coitus. In all instances, Ts embryos were identified by their developmental abnormalities and reduced size (*7*). **(B)** Examples of SKY analysis of metaphase spreads prepared from early passage (≤p3) Chr13 and Chr16 trisomic MEFs. Chromosomes and Robertsonian translocations are identified. **(C)** Gene-expression pattern of aneuploid cell lines and lines from euploid littermate controls (*12*). Transcripts were binned by chromosome and the average gene expression/total chromosome is shown. The asterisk indicates the identity of the trisomic chromosome. The increase in gene expression was highly significant ($P \leq 1 \times 10^{-74}$, all trisomies, Student's *t* test).

cultures is due to proliferation defects. These defects are more severe in cells carrying an extra copy of larger chromosomes.

To examine whether the cell proliferation defect observed in trisomic cells arose from delays in a specific cell-cycle stage, we compared the DNA content between asynchronously growing trisomic and euploid MEFs (*12*). The flow cytometric profile was similar in the trisomic cells and euploid controls examined (Fig. 2E and fig. S3F). Neither cell lysis, as judged by the presence of large amounts of cellular debris in the cell volume determination (Fig. 2C and figs. S2C and S3D), nor senescence-associated β-galactosidase activity (fig. S6) was increased in trisomic cell lines. Cell proliferation was also impaired in primary cells from humans with Down syndrome (trisomy 21), but a specific cell-cycle defect was

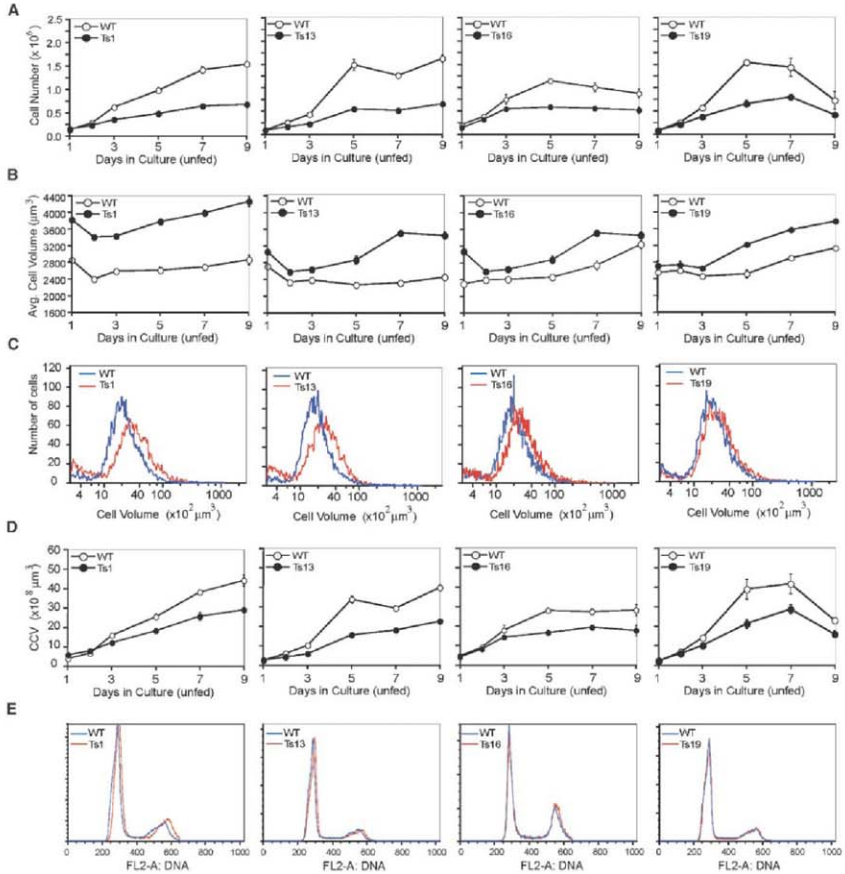


**Fig. 2.** Proliferation defects in trisomic MEFs. Wild-type (open circles) and Ts cells (solid circles) were plated and counted daily for cell number increase (*12*). Error bars are ±SD. The data for each column come from the same cell line. **(A)** Growth of early passage (p3) trisomic cells under "unfed" (medium was not changed) conditions. **(B** and **C)** Average cell volume of cells under growth conditions in which the medium was not changed [unfed (B)] and the distribution of cell volumes in the culture at day 5 of the accumulation assay (C). The low amounts of small-sized particles in (C) indicate that cells are not undergoing lysis. **(D)** Analysis of the CCV (number of cells times the average cell volume) during the proliferation assay in (A). Error bars are ±SD. **(E)** DNA content analysis of asynchronous wild-type and trisomic cells.

not observed either (*15*, *16*). It is possible that progression through the cell cycle is slowed overall in trisomic mouse and human cells. However, we favor the idea that specific cell-cycle defects exist but are too subtle to be detected in asynchronously growing cells. Although our results did not reveal a specific cell-cycle defect, they clearly show that aneuploidy hampers rather than promotes cell proliferation. Thus, during tumorigenesis, the aneuploid state of a cell would impair rather than accelerate the process.

**Altered metabolic properties of aneuploid cells.** Many metabolic pathways are altered in tumor cells (*17*). The trisomic MEFs we generated allowed us to examine whether the aneuploid state could contribute to these metabolic changes (*12*). We first analyzed the use of glucose, a carbon source of tissue culture cells, and of glutamine, another carbon source as well as a primary nitrogen source. To measure the amount of glucose and glutamine used by trisomic MEFs, we grew cells over 9 days

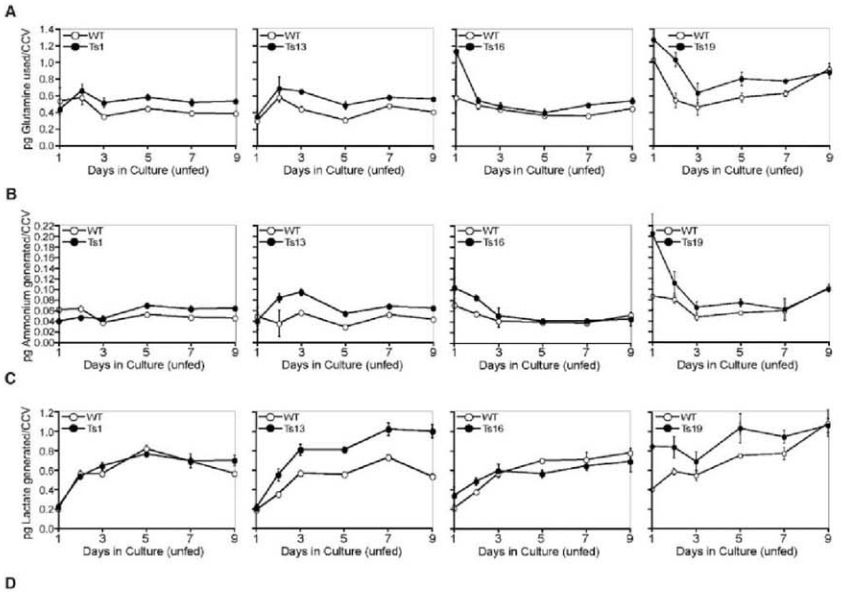


D

| Trisomy | Cell Lines | Proliferation | Cell Volume | CCV | Glucose/CCV | Glutamine/CCV | Glutamate/CCV | NH4+/CCV | Lactate/CCV |
|---|---|---|---|---|---|---|---|---|---|
| Ts1 | 3 | Reduced ($p<0.0001$) | Increased ($p<0.0001$) | Reduced ($p<0.0001$) | No change ($p=0.4667$) | Increased ($p<0.0001$) | Increased ($p<0.0001$) | Increased ($p<0.0001$) | Slightly Increased ($p=0.0585$) |
| Ts13 | 4 | Reduced ($p<0.0001$) | Increased ($p<0.0001$) | Reduced ($p<0.0001$) | Increased ($p=0.0400$) | Increased ($p<0.0001$) | Increased ($p<0.0001$) | Increased ($p<0.0001$) | Increased ($p<0.0001$) |
| Ts16 | 4* | Reduced ($p<0.0001$) | Increased ($p<0.0001$) | Reduced ($p=0.0012$) | No Change ($p=0.0513$) | Increased ($p<0.0001$) | Reduced ($p<0.0001$) | Increased ($p<0.0001$) | Increased ($p<0.0001$) |
| Ts19 | 4 | Reduced ($p=0.0253$) | Increased ($p<0.0001$) | No Change ($p=0.3918$) | No Change ($p=0.4667$) | Increased ($p<0.0001$) | Increased ($p<0.0001$) | Increased ($p=0.0005$) | Increased ($p<0.0001$) |

**Fig. 3.** Cellular metabolism in trisomic MEFs. (**A** to **C**) Tissue culture supernatants of proliferation experiments were subjected to metabolic analyses (*12*), and the amount of glutamine used (**A**) and ammonium (**B**) and lactate (**C**) generated per CCV was determined at the indicated times. The data for each column come from the same cell line. Error bars are ±SD. (**D**) The table summarizes the changes in cell proliferation, cell volume and CCV, as well as glucose and glutamine uptake and production of glutamate, ammonium, and lactate. These *P* values are shown for measurements of the proliferation assays. *P* values were determined through a two-way nested analysis of variance with standard statistical packages for values obtained for days 3, 5, and 7 (table S4). Values below $P = 0.05$ were interpreted to mean that the values obtained were either significantly increased or reduced. *P* values of >0.06 were interpreted to mean no difference between the Ts line and the wild type. The asterisk denotes that the cell number, cell volume, and CCV was determined for four trisomy 16-cell lines, whereas the metabolic analyses were performed with three Ts16 lines.

without changing the medium and then measured the amount of glucose and glutamine per CCV remaining in the medium (*12*). Glucose consumption was slightly increased in cells trisomic for chromosome 13 but was not affected in other trisomic cell lines (Fig. 3D and fig. S7, A and C). In contrast, glutamine consumption was increased in all trisomic cell lines. It was higher in cells trisomic for chromosome 1 and 13 and slightly though statistically significantly increased in cells carrying an extra copy of chromosome 16 or 19 (Fig. 3, A and D, and figs. S7C and S8A).

We also examined the production of the metabolites ammonium, glutamate, and lactate per CCV. Ammonium and glutamate are produced by the degradation of glutamine in tissue culture cells. Additionally, ammonium is produced as a result of the breakdown of amino acids because of higher rates of autophagy or perturbations in amino acid metabolism. We observed an increase in the production of ammonium in all trisomic cell lines (Fig. 3, B and D, and figs. S7C and S8B). Glutamate production was increased in Ts1, 13, and 19 cells but reduced in Ts16 cells (Fig. 3D and figs. S7, B and C, and S8C), which indicates that production of not all metabolites is increased in all trisomic cells. Lactate is produced when pyruvate accumulates in cells as a result of an increase in glycolysis, defects in mitochondrial function, the disruption of pyruvate import into the mitochondria, or an increased activity of lactate dehydrogenase. Lactate production was slightly though statistically significantly increased in Ts13, Ts16, and Ts19 cell cultures and was approaching significance in Ts1 cultures (Fig. 3, C and D, and fig. S8D). The changes in metabolism observed in aneuploid cells were specific to the presence of an additional chromosome and not to the Robertsonian fusion event. Analysis of euploid cells carrying 0, 1, or 2 Robertsonian translocations showed that the changes in metabolism were not due to the presence of fusion chromosomes in cells, because all the characteristics were indistinguishable between these cell lines (fig. S5D).

We conclude that primary aneuploid cells display alterations in glutamine use and the production of ammonium and lactate and speculate that these phenotypes may reflect a general alteration in energy production in the aneuploid cells. An increase in lactate production was first described nearly 100 years ago by Otto Warburg in Flexner-Jobling's rat carcinomas (*18*). It is now clear that many aspects of cellular metabolism are altered in tumor cells. Our results raise the possibility that one (but by no means the only) cause of the metabolic alterations observed in tumor cells is their aneuploid state.

**Effects of trisomy on immortalization.** Aneuploidy is a characteristic of many tumors and has been proposed to play a key role in promoting tumorigenesis (*19*). Consistent with this idea is the observation that the occurrence of acute lymphoblastic leukemia and acute megakaryoblastic leukemia is greatly increased in Down syndrome patients (*20*). However, the incidence of many solid tumors in these individuals is only half of that in the normal population, raising the possibility that aneuploidy also restricts the formation of certain tumors (*21*, *22*). Studies of mouse mutants that result in an increased frequency of aneuploidy also revealed mixed results. A mouse model in which chromosome mis-segregation was induced by the inactivation of a component of the chromosome segregation machinery (centromere protein E) indicated that aneuploidy acts in an oncogenic manner in some cell types but inhibits tumorigenesis in others (*23*). Random aneuploidy caused by transient overexpression of Mad2 in the mouse appears to initiate tumor formation only in certain cell types (*24*). A mouse model expressing a hypomorphic allele of the spindle-assembly checkpoint protein BubR1 displays progressive aneuploidy and exhibits an accelerated aging phenotype but without an increased incidence of tumorigenesis (*25*). Finally, segmental trisomy reduces the number of tumors in the colon cancer adenomatosis polyposis coli (APC) multiple intestinal neoplasia ($APC^{Min}$) mouse model (*26*). Thus, it is unclear whether aneuploidy inhibits or promotes tumorigenesis or does both. The primary trisomic cell lines we generated allowed us to begin to address this question and test the possibility that the identity of the additional chromosome determines whether aneuploidy promotes or inhibits tumor formation. We did this by examining the effects of specific additional chromosomes on immortalization induced by serial passage in vitro. Although it is clear that in vitro immortalization does not recapitulate all aspects of tumorigenesis, it is in most cases accompanied by two important characteristics of many solid tumors: (i) loss of p53 tumor suppressor pathway function and (ii) aneuploidy (*27*).

MEFs can be serially passaged, and after a period of reduced proliferation these cells will spontaneously overcome this period of reduced growth (*27*). This process of serial passaging until the culture fails, or until a subpopulation acquires the ability to grow indefinitely (which is usually caused by loss of p53 function), is referred to as a 3T3 protocol (*27*). We cultured four Ts16, three Ts13, and three Ts19 cell lines, and one Ts1 cell line in parallel with littermate euploid controls through serial passages, to analyze the number of passages required for trisomic MEFs to generate immortalized cells (*12*). To determine the passage at which immortalization occurred, we fit the population doublings for each culture to a double-linear fit model (*12*); the point at which the two lines intersect represents the passage by which immortalization had occurred. Immortalization was delayed in cell lines trisomic for Chr16. One line failed to immortalize and 3 lines showed a significant delay in the process as judged by their passage number ($P \leq 0.04$, Student's $t$ test) (Fig. 4, A and B). In the trisomic cell lines that spontaneously immortalized, immortalization required on average 39 (±4, SD) passages as compared with 30 (±4, SD) passages in matched euploid cultures (Fig. 4, A and B). Thus, the presence of an extra copy of Chr16 hampers

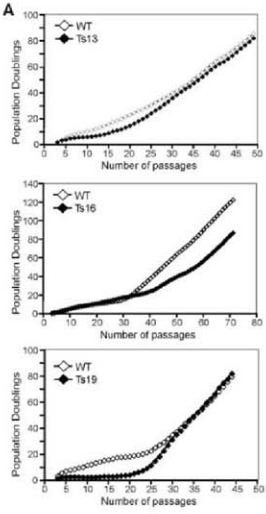


B

| Cell line | N | Passage | Std Dev. | p value (t test) |
|---|---|---|---|---|
| WT | 3 | 26.3 | 3.3 | 0.58 |
| Ts13 | 3 | 22.8 | 9.6 | |
| WT | 3 | 30.0 | 4.3 | 0.04 |
| Ts16 | 3 | 39.3 | 3.5 | |
| WT | 3 | 23.6 | 3.5 | 0.49 |
| Ts19 | 3 | 21.6 | 3.1 | |

**Fig. 4.** Rates of spontaneous immortalization of primary aneuploid MEFs. **(A)** Cells were serially passed in a 3T3 immortalization assay (*12*), and the number of population doublings are shown as a function of the number of passages. **(B)** The mean number of passages (passage) until immortalization was calculated, as described (*12*). The standard deviations are shown in the column to the right. *P* values are given in the last column. The average number of passages until immortalization for the Ts16 cell lines does not include the Ts16 cell line that failed to immortalize. For Ts19, two of the three immortalization assays were performed in independent experiments with cells obtained from the same embryo.

spontaneous immortalization. The one cell line that was trisomic for Chr1 failed to immortalize (fig. S9), which raises the possibility that an extra copy of Chr1 also antagonizes immortalization.

In contrast to cell cultures trisomic for chromosome 16 or 1, the number of passages necessary to achieve spontaneous immortalization was similar in control and Ts13 cell lines with 26 (±3, SD) passages in Ts13 as compared with 23 (±9, SD) passages in euploid cultures (Fig. 4, A and B). The number of passages was also indistinguishable from the euploid controls for the Ts19 cell lines analyzed. Ts19 cell lines required 22 (±3, SD) passages, whereas the euploid counterparts immortalized at 24 (±4, SD) passages (Fig. 4, A and B). These results indicate that although proliferation is slower in cells trisomic for chromosome 13 or 19, immortalization occurs after a similar number of passages as compared with that in the wild type. In fact, when the time of immortalization is described as a function of population doublings, Ts13 cells immortalize earlier than in wild-type controls. On average only 12 (±5, SD) doublings were necessary to immortalize Ts13 cell lines as compared with 27 (±8, SD) doublings in euploid controls ($P \leq 0.05$, Student's $t$ test). Our results indicate that aneuploidy affects the rate of immortalization in MEFs and this effect depends on the identity of the extra chromosome. These findings imply that the immortalization barrier caused by the proliferation defect due to aneuploidy (with perhaps the exception of that in Ts1) can eventually be overcome. The difference in the efficiency with which various trisomic lines overcome the proliferation barrier indicates that the underlying mechanism might differ in the individual aneuploid cell lines. However, once immortalized, trisomic cells do not consistently differ from immortalized euploid cells in their chromosome number. All immortalized trisomic and euploid cell lines were near tetraploid (table S3), which suggests that once immortalization occurs the degree of aneuploidy does not differ between euploid and trisomic cell lines.

**Discussion.** Our analysis of MEFs, each containing a different additional chromosome, revealed that in addition to chromosome-specific traits, the four trisomic MEFs share characteristics such as a cell-proliferation delay and an altered metabolism. MEFs carrying hypomorphic mutations in the spindle-checkpoint component BubR1 frequently carry one or two extra chromosomes, and their proliferation is also impaired (*25*), which indicates that at least the defect in cell proliferation is shared among different types of aneuploidies in the mouse. Primary foreskin fibroblasts of individuals with Down syndrome also exhibited a proliferation delay and an increase in cell volume (*16*, *28*), which suggests that aneuploidy may also hamper proliferation in human cells. In budding yeast, the proliferation defects of aneuploid cells is caused by imbalances in intracellular protein composition due to expression of genes on the additional chromosome (*1*). Because the genes present on the additional chromosome are also transcribed in the trisomic MEFs, and thus are probably also translated, the same could be true in mouse cells.

Most solid tumors are aneuploid. Our results and that of others indicate that aneuploidy suppresses rather than enhances tumorigenesis. We found that the presence of an extra chromosome hampered cell proliferation. There is also evidence to suggest that at least human Ts21 cells do not proliferate as well as euploid cells, either (*28*). Also, the percentage of cells undergoing DNA replication in solid tumors, which are mostly aneuploid, varies between 2 to 8%, whereas a normal renewing epithelium such as the intestine exhibits a DNA replication index of approximately 16% (*29*). Furthermore, individuals carrying an extra copy of chromosome 21 have a 50% lower probability of developing solid tumors than do individuals with the correct chromosome number (*21*, *22*). Segmental trisomy in the mouse has been shown to reduce incidence of neoplasia in the sensitized $APC^{Min}$ genetic background (*26*). Additionally, mouse models in which low-level aneuploidy was induced through interference with the chromosome segregation machinery prevented tumor formation in many tissues and caused tumor formation only relatively late in others (*23*–*25*).

A few findings, however, argue for a cancer-promoting role of aneuploidy. Loss of heterozygosity, which can arise from chromosome loss or aneuploidy, is detected in atypical ductal hyperplasias, which can be precursors of breast cancer (*30*) and in small (2 mm in diameter) adenomas, which are thought to represent early-stage colon cancers (*31*–*33*). Finally, even though tumors form late in mice carrying a low-level aneuploidy-inducing mutation, they do occur with an increased frequency in some tissues.

How can we reconcile these results? We propose that aneuploidy is a barrier toward tumorigenesis, but the very events that cause aneuploid cells to proliferate slowly, the cellular imbalances caused by aneuploidy and the stresses it is associated with, might promote tumorigenesis in a small fraction of aneuploid cells (*1*). The stresses associated with cellular imbalances could lead to an increase in mutation rate, gene amplification, and/or genomic instability. Precedents exist for all of these scenarios in bacteria, yeast, and tissue culture cells (*34*–*38*). Aneuploidy-tolerating and proliferation-promoting mutations could then eventually lead to the selection of tumor cells with a high proliferative capacity. Furthermore, aneuploidy would also shield the evolving tumor from lethal mutations. Thus, in a rather counterintuitive manner, as has been suggested for chemical carcinogens (*39*, *40*), the proliferation-inhibiting imbalances of aneuploidy may under some circumstances promote tumorigenesis.

Irrespective of whether or not aneuploidy can promote tumorigenesis, it is clear that aneuploidy causes a proliferative disadvantage in budding yeast (*1*), *Schizosaccharomyces pombe* (*2*, *3*), primary mouse cells (this study), and human cells (*28*). This property of aneuploidy functions as a barrier toward transformation, and this disadvantage must be overcome during tumorigenesis. Identifying mutations that can overcome the proliferation-inhibiting effects of aneuploidy may provide new pathways to exploit in cancer treatment. Given that most solid tumors are aneuploid, the cellular consequences of aneuploidy may also provide previously unidentified targets in cancer therapy. Characterizing the phenotypes associated with aneuploidy in human cells, as well as identifying small molecules that specifically target aneuploid cells, may provide new avenues in the treatment of cancer.

## References and Notes


1. E. M. Torres *et al.*, *Science* **317**, 916 (2007).
2. O. Niwa, Y. Tange, A. Kurabayashi, *Yeast* **23**, 937 (2006).
3. O. Niwa, M. Yanagida, *Curr. Genet.* **9**, 463 (1985).
4. D. L. Lindsley *et al.*, *Genetics* **71**, 157 (1972).
5. B. McClintock, *Genetics* **14**, 180 (1929).
6. K. Singh, D. S. Multani, G. S. Khush, *Genetics* **143**, 517 (1996).
7. A. P. Dyban, V. S. Baranov, *Cytogenetics of Mammalian Embryonic Development* (Oxford Univ. Press, New York, 1987).
8. A. Gropp, H. Winking, E. W. Herbst, C. P. Claussen, *J. Exp. Zool.* **228**, 253 (1983).
9. G. S. Pai, R. C. Lewandowski, D. S. Borgaonkar, *Handbook of Chromosomal Syndromes* (Wiley, New York, 2003).
10. A. Gropp, U. Kolbus, D. Giers, *Cytogenet. Cell Genet.* **14**, 42 (1975).
11. Chromosome size and coding gene statistics were obtained from the *National Center for Biotechnology Information* m37 mouse assembly; see www.ensembl.org/Mus_musculus/index.html.
12. Materials and methods are available as supporting material on *Science* Online.
13. R. Mao, C. L. Zielke, H. R. Zielke, J. Pevsner, *Genomics* **81**, 457 (2003).
14. M. Abercrombie, *Exp. Cell Res. Suppl.* **8**, 188 (1961).
15. K. Nielsen, M. Marcus, A. Gropp, *Hereditas* **102**, 77 (1985).
16. M. Rosner *et al.*, *J. Neurol Trans. Suppl.* **67**, 51 (2003).
17. R. Moreno-Sanchez, S. Rodriguez-Enriquez, A. Marin-Hernandez, E. Saavedra, *FEBS J.* **274**, 1393 (2007).
18. O. Warburg, K. Posener, E. Negelein, *Biochem. Z.* **152**, 309 (1924).
19. T. Boveri, *Verhandlungen der physikalisch-medizinischen Gesellschaft zu Würzburg Neu Folge* **35**, 67 (1902).
20. D. Satge *et al.*, *Am. J. Med. Genet.* **78**, 207 (1998).
21. H. Haase, L. H. Clemmensen, M. Mikkelsen, *Lancet* **355**, 165 (2000).
22. D. Satge, A. J. Sasco, B. Lacour, *Int. J. Cancer* **106**, 297 (2003).
23. B. A. Weaver, A. D. Silk, C. Montagna, P. Verdier-Pinard, D. W. Cleveland, *Cancer Cell* **11**, 25 (2007).
24. R. Sotillo *et al.*, *Cancer Cell* **11**, 9 (2007).
25. D. J. Baker *et al.*, *Nat. Genet.* **36**, 744 (2004).
26. T. E. Sussan, A. Yang, F. Li, M. C. Ostrowski, R. H. Reeves, *Nature* **451**, 73 (2008).
27. G. J. Todaro, H. Green, *J. Cell Biol.* **17**, 299 (1963).
28. D. J. Segal, E. E. McCoy, *J. Cell. Physiol.* **83**, 85 (1974).
29. I. Tannock, R. P. Hill, *The Basic Science of Oncology* (Pergamon Press, New York, 1987).
30. P. S. Larson *et al.*, *J. Pathol.* **209**, 307 (2006).
31. L. Bomme *et al.*, *Cancer Genet. Cytogenet.* **106**, 66 (1998).
32. L. Bomme *et al.*, *Int. J. Cancer* **92**, 816 (2001).
33. L. M. Shih *et al.*, *Proc. Natl. Acad. Sci. U.S.A.* **98**, 2640 (2001).
34. T. Edlund, S. Normark, *Nature* **292**, 269 (1981).
35. R. G. Ponder, N. C. Fonville, S. M. Rosenberg, *Mol. Cell* **19**, 791 (2005).
36. A. Selmecki, A. Forche, J. Berman, *Science* **313**, 367 (2006).
37. H. M. Sung, G. Yeamans, C. A. Ross, R. E. Yasbin, *J. Bacteriol.* **185**, 2153 (2003).
38. V. T. Mihaylova *et al.*, *Mol. Cell. Biol.* **23**, 3265 (2003).
39. E. Farber, *Biochem. Pharmacol.* **39**, 1837 (1990).

40. A. Haddow, *Acta Unio Int. Contra Cancrum* **3**, 342 (1938).
41. We thank E. Vazile in the Koch Institute Microscopy and Imaging Facility for help with SKY analysis; M. Luo in the MIT BioMicro Center for help with microarray analysis; L. Chan for assistance with the double linear fit models for immortalization kinetics; A. Regev and M. Guttman for advice and assistance with statistical analysis; and M. Dunham, M. Hemann, J. Lees, F. Solomon, and members of the Amon lab for critical reading of this manuscript. This work was supported by the Howard Hughes Medical Institute, a David Koch Research Award, a grant from the Curt W. and Kathy Marble Cancer Research Fund, and a David Koch Graduate Fellowship (V.R.P.). All microarray data are provided in final processed form in table S1 and as raw data through the Gene Expression Omnibus (www.ncbi.nlm.nih.gov/geo) under accession number GSE12501.

**Supporting Online Material**
www.sciencemag.org/cgi/content/full/322/5902/703/DC1
Materials and Methods
Figs. S1 to S9
Tables S1 to S4
References

5 May 2008; accepted 9 September 2008
10.1126/science.1160058

# Structure and Molecular Mechanism of a Nucleobase–Cation–Symport-1 Family Transporter

**Simone Weyand,[1,2,3]* Tatsuro Shimamura,[2,3,4]* Shunsuke Yajima,[2,3]*† Shun'ichi Suzuki,[5]*‡ Osman Mirza,[2]*§ Kuakarun Krusong,[2]‖ Elisabeth P. Carpenter,[1,2] Nicholas G. Rutherford,[5] Jonathan M. Hadden,[5] John O'Reilly,[5] Pikyee Ma,[5] Massoud Saidijam,[5,6] Simon G. Patching,[5] Ryan J. Hope,[5] Halina T. Norbertczak,[5] Peter C. J. Roach,[5] So Iwata,[1,2,3,4,7]¶ Peter J. F. Henderson,[5]¶ Alexander D. Cameron[1,2,3]**

The nucleobase–cation–symport-1 (NCS1) transporters are essential components of salvage pathways for nucleobases and related metabolites. Here, we report the 2.85-angstrom resolution structure of the NCS1 benzyl-hydantoin transporter, Mhp1, from *Microbacterium liquefaciens*. Mhp1 contains 12 transmembrane helices, 10 of which are arranged in two inverted repeats of five helices. The structures of the outward-facing open and substrate-bound occluded conformations were solved, showing how the outward-facing cavity closes upon binding of substrate. Comparisons with the leucine transporter $LeuT_{Aa}$ and the galactose transporter vSGLT reveal that the outward- and inward-facing cavities are symmetrically arranged on opposite sides of the membrane. The reciprocal opening and closing of these cavities is synchronized by the inverted repeat helices 3 and 8, providing the structural basis of the alternating access model for membrane transport.

Many membrane transporters are classified into three major groups. One group, the primary active transporters, uses the energy released from light, redox reactions, or adenosine triphosphate (ATP) hydrolysis to translocate substrates across the membrane. Another group, the secondary active transporters, uses the free energy stored in an ion gradient for substrate transport. A third group carries out facilitated diffusion without energy input. The kinetics and thermodynamics of all types of transporters can, in principle, be explained by the alternating access model of molecular transport (*1*, *2*). According to this model, a substrate-binding site located toward the center of the protein in the membrane has alternating access to either side of the membrane as a result of reciprocal opening and closing of cavities connecting the binding site to either side of the membrane. This model is well studied and was established for various transporters with use of kinetic and biochemical methods (*3*, *4*). For the P-type adenosine triphosphatases (ATPases) and the ATP binding cassette (ABC) transporters, the mechanism has also been studied on the basis of the structures of these proteins in various conformational states (*5*, *6*). Secondary transporters are biochemically well characterized, particularly lactose permease (*7*–*9*) and other members of the major facilitator superfamily (MFS) transporters (*10*, *11*), but here the structural basis of the alternating access mechanism is less well understood.

Here, we show how structural studies of the secondary active membrane transporter, Mhp1, from *Microbacterium liquefaciens* provide insight into the mechanism of alternating access. Mhp1 mediates the uptake of indolyl methyl- and benzyl-hydantoins into *M. liquefaciens*, as part of a metabolic salvage pathway for their conversion to amino acids (*12*). Mhp1 is a member of the so-called nucleobase–cation–symport-1, NCS1, family 2.A.39 (*13*, *14*) of transport proteins, which has at least 800 known homologs in eubacteria, archaea, fungi, and plants, according to the UNIPROT (www.uniprot.org) database. Known substrates for the other NCS1 subfamily transporters include allantoin, uracil, cytosine (including the antifungals, 5-fluorocytosine and 5-fluorouracil), purines, thiamine, pyridoxal-based compounds, and nicotinamide riboside (www.membranetransport.org/) (*15*, *16*). The x-ray structure of the Mhp1 protein described in this paper reveals similarities of this cation-coupled transporter to the *Aquifex aeolicus* leucine transporter $LeuT_{Aa}$ (*17*–*19*), a member of the neurotransmitter-sodium-symporter family, NSS 2.A.22, (*13*, *16*, *20*) and to the *Vibrio parahaemolyticus* sodium-galactose symporter vSGLT (*21*), a member of the solute-sodium-symporter family, 'SSS' 2.A.21. (*13*, *16*, *22*). Despite this structural similarity, the amino acid sequence of Mhp1 exhibits only an insignificant 15% identity to $LeuT_{Aa}$ and 16% to vSGLT, as calculated by the LALIGN algorithm (www.ch.embnet.org/software/LALIGN_form.html) (*23*).

The two x-ray structures of Mhp1, in the outward-facing open conformation and in the outward-facing occluded conformation with benzyl-hydantoin, demonstrate the conformational change consequent upon the binding of substrate from the outside of the membrane. Comparison of these Mhp1 structures with those of $LeuT_{Aa}$ and vSGLT

**Table 1.** Refinement statistics. Resolution numbers in parentheses refer to the statistics in the highest resolution shell. $R_{factor} = \sum|F_{obs} - F_{calc}|/\sum F_{obs}$. The $R_{free}$ is the same as the $R_{factor}$ but for the 5% of test reflections. Ramachandran plot outliers are as defined in MolProbity (*39*).

| Resolution (Å) | 30–2.85 (2.92–2.85) |
|---|---|
| $R_{factor}$ (%) | 24.0 (36.3) |
| $R_{free}$ (%) | 28.1 (41.8) |
| Average *B* value (Å$^2$) | 60.1 |
| RMSD from ideal values | |
| Bonds (Å) | 0.010 |
| Angle (°) | 0.982 |
| Ramachandran plot outliers (%) | 0.2 |

[1]Membrane Protein Laboratory, Diamond Light Source Limited, Harwell Science and Innovation Campus, Chilton, Didcot, Oxfordshire OX11 0DE, UK. [2]Division of Molecular Biosciences, Membrane Protein Crystallography Group, Imperial College, London SW7 2AZ, UK. [3]Human Receptor Crystallography Project, Exploratory Research for Advanced Technology (ERATO), Japan Science and Technology Agency, Yoshidakonoe-cho, Sakyo-ku, Kyoto 606-8501, Japan. [4]Department of Cell Biology, Graduate School of Medicine, Kyoto University, Yoshida-Konoe, Sakyo-Ku, Kyoto 606-8501, Japan. [5]Astbury Centre for Structural Molecular Biology, Institute for Membrane and Systems Biology, University of Leeds, Leeds LS2 9JT, UK. [6]School of Medicine, Hamedan University of Medical Sciences, Hamedan, Iran. [7]Systems and Structural Biology Center, RIKEN, 1-7-22 Suehiro-cho Tsurumi-ku, Yokohama 230-0045 Japan.

*These authors contributed equally to this work
†Present address: Department of Bioscience, Tokyo University of Agriculture, Sakuragaoka 1-1-1, Setagaya-ku, Tokyo 156-8502, Japan.
‡Present address: Aminosciences Laboratories, Ajinomoto Company Incorporated, 1-1 Suzuki-cho, Kawasaki-ku, Kawasaki-shi, Kanagawa 210-8681, Japan.
§Present address: Department of Medicinal Chemistry, Faculty of Pharmaceutical Sciences, University of Copenhagen, Universitetsparken 2, DK-2100, Denmark.
‖Present address: Department of Biochemistry, Faculty of Science, Chulalongkorn University, Phyathai Road, Patumwan, Bangkok 10330, Thailand.
¶To whom correspondence should be addressed. E-mail: s.iwata@imperial.ac.uk (S.I.); p.j.f.henderson@leeds.ac.uk (P.J.F.H.)

suggests a possible further conformational change, which allows the release of the substrate into the inside of the membrane. The inward- and outward-facing cavities of the transporters are symmetrically arranged on the opposite sides of the membrane by using two inverted repeated segments related by an internal pseudo-twofold axis parallel to the membrane. This comparative study suggests how the reciprocal opening and closing of inward-facing and outward-facing cavities could be synchronized by helices 3 and 8 that connect the two cavities on the opposite sides of the membrane.

**Structure determination.** For details, see (*24*). The structure of Mhp1 without substrate was solved by using multiple isomorphous replacement in combination with twofold cross-crystal averaging (*25*). The model was refined against data extending to a resolution of 2.85 Å with an $R_{factor}$ of 24.0% and a corresponding $R_{free}$ of 28.1% (Table1, table S1 and fig. S1) (*26*). The structure of the complex of Mhp1 with benzyl-hydantoin was solved from crystals grown in the presence of the substrate. Despite the limited resolution (4 Å), difference maps showed that the substrate is present in the binding site and that there is a structural rearrangement of residues 355-370. To avoid over-refinement, we only remodeled this region, followed by minimization with strict harmonic restraint (*24*). This partially remodeled structure gave an $R_{factor}$ of 34.2% and a corresponding $R_{free}$ of 39.2% (*24*).

**Transporter architecture.** The structure is composed of 12 membrane-spanning helices as was predicted (Fig. 1A) (*12*), although previous assignment of transmembrane helices (TMs) based on homologous yeast NCS-1 transporters needed a slight revision (fig. S2) (*15*). The 12 transmembrane helices (TMs) are arranged in two repeating units (TMs 1 to 5, residues 20 to 190, and TMs 6 to 10, residues 209 to 388) connected by an 18-residue loop and followed by an additional two transmembrane helices (Fig. 1, A and B). The similarity of the two repeating units is such that 65 out of a possible 170 Cα pairs can be superimposed with a root mean square deviation (RMSD) of 2.5 Å (*24*), despite the absence of significant sequence homology between the two units. The two units show an opposite topology with respect to the membrane and are related to each other by a rotation of 168° around an axis in the center of the membrane and parallel to its plane. An inverted topology repeat is commonly observed for many membrane transporters and channels (*17*, *21*, *27*–*31*). The two repeat units are completely intertwined, giving a central four-helix bundle consisting of the two broken TMs, 1 and 6, associated with TMs 2 and 7 (Fig. 1). This bundle is coated, on the side of TMs 1 and 6, by a layer formed by the other six helices; TMs 3 and 8, facing directly toward TMs 1 and 6, form a long antiparallel unit threading through two V-shaped structures formed by TMs 4 and 5 and TMs 9 and 10, respectively (Fig. 1A). The substrate- and cation-binding sites and the outward-facing cavity connecting these sites to the outsides of the

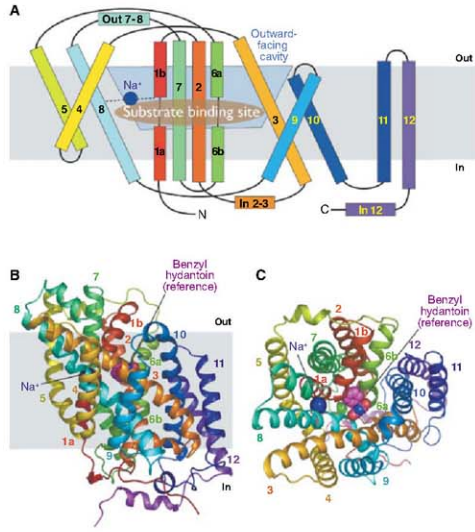


**Fig. 1.** Structure of Mhp1 from *M. liquefaciens*. **(A)** Mhp1 topology. The positions of the substrate- and the cation-binding sites are depicted as a brown ellipsoid and a blue circle, respectively. The membrane is shown in gray, and the outward-facing cavity observed in the structure is highlighted in light blue. The horizontal helices on the inside and outside of membrane are indicated as In and Out. TMs 3 and 8 pack onto each other in three-dimensional space. **(B)** The Mhp1 structure viewed in the plane of the membrane. The image is based on the high-resolution structure of the Mhp1 without benzyl-hydantoin. The position of the substrate in the Mhp1–benzyl-hydantoin complex structure is shown as a reference. A sodium ion is also shown and labeled. **(C)** View from the outside of the membrane.

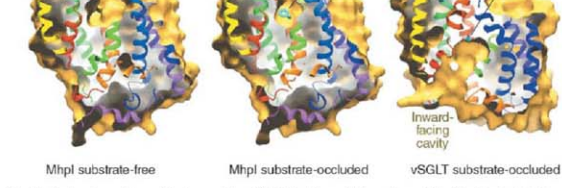


**Fig. 2.** Outward- and inward-facing cavities. **(A)** A slice through the surface of the Mhp1 substrate-free structure, viewed parallel to the membrane, showing the outward-facing cavity. The Connolly surface of Mph1 is shown in yellow (calculated with a probe radius of 2 Å). The ribbon representation of Mhp1 is colored as in Fig. 1. **(B)** As for (A) but for the Mhp1 substrate-occluded structure. Bound benzyl-hydantoin is shown in cyan. Note that the outward-facing cavity shown in (A) is blocked and the substrate is occluded from the outside of the membrane. **(C)** As for (A) but for the vSGLT substrate-occluded structure (PDB accession code 3DH4), showing the inward-facing cavity. Bound galactose is shown in cyan and red.

membrane are all located in the space between the central four-helix bundle and the outer helix layer (Figs. 1 and 2).

The amino acid sequence for TMs 11 and 12 and the C-terminal extension is poorly conserved among the NCS1 family (fig. S2), and the structural role of this region is unclear.

Although from the respective sequences it was not obvious, the fold of the core 10 helices of Mhp1 (TMs 1–10) is reminiscent of those of $LeuT_{Aa}$ (TMs 1-10) (*17*) and the recently solved structure of vSGLT (TMs 2-11) (*21*) (fig. S3). Overall, 249 out of a possible 460 Cα pairs between $LeuT_{Aa}$ and Mhp1 can be superimposed with a RMSD of 2.4 Å (*24*). Using the same algorithm to superpose Mhp1 and vSGLT, 172 Cα atom pairs have an rms deviation of 2.2 Å (fig. S4).

**Substrate binding and conformational changes.** In the electron density maps of the Mhp1 crystals with benzyl-hydantoin (Fig. 3, A and B), a V-shaped density was clearly observed at a position almost identical to that of the leucine in the $LeuT_{Aa}$ structure and close to that of the galactose in vSGLT (fig. S5). This site is located at the breaks in the discontinuous TMs 1 and 6 and facing TMs 3 and 8 (Fig. 1). It is located at the foot of the outward-facing cavity, which is composed of the neighboring surfaces of TMs 1, 3, 6, 8, and 10 and allows access of the substrate to the binding site (Figs. 1 and 2A). The structure of L-5-benzyl-hydantoin taken from the Cambridge Structural Database (accession code IWEYAK) was consistent with the shape of this density and the molecule was placed between $Trp^{117}$ (TM3) and $Trp^{220}$ (TM6) without requiring any modifications of torsion angles (Fig. 3, A and B).

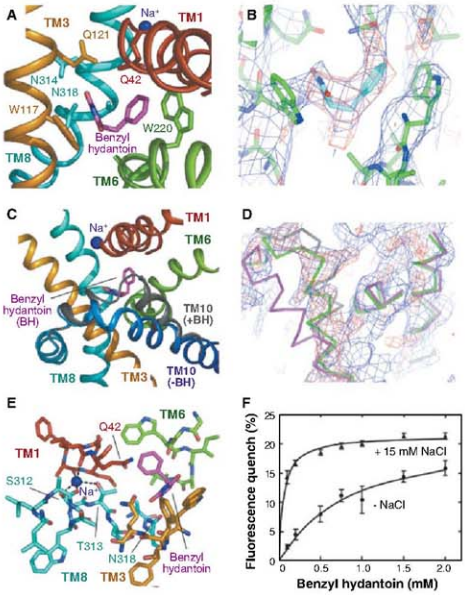


**Fig. 3.** Substrate- and cation-binding sites. **(A)** Substrate-binding site. The helices and key interacting residues (*36*) of the site are shown. The benzyl-hydantoin and the nearby sodium are shown in magenta and blue, respectively. **(B)** Electron density associated with benzyl-hydantoin. The $2F_o–F_c$ map (blue) has been contoured at 0.6σ and the $F_o–F_c$ map (red) at 3σ. **(C)** The conformational change upon the substrate binding. Transmembrane helix (TM) 10 and the loop between TMs 9 and 10 show a conformational change that occludes the bound substrate from the outside of the membrane. The trace of this region, shown in gray, is superimposed on the substrate-free structure. Benzyl-hydantoin is abbreviated as BH in the figure. **(D)** Electron density and model for TM10. The $2F_o–F_c$ map (blue) has been contoured at 0.6σ and the $F_o–F_c$ map (red) at 2σ. The trace for the benzyl-hydantoin free structure is shown in magenta and that for the benzyl-hydantoin complex is depicted in green. The gray trace is for the vSGLT structure (PDB accession code 3DH4) superimposed onto Mhp1. The maps in (B) and (D) were calculated on the basis of the molecular replacement solution by using the substrate-free structure with residues 355 to 370 omitted so is not biased by these residues [see (*24*) for details]. **(E)** Helices and key residues surrounding the cation- and substrate-binding sites. **(F)** Tryptophan-fluorescence-quenching by benzyl-hydantoin. The Mhp1 solution was titrated by benzyl-hydantoin and the decrease in the tryptophan fluorescence at 348 nm was monitored. The measurements were performed with (triangles) and without (circles) 15 mM NaCl in the solution. For details, see (*24*). Error bars indicate the standard error of the mean ($n$ = 3).

In the current model, the hydantoin moiety forms a *pi*-stacking interaction with the indole-ring of $Trp^{117}$ and is within hydrogen bonding distance of $Asn^{318}$ and $Gln^{121}$ (Fig. 3A). $Trp^{117}$ and $Asn^{318}$ are conserved amongst all the transporters in the family and $Gln^{121}$ only varies in the uridine transporter, FUI 1 (fig. S2). Another conserved residue, $Asn^{314}$, is within hydrogen bonding distance of $Asn^{318}$ such that it may hold the asparagine side chain in position to interact with the substrate. The benzyl group of the substrate is situated next to $Trp^{220}$ and $Gln^{42}$. The side chain of $Trp^{220}$ moves into the binding site with respect to its position in the substrate-free structure and forms a pi-stacking interaction with the benzyl moiety.

This binding mode is consistent with the observation that Mhp1 has a higher affinity for 5-indolyl-methyl-hydantoin than for benzyl-hydantoin (*12*), because the indole group in the hydantoin would form an even more extensive packing interaction with $Trp^{220}$ and, in addition, the side chain of $Gln^{42}$ could form a hydrogen bond with the nitrogen atom of the indole rings. This residue could play a role in the substrate specificity of the NCS1 transporters as suggested by sequence analysis (*15*).

The observed residues in the substrate-binding site are consistent with the results of mutational studies on a NCS1 family member, Fcy2, that transports cytosine into *Saccharomyces cerevisae* (*32–35*). Although Fcy2 is a distantly related homolog of Mhp1, the residues involved in the substrate and cation binding can be aligned with Mhp1 unambiguously (fig. S2). Three of the genetically selected Fcy2 mutants, which show an altered Michaelis constant $K_m$ of substrate uptake, were substitutions in the segment 371 I-A-N-N-I-P-N 377 (*36*) of Fcy2, which corresponds to the residues 311 to 318 of Mhp1 (*32–34*). Site-directed mutagenesis studies on these residues emphasized the role in the substrate binding of $Asn^{374}$ and $Asn^{377}$, which are equivalent to $Asn^{314}$ and $Asn^{318}$ of Mhp1, respectively (*35*).

In the benzyl-hydantoin complex structure, some conformational differences from the substrate-free Mhp1 structure are evident (Fig. 3, C and D). The N-terminal part of TM10 (residues 355 to 370) moves into the outward-facing cavity. This occludes the substrate-binding site from the outside space of the membrane (Figs. 2B and 3C).

This movement seems to be triggered by a repositioning of $Trp^{220}$ located on TM6, which is adjacent to TM10.

We, therefore, have two conformations of the protein. We refer to the substrate-free structure as outward-facing open and to the substrate bound structure as outward-facing occluded.

Occluding the substrate-binding site from the outside of the membrane is essential to prevent the leakage of any molecules across the membrane. In $LeuT_{Aa}$, it was proposed that this should be achieved by the interactions between TMs 1 and 8 and TMs 6 and 3 (*17*). The binding site is occluded by the side chains of selected residues that pack over the substrate in $LeuT_{Aa}$. The occluding mechanism of the outward-facing cavity for Mhp1, therefore, seems to be different from that for $LeuT_{Aa}$. It is noteworthy that in the closed vSGLT outward-facing cavity (*21*), TM11 (equivalent to TM10 of Mhp1) adopts a conformation similar to TM10 in the occluded form of Mhp1 (Fig. 3D).

**Cation-binding site.** The electron density map at 2.85 Å resolution indicates a possible cation-binding site at the C-terminal end of TM1a interacting with TM8. The site includes the carbonyl-oxygen-atoms of Ala 38, and Ile 41 of TM1 and the carbonyl-oxygen-atom of Ala 309, and the hydroxyl-oxygen-atoms of the side chains of Ser 312 and Thr 313, respectively (Fig. 3E and fig. S6). Presumably the dipole moment at the C terminus of TM1a contributes to the binding as seen for other transporters (*17*, *21*, *27*, *28*, *30*). Currently, a sodium ion is modeled at this position such that the substrate atoms form a square pyramidal arrangement with the bond distances between 2.2 and 2.7 Å, which is too short for a water molecule. An equivalent site was observed and assigned as a sodium binding site in the structures of $LeuT_{Aa}$ and vSGLT (fig. S6). The connection between the cation-binding site and the substrate-binding site could be made by residue $Asn^{318}$ on TM8 and $Gln^{42}$ on TM1. A requirement for cation-binding to form a proper substrate-binding site provides a basis for the coupling of the cation and substrate translocation.

To confirm the sodium dependency of Mhp1, which was not evident in whole cell uptake experiments (*12*), the binding of benzyl-hydantoin and/or sodium was measured using fluorescence quenching (Fig. 3F) (*37*). The results clearly show that the affinity of benzyl-hydantoin to the protein [apparent dissociation constant ($K_d$) of 0.88 ± 0.27 mM] is raised over 10-fold in the presence of 15 mM sodium (apparent $K_d$ 0.054 ± 0.007 mM). We have also observed that the benzyl-hydantoin increases the affinity of sodium to Mhp1; in the absence of benzyl-hydantoin, the apparent $K_d$ for sodium is 1.15 ± 0.28 mM, and in the presence of 2 mM benzyl-hydantoin, the value is 0.15 ± 0.04 mM. These results indicate that the binding of sodium and benzyl-hydantoin are tightly coupled in Mhp1.

Some of the NCS1 family transporters from yeasts and bacteria, including Mhp1, were thought to be proton- rather than sodium-dependent (*12*, *15*, *16*). Sodium dependence in whole cell transport assays may be obscured by the presence of a separate compensating sodium transport system in the membrane. In the case of Mhp1 the sensitivity of assays is reduced by the low solubility and the lipophilic nature of the substrate, preventing the testing of sodium dependence in proteoliposomes. It is also possible that Mhp1 and other NCS-1 transporters have a flexible cation selectivity, like the MelB sugar-cation symporter (*38*).

**Possible transport mechanism.** The two structures of Mhp1 reveal the conformational change of the transporter upon the binding of substrate from the outside of the membrane. The structure of vSGLT provides further insight into the transport process because it is in an inward-facing conformation closed with the substrate in its binding site (Figs. 2C and 4). We refer to this as an inward-facing, occluded conformation according to the assignment in (*21*). There, the cavity connecting the substrate-binding site to the inside of the membrane is observed although the site is still occluded (Fig. 2C and figs. S7 and S8). In this vSGLT structure the outward-facing cavity, as also observed in $LeuT_{Aa}$ and substrate-bound Mhp1, is completely closed (Fig. 2C). The observed inward-facing cavity in vSGLT is made of the neighboring surfaces of TMs 1, 3, 5, 6, and 8 (Fig. 2C and figs. S7 and S8), which are symmetrically related to the outward-facing cavity observed in Mhp1 on the opposite side of the membrane. Thus, these structures are related by an approximate two-fold axis that is parallel to the membrane (fig. S7). In Fig. 4, we compare the conformations of the core 10 helices (TMs 1 to 10) of outward-facing Mhp1 and inward-facing vSGLT. These structures suggest a reciprocating oscillation between symmetrical states opening alternately to each side of the membrane.

In the following, we propose a possible mechanism of molecular transport across the membrane by Mhp1 based on the x-ray structures (Fig. 4).

1) Change of the outward-facing open state to the outward-facing occluded state: In Mhp1, the outward-facing cavity is formed by TMs 1, 3, 6, 8, and 10 (Figs. 1C and 2A). Upon the binding of the substrate, TM10 moves toward the cavity closing access to the outside space of the membrane (Figs. 2B and 4).

2) Change of the outward-facing occluded state to the inward-facing occluded state: In vSGLT, the inward-facing cavity is formed by TMs 1, 3, 5, 6, and 8 (Mhp numbering, figs. S7 and S8). In the structure, the substrate-binding site is occluded from the inside of the membrane. In the outward-facing conformation of Mhp1 (and $LeuT_{Aa}$), the inward-facing cavity observed in vSGLT is occupied by TM8 (and partly by TM6). On the other hand, in the inward-facing conformation of vSGLT, the outward-facing cavity is occupied by TM3 (and partly TM6). It seems that the alternation of the outward- and inward-facing conformations is effected by the movement of the helix bundle of TMs 3 and 8. It is also possible that TMs 1 and 6 undergo a coordinated shift with TMs 3 and 8, as proposed by Gouaux and co-workers (*17*). Because of the substantial difference in the substrate binding sites of Mhp1 and vSGLT, it is difficult to estimate the extent of the movement of TMs 1 and 6; thus, in Fig. 4 only TMs 3 and 8 are shown for simplicity.

3) Change of the inward-facing occluded state to the inward-facing open state: This transition is required to release the substrates to the inside, but no structures are available to define this change. For vSGLT, it is proposed that the movement of $Tyr^{263}$ is enough to open up the cavity (*21*). For Mhp1, in addition, the opening up of TMs 4 and 5 might be necessary. The connection between TMs 4 and 5 is disordered and is not modeled in vSGLT. If this connection has a similar conformation to the one in Mhp1, it would block the cavity.

The site of the cation uptake and release is also controlled by the conformational changes, because the ion-binding site is located between TMs 1 and 8 (Fig. 4D). The cation-binding sites of Mhp1 and $LeuT_{Aa}$ are very similar (fig. S6) and are a part of the surface of the outward-facing cavity, whereas the one for vSGLT is very different and is a part of the inward-facing cavity, occurring as a consequence of the conformational change of TMs 3 and 8. This, together with the strong coupling of substrate and cation binding, should form the basis of substrate-cation symport. The coordinated and reciprocating conformational

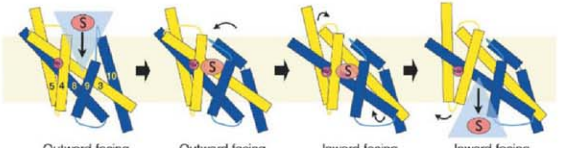


**Fig. 4.** Proposed substrate translocation mechanism by Mhp1. Schematic diagram showing four different conformational states: outward-facing open, outward-facing occluded, inward-facing occluded, and inward-facing open. Substrate- and sodium-binding sites are labeled as S and $Na^+$, respectively.

changes observed on both sides of the membrane provide a structural basis for the widely held view of an alternating access model deduced from kinetics data.

### References and Notes


1. O. Jardetzky, *Nature* **211**, 969 (1966).
2. C. Tanford, *Proc. Natl. Acad. Sci. U.S.A.* **80**, 3701 (1983).
3. H. R. Kaback *et al.*, *Proc. Natl. Acad. Sci. U.S.A.* **104**, 491 (2007).
4. D. D. F. Loo, B. A. Hirayama, M. H. Karakossian, A. K. Meinild, E. M. Wright, *J. Gen. Physiol.* **128**, 701 (2006).
5. C. Toyoshima, *Arch. Biochem. Biophys.* **476**, 3 (2008).
6. K. Hollenstein, R. J. Dawson, K. P. Locher, *Curr. Opin. Struct. Biol.* **17**, 412 (2007).
7. O. Mirza, L. Guan, G. Verner, S. Iwata, H. R. Kaback, *EMBO J.* **25**, 1177 (2006).
8. J. Abramson *et al.*, *Science* **301**, 610 (2003).
9. L. Guan, O. Mirza, G. Verner, S. Iwata, H. R. Kaback, *Proc. Natl. Acad. Sci. U.S.A.* **104**, 15294 (2007).
10. Y. Huang, M. J. Lemieux, J. Song, M. Auer, D. N. Wang, *Science* **301**, 616 (2003).
11. Y. Yin, X. He, P. Szewczyk, T. Nguyen, G. Chang, *Science* **312**, 741 (2006).
12. S. Suzuki, P. J. Henderson, *J. Bacteriol.* **188**, 3329 (2006).
13. M. H. Saier Jr., *Adv. Microb. Physiol.* **40**, 81 (1998).
14. M. H. Saier Jr., C. V. Tran, R. D. Barabote, *Nucleic Acids Res.* **34**, D181 (2006).
15. A. Pantazopoulou, G. Diallinas, *FEMS Microbiol. Rev.* **31**, 657 (2007).
16. Q. Ren, K. Chen, I. T. Paulsen, *Nucleic Acids Res.* **35**, D274 (2007).
17. A. Yamashita, S. K. Singh, T. Kawate, Y. Jin, E. Gouaux, *Nature* **437**, 215 (2005).
18. S. K. Singh, A. Yamashita, E. Gouaux, *Nature* **448**, 952 (2007).
19. Z. Zhou *et al.*, *Science* **317**, 1390 (2007); published online 9 August 2007 (10.1126/science.1147614).
20. L. Shi, M. Quick, Y. Zhao, H. Weinstein, J. A. Javitch, *Mol. Cell* **30**, 667 (2008).
21. S. Faham *et al.*, *Science* **321**, 810 (2008); published online 3 July 2008 (10.1126/science.1160406).
22. E. Turk *et al.*, *J. Biol. Chem.* **275**, 25711 (2000).
23. X. Huang, W. Miller, *Adv. Appl. Math.* **12**, 337 (1991).
24. Materials and methods are available as supporting material on *Science* Online.
25. K. Cowtan, *Joint CCP4 and ESF-EACBM Newsletter on Protein Crystallography* **31**, 34 (1994).
26. P. D. Adams *et al.*, *Acta Crystallogr. D* **58**, 1948 (2002).
27. C. Hunte *et al.*, *Nature* **435**, 1197 (2005).
28. D. Yernool, O. Boudker, Y. Jin, E. Gouaux, *Nature* **431**, 811 (2004).
29. D. Fu *et al.*, *Science* **290**, 481 (2000).
30. R. Dutzler, E. B. Campbell, M. Cadene, B. T. Chait, R. MacKinnon, *Nature* **415**, 287 (2002).
31. J. U. Bowie, *Nat. Struct. Mol. Biol.* **13**, 94 (2006).
32. M. R. Chevallier, R. Jund, F. Lacroute, *J. Bacteriol.* **122**, 629 (1975).
33. J. C. Bloch, H. Sychrova, J. L. Souciet, R. Jund, M. R. Chevallier, *Mol. Microbiol.* **6**, 2989 (1992).
34. D. Bréthes *et al.*, *Eur. J. Biochem.* **204**, 699 (1992).
35. T. Ferreira, D. Bréthes, B. Pinson, C. Napias, J. Chevallier, *J. Biol. Chem.* **272**, 9697 (1997).
36. Single-letter abbreviations for the amino acid residues are as follows: A, Ala; I, Ile; N, Asn; P, Pro; Q, Gln; S, Ser; T, Thr; and W, Trp.
37. P. J. Henderson, G. E. Martin, T. P. McDonald, A. Steel, A. R. Walmsley, *Antonie Leeuwenhoek* **65**, 349 (1994).
38. T. H. Wilson, P. Z. Ding, *Biochim. Biophys. Acta* **1505**, 121 (2001).
39. S. C. Lovell, *Proteins* **50**, 437 (2003).


40. This research was funded primarily by the Biotechnology and Biological Sciences Research Council (grant nos. B17935 and BB/C51725), with important contributions from Ajinomoto Incorporated, the European Membrane Protein consortium (grant no. LSHG-CT-2004-504601), the Membrane Protein Structure Initiative (grant no. BBS/B/14418), and the Wellcome Trust (grant no. 062164/Z/00/Z). We wish to thank the Membrane Protein Laboratory (MPL) at the Diamond Light Source Limited for use of the MPL facilities. J. Abramson kindly provided us with the coordinates of vSGlT before their release from the Protein Data Bank (PDB). We are also grateful to S. Phillips, S. Baldwin, P. Gilmartin, S. Radford, D. Drew, M. Jormakka, K. Watanabe, and M. Iwata for support or advice. The Japan Society for the Promotion of Science provided personal funding to S.Y. and the Leverhulme Trust to P.J.F.H. S.W. was a recipient of a European Molecular Biology Organization long-term fellowship. The coordinates and the structure factors for Mhp1 without substrate and the hydantoin complex have been deposited in the PDB (entries 2JLN and 2JLO, respectively).


### Supporting Online Material

www.sciencemag.org/cgi/content/full/1164440/DC1
Materials and Methods
Table S1
Figs. S1 to S8
References


8 August 2008; accepted 26 September 2008
Published online 16 October 2008;
10.1126/science.1164440
Include this information when citing paper.


REPORTS

# Magnetism on the Angrite Parent Body and the Early Differentiation of Planetesimals


**Benjamin P. Weiss,[1]* James S. Berdahl,[1] Linda Elkins-Tanton,[1] Sabine Stanley,[2] Eduardo A. Lima,[1] Laurent Carporzen[1]**



Angrites are among the oldest known pristine basaltic meteorites and record the earliest stages of planet formation and differentiation. Our paleomagnetic analysis of three angrites found that they record a past magnetic field of ~10 microteslas on the angrite parent body extending from 4564 to at least 4558 million years ago. Because the angrite paleomagnetic record extends beyond the expected lifetime of the early circumstellar disk, these paleofields were probably generated internally on the angrite parent body, possibly by an early dynamo in a rapidly formed metallic core.


Basaltic achondrites are thought to be igneous samples of the first differentiated planetary bodies. Several classes of these meteorites have crystallization ages within just ~3 million years (My) of the formation of the solar system and contain geochemical signatures of metal and silicate fractionation. Remanent magnetization has been detected in meteorites from five basaltic achondrite groups, indicating the presence of past magnetic fields on these bodies (*1*). However, these meteorites, as well as nearly all basaltic achondrite groups, were subjected to brecciation, shock, and metamorphic events tens to hundreds of millions of years after their formation that modified and, in many cases, reset their magnetization. Because magnetic fields can be generated by large impacts (*2*), the fields recorded on these bodies also may not have been generated internally.

An exception is the angrites, a group of twelve basaltic achondrites from an as yet unidentified parent body. Angrites have Pb/Pb and Hf/W ages of 4564 to 4558 million years ago (Ma) (*3*–*5*) that are within error of their (U-Th)/He ages for all but two meteorites (*6*). They entirely lack shock, post-cooling brecciation, and parent-body weathering textures (*7*–*12*), which makes them among the best preserved materials known from the early solar system. Angrites may therefore record two fundamental field-generating mechanisms postulated to exist in the early solar system: stellar and circumstellar disk fields external to the angrite parent body (APB) and an internal core dynamo on the APB.

Here we present a paleomagnetic investigation of 3 of the 12 known angrites: Angra dos Reis, D'Orbigny, and Asuka (A) -881371. We found that the angrites Northwest Africa (NWA) 2999 and NWA 4801 have been substantially remagnetized by collectors' hand magnets (as indicated by communication with previous owners of the samples and moments near saturation), whereas NWA 4931 has been heavily weathered


[1]Department of Earth, Atmospheric, and Planetary Sciences, Massachusetts Institute of Technology, 54-814, 77 Massachusetts Avenue, Cambridge, MA 02139, USA. [2]Department of Physics, University of Toronto, 60 St. George Street, Toronto, ON M5S 1A7, Canada.

*To whom correspondence should be addressed. E-mail: bpweiss@mit.edu

since arrival on Earth. Most of the remaining six angrites are either hot desert meteorites (probably subjected to weathering and magnet remagnetization) or not readily available to the scientific community.

Nearly all angrites contain several primary ferromagnetic minerals: low-Ti magnetite (*13*), titanomagnetite [typical composition of 71 to 77 mole percent (mol %) ulvöspinel, with 17 to 21 mol % magnetite] (*14*), and rarer kamacite (typically $Fe_{0.95}Ni_{0.05}$, except for D'Orbigny, which reportedly contains $FeNi_2$) and pyrrhotite (*7*, *14*). Our thermomagnetic, hysteresis, and other rock magnetic data [see the supporting online material (SOM)] indicate that the dominant ferromagnetic mineral in D'Orbigny and A-881371 is pseudo–single domain, low-Ti magnetite. Angra dos Reis contains two pseudo–single domain ferromagnetic minerals, one of which is probably low-Ti magnetite and the other a higher coercivity phase (either sulfide or metal). None of these meteorites exhibits a Verwey transition (see SOM), indicating that the magnetite is not stoichiometric and that any effects from inverse thermoremanent magnetization (ITRM) processes (*15*) must be modest [in any case, the high blocking coercivity of the natural remanent magnetization (NRM) in these meteorites implies that ITRM cannot be a major contributor]. Furthermore, none of these angrites contain appreciable quantities of ferromagnetic weathering minerals (see SOM). Angra dos Reis is particularly pristine because it was quickly recovered after it fell on Earth (*8*, *16*). The well-understood magnetic properties of magnetite mean that, relative to most other meteorites, angrites are very-high-fidelity magnetic recorders.

D'Orbigny is a pristine vesicular basalt containing undevitrified igneous glass (*7*). It is among the oldest known angrites, with final cooling ages only ~3 to 4 My younger than calcium- and aluminum-rich inclusions (CAIs) and the origin of the solar system (*3*, *4*, *17*). D'Orbigny's large size afforded us the opportunity to acquire samples ranging from the fusion crust to the center (150 mm deep) to identify preterrestrial remanence. Alternating field (AF) demagnetization, rock magnetic, and paleointensity studies of mutually oriented subsamples revealed that much of the exterior ~1 mm of the meteorite has been completely remagnetized by the collector's magnet (see SOM). Subsamples at 12 to 30 mm of depth had two main components of magnetization: (i) a nonunidirectional, near saturation, low-coercivity (LC) component from the collector's magnet (typically blocked up to ~5 to 10 mT) and (ii) a high-coercivity (HC) component (blocked up to at least ~40 to >290 mT, depending on the subsample) with a ratio of NRM to saturation isothermal remanent magnetization (IRM) <1%. The HC component trended to the origin and was unidirectional across all mutually oriented interior subsamples (fig. S1), consistent with a primary thermoremanence. Subsamples at ≥ 8 cm of depth had only a moderate LC overprint varying in intensity between that expected for a terrestrial viscous remanent magnetization and a low-field (<7 mT) IRM (Fig. 1A and fig. S2). Paleointensity experiments (*18*) on HC components from nine subsamples gave paleofield values of 17 ± 6 μT after normalizing to anhysteretic remanent magnetization (ARM) acquired in 50, 200, and 600 μT dc bias fields and 15 ± 5 μT after normalizing to IRM (uncertainties are SDs of values for nine subsamples) (table S3).

A-881371 is a fine-grained ophitic basalt with olivine megacrysts (*13*) and is nearly the same age as D'Orbigny (*5*). AF demagnetization of a single 66-mg grain from the interior of this tiny meteorite (≥5 mm from nearest fusion crust) revealed a LC component up to 7.2 mT (Fig. 1B and fig. S3A). Our magnetic viscosity experiments indicate that this component is almost certainly a viscous remanent magnetization acquired during residence on Earth (see SOM). A weaker HC magnetization is present up to at least 150 mT but does not notably decay in intensity during AF demagnetization due to the relatively high ARM noise from our AF system. AF demagnetization of a laboratory ARM acquired in a 7-μT dc bias field (chosen to yield a similar pa-

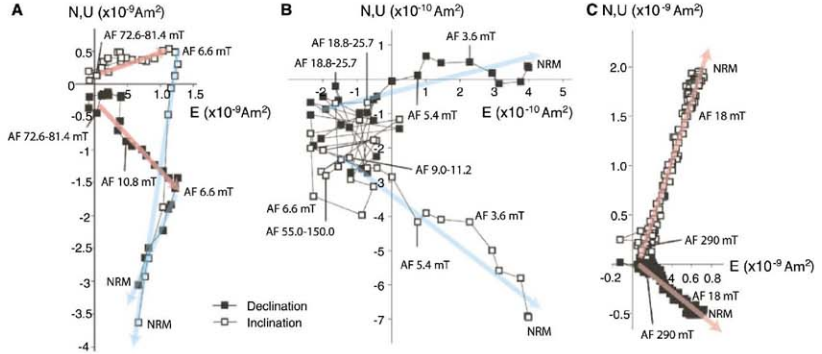


**Fig. 1.** NRM of angrites. A two-dimensional projection of the endpoint of the NRM vector during AF demagnetization is shown. Closed and open symbols represent end points of magnetization projected onto horizontal N-S-E-W and vertical U-D-E-W planes, respectively. Peak fields for selected AF demagnetization steps are labeled. One or two main components are visible: (i) sometimes a LC component (blue arrow) and (ii) always a HC component (red arrow). **(A)** D'Orbigny interior (~8 cm depth) sample F1. To reduce spurious ARM noise, steps from AF 7.2 to 8.4 mT were averaged over three consecutive steps, and steps from AF 9.0 to 83.6 mT were averaged over five consecutive steps. A least-squares fit to all HC steps without averaging from AF 6.6- to 50.6-mT deviates from the origin by dANG = 6° (calculated by anchoring to the AF 6.6-mT direction), which is less than the fit's uncertainty, represented as the maximum angular deviation (MAD) = 29.5°, consistent with the HC component trending to the origin. **(B)** A-881371 interior sample ,63. Two main components are visible: (i) a LC component (approximate direction given by blue arrow) and (ii) a HC component identified as an offset of the mean direction above AF 9.0 mT from the origin. High-AF directions are averages of multiple AF steps (compare with fig. S3A). **(C)** Angra dos Reis interior sample AMC-16. A least-squares fit to all HC steps without averaging from AF 18 to 74.8 mT gives dANG = 4.5° (anchored to the AF 18-mT direction), which is less than the fit's mean MAD = 5.7°, consistent with the HC component trending to the origin.

leointensity as that of the NRM) exhibits the same high AF-related noise (fig. S3B). If we assume this is the characteristic magnetization, then we obtain paleointensities of ~3 to 8 μT (ARM method) and ~2 μT (IRM method) (fig. S3, C and D, and table S3). D'Orbigny's and A-881371's great age, excellent preservation state, and nearly instantaneous (10 to 50°C hour$^{-1}$) primary igneous cooling rates (*19*) indicate that their HC magnetization is a truly ancient thermoremanence (*20*).

The coarse-grained younger angrite Angra dos Reis (Pb/Pb age of 4557.7 ± 0.1 Ma) (*3*) also has a preterrestrial magnetization acquired in a similarly substantial magnetic field. Our AF analyses of mutually oriented subsamples from a chip of Angra dos Reis from the American Museum of Natural History (AMNH) traversing the fusion crust to the interior revealed a unidirectional magnetization in the interior. Subsamples from within 2.7 mm of the fusion crust have directions divergent from (coincidentally nearly antipodal to) the interior and Earth-strength paleointensities. This is consistent with the outer few millimeters having been baked by atmospheric passage and indicates that the magnetization in the unbaked interior is preterrestrial (Fig. 2). This interior magnetization consisted of a HC primary magnetization component (extending from 15.8 to >290 mT) trending to the origin (Fig. 1C), usually overprinted by a weak LC component that is probably a terrestrial VRM (see SOM). AF demagnetization of five mutually oriented subsamples of a second chip of Angra dos Reis taken from the interior (≥6 mm from the nearest fusion crust) of the main mass in Museu Nacional, Brazil (MNB) revealed an intense LC overprint from previous sample handling and a unidirectional HC component trending to the origin interpreted as a primary thermoremanence (fig. S1). Two additional subsamples on the opposite side of the chip were nearly fully overprinted by the high intensity component and did not yield primary remanence. Paleointensity experiments on the HC component for seven subsamples from both the AMNH and MNB samples gave mean values and SDs of 17 ± 11 μT (ARM method) and 19 ± 9 μT (IRM method) (table S3).

Three angrites record magnetic fields on the order of 10 μT on the APB extending from at least 4564.4 ± 0.1 (Pb/Pb age of the oldest angrite, D'Orbigny) to ≥4557.7 ± 0.1 Ma (Pb/Pb age of the youngest studied angrite, Angra dos Reis) (Fig. 3). Our fusion-crust baked contact test on Angra dos Reis and unidirectional magnetization trending to the origin observed in the interiors of Angra dos Reis and D'Orbigny (with Angra dos Reis having an especially low-noise signal) are collectively strongly indicative of primary thermoremanence. The implied paleointensities are ~20% of Earth's field today and far larger than that of the galactic field, solar wind, Mercury's present surface field, and the expected time-averaged fields of the T Tauri Sun outside 0.2 astronomical units (AUs) (Fig. 3). Angrite HC magnetization is highly unlikely to be the product of nebular lightning (*21*), which cannot produce the observed low NRM/IRM values. On the other hand, the paleointensities are within the range expected for the disk dynamo excited by magnetorotational instabilities (*22*), T Tauri flares at ~0.2 AUs, magnetic fields generated by large impacts (*2*), strong crustal ferromagnetic anomalies, and a core dynamo. However, our data indicate that the paleofields on the APB lasted for at least 10 My after CAIs, beyond the likely lifetime of a circumstellar disk dynamo (*23*). The absence of shock textures in angrites means that it is highly unlikely that the HC magnetization, which is blocked to coercivities >290 mT in Angra dos Reis, can be a shock remanence created in an impact-generated field (*24*). Additionally, the slow cooling rates of the coarse-grained angrites like Angra dos Reis (*25*, *26*) mean that they would have acquired their thermoremanence over a period of thousands to millions of years, far longer than the expected lifetime of any impact-generated fields [which last just ~1 day, even for basin-scale impacts on a Moon-sized body (*27*)] or T Tauri flares [lifetimes of several hours (*28*)]. Such slow cooling rates also make it highly unlikely that these angrites could have been magnetized by the spatially complex fields expected from magnetorotational instabilities while situated on the translating, spinning APB. Crustal field sources could potentially account for angrite magnetization, but such strong crustal fields would probably demand a core dynamo for their formation.

This reasoning implies that the source of these fields was internal, most likely a convecting metallic core and dynamo. Angrites contain geochemical evidence for the formation of an Fe-Ni core with a mass ~8 to 60% of the APB (*7*, *29*) by 4 My after CAIs (*4*, *30*), possibly coincident with

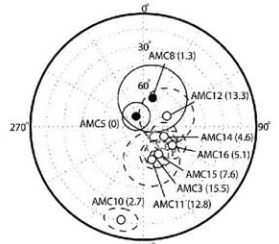


**Fig. 2.** Fusion-crust baked contact test on Angra dos Reis parent sample AMNH. HC magnetization directions of mutually oriented subsamples ranging from the fusion-crusted exterior to the interior are shown and plotted on an equal-area projection. Closed and open symbols represent projections of vector directions onto the lower and upper hemisphere, respectively. Ellipses give estimated orientation uncertainty (either MAD of least-squares fit or estimated sample positioning uncertainty, whichever is larger). Distance from fusion crust in millimeters is listed next to each sample. Only sample AMC5 contains fusion crust. The seven remaining samples are from the interior, with AMC8 and AMC10 apparently baked by atmospheric passage. Fisher mean direction (gray star) and associated 95% uncertainty confidence estimate ($\alpha_{95}$ = 10.7°) are shown for interior subsamples. The shallow depth of divergent magnetization directions (<3 mm) and the fact that measured samples have NRM/IRM < 1% throughout their full coercivity range indicate that the exterior has been thermally remagnetized by atmospheric passage rather than isothermally remagnetized by a magnet.

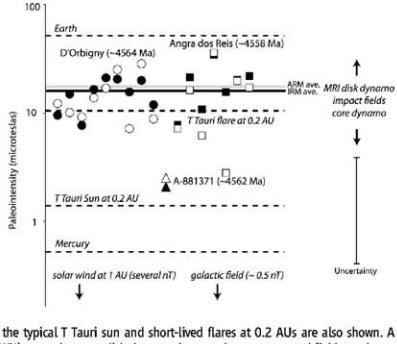


**Fig. 3.** Summary of paleointensity estimates for angrites. Each point is derived from the HC magnetization in a single subsample. Circles, D'Orbigny; triangles, A-881371; squares, Angra dos Reis (with approximate magnetization age labeled next to each meteorite). Solid symbols, IRM method; open symbols, ARM method using 50-μT bias field. Mean paleointensities from IRM and ARM methods are given by thick black and gray lines. For comparison, the surface fields of Earth and Mercury, the solar wind field at Earth's orbit (1 AU from the sun), the galactic field, and the inferred paleofields of the typical T Tauri sun and short-lived flares at 0.2 AUs are also shown. A magnetorotational instability (MRI) protoplanetary disk dynamo, impact plasma-generated fields, and core dynamos can produce paleointensities over a wide range of values, including values consistent with angrites. An estimate of the uncertainty range for an individual angrite paleointensity datum (primarily because of uncertainty in the ratio of ARM and IRM to thermoremanence) is shown at right.

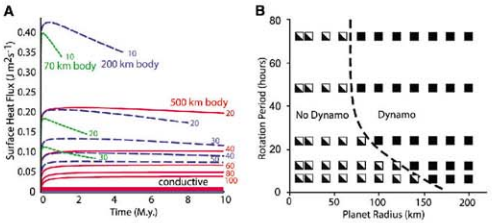


**Fig. 4.** Theoretical constraints on the possibility of dynamo generation on an early planetesimal. **(A)** Calculated outward heat flux from the surface of a model early planetesimal. The body is assumed to have a convecting magma ocean overlying a liquid Fe-Ni core and to be losing heat radiatively to space through a stagnant, conducting crustal lid (see SOM). The estimated power per unit surface area as a function of time after formation of the magma ocean [which is estimated to occur one to several My after accretion, see (*32*)] is shown. Calculations were conducted for bodies of radius 500 km (solid red lines), 200 km (dashed blue lines), and 70 km (dotted green lines) and for a variety of crustal thicknesses (numbers give thickness in kilometers). The dashed curves are terminated at the time when the magma ocean temperature drops below 850°C. Bold lines (all nearly overlapping at the bottom) indicate estimated maximum surface heat flux corresponding to a solely conductive adiabatic core. **(B)** Estimated conditions under which a planetesimal could produce a magnetic field like that recorded by angrites as a function of rotation period and planet size. Solid black squares indicate a supercritical magnetic Reynolds number and a planet surface field ≥20 μT (see SOM). Squares with lower left half in black indicate a surface field ≥20 μT, but a subcritical magnetic Reynolds number. The dashed line indicates the approximate boundary of angrite-like dynamo conditions.

an early magma ocean (*31*). Numerical modeling indicates that planetesimals will achieve >50 weight % melting and probably produce magma oceans if they accrete within ~1.3 My of CAIs and have radii exceeding ~20 km (*32*). On such bodies, it is conceivable that a metallic core would form quickly, setting the stage for an early, short-lived dynamo. We conducted two simple analytic calculations to assess this possibility (see SOM). Following (*32*), we assumed the core and silicate mantle of the body were initially molten and convecting beneath a solid conductive outer crust as a result of early internal heating by $^{26}$Al decay. We found that for bodies with radii of 70 to 500 km and a wide range of crustal thicknesses, the heat flux out of the core is superadiabatic, a likely requirement for dynamo production (*33*) for periods lasting for several to several tens of million years after the end of major $^{26}$Al heating (Fig. 4A). The main factor that terminates this early phase of superadiabatic heat flow is the progressive crystallization of the magma ocean: When the ocean temperature reaches ~850°C, we estimate that the ratio of crystals to liquid will be sufficiently high that convection will cease.

Second, we investigated the possibility that such bodies could produce a self-sustaining core dynamo and surface magnetic fields like that recorded in angrites (see SOM). Using various estimates of core convective velocities based on different scaling laws, we found that bodies with radii exceeding ~80 km and a wide range of spin rates, internal density distributions, and core sizes [including possibly ancient Mercury (*34*)] can have supercritical magnetic Reynolds numbers and produce surface fields exceeding 20 μT (Fig. 4B). These calculations are illustrative of the feasibility (perhaps even inevitability) of early planetesimal dynamos.

Magnetization in angrites pre-dates that in howardite-eucrite-diogenite meteorites (thought to be from the asteroid Vesta) (*35*) and lunar (*36*), martian (*37*), and terrestrial rocks (*38*) by ~100 to 1000 My. Our paleomagnetic data are a unique geophysical contribution to a growing body of geochemical evidence indicating that planets and large planetesimals formed metallic cores within just a few million years after CAIs. If the APB is representative of these quickly formed bodies, short-lived planetesimal core dynamos may have been a widespread process in the early solar system.

### References and Notes


1. Previous paleomagnetic studies have been conducted on five small-body basaltic achondrite groups: the howardite-eucrite-diogenites, Ibitira, ureilites, mesosiderite clasts, and aubrites.
2. D. A. Crawford, P. H. Schultz, *Int. J. Impact Eng.* **23**, 169 (1999).
3. Y. Amelin, *Geochim. Cosmochim. Acta* **72**, 221 (2008).
4. A. Markowski *et al.*, *Earth Planet. Sci. Lett.* **262**, 214 (2007).
5. R. E. Zartman, E. Jagoutz, S. A. Bowring, *Lunar Planet. Sci.* XXXVIII, 1580 (abstr.) (2006).
6. H. Busemann, S. Lorenzetti, O. Eugster, *Geochim. Cosmochim. Acta* **70**, 5403 (2006).
7. G. Kurat *et al.*, *Geochim. Cosmochim. Acta* **68**, 1901 (2004).
8. M. Prinz *et al.*, *Earth Planet. Sci. Lett.* **35**, 317 (1977).
9. D. W. Mittlefehldt, T. J. McCoy, C. A. Goodrich, A. Kracher, in *Planetary Materials*, J. J. Papike, Ed. (Mineralogical Society of America, Washington, DC, 1998), pp. 4-1–4-195.
10. G. McKay, D. Lindstrom, S.-R. Yang, J. Wagstaff, *Lunar Planet. Sci.* XIX, 762 (1988).
11. S. M. Kuehner *et al.*, *Lunar Planet. Sci.* XXXVII, 1344 (abstr.) (2006).
12. K. Yanai, *Proc. NIPR Symp. Antarc. Geosci.* **7**, 30 (1994).
13. P. H. Warren, A. M. Davis, *Antarct. Meteorites* XX, 257 (1995).
14. D. W. Mittlefehldt, in vol. 1 of *Treatise on Geochemistry*, H. D. Holland, K. K. Turekian, Eds. (Elsevier, Amsterdam, 2007), pp. 1–40.
15. D. J. Dunlop, *J. Geophys. Res.* **111**, B12S02 (2006).
16. O. A. Derby, *Revista do Observatorio* **3**, 33 (1888).
17. L. Spivak-Birndorf, M. Wadhwa, P. E. Janney, *68th Annual Meteoritical Society Meeting*, abstract 5091 (2005).
18. As discussed in the SOM, we conducted ARM and IRM paleointensity experiments but did not conduct thermal paleointensity experiments. Although thermal paleointensities are in principle the most accurate, our thermomagnetic data (fig. S9) suggest that the meteorites would probably alter during such experiments, which would compromise their efficacy while destroying the samples.
19. T. Mikouchi, M. Miyamoto, G. McKay, L. Le, *64th Annual Meteoritical Society Meeting*, abstract 5344 (2001).
20. These fast cooling rates mean that the Pb/Pb ages should provide a good estimate of the time by which the meteorites first cooled to ambient temperatures. Fast cooling also implies that the meteorites should be unaffected by low-temperature metal recrystallization that can complicate slower-cooled samples.
21. S. J. Desch, J. N. Cuzzi, *Icarus* **143**, 87 (2000).
22. S. A. Balbus, *Annu. Rev. Astron. Astrophys.* **41**, 555 (2003).
23. S. S. Russell *et al.*, in *Meteorites and the Early Solar System II*, D. S. Lauretta, H. Y. McSween, Eds. (Univ. of Arizona, Tucson, AZ, 2006), pp. 233–251.
24. J. Gattacceca *et al.*, *Phys. Earth Planet. Inter.* **166**, 1 (2008).
25. D. Stöffler, P. Pellas, *Earth Planet. Sci. Lett.* **35**, 285 (1977).
26. G. McKay, T. Ogawa, M. Miyamoto, H. Takeda, *Lunar Planet. Sci.* XXIV, 967 (1993).
27. L. L. Hood, N. A. Artemieva, *Icarus* **193**, 485 (2008).
28. J.-P. Vallée, *N. Astron. Rev.* **47**, 85 (2003).
29. K. Righter, *Lunar Planet. Sci.* XXXIX, 1936 (abstr.) (2008).
30. A. Shukolyukov, G. W. Lugmair, *Lunar Planet. Sci.* XXXVIII, 2423 (abstr.) (2007).
31. R. C. Greenwood, I. A. Franchi, A. Jambon, P. C. Buchanan, *Nature* **435**, 916 (2005).
32. P. J. Hevey, I. S. Sanders, *Meteorit. Planet. Sci.* **41**, 95 (2006).
33. D. J. Stevenson, *Earth Planet. Sci. Lett.* **208**, 1 (2003).
34. S. Stanley, J. Bloxham, W. E. Hutchison, M. T. Zuber, *Earth Planet. Sci. Lett.* **234**, 27 (2005).
35. D. W. Collinson, S. J. Morden, *Earth Planet. Sci. Lett.* **126**, 421 (1994).
36. I. Garrick-Bethell, B. P. Weiss, *Lunar Planet. Sci. Conf.* XXXVIII, 2405 (abstr.) (2007).
37. B. P. Weiss *et al.*, *Earth Planet. Sci. Lett.* **201**, 449 (2002).
38. C. J. Hale, *Earth Planet. Sci. Lett.* **86**, 354 (1987).
39. We thank T. Irving for introducing us to angrites and G. Hupé for providing NWA 2999, NWA 4801, and NWA 4931; E. Jagoutz and La Memoire de la Terre for D'Orbigny; D. Ebel and M. Zucolotto for Angra dos Reis; and the National Institute of Polar Research in Japan for A-881371. L. Bei and C. Ross gave us access to their vibrating sample magnetometer for rock magnetic analyses, N. Chatterjee assisted with electron microscopy, and D. Shim assisted with Raman spectroscopy. We also thank T. Bosak and M. Zuber for advice, M. Varela for information on the handling history of D'Orbigny, and K. Willis for administrative help. This study relied on automated paleomagnetic technology shared by J. Kirschvink. This work was partially supported by the NSF Instrumentation and Facilities Program (to B.P.W.).


### Supporting Online Material

www.sciencemag.org/cgi/content/full/322/5902/713/DC1
SOM Text
Figs. S1 to S12
Tables S1 to S5
References

27 June 2008; accepted 25 September 2008
10.1126/science.1162459

# The Role of Impulse on the Initiation of Particle Movement Under Turbulent Flow Conditions

Panayiotis Diplas,[1]* Clint L. Dancey,[2] Ahmet O. Celik,[1] Manousos Valyrakis,[1] Krista Greer,[1]† Tanju Akar[1]‡

Fundamental to our understanding of erosional and transport phenomena in earth-surface dynamics and engineering is knowledge of the conditions under which sediment motion will begin when subjected to turbulent flow. The onset criterion currently in use emphasizes the time-averaged boundary shear stress and therefore is incapable of accounting for the fluctuating forces encountered in turbulent flows. We have validated through laboratory experiments and analytical formulation of the problem a criterion based upon the impulse imparted to a sediment grain. We demonstrate that in addition to the magnitude of the instantaneous turbulent forces applied on a sediment grain, the duration of these turbulent forces is also important in determining the sediment grain's threshold of motion, and that their product, or impulse, is better suited for specifying such conditions.

The global amount of sediment delivered annually by rivers to the oceans is approximately 20 billion metric tons (*1*), whereas the overall erosion of the continental surface of the earth via the action of water and wind is estimated to be several times that amount (*2*). Shoreline retreat and stream migration have major impacts on humans and infrastructure. Despite the long study of geomorphology and the efforts in engineering, the precise determination of a criterion that identifies the flow conditions responsible for the erosion of a soil boundary remains elusive. Shields (*3*) was the first to propose a quantitative criterion based on the time- (and spatially) averaged boundary shear stress. This criterion has remained the standard method for describing threshold conditions of mobile sediment for more than 70 years, even though results from laboratory and field studies have shown more than an order of magnitude of variability in the value of this criterion for a hydraulically rough boundary (*4*). Although there are a number of possible explanations for the poor predictive ability of this threshold criterion, such as the variability of particle size and shape, the wide range of values also suggests that Shields' criterion does not properly capture turbulent flow processes and their fluctuating nature, which is responsible for particle entrainment. Many researchers, in an effort to overcome the limitations of the time-averaged wall shear stress approach, have explored and advocated the important role that peak turbulent-velocity values and the resulting hydrodynamic forces play on particle dislodgement, particularly for flow conditions near the threshold of movement (*5*–*12*). Despite these efforts, the actual physical processes responsible for grain entrainment and the accurate prediction of the initiation of movement are not well understood.

Initially, we performed laboratory flume experiments to examine the role of turbulent fluctuations on particle movement under incipient flow conditions by using 12.7-mm Teflon spheres. Details about the experiments are available in (*13*). We found that although all sediment movements coincided with high local instantaneous-velocity values, well above the mean value, very few resulted in particle movement. In Fig. 1, the streamwise velocity measured directly upstream of a mobile particle is displayed with an emphasis on seven separate extreme-velocity fluctuation events, labeled A to G. Though events A, C, and G have maximum velocities that are similar to those of events B, D, E, and F (approximately twice the mean), only the latter ones resulted in grain dislodgment. Thus, we conclude that peak values in the fluctuating velocity record indicate a necessary but not sufficient condition for particle dislodgement. The complete data record reveals that the majority of the events last over such a short period of time (milliseconds or tens of milliseconds) that, even though they may impart adequate force to move a particle within its pocket, they do not last sufficiently long to accomplish dislodgement. This is evident in Fig. 1 when comparing the duration of the peaks of events A, C, and G (28, 14, and 20 ms, respectively) with those of B, D, E, and F (93, 57, 60, and 48 ms, respectively). We therefore hypothesize that besides force magnitude, duration should also be considered in identifying the threshold of motion conditions. Impulse, which accounts for both aspects of force application, is proposed as the parameter suitable for determining particle movement.

In naturally occurring flows, variability of grains and their local arrangement will affect the hydrodynamic and resistive forces. In addition, for turbulent flow, the net hydrodynamic force, which represents the summation of the lift and drag contributions, will vary in time, magnitude, and direction. The complexities associated with grain and flow-field variability were removed to reduce the phenomenon to its essential features (including appropriate sediment bed characteristics, such as bed-pocket geometry, resistive forces, and the short duration forces that initiate motion) under well-controlled experimental conditions. We considered the dislodgement

[1]Baker Environmental Hydraulics Laboratory, Department of Civil and Environmental Engineering, Virginia Tech, Blacksburg, VA 24061, USA. [2]Department of Mechanical Engineering, Virginia Tech, Blacksburg, VA 24061, USA.

*To whom correspondence should be addressed. E-mail: pdiplas@vt.edu

†Present address: Rummel, Klepper and Kahl, LLP Consulting Engineers, Baltimore, MD 21217, USA.

‡Present address: Civil Engineering Department, Akdeniz University, Antalya 07058, Turkey.

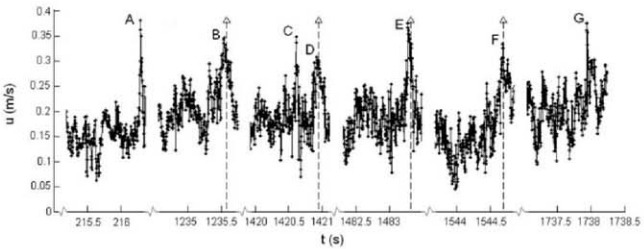


**Fig. 1.** Representative streamwise velocity $u$ time series. This velocity record was obtained in flume experiments with a laser Doppler velocimeter (LDV). The error in the velocity measurements is ±1.5%. The LDV measurement volume was located one diameter upstream of the target grain along its centerline. A separate laser-based tracking system was used to detect the instants of particle entrainment (*13*). Several velocity segments were spliced together for this illustration. The test particle entrainment instants are shown with dashed vertical arrows.

of a spherical particle under the two limiting conditions: pure drag and pure lift. The former was accomplished experimentally by using an electromagnet to apply forces of specified amplitude and duration. The latter was investigated theoretically with a simple but realistic mathematical model. Results from laboratory flume experiments were used to further evaluate the hypothesis.

A mobile steel sphere resting on a bed of Teflon spheres, representative of a particle fully exposed to turbulent flow conditions, was used together with an electromagnet to investigate the combinations of drag force magnitude $F_D$ and duration $T_D$, which barely lead to full dislodgment (Fig. 2). The preferred mode of particle movement under these conditions is rolling, consistent with observations made in the field for rounded or semirounded particles subjected to near-threshold conditions (*14*–*17*). The drag force was induced with the application of a top-hat pulse having a voltage $V$ to the electromagnet: $F_D = CV^2$ where $C$ is a characteristic of the experimental setup and the properties of the electromagnet, which is constant for a given arrangement. Many combinations of $V$ and $T_D$ were investigated for each of the particle arrangements tested (for a total of 328 separate experiments) in order to identify the minimum impulse values necessary to dislodge the steel ball from its pocket (*13*).

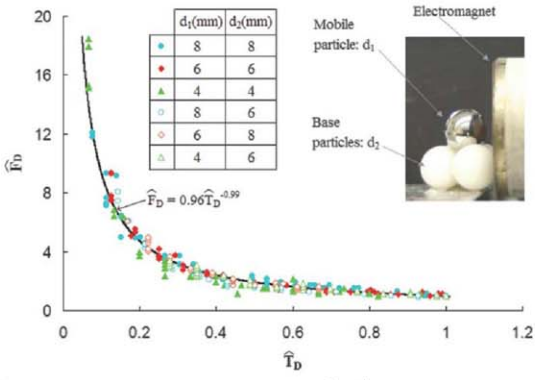


**Fig. 2.** Plot of the normalized applied electromagnetic force $\hat{F}_D = \frac{V^2}{V_{cr}^2}$ versus the normalized duration $\hat{T}_D = \frac{T_D}{T_{max}}$ at the threshold of motion from six particle configurations (data obtained from 328 tests). Errors in $V^2$ and $T_D$ are ±1.5% and ±3.6%, respectively; for $T_D$ values higher than 6 ms, which represent the vast majority of the tests, the error is smaller than ±3.6%. **(Inset)** Experimental setup photo showing the grain geometry and the electromagnet (right), and table indicating the various size combinations of magnetic test particle and base particles for the six arrangements considered in this study (left).

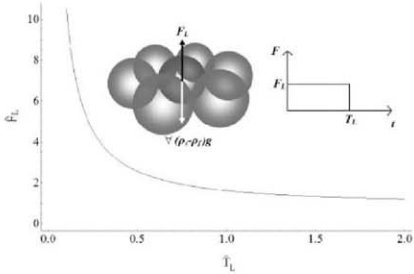


**Fig. 3.** Plot of the normalized lift force $\hat{F}_L$ versus the normalized duration $\hat{T}_L$ necessary to achieve vertical dislodgment, obtained from the theoretical lift analysis. **(Inset)** Driving and resisting forces acting upon a mobile sphere located within a bed of identical spheres, all at the same level and subject to vertical dislodgement (left), and demonstration of the lift-force pulse of magnitude $F_L$ and duration $T_L$ (right).

The results (Fig. 2) were used to delineate the relationship between normalized force $\hat{F}_D = \frac{F_D}{F_{Dmin}} = \frac{V^2}{V_{min}^2}$ and normalized duration $\hat{T}_D = \frac{T_D}{T_{max}}$, where $T_{max}$ is the duration required to dislodge the sphere at the minimum measurable applied force $F_{Dmin}$ with corresponding voltage $V_{min}$. Given the least-squares regression equation and the coefficient of determination $R^2 = 0.96$, this relationship is well represented by $\hat{F}_D = \hat{I}/\hat{T}_D$, where $\hat{I} = 1$ is the normalized critical impulse. Combinations of $\hat{F}_D$ and $\hat{T}_D$ that fall below the hyperbola are insufficient to cause full dislodgment of the sphere, whereas combinations above the curve result in dislodgment. Both of these assertions were verified through a large number of additional electromagnet experiments using the particle arrangements shown in the inset of Fig. 2. Assuming that each force applied by the electromagnet simulates in a rather simplified way an energetic turbulent event, Fig. 2 implies that the impulse potential of a turbulent stream is relevant to sediment entrainment and bed erosion. Given the wide range of force-magnitude values that are capable of barely dislodging the steel ball out of its pocket (Fig. 2) even under idealized conditions, the present results are consistent with the scatter in critical Shields stress values (*4*).

In contrast to a fully exposed particle, if a grain is imbedded in the uppermost surface of the sediment bed (Fig. 3) or slightly protruding into the turbulent flow, vertical movement represents the initial phase of dislodgment, when the streamwise drag force is ineffective and pure lift is most relevant. Using an approach similar to the electromagnet experiments, the sphere was subjected to a lift-force top-hat pulse of magnitude $F_L$ and duration $T_L$ necessary to lift the sphere to a specified elevation $z_{max}$, typically one- to two-grain diameters. This pulse can be represented by $F_L[H(t) - H(t - T_L)]$, shown as an inset in Fig. 3, where $H(t)$ is the Heaviside function defined by

$$H(t) = \begin{cases} 1 & t > 0 \\ 0 & t \le 0 \end{cases}$$

and so

$$F_L[H(t) - H(t - T_L)] = \begin{cases} F_L & 0 < t \le T_L \\ 0 & t > T_L \end{cases}$$

The resulting equation describing the purely vertical motion of a mobile grain is then

$$\forall(\rho_s + \rho_f C_m)\frac{d^2z}{dt^2} = F_L[H(t) - H(t - T_L)] - \forall(\rho_s - \rho_f)g \quad (1)$$

In Eq. 1, $\forall$ is the particle volume, $\rho_s$ is the solid-grain density, $\rho_f$ is the fluid density, $C_m$ is the added mass coefficient (*18*), $z$ is the elevation of the particle's center of mass above its initial location at time $t$, and $g$ is the gravitational

acceleration. Equation 1 is solved analytically to obtain the vertical height $z(t)$ at any time $t \geq T_L$:

$$z(t) = \frac{(\rho_s - \rho_f)gt^2}{2(\rho_s + \rho_f C_m)}\left[\frac{F_L}{W_{sub}}\left(1 - \left(1 - \frac{T_L}{t}\right)^2\right) - 1\right] \quad (2)$$

Equation 2 describes the decelerating phase of the particle motion after the application of the lift force has ceased (for $t > T_L$). The critical condition for full particle dislodgment is defined here by a specified vertical displacement, $z_{max}$. Using the time parameter $t_{ff} = \sqrt{\frac{2z_{max}}{g}}$, which may be interpreted as a characteristic free-fall time for the sphere, and the particle submerged weight $W_{sub}$, to normalize the time variables ($t$, $T_L$) and lift force respectively, yields (to achieve $z = z_{max}$)

$$1 = \frac{\rho_s - \rho_f}{\rho_s + \rho_f C_m}\frac{\hat{F}_L{}^2 \hat{T}_L{}^2}{2}\left(1 - \frac{1}{\hat{F}_L}\right) \quad (3)$$

with $\hat{F}_L$ and $\hat{T}_L$ (lift-force magnitude and duration, respectively) in normalized form. Equation 3 represents the threshold condition for vertical dislodgement and is plotted in Fig. 3. Consistent with the impulse concept, the critical lift-force magnitude necessary for initiating the particle dislodgement increases with decreasing duration. For the limiting case of critical conditions obtained by applying forces much greater than the submerged particle weight over very short durations, which are the conditions typically encountered in turbulent flows when saltation is the prevalent mode of entrainment (*14*), the normalized impulse $\hat{I}$ approaches an asymptotic value.

To explore our hypothesis further, we used laboratory flume experiments to study the interaction between turbulent channel flow and a mobile grain. Movement of a fully exposed 12.7-mm Teflon sphere (Fig. 4A) was detected with a He-Ne laser system simultaneously with the local flow velocity, which was obtained with a laser Doppler velocimeter (*13*). The hydraulic conditions were near threshold for the mobile test particle, and we observed that rolling was the mode of entrainment, in agreement with prior studies (*14–17*) and the electromagnet experiments.

A portion of the He-Ne detection system output that shows slight movement of the grain, as well as a complete dislodgment, is provided in Fig. 4B. The entire 30-min photodetector record was analyzed, and the times identified with full grain dislodgment were encoded within the corresponding flow-velocity record. This data series was further analyzed assuming that the form drag $F_D$ was the dominant hydrodynamic force acting on a test particle. The instantaneous drag force acting on the particle was estimated from the instantaneous local velocity measurements $u$, considering $F_D \propto u^2$ (*19*, *20*).

A moment balance approach was used to determine the minimum level of $u^2$necessary for moving the submerged grain ($\overline{u^2}_{crit}$) (*21*). All events with $u^2 \geq \overline{u^2}_{crit}$ were specified in the velocity record together with their times of occurrence and durations ($T_i$, duration over which $u^2_i \geq \overline{u^2}_{crit}$). In addition, time-averaged $u^2$ values ($\overline{u^2}_i$) were computed for each such event, representative of the average drag force ($\overline{F}_{Di}$). That is, each event for which $\overline{u^2}_i \geq \overline{u^2}_{crit}$ has associated with it a pair of values ($\overline{u^2}_i$, $T_i$) that represent ($\overline{F}_{Di}$, $T_i$). The impulse associated with any event is $I_i \propto \overline{u^2}_i T_i$. The results are shown in Fig. 4C, where ($I_i$, $\overline{u^2}_i$) combinations are plotted for all 1465 events for which $\overline{u^2}_i \geq \overline{u^2}_{crit}$, including 65 events associated with particle entrainment.

The Fig. 4C plot demonstrates that $F_D > F_{Dcrit}$ alone is not sufficient to predict grain dislodgment. Only particular combinations of ($\overline{F}_{Di}$, $T_i$) with sufficient impulse $I_i$ yield grain dislodgment; that is, a critical set of ($\overline{F}_{Di}$, $T_i$) values distinguish grain movement from no movement based upon the impulse they impart. Contrary to controlled pulses applied during the electromagnet experiments, turbulent channel flow naturally contains flow structures with the potential to apply a wide range of impulse levels to the mobile particle, above and below a critical value (Fig. 4C). The demarcation line KL separating movement from no movement in Fig. 4C is characterized by nearly constant impulse

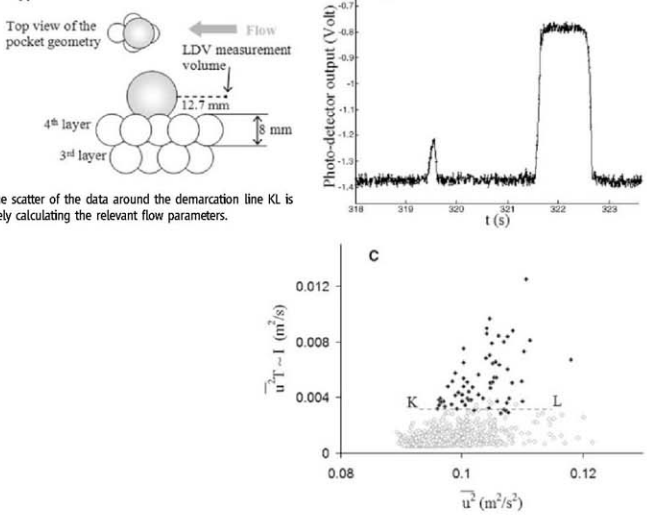


**Fig. 4.** Flume-bed arrangement and experimental results. **(A)** Detailed drawing of the pocket geometry and the mobile test particle on the flume bed. **(B)** A fraction of typical photodetector output. Examples of both rocking (left peak), and rolling (right peak) of the test particle are shown. **(C)** Corresponding $I_i - \overline{u^2}_i$ combinations of the events. Particle entrainment events are displayed with solid circles; open circles indicate flow events that did not result in particle dislodgement. The scatter of the data around the demarcation line KL is indicative of the difficulties in accurately calculating the relevant flow parameters.

values but widely ranging force magnitudes, which shows the relevance of impulse to grain entrainment.

Our experimental and theoretical analyses support the hypothesis that impulse rather than force is the relevant parameter for the incipient motion of mobile sediment under the two limiting conditions of pure drag and pure lift. Because impulse represents the criterion for particle dislodgement for lift and drag separately, it will remain valid for the more general case in which both forces contribute to particle dislodgement, a condition typically encountered when a particle is partially exposed to the flow. It is anticipated that the practical implementation of the impulse criterion will include a parametric characterization of the hydraulic forces acting on the sediment grains (much like the Shields' criterion), but in addition and in contrast to the traditional criterion, the time scales characteristic of the flow structures that impart the required impulse and their frequency will need to be properly parameterized as well.

### References and Notes


1. J. P. M. Syvitski, C. J. Vorosmarty, A. J. Kettner, P. Green, *Science* **308**, 376 (2005).
2. B. H. Wilkinson, B. J. McElroy, *Geol. Soc. Am. Bull.* **119**, 140 (2007).
3. A. Shields, *Anwendung der Aehnlichkeitsmechanik und der Turbulenzforschung auf die Geschiebebewegung*, *Mitteilungen der Preussischen Versuchsanstalt fur Wasserbau und Schiffbau* (Heft 26, Berlin, 1936) (W. P. Ott, J. C. van Uchelen, Transl., Publication No. 167, Hydrodynamics Laboratory, California Institute of Technology, Pasadena, CA, 1950).
4. J. M. Buffington, D. R. Montgomery, *Water Resour. Res.* **33**, 1993 (1997).
5. H. A. Einstein, E. A. El-Samni, *Rev. Mod. Phys.* **21**, 520 (1949).
6. A. J. Sutherland, *J. Geophys. Res.* **72**, 6183 (1967).
7. A. J. Grass, *J. Hydraul. Div.* **96**, 619 (1970).
8. A. S. Paintal, *J. Hydraul. Res.* **9**, 527 (1971).
9. A. D. Heathershaw, P. D. Thorne, *Nature* **316**, 339 (1985).
10. J. Nelson, R. L. Shreve, S. R. McLean, T. G. Drake, *Water Resour. Res.* **31**, 2071 (1995).
11. B. M. Sumer, L. H. C. Chua, N.-S. Cheng, J. Fredsoe, *J. Hydrol. Eng.* **129**, 585 (2003).
12. S. Vollmer, M. G. Kleinhans, *Water Resour. Res.* **43**, W05410 (2007).
13. Materials and methods are available as supporting material on *Science* Online.
14. R. A. Bagnold, *Proc. R. Soc. London Ser. A* **332**, 473 (1973).
15. J. R. D. Francis, *Proc. R. Soc. London Ser. A* **332**, 443 (1973).
16. T. G. Drake, R. L. Shreve, W. E. Dietrich, P. J. Whiting, L. D. Leopold, *J. Fluid Mech.* **192**, 193 (1988).
17. C. L. Dancey, P. Diplas, A. Papanicolaou, M. Bala, *J. Hydrol. Eng.* **128**, 1069 (2002).
18. T. R. Auton, *J. Fluid Mech.* **183**, 199 (1987).
19. M. W. Schmeeckle, J. M. Nelson, R. L. Shreve, *J. Geophys. Res.* 10.1029/2006JF000536 (2007).
20. B. Hofland, J. Battjes, *J. Hydrol. Eng.* **132**, 1169 (2006).
21. A. N. Papanicolaou, P. Diplas, N. Evaggelopoulos, S. Fotopoulos, *J. Hydrol. Eng.* **128**, 369 (2002).


22. We thank the NSF for financially supporting this study (grant EAR-0439663 to P.D. and C.L.D).


### Supporting Online Material

www.sciencemag.org/cgi/content/full/322/5902/717/DC1
Materials and Methods

10 April 2008; accepted 24 September 2008
10.1126/science.1158954

# Molecular Confinement Accelerates Deformation of Entangled Polymers During Squeeze Flow

Harry D. Rowland,[1] William P. King,[1] John B. Pethica,[2] Graham L. W. Cross[2]*

The squeezing of polymers in narrow gaps is important for the dynamics of nanostructure fabrication by nanoimprint embossing and the operation of polymer boundary lubricants. We measured stress versus strain behavior while squeezing entangled polystyrene films to large strains. In confined conditions where films were prepared to a thickness less than the size of the bulk macromolecule, resistance to deformation was markedly reduced for both solid-glass forging and liquid-melt molding. For melt flow, we further observed a complete inversion of conventional polymer viscosity scaling with molecular weight. Our results show that squeeze flow is accelerated at small scales by an unexpected influence of film thickness in polymer materials.

Polymeric materials have become common in manufacturing because they combine favorable, tunable properties with ease and economy of production and processing. Nanoimprint lithography (NIL) (*1*) exploits nanometer-scale polymer flow to form patterns during the manufacture of semiconductor devices, organic electronics, and optics (*2*, *3*). During NIL, a rigid, patterned die squeezes a supported polymer thin film at dimensions that are comparable to the size of the polymer molecule. The squeeze flow between protruding die regions and the supporting substrate governs the dynamics of NIL (*4*–*6*). Filling of the die requires large-strain lateral flow of polymer through gaps that approach a few nanometers in size as cavities progressively fill (*5*, *7*, *8*). The polymer properties, the film thickness, and the distribution of cavity sizes and shapes affect the processing conditions required for NIL and ultimate replication fidelity.

The dynamics of amorphous polymer systems with long, flexible molecular chains are governed by a spectrum of relaxation time scales linked to available modes of motion, constrained by dynamic networks of entanglements. Near a wall, the behavior becomes more complex as symmetries are broken by geometric constraints and interaction with the wall surface. The segmental and whole-chain motion that governs these interfacial chain dynamics is not well understood. In the case of segmental motion, experiments with high spatial resolution normal to the plane of the film have revealed both enhanced segmental mobility (*9*) and reduced segmental mobility at surfaces (*10*). Conflicting experimental evidence also exists in the case of whole-chain motion; viscous-melt thinning (*11*) and thin-film stretching (*12*) suggest enhanced whole-chain motion, whereas suppressed diffusion (*13*) suggests reduced whole-chain motion.

We used a nanometer-scale indentation technique (*14*) to show how both dimensional reduction and molecular confinement affect polymer mechanics during NIL while forming temperature and molecule size are varied. Nearly all investigations of nanometer-scale polymer mechanical behavior have been at zero strain or small strain. In contrast, NIL squeeze flow features a large hydrostatic pressure, rapid shearing, extremely large strains, and unknown wall interactions. Even macroscopically, squeeze flow measurements involve transient, inhomogeneous flow with nontrivial, evolving boundary conditions (*15*). Nonetheless, by careful control of initial conditions, boundary conditions, and deformation history, there emerges a consistent and reproducible alteration of stress-strain squeeze flow response with dimensional and macromolecular confinement.

Figure 1 shows the experimental approach, which allows high-resolution measurement of stress and strain during polymer squeeze flow over a broad range of temperature, strain, and loading conditions (*16*). A flat-punch nanoindenter performed large-strain squeeze flow indentation on three thicknesses ($H_i$) of monodisperse polystyrene (PS) films—170 nm, 80 nm, and 36 nm—prepared with weight-average molecular weights ($M_w$) of 44 kD, 900 kD, and 9000 kD. Measurements were performed above and below the bulk glass transition temperature $T_g$ (100°C) at temperatures of 20° to 125°C (a representative measurement set is shown in Fig. 1C). Linear loading ramps ensured repeatable experimental conditions similar to NIL practice.

To ensure a formal similarity of flow field geometry, we dimensionally scaled the squeezed volumes such that the die diameter was always 10 times the initial film thickness. The isothermal testing conditions produced either glassy or melt-like conditions. The die surface roughness and contact misalignment were less than 2 nm, pro-

[1]Department of Mechanical Science and Engineering, University of Illinois, Urbana, IL 61801, USA. [2]School of Physics and Centre for Research on Adaptive Nanostructures and Nanodevices (CRANN), Trinity College, Dublin 2, Ireland.

*To whom correspondence should be addressed. E-mail: graham.cross@tcd.ie

viding near-ideal squeeze flow between flat, parallel plates (*14*).

Several key features are apparent in the measured stress-strain curves (Fig. 1, C and D). At low strain, an elastic contact modulus was defined from the largely recoverable, linear slope deformation (*16*, *17*). Beyond this point, a distinct and characteristic step-like feature appears in the curve. The leading edge of the step signals a transition from recoverable (elastic) to irrecoverable plastic strain (*17*), which we associate with plastic yield of a glassy form of the thin-film polymer. We label the measured value of stress at this transition point the forming stress.

In entangled polystyrene, film thickness affects $T_g$ at about 100 nm (*18*) with a 5°C depression at 36 nm (*19*) and affects elastic modulus at around 30 to 40 nm (*20*). We found that initial film thickness affects squeeze flow stress-strain response in various ways. Where glass-like characteristics appeared at low strain, they were similar for the 170-nm and 80-nm films over all tested conditions. However, the 36-nm films exhibited a pronounced increase in compliance on the order of 40% for contact modulus and decrease in strength with a 30% reduction of forming stress. This occurred over two decades of $M_w$ and temperatures of 20° and 80°C; it is shown explicitly (Fig. 2A) for 80°C in comparative stress-strain curves and summarized for our full data set in Fig. 2B (contact

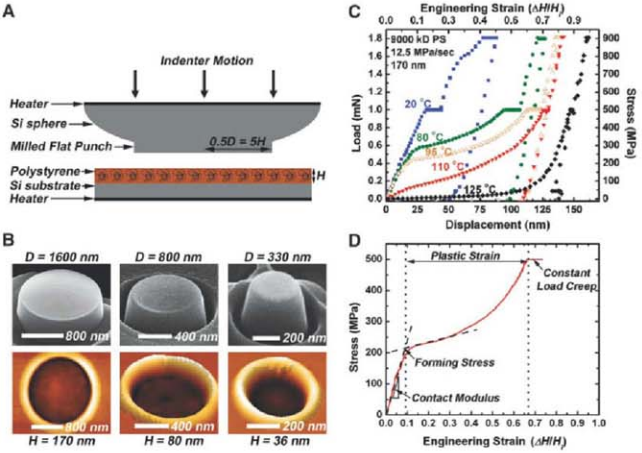


**Fig. 1.** **(A)** Flat-punch silicon dies, with 10:1 aspect ratio of punch diameter to initial film thickness, emboss thin PS films supported by silicon. **(B)** Scanning electron micrographs of the three flat-punch silicon dies used in this work (diameters 1600, 800, and 330 nm) and atomic force microscopy scans of imprints into 9000-kD polystyrene (PS) films of 170, 80, and 36 nm, respectively. **(C)** Representative family of stress-strain measurements recorded above and below nominal bulk $T_g$, at a linear loading ramp of 12.5 MPa/s with the 1600-nm die on a 9000-kD, 170-nm PS film. **(D)** Features of the stress-strain curve used to extract modulus, forming stress, and plastic strain.

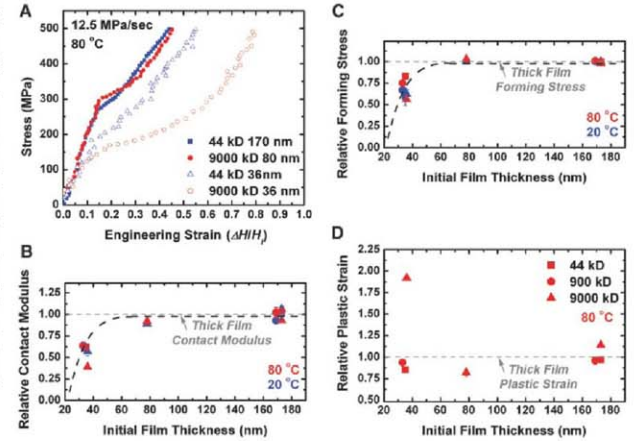


**Fig. 2.** **(A)** Effects of film thickness and molecular confinement shown explicitly for squeeze flow stress-strain curves collected using a 12.5 MPa/s load ramp at 80°C. Data are shown for 170-nm and 36-nm films of shortest-chain (44 kD) PS (blue) and for 80-nm and 36-nm longest-chain (9000 kD) PS (red). Curves from 170-nm and 80-nm films show identical stress versus strain response to squeeze strains of 0.45 for entangled polymers, despite molecular weight spanning two decades (solid squares and circles). **(B** to **D)** Contact modulus (B), forming stress (C), and plastic strain (D) for polymers with $M_w$ of 44 kD (squares), 900 kD (circles), and 9000 kD (triangles) plotted versus initial film thickness. Dashed line is to guide the eye. For each temperature tested (20°C, blue; 80°C, red), the parameters are normalized by the corresponding value measured for the short-chain polymer in thick films (44 kD, 170 nm).

modulus) and Fig. 2C (forming stress). For each temperature, parameter values for a particular measured film were normalized to the average value of 170-nm film measurements (including all molecular weights) to allow direct comparison of the relative effect of film thickness. In contrast, large-strain behavior is similar for all films except for the case of the highest $M_w$, shown as relative plastic strain in Fig. 2D for the experiment at 80°C. In a manner similar to the contact modulus and forming stress, the relative plastic strain parameter refers to the plastic strain normalized by the average value of plastic strain, as defined in Fig. 1D, for all 170-nm films at 80°C. These observations remain qualitatively unchanged for load rate variation over two decades, provided the forming-stress step is present.

To highlight the anomaly in the strain behavior of the longest-chain weight and thinnest film, we compared stress versus strain for thick (170 nm) and thin (36 nm) films measured at 20° and 80°C during initial loading to 500 MPa (Fig. 3). The three $M_w$ values of 44 kD, 900 kD, and 9000 kD (blue, green, and red traces, respectively) are shown. The ratios of film thickness to the unperturbed (i.e., bulk) radius of gyration $R_g$ are 28, 6.5, and 2.0 for the thick film (i.e., far from confinement), whereas for the thin film the factors are 6.0, 1.4, and 0.43, with the last factor indicating highly confined molecules. The forming stress step is visible in all but the thick-film 20°C data in Fig. 3A, where it occurs at about 750 MPa (see Fig. 1D). The stress-strain curves of unconfined polymer show remarkable overlap at a given temperature. In the thin-film case, the unconfined polymer curves exhibit a $M_w$-independent increase in compliance and softness with absolute film thickness, whereas the anomalous confined-film case shows reduced stress for equivalent large strain that becomes relatively more pronounced with increasing temperature.

Hot embossing NIL achieves high-quality replication (*17*) by heating the polymer to a softened state, eliminating plastic yield, and reducing elastic storage. Figure 4 shows the effect of confinement on polymer flow characteristics in a melt-like state. For the 170-nm film at 115°C (Fig. 4A), no forming stress was observed, and the three curves lie fully separated with thickened flow at higher $M_w$, consistent with a conventional bulk response. In the 36-nm film, forming stress disappeared at 110°C (Fig. 4B). Confinement, however, profoundly affects the resistance to deformation. The ordering of increased flow stress with $M_w$ in curves free of forming stress has been completely reversed: The data for the 900-kD film near confinement (confinement ratio 1.4) overlap the data for the unconfined 44-kD film, whereas the behavior of the 9000-kD film has flipped position to lie well below the shorter-chain films. A stress reduction for the 0.43 confinement ratio of nearly 70% at 0.5 strain extends the trend of an increased softening effect with temperature seen in Fig. 3.

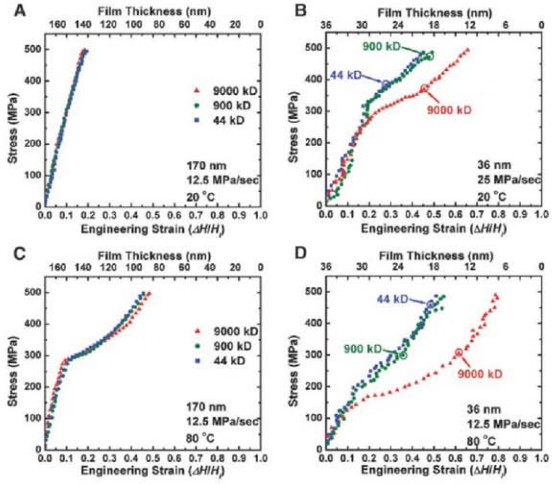


**Fig. 3.** Squeeze flow stress-strain curves (loading at 12.5 MPa/s to peak stress of 500 MPa) show identical mechanical behavior with respect to $M_w$ of 44 kD, 900 kD, and 9000 kD in 170-nm films at 20°C (**A**) and 80°C (**C**), and for $M_w$ of 44 kD and 900 kD in 36-nm films at 20°C (**B**) and 80°C (**D**). Note that in (A), inelastic behavior cannot be seen because the forming stress is about 750 MPa for all films at this temperature (see Fig. 1C). The curve overlap is broken at large strain for the confined 9000-kD film at both temperatures, but with a more pronounced effect at 80°C.

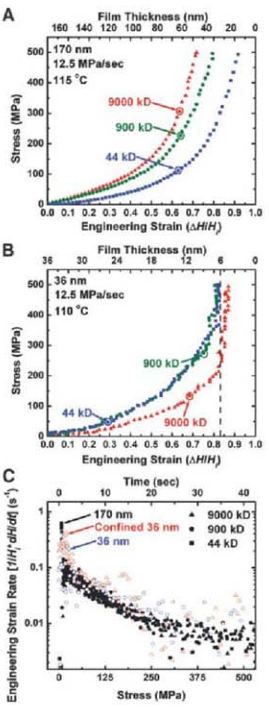


**Fig. 4.** (**A**) Stress-strain curves (loading at 12.5 MPa/s) at 115°C for 170-nm polystyrene films with $M_w$ of 44 kD, 900 kD, and 9000 kD (blue, green, and red, respectively). The forming stress has vanished in all curves that show conventional separation of stress-strain curves for melt flow by thickening with $M_w$. (**B**) Stress-strain curves at 110°C for 36-nm polystyrene films with $M_w$ of 44 kD, 900 kD, and 9000 kD. The 900-kD film, which is close to being confined, shows a similar response to the 44-kD film, whereas the deeply confined 9000-kD film curve lies well below both the shorter-chain curves. Confinement inverts the order of separated stress-strain curves for melt flow by instead thinning with $M_w$. (**C**) Mean forming strain rate versus applied mean die stress at 110°C for all three molecular weights in 170-nm films (black markers) and 36-nm films for unconfined 44-kD and 900-kD films (blue) and the confined 9000-kD film (red).

The observed polymer mechanical behavior differs from expected bulk scaling of polymer mechanical behavior in two ways. When the squeeze flow conditions induce a forming stress in the polymer film, the polymer mechanical response is anomalous when the film is in an initially confined state, giving accelerated deformation. In the absence of forming stress, unconfined films lead to a net thickened scaling with $M_w$, whereas films prepared so that the molecules are confined show inverted behavior, with the flow thinning at high $M_w$. Although indentation to large strain also serves to confine the longer polymer molecules, we found no evidence of a shift in mechanical behavior during the deformation process itself. This is consistent with our previous observations for thick films (*21*).

The measured polymer response cannot be attributed to phenomena known from conventional polymer processing, even though complex effects are not uncommon in these flows. This complexity arises when inelastic deformation localizes at different length scales as shear bands, entanglement depletion, and wall slip. Shear bands with dimensions down to several tens of nanometers have been observed in annealed polystyrene glass compression (*22*), and there is recent evidence for strain localization in deformed melts (*23*). However, in nanoindentation of metallic crystals and glass-forming systems, small contact stress fields have been found to probe a natural spatial distribution of localized defects, leading to, for example, delayed plasticity (hardening) and single shear band emission (*24*). We similarly expect stress localization of our present experiments to, if anything, suppress the formation of topological defects. Therefore, such defect activity is highly unlikely to be responsible for the accelerated deformation we observe.

At smaller scales, high shear rate can induce local entanglement depletion, which results in shear thinning. The polymer strains and strain rates in our experiments represent conditions typical for nanoimprint manufacturing and are all well into the nonlinear flow regime. Nonetheless, our results cannot be explained by standard polymer nonlinear shear or extensional effects. In Fig. 4C, the mean compressive strain rate (corresponding to the rate of gap closure) produced by our linear loading history is compared for the confined-film and unconfined-film experiments. At early times, the strain rates are distributed over the region 0.05 to 0.5 $s^{-1}$ before converging and slowly decreasing to 0.01 $s^{-1}$ at long times. Conventional shear thinning leads to reemergent Newtonian flow with viscosity reduction bounded by linear Rouse-mode $M_w$ scaling (*25*), whereas extensional flows thicken with a further linear $M_w$ prefactor (*26*, *27*). Shear thinning may partially account for the relatively modest increase in stress versus strain scaling with $M_w$ in the thick film at 115°C (Fig. 4A). The reversal of $M_w$ scaling for the confined entangled polymer melt of Fig. 4B cannot be explained by any standard nonlinear polymer mechanical response.

In channeled flows of dimension less than the Navier–de Gennes slip length, the die wall can further provide a mechanism for strain localization by allowing slip at the interface (*28*). In general, slip can be controlled by lubricants that concentrate shear at a sharp rheological gradient near die walls (*29*). Natural mobility gradients reported for cooperative chain segment motion (*9*, *10*) across thin films may result in slip and reduced effective frictional wall traction. However, in the present experiment, chain confinement does not affect contact modulus or forming stress, as these properties are uniformly affected for all chain lengths (Fig. 2, B and C), from which we conclude that effective small-strain lubrication is not altered by confinement. At large strain, squeeze flows may suffer a loss of lubrication (*29*); however, any similar confinement-related effect would produce a flow thickening opposite to what we observe.

The experiments show a breakdown of well-established scaling order in polymer physics. In the limit of zero shear, the viscosity scales as $M_w^{3.4}$, as explained to the leading digit by the reptation theory of entangled polymer melt dynamics (*30*). In the absence of shear thinning, conventional scaling would predict a (9000 kD/44 kD)$^{3.4} \approx 10^8$ increase in flow resistance from the lowest- to highest-$M_w$ polymers. Even at the shear thinning limit, the $M_w$ scaling approaches unity and the flow resistance should increase by a factor of more than 100 from the lowest- to highest-$M_w$ films. The approximate factor of 3 reduction for the highest-$M_w$ stress versus strain scaling observed in Fig. 4B is highly different from bulk mechanics.

Our experiments, which show fluid-like behavior of a confined polymeric solid, are contrary to previous experiments that found solid-like behavior for unentangled polymer fluids during small-strain deformation in narrow gaps (*31*). In the latter, solidification is thought to arise from ordering and bridging effects in the gap that are attributable to short molecular relaxation times. In our films, long relaxation times preclude the development of such networks on experimental time scales. Instead, we propose that the experiments reveal the effect of an altered entanglement network, where two-dimensional confinement modifies chain packing during film preparation (*32*, *33*). This manifests as a suppression of bulk entanglements by reduced interpenetration of neighboring chains in favor of self-penetration, effectively weakening the overall polymer network. The concept has been used to explain enhanced deformation of tension-loaded, free-standing, confined glassy polystyrene films (*12*).

The altered entanglement network does not appear to affect the small-strain properties of the polymer. In bulk polymers in the glassy state, small-strain deformations related to both elasticity and yield perturb segments of polymer chain shorter than the entanglement spacing or tube diameter (*34*). Because the small-strain properties observed here in thin films are uniformly affected regardless of $M_w$, we suspect that they are likely caused by enhanced segmental (not whole-chain) mobility, similar to observations (*9*) during investigation of $T_g$ at the surfaces of thin films. Both large-strain glassy plastic and melt flow stress are strongly linked to entanglement network effects (*35*); therefore, network weakening by confinement provides a unifying picture explaining our observations at both small and large strain.

Our results show that molecular confinement accelerates deformation of entangled polymers during squeeze flow, and that confined entangled polymer films exhibit $M_w$ dependence opposite to what is found for unconfined entangled polymer films. Glassy entangled polymer films exhibit elastic stiffness and yield stress that is lower for thin films than for thick films, regardless of confinement. The observed phenomena cannot be explained by boundary effects or known nonlinear mechanical polymer response. The results suggest that polymer flow during NIL may be enhanced by selecting polymers of increased molecular weight. Although they are directly relevant to NIL and nanomanufacturing, the results also have implications for wear in ultrathin polymer coatings, the operation of polymer-based lubricants and additives, and the strength and fatigue of layered polymer composites.

## References and Notes


1. S. Y. Chou, P. R. Krauss, P. J. Renstrom, *Science* **272**, 85 (1996).
2. L. J. Guo, *J. Phys. D* **37**, R123 (2004).
3. S. R. Forrest, *Nature* **428**, 911 (2004).
4. L. J. Heyderman, H. Schift, C. David, J. Gobrecht, T. Schweizer, *Microelectron. Eng.* **54**, 229 (2000).
5. H. D. Rowland, W. P. King, A. C. Sun, P. R. Schunk, *J. Micromech. Microeng.* **15**, 2414 (2005).
6. H. Schulz, M. Wissen, H. C. Scheer, *Microelectron. Eng.* **67–68**, 657 (2003).
7. G. L. W. Cross, *J. Phys. D* **39**, R363 (2006).
8. H.-C. Scheer, H. Schulz, D. Lyebyedyev, *Proc. SPIE* **4349**, 86 (2001).
9. C. J. Ellison, J. M. Torkelson, *Nat. Mater.* **2**, 695 (2003).
10. S. Sills *et al.*, *J. Chem. Phys.* **120**, 5334 (2004).
11. A. Tuteja, P. M. Duxbury, M. E. Mackay, *Macromolecules* **40**, 9427 (2007).
12. L. Si, M. V. Massa, K. Dalnoki-Veress, H. R. Brown, R. A. L. Jones, *Phys. Rev. Lett.* **94**, 127801 (2005).
13. B. Frank, A. P. Gast, T. Russell, H. R. Brown, C. Hawker, *Macromolecules* **29**, 6531 (1996).
14. G. L. W. Cross, B. S. O'Connell, J. B. Pethica, H. D. Rowland, W. P. King, *Rev. Sci. Instrum.* **79**, 013904 (2008).
15. J. Engmann, C. Servais, A. S. Burbidge, *J. Non-Newtonian Fluid Mech.* **132**, 1 (2005).
16. See supporting material on *Science* Online.
17. G. L. W. Cross, B. S. O'Connell, J. B. Pethica, *Appl. Phys. Lett.* **86**, 081902 (2005).
18. J. L. Keddie, R. A. L. Jones, R. A. Cory, *Europhys. Lett.* **27**, 59 (1994).
19. S. Kawana, R. A. L. Jones, *Phys. Rev. E Stat. Nonlin. Soft Matter Phys.* **63**, 021501 (2001).
20. C. M. Stafford *et al.*, *Nat. Mater.* **3**, 545 (2004).
21. H. D. Rowland, W. P. King, G. L. W. Cross, J. B. Pethica, *ACS Nano* **2**, 419 (2008).
22. J. B. C. Wu, J. C. M. Li, *J. Mater. Sci.* **11**, 434 (1976).
23. P. Tapadia, S. Ravindranath, S.-Q. Wang, *Phys. Rev. Lett.* **96**, 196001 (2006).
24. C. A. Schuh, T. C. Hufnagel, U. Ramamurty, *Acta Mater.* **55**, 4067 (2007).
25. C. Tsenoglou, *Macromolecules* **34**, 2148 (2001).
26. J. K. Nielsen, H. K. Rasmussen, O. Hassager, G. H. McKinley, *J. Rheol.* **50**, 453 (2006).
27. A. Bach, H. K. Rasmussen, O. Hassager, *J. Rheol.* **47**, 429 (2003).
28. S. Wang, *Adv. Polym. Sci.* **138**, 229 (1999).

29. C. W. Macosko, *Rheology Principles, Measurements, and Applications* (Wiley-VCH, New York, 1994).
30. M. Doi, S. F. Edwards, *The Theory of Polymer Dynamics* (Oxford Univ. Press, Oxford, 1986).
31. J. Peanasky, L. L. Cai, S. Granick, C. R. Kessel, *Langmuir* **10**, 3874 (1994).
32. P. G. De Gennes, *Scaling Concepts in Polymer Physics* (Cornell Univ. Press, Ithaca, NY, 1979).
33. H. R. Brown, T. P. Russell, *Macromolecules* **29**, 798 (1996).
34. B. Crist, in *The Physics of Glassy Polymers*, R. N. Haward, R. J. Young, Eds. (Chapman & Hall, London, 1997), pp. 155–212.
35. M. C. Boyce, R. N. Haward, in *The Physics of Glassy Polymers*, R. N. Haward, R. J. Young, Eds. (Chapman & Hall, London, 1997), pp. 213–294.
36. Supported by Science Foundation of Ireland grant 00/PI.1/C028, NSF grants CMMI 07-32114 and DMI 03-28162, the Center for Nanoscale Chemical-Electrical-Mechanical Manufacturing Systems, NSF Faculty Early Career Development grant CBET 07-31930, and a U.S. Department of Energy Presidential Early Career Award for Scientists and Engineers. H.D.R. is vice president for engineering, Endotronix Inc., Peoria, IL.

**Supporting Online Material**
www.sciencemag.org/cgi/content/full/1157945/DC1
Materials and Methods
Figs. S1 to S3
Tables S1 and S2
References

18 March 2008; accepted 16 September 2008
Published online 2 October 2008;
10.1126/science.1157945
Include this information when citing this paper.

# Peptides Enhance Magnesium Signature in Calcite: Insights into Origins of Vital Effects

A. E. Stephenson,[1]* J. J. DeYoreo,[2] L. Wu,[2,3] K. J. Wu,[2] J. Hoyer,[4] P. M. Dove[1]*

Studies relating the magnesium (Mg) content of calcified skeletons to temperature often report unexplained deviations from the signature expected for inorganically grown calcite. These "vital effects" are believed to have biological origins, but mechanistic bases for measured offsets remain unclear. We show that a simple hydrophilic peptide, with the same carboxyl-rich character as that of macromolecules isolated from sites of calcification, increases calcite Mg content by up to 3 mole percent. Comparisons to previous studies correlating Mg content of carbonate minerals with temperature show that the Mg enhancement due to peptides results in offsets equivalent to 7° to 14°C. The insights also provide a physical basis for anecdotal evidence that organic chemistry modulates the mineralization of inorganic carbonates and suggest an approach to tuning impurity levels in controlled materials synthesis.

Over the past 50 years, the Mg/Ca ratio in marine cements (*1–4*) and calcified skeletal structures (*5–9*) has become a widely used proxy for reconstructing past Earth environments. Elemental proxy models for temperature and seawater chemistry begin by assuming that compositional signatures reflect environmental conditions of formation. Yet, the impurity contents of biominerals are subject to "vital effects" that can induce large offsets from equilibrium values (*7*). These "vital effects" are believed to have kinetic and taxonomic origins, but the mechanistic basis for measured offsets is not well understood. A complicating factor is that mineralization is isolated from the external environment and occurs within an organic-rich matrix (*10*) whose roles in mineralization are recognized but difficult to assess. At sites of calcification, this microenvironment contains complex assemblages of proteins and polysaccharides (*10*) whose structures and amino acid sequences are species-specific (*5, 10–12*). Moreover, calcifying macromolecules are unusually enriched in the carboxyl-rich acidic amino acids aspartate and glutamate (*10, 11*), and their presence is implicated in modulating biomineral formation (*13, 14*). Similarly, a number of widely cited studies of nonskeletal carbonates have questioned whether humic and protein substances (also enriched in acidic amino acids) in marine sedimentary environments could influence mineralization (*2, 3*).

Many observations and in vitro experimental studies show that aspartate-rich biomolecules enhance calcite growth (*11, 13, 14*). Indeed, a recent study found that nanomolar concentrations of acidic amino acids, peptides, and full proteins accelerate calcite growth rate (up to 25 times) by a relation that correlates with the hydrophilicity of biomolecules (*14*), a measure of their interactions with water. These insights led us to hypothesize that because (i) cation incorporation is the rate-limiting step to growth (*15*) and (ii) Mg is more strongly solvated than Ca (*16*), then rate-modifying peptides could also lower the desolvation barrier to Mg incorporation relative to Ca and thereby alter Mg content.

To test this idea, we grew calcite under controlled chemical conditions within a flow-though cell of an atomic force microscope (AFM). Growth was observed in situ for the duration of each experiment while kinetic and surface thermodynamic properties were simultaneously measured. We monitored the propagation of steps at dislocation hillocks to observe the growth process during each treatment. Using established methods (*17–19*), we conducted experiments at a constant supersaturation (defined with respect to pure calcite), $\sigma$, of 1.6 where

$$\sigma = \ln\left(a_{Ca^{2+}} a_{CO_3^{2-}} / K_{sp}\right) \quad (1)$$

such that $a_i$ is the activity of species i, and $K_{sp}$ is the equilibrium solubility constant ($10^{-8.48}$ for pure calcite at 25°C). The $Ca^{2+}$:$CO_3^{2-}$ ratio was

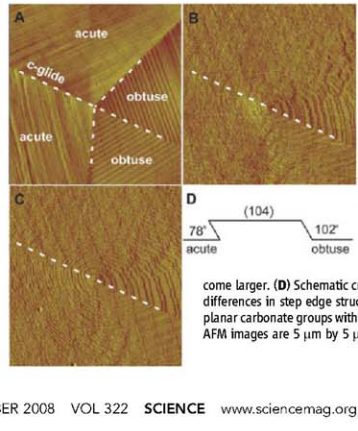


**Fig. 1.** AFM images of calcite growth hillocks. **(A)** In the absence of Mg or peptide modifiers, growth hillocks develop by the propagation of straight steps that lack visible roughening. The c-glide plane bisects two types of symmetrically equivalent step edges that define the obtuse and acute step directions to give four hillock flanks. **(B)** With $3 \times 10^{-4}$ M Mg, step edges, particularly on acute flanks, become roughened and hillock morphology is elongated parallel to the c-glide axis. **(C)** With peptide and $3 \times 10^{-4}$ M Mg, acute step edges are roughened as before, and the terrace widths become larger. **(D)** Schematic cross section of the step risers illustrates differences in step edge structure that arise from the orientation of planar carbonate groups with respect to the (104) growth surface. All AFM images are 5 μm by 5 μm.

[1]Department of Geosciences, Virginia Tech, Blacksburg, VA 24061, USA. [2]Chemistry and Materials Science Directorate, Lawrence Livermore National Lab, Livermore, CA 94551, USA. [3]Department of Applied Science, University of California–Davis, Davis, CA 95616, USA. [4]Department of Biological Sciences, University of Delaware, Newark, DE 19716, USA.

*To whom correspondence should be addressed. E-mail: dove@vt.edu (P.M.D.) and aestephe@vt.edu (A.E.S.)

held at 1:1 to maximize growth rate (*15*), pH was constant at 8.5, and Mg concentrations were varied from 0 to $4 \times 10^{-4}$ M. Control experiments established an inorganic baseline for comparisons to calcites grown in solutions containing 10 nM $(Asp_3Gly)_6Asp_3$, a synthetic 27–amino acid peptide. This biomolecule was chosen for its similarity to Asp-rich peptide sequences found in proteins isolated from sites of calcification (*11*). The 10 nM concentration was selected to maximize the rate-enhancing effect without visibly roughening step edges at the micrometer scale (*14*). For experiments at the highest Mg concentration ($4 \times 10^{-4}$ M), where slow growth made measurements difficult, peptide concentration was reduced to 1 nM.

In the absence of Mg or peptides, growth hillocks form by propagation of straight steps along four crystallographically defined directions (Fig. 1A). When Mg was introduced to the solution, steps along acute directions showed characteristic (*18*) rounding and roughening (Fig. 1B). With the addition of peptide, step spacing increased but hillock morphology did not appreciably change (compare Fig. 1, B and C).

The Mg contents of AFM-prepared overgrowths were determined by time-of-flight–secondary ion mass spectrometry (ToF-SIMS) with a calibration curve established from NIST (National Institute of Standards and Technology) glass standards by inductively coupled plasma mass spectrometry. Control experiments established a baseline relation between Mg content and Mg concentration ([Mg]) in solution:

$$\text{mol\% } MgCO_{3\ \text{obtuse}} = 1.02 \pm 0.34\ [\text{Mg, mM}] \quad (2a)$$

$$\text{mol\% } MgCO_{3\ \text{acute}} = 1.03 \pm 0.08\ [\text{Mg, mM}] \quad (2b)$$

Obtuse and acute step edge directions incorporate Mg such that the contents of hillock flanks exhibit a linear dependence on solution concentration that is the same within experimental errors (Fig. 2, A and B). This is consistent with previous studies showing that transport conditions influence Mg uptake (*20*). In contrast to growth in diffusion-limited environments that results in differential uptake, acute and obtuse steps incorporate similar amounts of Mg during growth under surface reaction-limited conditions (*17*, *20*).

Calcites grown in the presence of Asp-rich peptide incorporate 50 to 75% more Mg (Fig. 2, A and B) by the relations

$$\text{mol\% } MgCO_{3\ \text{obtuse, peptide}} = 1.75 \pm 0.34\ [\text{Mg, mM}] \quad (3a)$$

$$\text{mol\% } MgCO_{3\ \text{acute, peptide}} = 1.55 \pm 0.08\ [\text{Mg, mM}] \quad (3b)$$

such that Mg content is increased by up to ~3 mol% $MgCO_3$ at the highest solution concentration of Mg and indicates preferential uptake across obtuse steps.

Insights into the origin of this behavior are found in kinetic measurements of step propagation rates, $v$ (nm $s^{-1}$). For calcite growth at $\sigma$ = 1.6, step velocity is given by

$$v = \omega\beta\,(a_{Ca^{2+}} - a_{Ca^{2+}e}) \quad (4)$$

where step velocity ($v$, nm $s^{-1}$) is given by the molecular volume of calcite ($\omega$, $6.13 \times 10^{-23}$ $cm^3$ per molecule), the kinetic coefficient ($\beta$), the local activity of $Ca^{2+}$ at the growing surface ($a_{Ca^{2+}}$), and the equilibrium $Ca^{2+}$ activity for the crystal that forms and is the value of calcium activity for which step speed extrapolates to zero ($a_{Ca^{2+}e}$) (*17*, *18*). Calcite growth velocity decreased with increasing Mg concentration in the inorganic control solutions (Fig. 3A), as expected (*18*).

In contrast, growth in solutions that also contain peptide offset growth rate to 25 to 50% faster velocities (Fig. 3A). This enhanced growth rate could be responsible for the increased Mg contents because studies have shown that impurity contents correlate with faster growth (*21*), though no mechanism for this correlation has yet been established. Elhadj *et al.* (*14*) showed that biomolecule-induced increases in growth rate arise from increases in $\beta$. The magnitude of $\beta$ is controlled by two primary factors: (i) density of kink sites along the step, $n_k$; and (ii) net probability of attachment to a site, which we write as $\exp(-E_k/kT)$, where $k$ = Boltzmann's constant, $T$ is temperature, and $E_k$ is an effective barrier to attachment (*17*) of Ca or Mg at a kink such that

$$\beta \sim n_k \exp(-E_k/kT) \quad (5)$$

Assuming that $v$ remains linear versus $(a - a_e)$ in the presence of impurities, which is documented for the range of Mg (*18*) and value of $\sigma$ used here (*18*), then we must conclude that $n_k$ is a constant (*19*), although it may be reduced in magnitude relative to the pure system when impurities bind to the step. Thus, under these conditions, $n_k$ is at its maximum value and impurities can only decrease $n_k$ by blocking active kinks (*22*).

Allowing these constraints, the most likely origin of enhanced $\beta$ is reductions in $E_k$. This interpretation is evidenced by a previous study showing that biomolecules promote calcite growth in proportion to their hydrophilic character (*14*). Analysis of those data suggests that acidic bio-

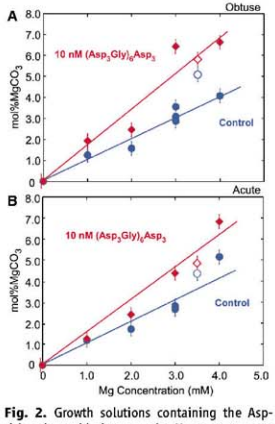


**Fig. 2.** Growth solutions containing the Asp-rich polypeptide increase the Mg content up to 3 mol% $MgCO_3$ into calcite overgrowths (red trend line) compared to the inorganic controls (blue trend line). The enhancement due to peptide is greater on flanks comprising obtuse steps **(A)** than on those comprising acute steps **(B)**. Open symbols show data with larger uncertainties. They are reported in the figure but are not included in the regressions (Eqs. 2a and 2b, and 3a and 3b).

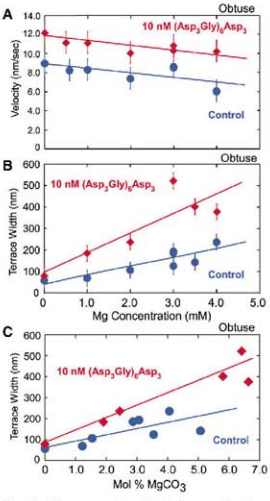


**Fig. 3.** Measurements of calcite growth show that **(A)** the rate of step propagation in the presence of peptides (red) is 25 to 50% faster than in the presence of inorganic controls (blue) for experimental conditions that are otherwise the same. **(B)** Terrace widths increase with increasing solution [Mg], reflecting the formation of an increasingly soluble Mg-enriched overgrowth (compare to Fig. 2) and the consequent decrease in apparent supersaturation of the solid solution. **(C)** Terrace widths increase with Mg content. The offset between trends for the inorganic control (blue) and the peptide-bearing experiments (red) demonstrates that the biomolecules increase the step edge energy of calcite by 20 to 80%.

molecules create a lower-energy pathway for desolvating strongly hydrated cations as they approach the growing step edge (*14*). A similar mechanism was invoked to explain Mg uptake into calcites grown in alcohol-water mixtures (*23*) and was supported by molecular dynamics simulations showing that aspartic acid monomers enhance the rate of $Ba^{2+}$ desolvation in the barite ($BaSO_4$) system (*24*). Recent AFM observations of calcium oxalate monohydrate show that acidic biomolecules are weakly attracted to the surface and appear to serve as nutrient sources by promoting faster growth as steps propagate beneath the biomolecules (*25*). When one considers the extent of cation interactions with the acidic domains of biomolecules as a proxy for their ability to attract and desolvate cations, a plausible mechanistic picture emerges whereby biomolecules facilitate the uptake, desolvation, and transport of cations from bulk solution to the mineral surface.

Although this study cannot fully assess the physical model for enhancement, we can conclude that peptides affect Mg more strongly than Ca. If this peptide-induced perturbation were equivalent, the Mg/Ca ratio would be unchanged. Our analysis suggests that the only way to increase the proportion of Mg is to induce a drop in the barrier to Mg uptake that is greater than that for Ca. This can be understood by comparing the enthalpy of dehydration, $\Delta H°_{rxn}$, for $Mg^{2+}$ (−1882 kJ/mol) versus $Ca^{2+}$ (−1569 kJ/mol) at 25°C (*16*). If, for example, biomolecules reduce $\Delta H°_{rxn}$ by 10%, then the energy barrier is reduced by almost 190 kJ/mol for Mg but only 157 kJ/mol

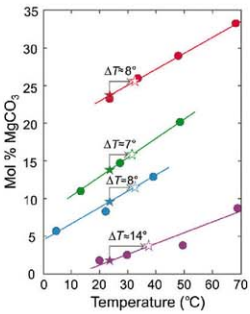


**Fig. 4.** Published correlations between Mg content and temperature show that if biomolecules induce a modest 2 mol% increase in Mg content, the corresponding temperature offset could be as much as 7° to 14°C. The different ionic strengths and superaturations used in these studies do not allow a direct prediction, but only a general comparison. Legend: purple: Chilingar, 1962 (*30*); blue: Mucci, 1987 (*31*); green: Fuchtbauer and Hardie, 1976 (*32*); and red: Katz, 1973 (*33*).

for Ca. This kind of analysis raises two questions: (i) What is the "real" equilibrium distribution of Mg in calcite? Our findings suggest that Mg contents must be highly limited by kinetic factors. (ii) Do biomolecules also modify the hydration properties of other IIA cations and thus also modulate their incorporation? If true, this suggests the potential for selectively applying macromolecules during controlled materials synthesis to tune impurity or dopant levels.

Measurements of terrace width, or spacing between steps (Fig. 3C), indicate that surface thermodynamic properties of calcite may also be modified by peptides. Terrace width, λ, is controlled by the Gibbs-Thomson relation through

$$\lambda = (2.04\ \omega\alpha)/kT\sigma \qquad (6)$$

where α = step edge free energy per unit step height (*18*). Though λ increases with increases in ω and/or decreases in σ, we deduce here that α is the origin of this effect. First, we assume changes in the molecular volume of calcites containing 0 to 6 mol% Mg are small relative to increases in λ. Next, we consider the influence of σ on λ. When the solid contains sufficiently high amounts of Mg, σ is reduced through increases in the apparent solubility (Eq. 1) (*26*, *27*). However, comparisons to a previous study (*18*) show that the ratio of terrace widths for the peptide-bearing and control experiments is far too large to be explained by reductions in σ; that is, the $K_{sp}$ of calcites containing up to 4 mol% $MgCO_3$ are not sufficiently different to explain the differences in terrace width for the Mg contents reported here. The peptide could also influence local σ by binding with Ca to reduce $a_{Ca^{2+}}$ (Eq. 1), but two quantitative measurements show that these peptides have negligible effects on $a_{Ca^{2+}}$ (*28*, *29*). Citrate, an inhibitor with three carboxylic groups, does not measurably modify σ for calcium oxalate monohydrate systems until citrate concentrations are ≥2 μM, and no change can be discerned below 10 μM (*28*). Moreover, a study of calcite that used large amounts of $Asp_1$ (*29*) indicates that nanomolar concentrations of $(Asp_3Gly)_6Asp_3$ are unlikely to substantially reduce σ. Even if every carboxylic of this 27–amino acid peptide acted independently, we would expect no effect for peptide concentrations of ≤1 μM. Therefore, wider terraces that develop in peptide-bearing solutions must be due, at least in part, to increased α. This is consistent with evidence that aspartate monomers also induce small increases in α (*28*).

Our findings also raise new questions regarding carbonate mineralization and interpretations of their formation environments. In particular, do biomolecules substantially offset Mg signatures in natural calcites relative to the amounts attributed to temperature differences? Assuming a modest increase of 2.0 mol% $MgCO_3$, comparisons to published studies (*30*–*33*) show that an equivalent Mg enhancement corresponds to an offset of 7° to 14°C (Fig. 4). This crude comparison is not a prediction but nonetheless illustrates that because the growth enhancement is specific to biomolecule chemistry (*14*) and acidic biomolecules induce greater Mg contents, perhaps some signatures are altered by macromolecule chemistry. These findings suggest that the basic assumption of paleotemperature reconstruction models would be degraded if the vital effect due to biomolecules were to change over time. One could also ask if biomolecules are a source of the vital effects long reported for stable isotopic signatures (*34*).

This study may also provide mechanism-based insights into factors that influence the stability of carbonate minerals in biological and sedimentary settings (*35*). Marine sediments contain organic matter that is frequently enriched in aspartate and glutamate (*3*). Because carbonate surfaces in these environments interact preferentially with aspartate-rich domains (*3*), findings that $Asp_1$ and $(Asp_3Gly)_6Asp_3$ have compound-specific effects on α suggest a means by which biomolecule chemistry could passively influence polymorph selection. Although step edge energy cannot be equated to surface energy, the generally accepted practice is to estimate step edge energy as the surface energy for the face that defines the step riser (Fig. 1D) times the step height. So, greater step edge energy implies greater surface energy. The increased surface energy of a phase makes nucleation of that phase less likely to occur. Thus, one polymorph becomes favored over another (*36*). Hence, if biomolecules increase $\alpha_{calcite}$ more than $\alpha_{aragonite}$, organics could induce preferential formation of aragonite. Aside from the well-documented influence of Mg on the stability of carbonate polymorphs, shifts in α could offer an alternative explanation for occurrences of aragonite needles in carbonate muds containing proteinaceous compounds enriched in acidic amino acids (*2*, *3*). Formation of skeletal and inorganic carbonates alike may be better understood by considering biomolecule influences on kinetics and thermodynamics of mineral growth and stability.

### References and Notes


1. A. P. Vinogradov, *The Elementary Chemical Composition of Marine Organisms* (Yale University, New Haven, CT, 1953).
2. R. A. Berner, J. T. Westrich, R. Graber, J. Smith, C. S. Martens, *Am. J. Sci.* **278**, 816 (1978).
3. P. W. Carter, R. M. Mitterer, *Geochim. Cosmochim. Acta* **42**, 1231 (1978).
4. R. L. Folk, *J. Sediment. Petrol.* **44**, 40 (1974).
5. S. Bentov, J. Erez, *Geochem. Geophys. Geosyst.* **7**, Q01P08 (2006).
6. H. Elderfield, G. Ganssen, *Nature* **405**, 442 (2000).
7. D. W. Lea, in *The Oceans and Marine Geochemistry*, H. Elderfield, Ed., vol. 6 of *Treatise on Geochemistry*, H. D. Holland, K. K. Turekian, Eds. (Elsevier-Pergamon, Oxford, 2003), pp. 365–390.
8. J. A. D. Dickson, *Science* **298**, 1222 (2002).
9. S. M. Stanley, L. A. Hardie, *Palaeogeogr. Palaeoclimatol. Palaeoecol.* **144**, 3 (1999).
10. L. Addadi, S. Weiner, *Proc. Natl. Acad. Sci. U.S.A.* **82**, 4110 (1985).
11. L. Addadi, A. Berman, J. Moradianoldak, S. Weiner, *Croat. Chem. Acta* **63**, 539 (1990).

12. A. Puverel *et al.*, *Comp. Biochem. Physiol. B Biochem. Mol. Biol.* **141**, 480 (2005).
13. G. Fu, S. R. Qiu, C. A. Orme, D. E. Morse, J. J. De Yoreo, *Adv. Mater.* **17**, 2678 (2005).
14. S. Elhadj, J. J. De Yoreo, J. R. Hoyer, P. M. Dove, *Proc. Natl. Acad. Sci. U.S.A.* **103**, 19237 (2006).
15. M. Kowacz, C. Putnis, A. Putnis, *Geochim. Cosmochim. Acta* **71**, 5168 (2007).
16. J. E. Huheey, *Inorganic Chemistry: Principles of Structure and Reactivity* (Harper and Row, New York, ed. 3, 1983).
17. L. E. Wasylenki, P. M. Dove, J. J. De Yoreo, *Geochim. Cosmochim. Acta* **69**, 4227 (2005).
18. K. J. Davis, P. M. Dove, J. J. De Yoreo, *Science* **290**, 1134 (2000).
19. H. H. Teng, P. M. Dove, C. A. Orme, J. J. De Yoreo, *Science* **282**, 724 (1998).
20. R. J. Reeder, *Geochim. Cosmochim. Acta* **60**, 1543 (1996).
21. R. B. Lorens, *Geochim. Cosmochim. Acta* **45**, 553 (1981).
22. A. A. Chernov, *Theor. Technol. Aspects Cryst. Growth* **276-2**, 57 (1998).
23. G. Falini, M. Gazzano, A. Ripamonti, *Chem. Commun.* **9**, 1037 (1996).
24. S. Piana, F. Jones, J. D. Gale, *J. Am. Chem. Soc.* **128**, 13568 (2006).
25. J. J. De Yoreo, paper presented at the 233rd Annual Meeting of the American Chemical Society, Chicago IL, 25 to 29 March 2007.
26. J. M. Astilleros, C. M. Pina, L. Fernández-Díaz, A. Putnis, *Geochim. Cosmochim. Acta* **67**, 1601 (2003).
27. M. Prieto, J. M. Astilleros, C. M. Pina, L. Fernández-Díaz, A. Putnis, *Am. J. Sci.* **307**, 1034 (2007).
28. M. L. Weaver *et al.*, *J. Cryst. Growth* **306**, 135 (2007).
29. C. A. Orme *et al.*, *Nature* **411**, 775 (2001).
30. G. V. Chilingar, *Bull. South. Calif. Acad. Sci.* **61**, 45 (1962).
31. A. Mucci, *Geochim. Cosmochim. Acta* **51**, 1977 (1987).
32. H. Fuchtbauer, L. A. Hardie, *Geol. Soc. Am. Abstr.* **8**, 87719 (1976).
33. A. Katz, *Geochim. Cosmochim. Acta* **37**, 1563 (1973).
34. S. Epstein, *Geol. Soc. Am. Bull.* **62**, 417 (1951).
35. J. W. Morse, A. J. Andersson, F. T. Mackenzie, *Geochim. Cosmochim. Acta* **70**, 5802 (2006).
36. A. Navrotsky, *Proc. Natl. Acad. Sci. U.S.A.* **101**, 12096 (2004).
37. We thank J. F. Read and D. Rimstidt for thoughtful discussions. This research was supported by awards to P.M.D. from the NSF (grant OCE-052667) and U.S. Department of Energy (grant FG02-00ER15112). This work was also performed under the auspices of the U.S. DOE by an award to J.D.Y. at the University of California, Lawrence Livermore National Laboratory, under Contract No. W-7405-Eng-48. Opinions, findings, and conclusions or recommendations expressed in this material are those of the authors and do not necessarily reflect the views of the NSF or DOE.

21 April 2008; accepted 26 September 2008
10.1126/science.1159417

# Trampoline Effect in Extreme Ground Motion

**Shin Aoi,* Takashi Kunugi, Hiroyuki Fujiwara**

In earthquake hazard assessment studies, the focus is usually on horizontal ground motion. However, records from the 14 June 2008 Iwate-Miyagi earthquake in Japan, a crustal event with a moment magnitude of 6.9, revealed an unprecedented vertical surface acceleration of nearly four times gravity, more than twice its horizontal counterpart. The vertical acceleration was distinctly asymmetric; the waveform envelope was about 1.6 times as large in the upward direction as in the downward direction, which is not explained by existing models of the soil response. We present a simple model of a mass bouncing on a trampoline to account for this asymmetry and the large vertical amplitude. The finding of a hitherto-unknown mode of strong ground motion may prompt major progress in near-source shaking assessments.

The deployment of high-density seismograph networks has contributed to recent discoveries concerning ground shaking and complex wave propagation (*1*–*3*) and to the development of ShakeMap, a tool for real-time seismology and earthquake hazard mitigation (*4*, *5*). As more and more near-source data have become available, the stockpile of extreme ground motion observations has become ever larger, with potentially rich implications for earthquake engineering and building design.

Japan has deployed and maintained nationwide networks of strong motion seismographs (*6*–*9*), with about 1800 stations. A station of the KiK-net (*10*) recorded ground acceleration exceeding four times gravity (*11*), the largest ever reported to date, during the 14 June 2008 Iwate-Miyagi earthquake, a reverse-fault type crustal event extending roughly 30 km in strike and 20 km in dip directions (Fig. 1A). The motion in question was recorded at the IWTH25 (West Ichinoseki) station, located on the hanging-wall side of the fault (*12*), 3 km southwest of the epicenter. The IWTH25 station is equipped with three-component accelerometers, installed at both the free surface and the bottom of a 260-m borehole (Fig. 1B). It lies in a volcanic zone where volcaniclastic rocks, such as tuff breccia, are covered with a surface layer of river terrace deposits (*S*-wave velocity 430 m/s in the shallowest surface layer) (fig. S1A).

National Research Institute for Earth Science and Disaster Prevention, 3-1 Tennodai, Tsukuba, Ibaraki 305-0006, Japan.

*To whom correspondence should be addressed. E-mail: aoi@bosai.go.jp

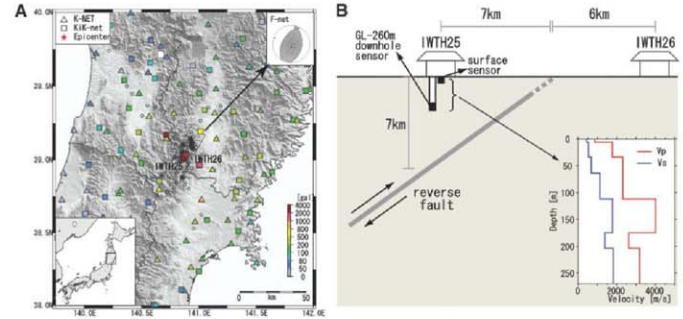


**Fig. 1. (A)** Map of the source region of the Iwate-Miyagi earthquake in Japan [14 June 2008; moment magnitude ($M_w$) = 6.9]. Triangles and squares, K-NET and KiK-net stations, respectively, colored according to the peak ground accelerations. Red star and black circles, epicenters of the mainshock and the aftershocks. Black rectangle, ground surface projection of the earthquake source fault. The focal mechanism, estimated using F-net broadband data, is also demonstrated. **(B)** Schematic diagram of the relative geometry of the KiK-net IWTH25 station with respect to the source fault. The downhole sensor, contained in a watertight pressure-resistant casing made of stainless steel, is fixed with a latch to the bottom of the borehole. The surface sensor is anchor-bolted to the bottom of an empty 45 cm-deep pit with a metal lid firmly glued shut (*19*). Inset, the *P*- and *S*-wave velocity measured by geophysical logging.

The peak acceleration at the surface (Fig. 2A) was 3866 gal in the vertical direction and 1435 gal in the horizontal (*13*). In strong motion seismology, the focus has customarily been on horizontal motion, because they are usually much larger in amplitude than their vertical counterparts, so the evidence of an extreme vertical acceleration, more than twice the horizontal, should merit special attention. The downhole [(ground level) GL −260 m] sensor set in a soft rock (*S*-wave velocity 1810 m/s) (Fig. 1B and fig. S1A) recorded peak accelerations of 683 and 1036 gal in the vertical and horizontal directions, respectively. This means that the large accelerations on the surface are partly due to the large incident amplitudes at the subsurface layer, but the unusually large vertical-to-horizontal peak acceleration ratio at the surface should be attributed to the effects of near-surface layers.

The waveform of the vertical surface motion is strongly asymmetric with respect to the zero axis (Fig. 2A). By contrast, the horizontal surface components and the downhole records are largely symmetric. This indicates that the waveform asymmetry, peculiar to the vertical surface record, also originated between the 260-m depth and the surface. In terms of spectral composition, the waveform asymmetry in the vertical surface record is visible only above 8 Hz (fig. S2).

We determined envelopes, independently for the positive- and negative-polarity motions, by applying a triangular smoothing filter (duration 1 s) to the sequence of maximum positive and negative values, taken from every consecutive 0.1 s interval of the vertical- and two horizontal-component records (red and blue areas in Fig. 2A). Only for the surface vertical acceleration in the time window of 4 to 14 s, roughly corresponding to the largest amplitudes, the envelope determined for the positive polarity is visibly larger than the negative-polarity envelope, with the peak amplitudes differing by a factor of 1.6. After 14 s, the amplitudes became similar for both envelopes.

In the vertical surface record from 4 to 14 s, not only were the upward pulses larger in amplitude than the downward ones but also they tended to be narrow and sharp, whereas the downward pulses were broader and longer lasting (inset of Fig. 2A). These features are not evident in the corresponding downhole record. We have taken statistics of the periods of the positive and negative pulses, defined here for convenience as twice the time between two consecutive zero crossings. Despite the large dispersions, the periods are visibly shorter for the positive pulses (Fig. 2B). Histograms of the positive and negative local peak accelerations (fig. S3) demonstrate that, between 5 and 15 s, positive peaks in the surface record tend to scatter farther away from zero than their negative counterparts. The negative local peak accelerations have a sharp peak of frequency near −800 gal in the 5- to 10-s time window. It is worthy of note that the positive pulse, taller and sharper, and the negative pulse, smaller and broader, cover similar areas when integrated along the time axis for one cycle. This means that the disparity in peak amplitudes for both polarities does not lead to one-sided shifts in velocity or displacement seismograms.

To search for similar asymmetry in other earthquakes, we picked out, from among the ~200,000 records in the K-NET and KiK-net database from more than 1800 stations and about 6800 events, 14 seismograms for which the acceleration (vector summation of all three components) exceeded gravity (table S1). We use two indexes as measures of the waveform asymmetry, namely the ratio of the areas of the upward (S+) and downward (S−) envelopes and the ratio of the average pulse periods of the downward (T−) and upward (T+) motions. These two indexes were calculated for the longest continuous time window over which the envelope amplitudes stayed larger than 5% of the maximum value (Fig. 3). For the vertical surface record of the Iwate-Miyagi event at IWTH25 (#1 in a black circle in Fig. 3A and table S1), S+/S− = 1.29 and T−/T+ = 1.15. Two other surface records (#2 and #3 in black circles in Fig. 3A and table S1) demonstrated pronounced asymmetry, where our threshold for selection is S+/S− > 1.15 and T−/T+ > 1.10 (pink area in Fig. 3A). Noticeably, the S+/S− and T−/T+ ratios (especially the former) seldom fall too far below unity. The S+/S− and T−/T+ ratios were near unity (no asymmetry) for all vertical downhole records (white circles in Fig. 3A).

Both ratios have the tendency to increase with peak ground acceleration, although there are cases in which strong shaking was not accompanied by pronounced asymmetry. The number and the frequency of large-amplitude pulses may potentially be involved in the development of asymmetry, but that remains inconclusive at the moment. At IWTH25, the largest aftershock of the Iwate-Miyagi event (#12 in a black circle in Fig. 3A and table S1) produced largely symmetrical ground acceleration, indicating that asymmetry is not characteristic of this site. Relatively strong asymmetry is present in the record from event #5 (black circle in Fig. 3A and highlighted in blue in table S1), the only strike-slip type earthquake among the 14 listed events.

Earthquake ground motion is generally well described by wave propagation in an elastic medium satisfying a linear wave equation, so there

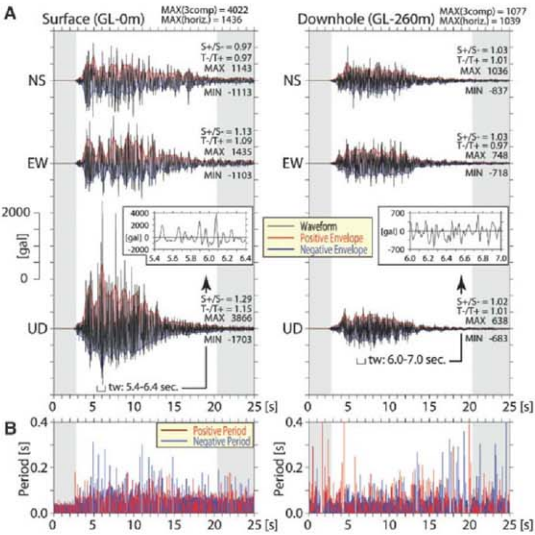


**Fig. 2. (A)** Acceleration at IWTH25 during the Iwate-Miyagi earthquake. Left, surface records. Right, downhole (GL −260 m) records. The origin of the time axis is 8:43:44 Japan Standard Time. Red and blue areas, envelopes of the upward and downward pulses. White background, time window used in the calculation of the S+/S− and T−/T+ ratios. Insets, magnified views of the vertical component acceleration during a 1-s interval that includes the maximum amplitude (indicated by brackets beneath the original seismograms). **(B)** Periods of the positive (red) and negative (blue) pulses, estimated by doubling the time between two consecutive zero crossings.

should basically be no asymmetry of amplitudes arising during propagation. During strong shaking, nonlinear behavior of soil becomes important (*14*, *15*). When the incident motion is large, nonlinearity reduces the surface soil amplification factors and shifts the peak amplification factor to lower frequencies with respect to what is expected from the linear theory (*16*, *17*). These phenomena are in fact observed for the horizontal motion record of the Iwate-Miyagi event (fig. S4), consistently with existing knowledge. However, such conventional models of nonlinearity do not satisfactorily explain the waveform asymmetry in the vertical component.

To explain this asymmetry, we propose a new model of soil's nonlinear behavior. We hypothesize that, when dilatational strains become large enough during strong downgoing acceleration, the bulk tensile strength of the near-surface material is reached, so that soil and rocks lose their cohesion through the development of tensile cracks and apertures. Let us consider, by way of analogy, an open box filled with sand. When there is upgoing acceleration, the sand, subject to compressional stress, behaves elastically, and this may continue to be true under moderate downgoing acceleration. As the downgoing acceleration increases, however, the sand particles may begin to lose mutual contact and fall into a virtual free-fall state.

Another familiar analogy would be that of an athlete bouncing on a trampoline (Fig. 4A). There are two forces acting on the athlete, namely the downward-directed gravity and the upward-directed repulsion of the trampoline hit by the athlete. The trampoline's repellent force is larger than gravity. This analogy apparently helps to account for the two aspects of waveform asymmetry we have described so far: First, the asymmetry in acceleration amplitudes—the downgoing acceleration should basically be bounded at $-1 \times g$, whereas there is no intrinsic bound on the upgoing acceleration; and second, the asymmetry in pulse periods—the time for the athlete to be repelled upward is shorter than the time for the athlete to fall freely.

A simple mathematical illustration of this trampolining model is given in Fig. 4. By way of simplification, we represent the motion of an undeformable mass bouncing on a trampoline by cyclic oscillations with distinct polarity asymmetry (Fig. 4A) (*18*). A selected part of the IWTH25 downhole record from the Iwate-Miyagi earthquake, which is thought to be elastically behaved, is used to represent the elastic deformation of a deformable mass (Fig. 4B). Figure 4C shows the sum of the two waveforms, which should correspond to the motion of a deformable mass bouncing on a trampoline. This graph is qualitatively similar to the asymmetric vertical surface acceleration observed at IWTH25 (inset of Fig. 2A). The tendency for the downgoing accelerations to be bounded near $-1 \times g$ is also reproduced.

Because real soil or rock is not likely to become entirely cohesionless under dilatational stress, and should be subject to a wealth of natural factors such as friction and medium complexity, its true behavior should be appreciably more complicated than the trampoline analogy. However, the fundamental features of the asymmetrical ground motion we have found at IWTH25 are apparently in good accordance with our simple trampolining model. The search for other instances of similar asymmetry should be precipitated, so that we can have a better understanding of the nature and origin of this phenomenon and find out the key conditions for it to take place or not to take place during strong ground shaking. An explanation of this phenomenon is expected to bring about major progress in earthquake hazard assessment studies for near-source areas.

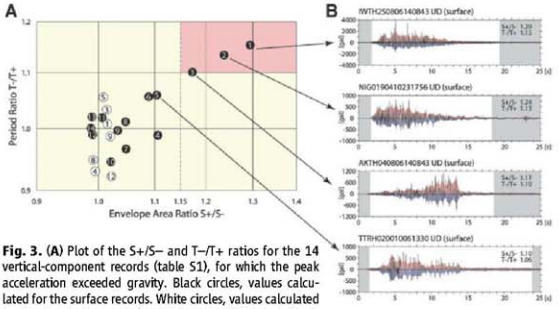


**Fig. 3. (A)** Plot of the S+/S– and T–/T+ ratios for the 14 vertical-component records (table S1), for which the peak acceleration exceeded gravity. Black circles, values calculated for the surface records. White circles, values calculated for the downhole records (available only at KiK-net stations). Pink, region of strong waveform asymmetry, defined by S+/S– > 1.15 and T–/T+ > 1.10. **(B)** Four vertical surface records with the strongest degrees of asymmetry. White background, time windows used in the calculation of the S+/S– and T–/T+ ratios.

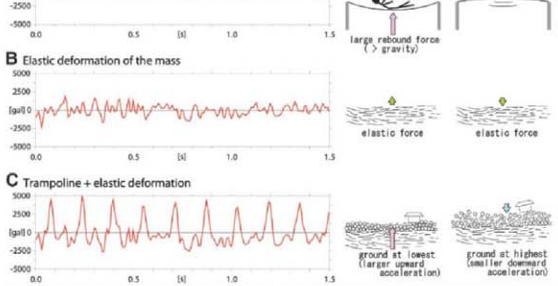


**Fig. 4. (A)** Simplified model of the motion of an undeformable mass bouncing on a trampoline. **(B)** Elastic deformation of a deformable mass, represented by a selected part of a downhole seismic record. **(C)** Simulated motion of a deformable mass bouncing on a trampoline, obtained as the sum of (A) and (B). To be compared with the seismogram in the left inset of Fig. 2A.


**References and Notes**

1. A. D. Frankel, *Science* **283**, 2032 (1999).
2. K. Koketsu, M. Kikuchi, *Science* **288**, 1237 (2000).
3. S. Aoi *et al.*, *J. Geophys. Res.* **113**, B07302 (2008).
4. H. Kanamori, E. Hauksson, T. Heaton, *Nature* **390**, 461 (1997).
5. D. J. Wald *et al.*, *Earthquake Spectra* **15**, 537 (1999).
6. S. Kinoshita, *Seismol. Res. Lett.* **69**, 309 (1998).
7. S. Aoi *et al.*, *Eos Trans. AGU* **81**, S71A-05 (2000).
8. S. Aoi, T. Kunugi, H. Fujiwara, *J. Japan Assoc. Earthq. Eng.* **4**, 65 (2004).
9. Y. Okada *et al.*, *Earth Planets Space* **56**, xv (2004).
10. All KiK-net stations have recently been re-equipped by new instruments. The surface sensors have been upgraded from 2000 to 4000 gal in maximum measurable acceleration.

11. 1 g (gravity) = 980 gal ("gal" is equivalent to "cm/s$^2$"). The peak ground acceleration at IWTH25 was 4022 gal, in terms of the vector summation of all three components. The peaks in the north-south, east-west, and up-down (vertical) accelerations were 1143, 1435, and 3866 gal, respectively.
12. D. D. Oglesby, R. J. Archuleta, S. B. Nielsen, *Science* **280**, 1055 (1998).
13. During a field survey performed by the National Research Institute for Earth Science and Disaster Prevention (NIED) one week after the earthquake, we found no trace, in the neighborhood of the IWTH25 station, of stones displaced and tossed around during the strong shaking.
14. E. H. Field, P. A. Johnson, I. A. Beresnev, Y. Zeng, *Nature* **390**, 599 (1997).
15. L. F. Bonilla, R. J. Archuleta, D. Lavallee, *Bull. Seismol. Soc. Am.* **95**, 2373 (2005).
16. L. F. Bonilla, J. H. Steidl, J. C. Gariel, R. J. Archuleta, *Bull. Seismol. Soc. Am.* **92**, 3165 (2002).
17. I. M. Idriss, H. B. Seed, *Bull. Seismol. Soc. Am.* **58**, 2013 (1968).
18. The pulse waveform in Fig. 4A was obtained using the Gaussian function $\sum_i A_i \times \exp\{-(t - T_i)^2 f_i^2\} - g$, where $A_i$ is the peak-to-peak amplitude, $t_i$ the characteristic pulse duration, $T_i$ the reference time for the $i$-th cyclic pulse, and $g$ the gravity. The only constraint on this set of values is that the pulse shape should integrate to zero over each single cycle.
19. We checked the sensors in person after the Iwate-Miyagi mainshock to ensure that no abnormal circumstances had affected the records. The sensors successfully recorded a large number of aftershocks, including one event with acceleration exceeding gravity.
20. We thank T. Tada and N. Pulido for helpful discussions.


**Supporting Online Material**

www.sciencemag.org/cgi/content/full/322/5902/727/DC1
Figs. S1 to S4
Table S1

11 July 2008; accepted 24 September 2008
10.1126/science.1163113

# Tracing the Origin and Fate of $NO_x$ in the Arctic Atmosphere Using Stable Isotopes in Nitrate

Samuel Morin,[1,2]* Joël Savarino,[1,2] Markus M. Frey,[1,2]† Nicolas Yan,[1,3] Slimane Bekki,[1,3] Jan W. Bottenheim,[4] Jean M. F. Martins[1,5]

Atmospheric nitrogen oxides ($NO_x$ = NO + $NO_2$) play a pivotal role in the cycling of reactive nitrogen (ultimately deposited as nitrate) and the oxidative capacity of the atmosphere. Combined measurements of nitrogen and oxygen stable isotope ratios of nitrate collected in the Arctic atmosphere were used to infer the origin and fate of $NO_x$ and nitrate on a seasonal basis. In spring, photochemically driven emissions of reactive nitrogen from the snowpack into the atmosphere make local oxidation of $NO_x$ by bromine oxide the major contributor to the nitrate budget. The comprehensive isotopic composition of nitrate provides strong constraints on the relative importance of the key atmospheric oxidants in the present atmosphere, with the potential for extension into the past using ice cores.

The atmospheric cycle of reactive nitrogen (*1*) has a profound influence on the chemical composition of the lower atmosphere and the deposition pattern of nutrients at Earth's surface. $NO_x$ contributes to the formation of ozone and particulate matter (*2*) and is thus important for regional air quality (*3*) and radiative balance (*4*). Atmospheric nitrate, produced upon oxidation of $NO_x$, is the main source of reactive nitrogen to remote ecosystems (*5*). Understanding the budget of $NO_x$ and nitrate in the Arctic atmosphere is necessary to assess their environmental impact.

The input of reactive nitrogen to the Arctic proceeds mainly through long-range transport within the troposphere (*6*) and the deposition of atmospheric nitrate, associated with the so-called Arctic haze phenomenon (*7*, *8*), which has hitherto been confined to winter and spring. A substantial direct contribution from the stratosphere to the budget of reactive species in the Arctic marine boundary layer has been ruled out on the basis of meteorological evidence and patterns of atmospheric transport (*6*). Local oxidation of $NO_x$ is generally thought to be limited because the release of appreciable amounts of $NO_x$ to the Arctic atmosphere from the thermal decomposition of peroxyacetylnitrate [PAN, the main reservoir species of $NO_x$ in the atmosphere (*9*)] is prevented by the low temperatures prevailing during winter and spring (*10*) and because PAN levels are too low during summer. However, the possible recycling of nitrate deposited on snow, leading to the release of $NO_x$ to the atmosphere (*11*–*14*) and interactions with halogen oxides such as bromine oxide (BrO) during the spring (*15*), complicates the atmospheric budget of reactive nitrogen in the Arctic atmosphere (*16*). In situ emissions of $NO_x$ may occur in the future during the summer, with the development of shipping routes associated with the reduction of sea-ice cover (*17*).

In general, closing the budget of atmospheric species requires the quantification of both the burden and the fluxes (that is, source/sink rates) associated with the different processes acting on them, such as emissions, chemical reactions, and transport. Conventional methods rely mostly on models that are evaluated and constrained with atmospheric concentration measurements, because there is no direct means of measuring chemical fluxes associated with individual reactions. In contrast, the measurement of isotopic ratios (*18*) provides direct insights into the nature and importance of individual fluxes (*19*). First, changes in the $\delta^{15}N$ values during the conversion of $NO_x$ to nitrate are minor, therefore $\delta^{15}N$ traces $NO_x$ sources (*20*). Second, because of mass-independent fractionation during its formation process (*21*),

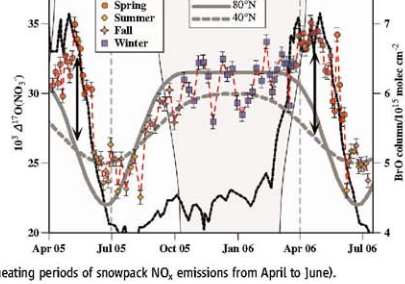


**Fig. 1.** Seasonal cycle of concentrations and $\Delta^{17}O$ of atmospheric nitrate at Alert. Also shown is the day length (from 0 to 24 hours, the shaded area corresponding to nighttime conditions). The black dashed line represents a satellite-retrieved column of BrO north of 70°N (*32*). Thick gray lines correspond to the calculated $\Delta^{17}O$ value in atmospheric nitrate formed at 40° and 80°N, respectively. The black vertical arrows indicate the strong deviation from these seasonal cycles in spring, due to the interaction of BrO with snowpack-emitted $NO_x$. The vertical dotted lines are identical to those in Fig. 2 (delineating periods of snowpack $NO_x$ emissions from April to June).

[1]CNRS, Institut National des Sciences de l'Univers, France. [2]Laboratoire de Glaciologie et de Géophysique de l'Environnement, Université Joseph Fourier (UJF), Grenoble, France. [3]Service d'Aeronomie, Institut Pierre-Simon Laplace, Université Pierre et Marie Curie, Paris 6, Paris, France. [4]Environment Canada, Toronto, Ontario, Canada. [5]Laboratoire d'Etude des Transferts en Hydrologie et Environnement, UJF, Grenoble, France.

*To whom correspondence should be addressed. E-mail: samuel.morin@ujf-grenoble.fr

†Present address: British Antarctic Survey, Physical Sciences Division, Cambridge, UK.

ozone possesses a strong isotope anomaly ($\Delta^{17}O = \delta^{17}O - 0.52 \times \delta^{18}O$), which is transferred to most short-lived oxygen-bearing species, including $NO_x$ and nitrate. The isotope anomaly of nitrate depends on the relative importance of ozone and other key oxidants in $NO_x$ oxidation, thus $\Delta^{17}O$ measurements in nitrate allow researchers to identify and apportion $NO_x$ sinks (*16*, *22*).

This study combines atmospheric concentration and isotopic composition ($\delta^{15}N$, $\Delta^{17}O$) of nitrate sampled at Alert, Nunavut, Canada (82.5°N, 190 m above sea level), in order to infer a detailed budget of $NO_x$ and nitrate on a seasonal time scale (*23*). The nitrate concentrations measured at Alert are typical of the yearly cycle in the Arctic lower atmosphere (Fig. 1) (*8*). They show a marked seasonal cycle with maximum values between November and May (on average 140 ± 50 ng $m^{-3}$) and minimum values between June and October (40 ± 20 ng $m^{-3}$).

Throughout the year, $\delta^{15}N$ exhibits pronounced variations, spanning a very large range [between −42 and 3 per mil (‰)], which encompasses previous measurements carried out in the Arctic (Fig. 2) (*24*, *25*). Summer months exhibit the highest values (on average −1‰ in July and August), smoothly decreasing to reach values on the order of −15‰ in winter (until March), which is consistent with seasonal variations inferred from a Greenland snowpit (*25*). This seasonal cycle is more pronounced than and opposite to seasonal variations observed at industrialized midlatitude sites (*26*, *27*) that are driven by isotopic exchange between NO and $NO_2$ (*26*). During most of the year (between July and March), $\delta^{15}N$ variations are strongly correlated with air temperature ($T$) [$10^3\ \delta^{15}N = 0.37 \times T$ (in °C) − 1.8, $R^2 = 0.81$, $n = 41$, $P < 0.001$, fig. S2]. This relationship points toward an isotopic effect arising from physicochemical transformations within the Arctic region and during the transport of nitrate and reactive nitrogen species from midlatitudes (*26*), although the driving factor cannot be identified on the basis of this sole data set. The compact relationship between $\delta^{15}N$ and temperature breaks down completely during spring, suggesting the onset and predominance of a process anomalous with respect to the rest of the year. $\delta^{15}N$ becomes extremely variable and reaches record low values: They are matched only by measurements carried out in coastal Antarctica (*28*, *29*) that have unambiguously been attributed to emissions of reactive nitrogen from the snowpack (*11*, *14*, *29*). The $^{15}N$ isotopic effect associated with this snowpack recycling loss is large, with a fractionation constant (ε) on the order of −54‰ in central Antarctica (*30*), leading to elevated $\delta^{15}N$ values in nitrate remaining in the snow (*30*) and, as a consequence of mass conservation, depleted $\delta^{15}N$ values in the emitted species (*29*). Assuming that, without snowpack emissions, $\delta^{15}N$ would correlate with temperature year-round, and using the ratio of the deviation of $\delta^{15}N$ data from this seasonal trend with ε measured in Antarctica (*30*) (due to the lack of Arctic measurements), it is found that snowpack emissions can contribute to at least a third of the budget of $NO_x$ and nitrate during spring [Fig. 2 and supporting online material (SOM) text]. Although snowpack emissions do not represent a net source of reactive nitrogen to the Arctic, they do have a substantial impact on the seasonality of its concentrations and the oxidative capacity of the lower Arctic troposphere, especially in spring. In the same way, this phenomenon can also explain the absence of a correlation between the atmospheric nitrate concentration record and the concentration time series of other anthropogenic species (*31*). As shown by Fig. 2, the derived contribution of snowpack emissions correlates with the amount of ultraviolet (UV) (calculated for 80°N) interacting with snow surfaces in the Arctic basin, suggesting that snow photochemistry drives much of these reactive nitrogen emissions: The calculated impact of snowpack emissions is maximal when both snow and UV radiation coexist during spring. During winter, permanent nighttime conditions prevent photochemistry, and in summer and fall the snow cover is minimal.

Oxygen isotopic data are represented as a function of the season (Figs. 1 and 3). Summer corresponds to permanent sunlight conditions, and fall corresponds to the sharp transition into the winter, during which sunlight is permanently absent. The spring period corresponds to polar sunrise, when frequent surface ozone depletion events (ODEs) are observed at Alert, due to active halogen chemistry (*15*, *32*). The seasonal pattern of $\Delta^{17}O$ (Fig. 1) is strongly asymmetrical, with lowest values in summer, whereas the highest $\Delta^{17}O$ values correspond to the spring, followed by the winter and fall. The highest variability is observed during spring. Variations of the $\Delta^{17}O$ of nitrate can be understood in terms of the transfer of the isotope anomaly from ozone to nitrate through different formation pathways (*16*, *22*).

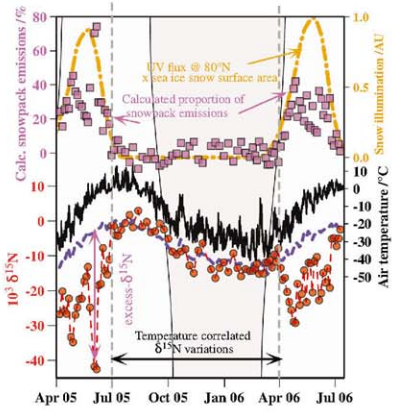


**Fig. 2.** Temporal evolution of $\delta^{15}N$ of atmospheric nitrate at Alert (red dots). Shaded areas are identical to those in Fig. 1. Also shown is the air temperature record (black solid line). The blue dashed line represents the seasonal cycle of $\delta^{15}N$ inferred from temperature variations (between July and March). Purple squares represent the calculated contribution of snowpack emissions inferred from an isotopic mass balance, which qualitatively correlates with the normalized UV radiation at 80°N interacting with snow surfaces in the Arctic basin (termed snow illumination).

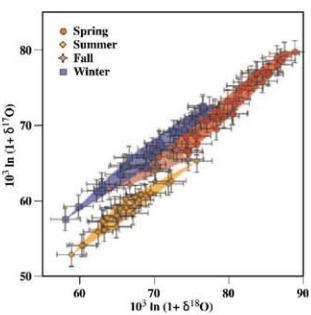


**Fig. 3.** Three-isotope plot of atmospheric nitrate oxygen isotopes at Alert. Symbols and colors refer to the seasons delineated in Fig. 1. Summer, spring, and winter correspond to $NO_x$ oxidation pathways involving OH, BrO, and $NO_3$, respectively, so that reporting oxygen isotopic measurements on this plot offers a way to unambiguously identify (and possibly apportion) $NO_x$ oxidation pathways. The slopes (intercepts) of the linear regression lines are 0.88, 0.71, and 0.74 (2.4, 11.6, and 15.0) for spring, summer, and winter, respectively.

Regardless of the $NO_x$ source, $\Delta^{17}O$ of $NO_2$ is a direct function of the isotope anomaly of ozone and the concentration of NO oxidants ($O_3$, BrO, and $RO_2$) due to rapid photochemical recycling (*16*, *22*, *33*). When $NO_2$ is oxidized to nitrate, an additional O atom is incorporated from various source molecules, depending on the $NO_2$ oxidation pathway (*16*, *22*), which results in characteristic $\Delta^{17}O$ values in the nitrate produced. Three groups of nitrate formation pathways need to be considered, depending on the nature of the $NO_2$ oxidant: (i) OH radicals, (ii) $O_3$, and (iii) BrO. The first case (i) corresponds to the reaction of OH with $NO_2$ (directly producing $HNO_3$), which operates only during the day because OH levels are negligible at night. The reaction of $NO_2$ with ozone (ii) yields the nitrate radical, which can react either with hydrocarbons and reduced sulfur compounds to give $HNO_3$ or with $NO_2$ to form dinitrogen pentoxide, $N_2O_5$, whose heterogeneous hydrolysis leads to nitrate formation (*3*). These channels (ii) essentially operate at night because $NO_3$ is rapidly photolysed back to $NO_2$ during the day. The reaction of $NO_2$ with BrO (iii) yields the reservoir species bromine nitrate ($BrONO_2$), which can in turn hydrolyze into nitrate. Each of these channels results in a different $\Delta^{17}O$ value in the produced nitrate, thus providing an easy way to tabulate the isotopic signature of each $NO_x$ sink (table S1). An atmospheric chemistry box model was used to compute the $\Delta^{17}O$ of nitrate produced in winter and summer at middle (40°N) and polar (80°N) latitudes (SOM text). These two extreme cases represent the two sources of Arctic nitrate that is, long-range transport and local production, respectively). Halogen chemistry was not taken into account because it does not operate significantly in summer and winter (*15*, *32*). In winter, $NO_x$ is mostly oxidized through the ozone channels (ii). In summer, the reaction OH + $NO_2$ (i) is the main $NO_x$ oxidation channel. The seasonal contrast is more pronounced in polar regions as compared to middle latitudes because of permanent nighttime conditions in winter and permanent daytime in summer, so that predominant channels are more exclusive. Under the assumption that changes in actinic flux are the main drivers of the seasonal changes in $NO_x$ oxidation pathways (*22*), the annual cycle of $\Delta^{17}O$ can then be inferred from the two model-calculated values (winter and summer) and the solar zenith angle. These calculations are shown in Fig. 1, along with the field measurements. For most of the year (from July to March), measured $\Delta^{17}O$ values fall by and large between the modeled values, with a tendency to better follow the temporal evolution of the modeled $\Delta^{17}O$ at 40°N, especially in summer, despite some scatter in the data. Oxygen isotopic measurements are consistent with the idea that atmospheric nitrate mostly originates from long-range transport from midlatitudes at this time of the year (*6*, *8*). In contrast, $\Delta^{17}O$ measurements during spring are found far away from the range of model-calculated values. The concurrence of elevated $\Delta^{17}O$ values and large-scale observations of enhanced BrO levels in the polar lower atmosphere (Fig. 1) (*32*) strongly suggests that $NO_x$ is mainly oxidized to nitrate within the Arctic basin through the hydrolysis of $BrONO_2$ (*16*).

Scrutiny of the $\delta^{15}N$ and $\Delta^{17}O$ time series shows that abnormally high $\Delta^{17}O$ values, indicative of local $NO_x$-halogen chemistry, are recorded only when low $\delta^{15}N$ values, indicative of snowpack $NO_x$ emissions, occur. The scenario emerging from this dual isotopic approach, complemented by the regional BrO measurements (*32*), is that interactions of UV light with snow surfaces drive photochemical loss of nitrate in the snowpack and the concomitant release of $NO_x$ during spring. In turn, $NO_x$ interacts with BrO to profoundly modify the budget of atmospheric nitrate, which is then formed almost exclusively by $BrONO_2$ hydrolysis. This implies that snowpack $NO_x$ emissions are key to the atmospheric budget of $NO_x$ and nitrate at high latitudes during springtime, confirming the significant impact of snow on the ground on the overlying atmosphere (*12*). $NO_x$ emissions also play a role in the recycling of atmospheric reactive halogen species, in particular through the role of $BrONO_2$, thereby forming a link between the chemistry of $NO_x$ and reactive halogens. The latter observation may explain why ODEs do not occur in fall, because at this time of the year the interaction of UV light (maximal in June) and snow surfaces is minimal (see Fig. 2, fig. S3, and SOM text for details). It could imply either that bromine activation requires the simultaneous occurrence of UV light and the presence of snow, as for snowpack $NO_x$ emissions, or that snowpack $NO_x$ emissions themselves play a role in bromine explosion.

Another important implication of oxygen isotopic measurements is the determination of purely chemical budgets. The data set can be used to identify the isotopic signature of almost pure $NO_x$ oxidation channels. Figure 3 summarizes all the oxygen isotopic data on a three-isotope plot, where seasonally labeled data plot on distinct arrays. Each of these seasonal arrays broadly represents the signature of predominant nitrate formation mechanisms at the hemispheric scale (summer, OH + $NO_2$; winter, $NO_3$ radical; spring, halogen chemistry). Hence the oxygen isotopic composition of atmospheric nitrate offers a way to identify and apportion $NO_x$ oxidation pathways. In contrast to elaborate in situ concentration measurements [as in (*3*)], this "geochemical" approach relies on standard aerosol sampling techniques, which are easy to implement on large geographical scales and for long-term studies, and on stable isotope measurements, which can be performed in the laboratory weeks or months after the sampling. The isotope tool is thus able to assist in identifying sources and sinks of reactive nitrogen in complex environments or matrices, such as polluted areas or polar ice cores.

### References and Notes


1. Atmospheric reactive nitrogen encompasses here nitrogen oxides ($NO_x$ = NO + $NO_2$) and their oxidation products.
2. P. J. Crutzen, *Q. J. R. Meteorol. Soc.* **96**, 320 (1970).
3. S. S. Brown *et al.*, *Science* **311**, 67 (2006).
4. D. Shindell, *Geophys. Res. Lett.* **34**, L14704 (2007).
5. J. N. Galloway *et al.*, *Science* **320**, 889 (2008).
6. A. Stohl, *J. Geophys. Res.* **111**, D11306 (2006).
7. K. S. Law, A. Stohl, *Science* **315**, 1537 (2007).
8. P. K. Quinn *et al.*, *Tellus* **59B**, 99 (2007).
9. H. B. Singh, M. Kanakidou, P. J. Crutzen, D. J. Jacob, *Nature* **378**, 50 (1995).
10. H. J. Beine, T. Krognes, *Atmos. Environ.* **34**, 933 (2000).
11. R. E. Honrath *et al.*, *Geophys. Res. Lett.* **26**, 695 (1999).
12. F. Dominé, P. B. Shepson, *Science* **297**, 1506 (2002).
13. H. J. Beine *et al.*, *Atmos. Chem. Phys.* **3**, 335 (2003).
14. A. M. Grannas *et al.*, *Atmos. Chem. Phys.* **7**, 4329 (2007).
15. W. R. Simpson *et al.*, *Atmos. Chem. Phys.* **7**, 4375 (2007).
16. S. Morin, J. Savarino, S. Bekki, S. Gong, J. W. Bottenheim, *Atmos. Chem. Phys.* **7**, 1451 (2007).
17. C. Granier *et al.*, *Geophys. Res. Lett.* **33**, L13807 (2006).
18. Isotopic enrichments are expressed with the δ notation: $\delta^{x}O = R_{x,sample}/R_{x,reference} - 1$, where $R_x$ refers to $^{x}O/^{16}O$ mole ratio for $x$ = 17 or 18, or the $^{15}N/^{14}N$ mole ratio, in the sample and the reference material (standard mean ocean water for oxygen, atmospheric $N_2$ for nitrogen).
19. C. A. M. Brenninkmeijer *et al.*, *Chem. Rev.* **103**, 5125 (2003).
20. C. Kendall, E. M. Elliott, S. D. Wankel, *Stable Isotopes in Ecology and Environmental Science, 2nd Edition* (Blackwell, Oxford, 2007), chap. 12.
21. M. H. Thiemens, *Annu. Rev. Earth Planet. Sci.* **34**, 217 (2006).
22. G. Michalski, Z. Scott, M. Kabiling, M. H. Thiemens, *Geophys. Res. Lett.* **30**, 1870 (2003).
23. Nitrate (both particulate and gas-phase $HNO_3$) trapped on Whatman 41 filters by means of high-volume sampling at a subweekly resolution between April 2005 and July 2006 was dissolved in ultrapure water and analyzed for its oxygen and nitrogen isotope ratios using an automated version of the denitrifier technique (*34*). Uncertainties (1σ) pertaining to $\delta^{18}O$, $\Delta^{17}O$, and $\delta^{15}N$ measurements are 2, 0.4, and 0.5‰, respectively (see SOM for details).
24. T. H. E. Heaton, P. Wynn, A. Tye, *Atmos. Environ.* **38**, 5611 (2004).
25. M. G. Hastings, E. J. Steig, D. M. Sigman, *J. Geophys. Res.* **109**, D20306 (2004).
26. H. D. Freyer, D. Kley, A. Volz-Thomas, K. Kobel, *J. Geophys. Res.* **98**, 14791 (1993).
27. E. M. Elliott *et al.*, *Environ. Sci. Technol.* **41**, 7661 (2007).
28. D. Wagenbach, M. Legrand, H. Fischer, F. Pichlmayer, E. W. Wolff, *J. Geophys. Res.* **103**, 11007 (1998).
29. J. Savarino, J. Kaiser, S. Morin, D. M. Sigman, M. H. Thiemens, *Atmos. Chem. Phys.* **7**, 1925 (2007).
30. T. Blunier, G. L. Floch, H.-W. Jacobi, E. Quansah, *Geophys. Res. Lett.* **32**, L13501 (2005).
31. A. Sirois, L. A. Barrie, *J. Geophys. Res.* **104**, 11599 (1999).
32. A. Richter, F. Wittrock, A. Ladstätter-Weissenmayer, J. P. Burrows, *Adv. Space Res.* **29**, 1667 (2002).
33. J. Savarino, S. K. Bhattacharya, S. Morin, M. Baroni, J.-F. Doussin, *J. Chem. Phys.* **128**, 194303 (2008).
34. J. Kaiser, M. G. Hastings, B. Z. Houlton, T. Röckmann, D. M. Sigman, *Anal. Chem.* **79**, 599 (2007).


35. Thanks are due to the Alert Global Atmospheric Watch station personnel for aerosol field sampling in rough conditions; to E. Vince for help with bacterial cultures; to J. Kaiser, D. Sigman, and M. Hastings for their help with setting up the analytical technique; to G. Picard, F. Dominé, and M. Thiemens for helpful discussions; and to J.-Ph. Balestrieri for technical support. Funding was provided by the Institut Polaire–Paul-Émile Victor, Institut National des Sciences de l'Univers LEFE-CHAT, and the European Science Foundation under the EUROCORES Programme EuroCLIMATE, through contract no. ERAS-CT-2003-980409 of the European Commission, DG Research, FP6. S.M. acknowledges the École National des Ponts et Chaussées for financial support.


### Supporting Online Material

www.sciencemag.org/cgi/content/full/322/5902/730/DC1
Materials and Methods
SOM Text
Figs. S1 to S3
Table S1
References

17 June 2008; accepted 26 September 2008
10.1126/science.1161910

# Ages for the Middle Stone Age of Southern Africa: Implications for Human Behavior and Dispersal

Zenobia Jacobs,[1]* Richard G. Roberts,[1] Rex F. Galbraith,[2] Hilary J. Deacon,[3] Rainer Grün,[4] Alex Mackay,[5] Peter Mitchell,[6] Ralf Vogelsang,[7] Lyn Wadley[8]

The expansion of modern human populations in Africa 80,000 to 60,000 years ago and their initial exodus out of Africa have been tentatively linked to two phases of technological and behavioral innovation within the Middle Stone Age of southern Africa—the Still Bay and Howieson's Poort industries—that are associated with early evidence for symbols and personal ornaments. Establishing the correct sequence of events, however, has been hampered by inadequate chronologies. We report ages for nine sites from varied climatic and ecological zones across southern Africa that show that both industries were short-lived (5000 years or less), separated by about 7000 years, and coeval with genetic estimates of population expansion and exit times. Comparison with climatic records shows that these bursts of innovative behavior cannot be explained by environmental factors alone.

Anatomical and genetic evidence suggests that modern humans (*Homo sapiens*) originated in Africa during the Middle Stone Age (MSA), which lasted from about 280 to 30 thousand years ago (ka) (*1*). The later part of the MSA in southern Africa includes two distinct industries notable for their technological and behavioral innovation, the Still Bay (SB) and the Howieson's Poort (HP), which are found in diverse climatic and biogeographic contexts (Fig. 1). SB flake-based technology includes finely shaped, bifacially worked, lanceolate points that were probably parts of spearheads (*2*), whereas the blade-rich HP is associated with backed (blunted) tools (*3*) that most likely served as composite weapons, made of multiple stone artifacts, and with tools that differ from those in the SB. Evidence from use-wear and residue analysis demonstrates that the SB and HP weapons were hafted (*4*, *5*). Recent discoveries of associated bone points and tools (*6*, *7*), engraved ochres and ostrich eggshells (*8*–*10*), and shell beads (*11*, *12*) validate the interpretation of the SB and HP as innovative (*1*). Increasingly complex technological and social organization, accompanied by expansion in human populations and densities, is implied by the use of bone tools, symbols, and personal ornaments (*13*). No consensus exists, however, on the possible causes or consequences of these innovative technologies.

Genetic studies of expansions, migrations, and isolations of modern human populations within Africa (*14*, *15*) and their initial exodus out of Africa (*16*, *17*) have been temporally associated with the SB and HP (*13*). The establishment of evidence for these hypothesized connections, any link to the origins of click languages (*18*), and putative technological responses to environmental pressures (*13*) has been hindered by a lack of reliable chronological control for the SB and HP. Until now, it was not known whether these industries fell into two discrete periods of relatively short duration or formed a continuum of longer duration. These uncertainties persisted partly because of the chronological "haze" resulting from different sites being dated by means of different methods. Even for a single method, experimental factors typically vary between dating laboratories, owing to the use of different instruments, calibration standards, and procedures for sample preparation, measurement, and data analysis. Here we report the results of a systematic dating study, subcontinental in scope, of the timing of the SB and HP.

We used single-grain optical dating (*19*), combined with statistical modeling, to determine the time of deposition of the artifact-bearing deposits at nine geographically widespread sites across southern Africa (Fig. 1) (*20*). Optical ages indicate the burial times of artifacts in primary context. We have minimized the extent of interfactorial variance by holding the main experimental parameters constant and by having one operator (Z.J.) make all measurements on a single instrument and analyze the data using a common set of procedures. Dating of individual sand-sized grains of quartz allows a direct assessment of stratigraphic integrity and of any evidence for sediment mixing, so that both the accuracy and precision of the ages are optimized (*19*).

Our survey includes "classic" MSA sites, which we have redated (such as Klasies River), and SB and HP deposits not dated previously. The coastline of South Africa is represented in our survey (Fig. 1), as are near-coastal areas and the continental interior of Lesotho and Namibia to altitudes of up to 1850 m. Most major present-day climatic ranges and ecological zones are encompassed in our survey, but we recognize that the position and extent of these biomes will have varied during the late Pleistocene because of changes in ocean/atmosphere circulation patterns (*21*). Fifty-four sediment samples were dated from stratigraphic units containing unambiguous evidence for the HP ($n = 22$) and SB ($n = 4$), and from units immediately before ($n = 10$) and after ($n = 18$) these industries. Details of sites, samples,

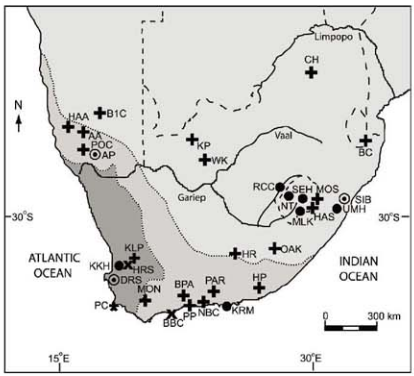


**Fig. 1.** Locations of sites at which SB and HP artifacts have been found. Solid circles indicate those sites where HP deposits, have been dated in this study, whereas open circles with a central dot denote study sites that contain both dated SB and HB industries. The symbols x and + indicate other known (or claimed) occurrences of SB and HP, respectively; these sites may have associated independent age estimates. Also shown are the modern rainfall zones: winter (dark gray), all year (medium gray), and summer (light gray). Site acronyms are defined in (*20*).

[1]GeoQuEST Research Centre, School of Earth and Environmental Sciences, University of Wollongong, Wollongong, New South Wales 2522, Australia. [2]Department of Statistical Science, University College London, London WC1E 6BT, UK. [3]Iziko Museums of Cape Town, Cape Town 8000, South Africa. [4]Research School of Earth Sciences, Australian National University, Canberra, Australian Capital Territory (ACT) 0200, Australia. [5]School of Archaeology and Anthropology, Australian National University, Canberra, ACT 0200, Australia. [6]School of Archaeology, University of Oxford, Oxford OX1 2PG, UK. [7]Institute of Prehistoric Archaeology, African Archaeology Unit, University of Cologne, Köln 50823, Germany. [8]School of Geography, Archaeology and Environmental Sciences, and Institute for Human Evolution, University of the Witwatersrand, WITS 2050, South Africa.

*To whom correspondence should be addressed. E-mail: zenobia@uow.edu.au

and dating procedures are given in (*20*). It is unlikely that each site will cover the entire age range of each industry, but we consider that sufficient samples have been dated to recognize chronological patterns for each industry. In particular, we have obtained reliable estimates of the timing and duration of the HP.

The ages are summarized in Fig. 2. They are plotted according to site location (west, or east and south) to illuminate any tendencies for spatial variation across geographic and climatic boundaries. No spatial patterns could be discerned, so both data sets were combined for all subsequent statistical analyses (*20*). We determined, by maximum likelihood estimation, that the composite data set is not consistent with a continuum of ages between the SB and HP ($P = 0.008$) but rather with a gap of 6.7 thousand years (ky) [95% confidence interval (CI): 2.7 to 9.3 ky]. We then estimated that the HP started 64.8 ka (95% CI: 68.2 to 61.6 ka) and ended 59.5 ka (95% CI: 62.7 to 56.5 ka), with a duration of 5.3 ky (95% CI: 2.0 to 8.3 ky). The start and end ages for SB were calculated as 71.9 and 71.0 ka, respectively, but there are too few data to reliably constrain their 95% CIs to better than 4 to 5 ky. The current ages are consistent with it being of short duration (<1 ky), but additional ages for the SB would help refine this estimate. The 10 earliest post-HP ages agree with a common value (56.5 ka; 95% CI: 59.0 to 54.0 ka); assuming that this marks the start of this period, we estimated a gap ($P = 0.02$) of about 4.2 ky (95% CI: 1.9 to 6.6 ky) between the end of the HP and the start of the post-HP period (*20*). The CIs for all of the start and end ages include a calibration uncertainty of 2% (associated with the laboratory beta source), but this uncertainty does not apply to estimates of duration (which are differences of ages).

| | | Age | $\sigma_1$ | $\sigma_2$ |
|---|---|---|---|---|
| **West** | | | | |
| later MSA | *KKH–8* | 33.3 | 1.1 | 1.3 |
| post–HP | *AP–9* | 57.9 | 2.5 | 2.6 |
| | *DRS–9* | 47.7 | 1.4 | 1.7 |
| | *DRS–8* | 55.4 | 1.7 | 2.0 |
| | *KKH–4* | 55.6 | 2.4 | 2.7 |
| | *KKH–3* | 55.2 | 1.7 | 2.0 |
| | *KKH–1* | 57.8 | 2.1 | 2.4 |
| HP | *AP–4* | 63.2 | 1.9 | 2.2 |
| | *DRS–6* | 60.5 | 1.5 | 1.9 |
| | *DRS–10* | 61.8 | 1.2 | 1.7 |
| | *DRS–5* | 60.3 | 1.6 | 2.0 |
| | *DRS–4* | 58.1 | 1.5 | 1.9 |
| | *DRS–7* | 61.3 | 1.4 | 1.9 |
| | *DRS–11* | 63.3 | 1.7 | 2.1 |
| | *KKH–5* | 64.7 | 2.7 | 3.0 |
| | *KKH–6* | 59.7 | 2.5 | 2.7 |
| | *KKH–2* | 56.0 | 3.2 | 3.4 |
| | *KKH–7* | 64.0 | 2.5 | 2.8 |
| pre–HP | *AP–5* | 66.9 | 2.2 | 2.6 |
| SB | *AP–6* | 70.7 | 2.1 | 2.5 |
| | *DRS–13* | 70.8 | 1.8 | 2.3 |
| | *DRS–14* | 73.6 | 2.1 | 2.5 |
| pre–SB | *DRS–15* | 84.9 | 2.4 | 2.9 |
| | *DRS–16* | 92.4 | 4.2 | 4.6 |
| | *DRS–17* | 86.6 | 4.0 | 4.4 |
| **East + South** | | | | |
| later MSA | *SEH–4* | 31.6 | 1.2 | 1.4 |
| | *SEH–3* | 30.3 | 3.3 | 3.4 |
| | *SIB–10* | 37.6 | 2.2 | 2.4 |
| | *SIB–22* | 48.0 | 2.1 | 2.4 |
| post–HP | *ZKR–5* | 57.9 | 1.9 | 2.3 |
| | *MLK–4* | 50.0 | 1.6 | 1.8 |
| | *NT–2* | 56.0 | 1.4 | 1.8 |
| | *SEH–2* | 46.5 | 2.3 | 2.5 |
| | *SEH–1* | 57.6 | 2.0 | 2.3 |
| | *SIB–9* | 56.7 | 1.7 | 2.1 |
| | *RCC–5* | 56.0 | 2.3 | 2.6 |
| HP | *ZKR–9* | 63.4 | 2.2 | 2.6 |
| | *ZKR–10* | 65.5 | 1.9 | 2.3 |
| | *ZKR–6* | 64.1 | 2.2 | 2.6 |
| | *MLK–3* | 61.0 | 2.1 | 2.5 |
| | *NT–1* | 60.9 | 2.5 | 2.8 |
| | *RCC–2* | 63.0 | 1.9 | 2.3 |
| | *RCC–1* | 63.2 | 1.9 | 2.3 |
| | *RCC–3* | 65.0 | 2.7 | 3.0 |
| | *SIB–15* | 61.7 | 1.5 | 2.0 |
| | *SIB–17* | 63.8 | 2.5 | 2.8 |
| | *SIB–19* | 64.7 | 1.9 | 2.3 |
| pre–HP | *ZKR–8* | 71.6 | 2.5 | 2.9 |
| | *ZKR–4* | 72.1 | 3.1 | 3.4 |
| | *MLK–2* | 79.5 | 2.6 | 3.1 |
| SB | *SIB–20* | 70.5 | 2.0 | 2.4 |
| pre–SB | *SIB–21* | 72.5 | 2.0 | 2.5 |
| | *SIB–24* | 73.2 | 2.3 | 2.7 |
| | *SIB–23* | 77.2 | 2.1 | 2.6 |

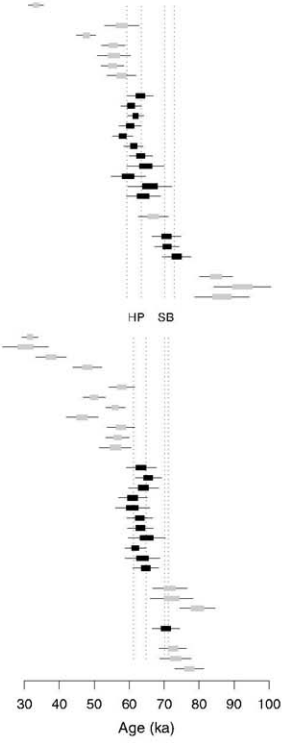


**Fig. 2.** Optical age estimates (ka) classified by region, archaeological association, and site. Samples are listed in stratigraphic order within each site. Samples with the association "pre-HP" have been identified as being before the start of the HP but not necessarily after the end of the SB. Standard errors $\sigma_1$ and $\sigma_2$ exclude and include, respectively, possible systematic error (any systematic error is the same for each estimate and does not affect comparisons between estimates). Shaded boxes and error bars denote 50 and 95% CIs, respectively, calculated using $\sigma_1$. Intervals for samples from the HP and SB are highlighted in black. Dotted lines indicate the start and end ages of the HP and SB, estimated separately for each region. ZKR denotes samples from Klasies River; other site acronyms are defined in (*20*).

Our SB and HP ages are plotted in Fig. 3 with other chronological estimates obtained previously (table S1). For these comparisons, the total uncertainty on the optical ages includes the calibration uncertainty of 2%. Nearly all of the previous HP ages are consistent with being inside our estimated HP period, and all of the SB estimates are consistent with a single common age (*20*). But our optical ages are more precise, being compatible with the most accurate and precise estimates available [from uranium-series dating of speleothems (Fig. 3) and acid-base-wet oxidation pretreatment with stepped combustion (ABOX-SC) radiocarbon dating of charcoal from post-HP levels at Border Cave (*22*)].

Southern Africa lacks continuous and well-dated paleoenvironmental records for the time interval of interest across the full range of biomes (*21*). But we argue against a substantial influence of local- to regional-scale climatic variations on the archaeological record because HP and SB sites cross-cut climatic and ecological zones. At a subcontinental scale, the climatic records identified in ice cores from West and East Antarctica (*23*, *24*) (Fig. 4) can be used for comparison, bearing in mind the detailed differences in timing and amplitude of changes in the Antarctic records and the additional uncertainties associated with extrapolating climatic changes in Antarctica to southern Africa. Although the HP occurred during a period of climatic warming, this was also the case for the late and final MSA occupations at Sibudu (*25*, *26*). The SB and post-HP periods cannot be reliably associated with either warm or cool intervals (Fig. 4). Accordingly, we cannot identify any particular climatic attribute that is consistently and uniquely associated with any MSA industry. Other differences also occur; for example, the SB coincided (within error) with the Toba volcanic super-eruption (*27*) and with the end of megadroughts in tropical Africa (*28*), whereas the HP is not associated with any such known events. Environmental factors may have been responsible for episodic occupation and abandonment of rock shelters (*26*), but they were not necessarily the driving force behind technological change.

The age and duration of the HP have been long-standing topics of dispute (*29*). We have resolved, with useful precision and over a broad geographical range, start and end ages for the HP (which is of sufficiently short duration that it represents a marker horizon of about 62 ka for southern Africa), the probable brief duration of the SB, and the existence of an age gap of several millennia between the SB and HP. The cause of these two bursts of technological innovation, closely spaced yet separated in time, remains an enigma, as does the reason for their disappearance. But, intriguingly, both fall within the genetic bottleneck that occurred 80 to 60 ka and the subsequent expansions of modern human populations within (*14*, *15*) and out of (*16*, *17*) Africa. Determining whether the emergence of innovative technology in southern Africa was a precursor to the latter exodus (*13*), or whether population expansions were the stimulus for the SB and HP (*15*, *28*), requires that similar chronological data sets be compiled and evaluated for comparable lithic technologies in East and North Africa (*30*).

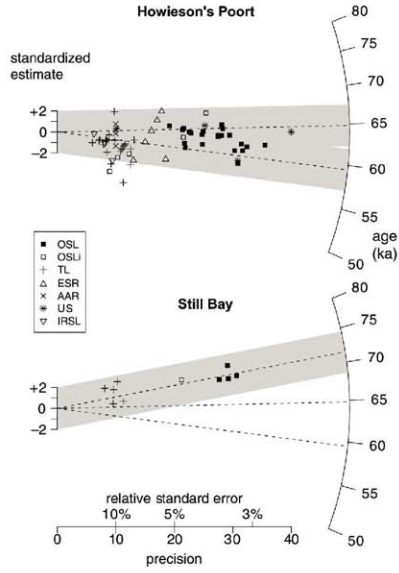


**Fig. 3.** Radial plots comparing age estimates of samples from the HP and SB obtained in different studies. Solid squares denote estimates from this study presented in Fig. 2, with precisions obtained using $\sigma_2$ (that is, including possible systematic error). Other symbols denote estimates obtained independently by various researchers using different dating methods (table S1). Dashed lines show the estimated start and end ages of the HP period and the midpoint of the SB. Shaded bands indicate ±2 SE (for any age estimate) about each of these lines. Estimates consistent with a common age should scatter mostly within such a band.

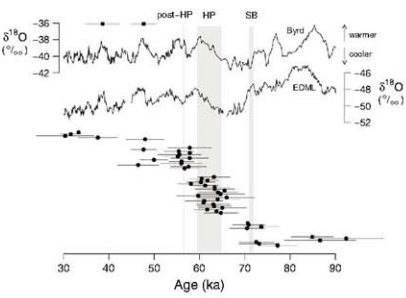


**Fig. 4.** Age estimates (with 95% CIs) from Fig. 2 plotted alongside oxygen isotope data (‰, per mil) from the Byrd and European Project for Ice Coring in Antarctica (EPICA) Dronning Maud Land (EDML) ice cores from Antarctica (*23*, *24*). Both records are plotted on a common time scale, achieved by synchronization with Greenland ice core data (*24*), and the EDML data are lowess-smoothed to 100-year resolution. Ages labeled "pre-HP" in Fig. 2 are omitted here, as they cannot be identified with a specific period. Vertical gray bands show our estimates of the HP and SB periods as well as the pulse immediately post-HP. The gray horizontal bars show mean age estimates and 95% CIs for the late and final MSA periods obtained in (*26*).


**References and Notes**

1. S. McBrearty, A. S. Brooks, *J. Hum. Evol.* **39**, 453 (2000).
2. L. Wadley, *J. Hum. Evol.* **52**, 681 (2007).
3. S. Wurz, *S. Afr. Archaeol. Bull.* **54**, 38 (1999).
4. M. Lombard, *S. Afr. Archaeol. Bull.* **62**, 62 (2007).
5. M. Lombard, *J. Archaeol. Sci.* **35**, 26 (2008).
6. C. S. Henshilwood, F. d'Errico, C. W. Marean, R. G. Milo, R. Yates, *J. Hum. Evol.* **41**, 631 (2001).
7. L. Backwell, F. d'Errico, L. Wadley, *J. Archaeol. Sci.* **35**, 1566 (2008).
8. C. S. Henshilwood *et al.*, *Science* **295**, 1278 (2002).
9. A. Mackay, A. Welz, *J. Archaeol. Sci.* **35**, 1521 (2008).
10. J.-P. Rigaud, P.-J. Texier, J. E. Parkington, C. Poggenpoel, *C. R. Palevol.* **5**, 839 (2006).
11. C. S. Henshilwood, F. d'Errico, M. Vanhaeren, K. van Niekerk, Z. Jacobs, *Science* **304**, 404 (2004).
12. F. d'Errico, M. Vanhaeren, L. Wadley, *J. Archaeol. Sci.* **35**, 2675 (2008).
13. P. Mellars, *Proc. Natl. Acad. Sci. U.S.A.* **103**, 9381 (2006).
14. P. Forster, *Philos. Trans. R. Soc. London Ser. B* **359**, 255 (2004).
15. D. M. Behar *et al.*, *Am. J. Hum. Genet.* **82**, 1130 (2008).
16. V. Macaulay *et al.*, *Science* **308**, 1034 (2005).
17. H. Liu, F. Prugnolle, A. Manica, F. Balloux, *Am. J. Hum. Genet.* **79**, 230 (2006).
18. S. A. Tishkoff *et al.*, *Mol. Biol. Evol.* **24**, 2180 (2007).
19. Z. Jacobs, R. G. Roberts, *Evol. Anthropol.* **16**, 210 (2007).
20. Materials and methods are available as supporting material on *Science* Online.
21. B. M. Chase, M. E. Meadows, *Earth-Sci. Rev.* **84**, 103 (2007).
22. M. I. Bird *et al.*, *Quat. Sci. Rev.* **22**, 943 (2003).
23. T. Blunier, E. J. Brook, *Science* **291**, 109 (2001).
24. EPICA Community Members, *Nature* **444**, 195 (2006).
25. S. Soriano, P. Villa, L. Wadley, *J. Archaeol. Sci.* **34**, 681 (2007).
26. Z. Jacobs, A. G. Wintle, G. A. T. Duller, R. G. Roberts, L. Wadley, *J. Archaeol. Sci.* **35**, 1790 (2008).
27. S. H. Ambrose, *J. Hum. Evol.* **34**, 623 (1998).
28. C. A. Scholz *et al.*, *Proc. Natl. Acad. Sci. U.S.A.* **104**, 16416 (2007).
29. Z. Jacobs, R. G. Roberts, *S. Afr. Archaeol. Soc. Goodwin Ser.* **10**, 8 (2008).
30. A. Bouzouggar *et al.*, *Proc. Natl. Acad. Sci. U.S.A.* **104**, 9964 (2007).


31. We acknowledge support from the Australian Research Council (R.G.R., R.G., and Z.J.), Deutsche Forschungsgemeinschaft, and National Museum of Namibia (R.V.). The South African Heritage Resource Agency, Amafa, the Namibian Heritage Council of Namibia, and the Protection and Preservation Commission of Lesotho (N. Khitsane) issued permits.


**Supporting Online Material**

www.sciencemag.org/cgi/content/full/322/5902/733/DC1
Materials and Methods
Figs. S1 to S29
Tables S1 to S29
References


24 June 2008; accepted 25 September 2008
10.1126/science.1162219

# Energy Uptake and Allocation During Ontogeny

Chen Hou,[1]* Wenyun Zuo,[2] Melanie E. Moses,[3] William H. Woodruff,[1,4] James H. Brown,[1,2] Geoffrey B. West[1,4]

All organisms face the problem of how to fuel ontogenetic growth. We present a model, empirically grounded in data from birds and mammals, that correctly predicts how growing animals allocate food energy between synthesis of new biomass and maintenance of existing biomass. Previous energy budget models have typically had their bases in rates of either food consumption or metabolic energy expenditure. Our model provides a framework that reconciles these two approaches and highlights the fundamental principles that determine rates of food assimilation and rates of energy allocation to maintenance, biosynthesis, activity, and storage. The model predicts that growth and assimilation rates for all animals should cluster closely around two universal curves. Data for mammals and birds of diverse body sizes and taxa support these predictions.

The "food of life" and the "fire of life"—the combustion of food to supply the energy that fuels growth, maintenance, and activity—is fundamental to animal survival (*1*). A large body of previous work used energy budget models to understand ontogenetic growth (*1–7*). These models have contributed importantly to many conceptual and applied problems, including life history theory, animal husbandry, and biomedicine. Still largely missing, however, is a complete quantitative framework that specifies how food is transformed into metabolic energy and stored biomass. Here, we present such a framework, which quantifies explicitly how assimilated food is transformed into biomass and metabolic energy during ontogeny.

When an animal is growing, some fraction of the assimilated food is oxidized to fuel the total metabolic rate, $B_{tot}$, whereas the remaining fraction is synthesized and stored as biomass, $S$ (Fig. 1). Thus, the energy flux of assimilated food, $A$, sometimes called the rate of intake of metabolizable energy (*1*, *2*), is expressed as

$$A = B_{tot} + S = B_{tot} + E_c\,dm/dt \qquad (1)$$

where $A$ is defined as the combustion energy content of ingested food per unit time minus the combustion energy content of excreta per unit time, $E_c$ is the combustion energy content of a unit biomass, and $dm/dt$ is the rate of change in biomass, $m$, at time, $t$.

We build on an ontogenetic growth model (OGM), which specifies the allocation of metabolic energy between growth and maintenance and views the scaling of metabolic rate with body size as the primary constraint on growth (*7*). It partitions the basal metabolic rate, $B_{basal}$, between the rate of energy expenditure to maintain the existing biomass, $B_{maint}$, and the rate to synthesize the new biomass, $B_{syn}$ (Fig. 1): so, $B_{basal} = B_{maint} + B_{syn} = B_m m + E_m dm/dt$, where $B_m \sim M^{-1/4}$ is the mass-specific maintenance metabolic rate, $M$ is the adult body mass, and $E_m$ is the energy required to synthesize a unit of biomass.

It is difficult to measure $B_{basal}$ over ontogeny because animals grow even while resting. Therefore, for growing animals a more operational and realistic parameter is resting metabolic rate, $B_{rest}$, which is the sum of $B_{basal}$ and specific dynamic action (SDA), the increment resulting from digestion. SDA is the energy expended for intestinal absorption, nutrient transport, amino acid oxidation, and protein synthesis (*8*, *9*). Because some fraction of metabolic rate is allocated to SDA during growth (*8–11*), we modify the OGM to obtain

$$B_{rest} = B_{maint} + B_{syn} = B_m m + E_m dm/dt \qquad (2)$$

where $B_m$ is larger here than in the OGM, which ignored SDA.

It is important to recognize the difference between the terms $S = E_c dm/dt$ in Eq. 1 and $B_{syn} = E_m dm/dt$ in Eq. 2 and, consequently, the difference between $E_m$ and $E_c$. Energy expended during growth is partitioned between the energy content stored in the newly synthesized biomass and the energy expended in synthesizing this biomass from the constituent materials. So, $S$ is the rate of accumulated energy content of new biomass, and $E_c$ is its combustion energy content. On the other hand, $B_{syn}$ is the metabolic power expended on biosynthesis, and $E_m$ is the energy expended to synthesize a unit of biomass. The term $B_{syn}$ corresponds to the organizational work of growth (*2*) and is completely dissipated as heat, not conserved in stored biomass. In the OGM, the energy expended on biosynthesis was incorrectly estimated by using the empirical combustion energy (*7*).

For adult mammals and birds, the total metabolic rate is typically referred to as field metabolic rate, and the relationship between total and resting metabolic rates is expressed as $B_{tot}(M) = B_{act}(M) + B_{rest}(M) = fB_{rest}(M)$, where $B_{act}$ is the rate of energy expenditure for locomotion, feeding, and other activities and $f$, the activity scope, is a dimensionless parameter (*12–14*). In adult endotherms, $f$ is about 2 to 3 and independent of body mass (*12–14*). Assuming that a similar relationship holds during growth, we can write, using Eq. 2, $B_{tot}(m) = fB_{maint}(m) + fB_{syn}(m)$. We define the dimensionless storage coefficient, $\gamma = S/B_{syn} = E_c/E_m$, as the ratio of the energy stored in a unit of biomass to the energy expended to synthesize this biomass. Substituting $\gamma$ and $B_{tot}$ into Eqs. 1 and 2 gives

$$A(m) = B_{maint}(m) + B_{act}(m) + B_{syn}(m) + S(m)$$
$$= (f+\gamma)B_{rest}(m) - \gamma B_{maint}(m) \qquad (3)$$

Equation 3 is quite general, independent of how $B_{rest}$, $B_{maint}$, or $f$ scale with $m$. Empirical measurements of metabolic rate over ontogeny and theoretical evidence linking growth and metabolism show that resting metabolic rate $B_{rest}(m) \approx B_0 m^{3/4}$ over ontogeny, where $B_0$ is constant for a given taxon (*14*, *15*). The mass-specific maintenance rate, taking into account SDA, is $B_m \approx$

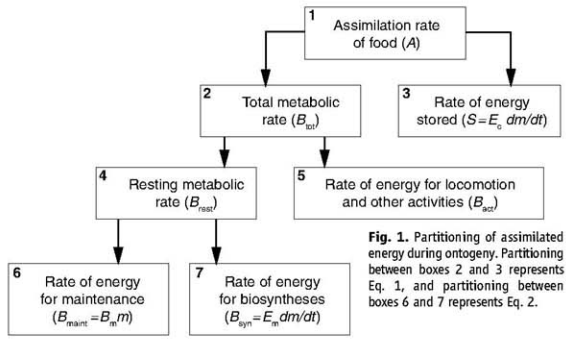


**Fig. 1.** Partitioning of assimilated energy during ontogeny. Partitioning between boxes 2 and 3 represents Eq. 1, and partitioning between boxes 6 and 7 represents Eq. 2.

[1]Santa Fe Institute, 1399 Hyde Park Road, Santa Fe, NM 87501, USA. [2]Department of Biology, University of New Mexico, Albuquerque, NM 87131, USA. [3]Department of Computer Science, University of New Mexico, Albuquerque, NM 87131, USA. [4]Los Alamos National Laboratory, Los Alamos, NM 87545, USA.

*To whom correspondence should be addressed. E-mail: houc@santafe.edu

$B_0M^{-1/4}$ (*7*). The use of these scaling relations in Eq. 3 yields

$$A(m) = (f+\gamma)B_0m^{3/4} - \gamma B_0M^{-1/4}m$$
$$= B_{\text{rest,adult}}[(f+\gamma)\mu^{3/4} - \gamma\mu] \quad (4)$$

where $\mu$ ($=m/M$) is relative mass and $B_{\text{rest,adult}} \approx B_0M^{3/4}$ is the resting metabolic rate at the adult size.

Note that Eq. 4 predicts that during ontogeny the food assimilation rate, $A$, unlike metabolic rate, does not obey a simple power law as a function of body mass, $m$. This prediction is well supported (*14*). In Fig. 2, we plot some examples of the normalized assimilation rate ($A/B_{\text{rest,adult}}$) versus $\mu$ for six different animals and fit the data with Eq. 4. Values of $f$, $\gamma$, and $R^2$ from the nonlinear least squares regression for these and several other bird and mammal species are in table S1 (*14*). The storage coefficient, $\gamma = E_c/E_m$, can in principle be determined independently from the energetics of biosynthesis. The energy content of biomass, $E_c$, averages about 24,000 J/g for dry mass (*16*), with fourfold variation across vertebrates of different taxa and ontogenetic stages (*17*). In contrast to $E_c$, $E_m$, the energy expended to synthesize a unit of biomass, is difficult to determine empirically [but see (*14*)]. Theoretical considerations suggest that the average energy required for biosynthesis of macromolecules from monomers is about 2400 J/g (*14*). This theoretical value of $E_m$ gives an upper bound of $\gamma \sim 10$, the precise value depending on the additional energy expended on biosynthesis, metabolism, and excretion (*3*). For mammals and birds, $\gamma$ averages about 3 and ranges from 1 to 9 depending on species, diet, and age (*3*, *14*, *18*). This result is consistent with values ranging from 0.8 to 7 for fish, birds, and mammals estimated from the OGM (*14*, *15*). We estimated from food assimilation that $\gamma$ ranges from 0.6 to 5.3 with an average of 2.71 ± 1.18 (table S1), showing that, despite some variation, the empirical measurements are in agreement with the theoretical prediction. Values of $f$ vary somewhat, depending on activity levels and behavior. The mean value of $f$ estimated from food assimilation is 2.67 ± 0.61 (table S1), also in agreement with data for adult mammal and bird species (*14*).

When growth ceases, that is, $\mu = 1$ ($m = M$), Eq. 4 predicts that the food assimilation rate equals the total metabolic rate, which scales with mass, $M$. So, $A$ is equal to $fB_0M^{3/4}$ across adults of different species. Data for ad libitum energy intake from food of 120 species of zoo mammals with body masses ranging from 0.025 kg to 3000 kg show $A = 7.07M^{0.75}$, supporting the prediction (*14*, *19*, *20*). Taking the average value of $B_0$ for resting metabolic rates of mammals, 3.92 W/kg$^{3/4}$ (*14*), gives $f \approx 1.8$. This is somewhat less than that expected for wild animals, which may reflect lower activity levels in captivity.

Our model predicts that growth rates of diverse animals should exhibit universal properties. The fraction of energy assimilation rate allocated to growth is the sum of $S$ and $B_{\text{syn}}$. With Eq. 2 and the definition of $\gamma$, this fraction becomes $S + B_{\text{syn}} = (1+\gamma)B_{\text{rest,adult}}(\mu^{3/4} - \mu)$. If we normalize this quantity with respect to $(1+\gamma)B_{\text{rest, adult}}$, then all animal species, regardless of taxon or adult mass, should fall on the same parameterless universal curve, $\mu^{3/4} - \mu$. This further predicts that the maximum energy utilization rate for growth occurs when $d(\mu^{3/4} - \mu)/d\mu|_{\mu=\mu_0} = 0$, which gives $\mu_0 = (3/4)^4 = 0.316$. Equation 3 suggests a way to test these predictions. If we subtract the rate of metabolism for activity, $B_{\text{act}}$, and maintenance, $B_{\text{maint}}$, from the assimilation rate, $A$, the difference gives the rate of energy assimilation allocated to growth, $S + B_{\text{syn}}$. This quantity, normalized as above, is plotted as a function of the relative mass $\mu$ in Fig. 3A. The normalized assimilation rates for mammals and birds of widely varying body sizes and taxa show such universal properties, clustering closely around the predicted parameterless curve with a peak at ~0.316.

Additionally, the rate of energy allocation to growth must be proportional to the growth rate, $dm/dt$, so the universal curve and the value of $\mu_0 = (3/4)^4 = 0.316$ can be derived independently from the growth rate equation, Eq. 2, $dm/dt = (B_0/E_m)m^{3/4}[1 - (m/M)^{1/4}]$. This can be re-expressed as $(E_mM^{1/4}/B_0)d\mu/dt = \mu^{3/4} - \mu$. Data for normalized growth rates, $(E_mM^{1/4}/B_0)d\mu/dt$, for diverse mammals and birds measured independently from the above measurements of assimilation rate support this prediction (Fig. 3B). So, estimations from the rate of food assimilation and the rate of change in body mass independently predicted analogous universal curves with a maximum at a normalized body mass of ~0.316.

The predicted allometric scalings of metabolic energy allocation are summarized in Fig. 4A, which shows the rates of food assimilation and total, resting, and maintenance metabolism for two individuals of different adult size depicted by different colors. The figure illustrates the complete energy budget during growth, $A = B_{\text{maint}} + B_{\text{act}} + B_{\text{syn}} + S$, and allocation of energy at any given size is shown by the colored vertical lines. The assimilation rate, $A$, of a growing individual does not scale as a power law with mass, whereas its rates of total and resting metabolism, $B_{\text{tot}}$ and $B_{\text{rest}}$, both scale as $m^{3/4}$ and its maintenance rate, $B_{\text{maint}} = B_m m$, scales linearly. In contrast, for adults of different sizes, rates of assimilation and total (dashed line) and resting (maintenance, solid black line) metabolism all scale as $M^{3/4}$. Across species of different adult masses, growth ceases when all resting metabolism is allocated to maintenance (*7*) so that $B_{\text{rest}} = B_{\text{maint}}$, as indicated in Fig. 4A (circles) representing two different adult masses, $M_1$ and $M_2$. Lastly, if otherwise identical individuals vary in energy allocated to activity, thereby having different values of $B_{\text{act}}$ and $B_{\text{tot}}$, they must compensate by adjusting their assimilation rates, $A$, if they are to mature at the same adult mass, $M$.

One implication of the model is that when two individuals with the same $B_0$, $f$, and $\gamma$ but different adult body masses, $M_1$ and $M_2$ ($M_1 > M_2$), have the same body mass, $m$, during growth, the assimilation rate of the one with the greater adult mass, $M_1$, must be larger than the one with the smaller adult mass, $M_2$, that is,

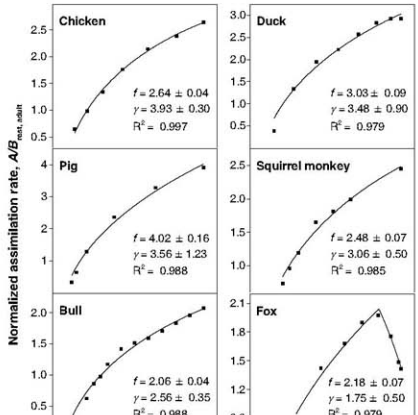


**Fig. 2.** Examples of normalized assimilation rate as a function of relative body mass for six mammals and birds (squares). The solid lines are fits of our model to these data with use of Eq. 4. (Parameters $f$ and $\gamma$ were estimated by using a nonlinear least squares regression method based on the Levenberg-Marquardt algorithm.) The majority of assimilation rate curves reported in the literature are monotonic, but a few, including curves for furbearers such as fox, are peaked relationships (*14*).

$A(m, M_1) - A(m, M_2) \propto (M_2^{-1/4} - M_1^{-1/4})m > 0$. To test this prediction, we plotted the assimilation rates of three pairs of closely related animals assumed to have the same $B_0$, $f$, and $\gamma$ as a function of body mass $m$ during growth. As illustrated in Fig. 4B, when members of each pair had the same body mass, $m$, during growth, the one with larger adult size ($M$) had a higher assimilation rate.

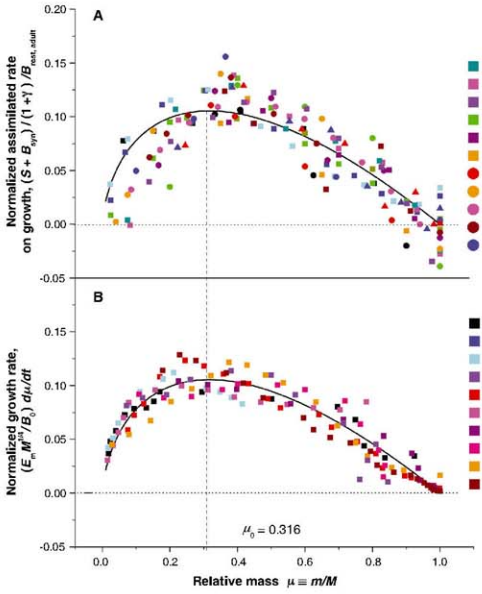


**Fig. 3.** Two growth curves that are universal in the sense that they have their bases in principles of energy allocation and are predicted to be independent of taxon and body size: **(A)** universal rate of assimilation of food for growth and **(B)** universal rate of change in body mass. The empirical estimates [colored symbols for different organisms, with assimilation and growth rates measured independently in different studies (*14*)] closely match the theoretical predictions (continuous curves that peak at 0.316).

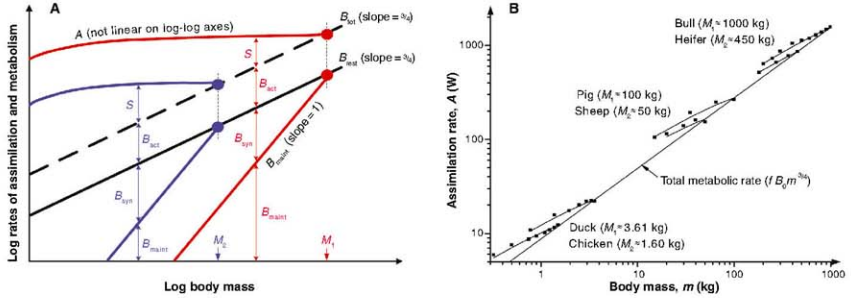


**Fig. 4.** **(A)** Schematic illustrating the allometric scalings of energy allocation during growth for two individual organisms (shown with different colors) of different adult sizes, $M_1$ and $M_2$. For each individual, the colored vertical lines illustrate how, at any given body mass during ontogeny, the rates of energy allocated to maintenance ($B_{maint}$), biosynthesis ($B_{syn}$), activity ($B_{act}$), and storage ($S$) sum to equal the rate of assimilation, $A$. The scalings across individuals of two different body sizes are shown as dashed and solid black lines for total and resting metabolic rates, respectively, with the colored dots corresponding to these rates at the adult sizes, $M_1$ and $M_2$. **(B)** Assimilation rate as function of body mass for three pairs of mammals or birds. To facilitate comparison, we assumed that $f = 2.67$ for all animals.

Our quantitative, predictive model for the energy budget of an individual during growth differs from phenomenological models that fit curves to data. It also differs from dynamic energy budget theory (DEB), which assumes a 2/3 power scaling of food assimilation rate during ontogeny, on the basis that energy uptake is limited by absorptive surface area, which scales like any simple geometric surface (*4*). By contrast, our model predicts that food assimilation rate cannot have a simple power-law scaling relation with body mass during ontogeny. Furthermore, DEB assumes that food assimilation rate is supply-limited, whereas our model views assimilation rate as arising from the developing organism matching food supply to metabolic energy demand. Our model provides a point of departure for addressing pathological cases of imbalance between supply and demand such as starvation or overeating. It captures the salient features of energy acquisition and allocation during ontogenetic development and quantitatively predicts universal assimilation and growth rate curves in agreement with data for mammals and birds. How well it captures the fundamental features of growth in other organisms, such as ectothermic vertebrates, insects, aquatic invertebrates, plants, and unicellular algae and protists, remains to be seen.

### References and Notes


1. M. Kleiber, *The Fire of Life: An Introduction to Animal Energetics* (Wiley, New York, 1961).
2. S. Brody, *Bioenergetics and Growth* (Hafner, Darien, CT, 1964).
3. P. C. Withers, *Comparative Animal Physiology* (Saunders College/Harcourt College, Fort Worth, TX, 1992).
4. S. A. L. M. Kooijman, *Dynamic Energy and Mass Budgets in Biological Systems* (Cambridge Univ. Press, Cambridge, 2000).
5. R. E. Ricklefs, *Funct. Ecol.* **17**, 384 (2003).
6. A. M. Makarieva, V. G. Gorshkov, B. L. Li, *Ecol. Model.* **176**, 15 (2004).
7. G. B. West, J. H. Brown, B. J. Enquist, *Nature* **413**, 628 (2001).
8. M. Jobling, *J. Fish Biol.* **23**, 549 (1983).
9. M. D. McCue, *Comp. Biochem. Physiol. A* **144**, 381 (2006).
10. A. Ashworth, *Nature* **223**, 407 (1969).
11. I. Krieger, *Am. J. Clin. Nutr.* **31**, 764 (1978).
12. K. L. Blaxter, *Energy Metabolism in Animals and Man* (Cambridge Univ. Press, Cambridge, 1989).
13. K. A. Nagy, I. A. Girard, T. K. Brown, *Annu. Rev. Nutr.* **19**, 247 (1999).
14. Materials and methods are available as supporting material on *Science* Online.
15. M. E. Moses *et al.*, *Am. Nat.* **171**, 632 (2008).
16. K. W. Cummins, J. C. Wuycheck, *Mitt. Int. Ver. Theor. Angew. Limnol.* **18**, 1 (1971).
17. C. T. Robbins, *Wildlife Feeding and Nutrition* (Academic Press, New York, 1983).
18. R. E. Ricklefs, in *Avian Energetics*, R. A. Paynter Jr., Ed. (Nuttall Ornithological Club Publication Number 15, Cambridge, MA, 1974).
19. E. Evans, D. S. Miller, *Proc. Nutr. Soc.* **27**, 121 (1968).
20. J. K. Kirkwood, *J. Nutr.* **121** (suppl. 11), 29 (1991).


21. Supported by NIH grants P20 RR-018754 (for M.E.M.) and DK36263 (for W.H.W.) and by NSF grants DEB-0083422 and CCF0621900 (for J.H.B.) and PHY 0706174 and PHY 0202180 (for G.B.W.) G.B.W. also acknowledges the Thaw Charitable Trust for its support.


### Supporting Online Material

www.sciencemag.org/cgi/content/full/322/5902/736/DC1
Materials and Methods
Tables S1 to S7
References and Notes


25 June 2008; accepted 19 September 2008
10.1126/science.1162302


# Experimental Evidence for Spatial Self-Organization and Its Emergent Effects in Mussel Bed Ecosystems


Johan van de Koppel,[1]* Joanna C. Gascoigne,[2] Guy Theraulaz,[3] Max Rietkerk,[4] Wolf M. Mooij,[5] Peter M. J. Herman[1]



**Spatial self-organization is the main theoretical explanation for the global occurrence of regular or otherwise coherent spatial patterns in ecosystems. Using mussel beds as a model ecosystem, we provide an experimental demonstration of spatial self-organization. Under homogeneous laboratory conditions, mussels developed regular patterns, similar to those in the field. An individual-based model derived from our experiments showed that interactions between individuals explained the observed patterns. Furthermore, a field study showed that pattern formation affected ecosystem-level processes in terms of improved growth and resistance to wave action. Our results imply that spatial self-organization is an important determinant of the structure and functioning of ecosystems, and it needs to be considered in their conservation.**


Self-organized spatial patterns in ecological communities have been observed in arid ecosystems (*1–3*), peat lands (*4*), tidal wetlands (*5*), mussel beds (*6*), and rocky shores (*7–9*). These patterns are thought to result from local, nonlinear interactions between organisms or between organisms and the environment, developing even on completely homogeneous substrates. Models predicted that self-organized patterns can affect ecosystem-level processes, for instance, by improving resilience to perturbation, resistance to environmental change, and primary or secondary production (*3*, *6*). Most studies of self-organization in ecological systems combine observational studies with mathematical modeling (*2*, *10*) or experimentally test the mechanisms that underlie the self-organization process (*11*). Experimental demonstrations of self-organization—as have been accumulated for physical, chemical (*12*, *13*), sociobiological (*14*), and microbial systems (*15*, *16*)—are rare for ecological systems (*17*, *18*).

We investigated the origin of regular patterns in beds of the blue mussel *Mytilus edulis* (in the Menai Strait near Bangor, UK) on intertidal flats under wind-sheltered conditions (*19*). *M. edulis* is a filter-feeding animal exploiting algal plankton and detritus in the water column. Patterns consist of regularly spaced clusters of 5 to 10 cm in width that form a coherent, labyrinth-like pattern (Fig. 1A). In areas where mussel densities are lower, clusters are more isolated (Fig. 1B), whereas beds are near-homogeneous in very dense areas. Point pattern analysis based on Ripley's $K$ (*19*) revealed clear, regularly spaced mussel clusters of ~3 to 5 cm across at ~10 cm distance from each other (fig. S1). Despite an order of magnitude difference in mussel biomass at the scale of meters, we found no significant difference in within-cluster biomass (fig. S2), suggesting that mussels self-organize to a certain local, within-cluster density, possibly to minimize predation or dislodgement losses (*20*). This concurs with a number of mathematical studies pointing at the possibility of self-organized pattern formation in mussel beds (*6–8*) and experimental studies in other intertidal ecosystems (*18*, *21*). Because of their small spatial scale, fast temporal development, and easy manipulation and observation of individuals, mussel beds are particularly suited for experimental testing of self-organization principles.

We tested in the laboratory the hypothesis that the observed patterns are self-organized and hence would develop spontaneously from homogeneity. Mussels that were laid out evenly in laboratory mesocosms developed coherent nonrandom spatial patterns within a day. These patterns were statistically similar to the patterns observed in the field (Fig. 1, C and D; movie S1; and see fig. S3, A and B, for a statistical description). When mussel densities in the laboratory were decreased, the spatial pattern became more open and clumps became more isolated (Fig. 1, E and F; movie S2; and fig. S3, C to D), as was observed under natural conditions (fig.


[1]Spatial Ecology Department, The Netherlands Institute of Ecology (NIOO-KNAW), Post Office Box 140, 4400 AC Yerseke, Netherlands. [2]School of Ocean Sciences, University of Wales Bangor, Askew Street, Menai Bridge LL59 5AB, UK. [3]Centre de Recherches sur la Cognition Animale, CNRS UMR 5169, Universite Paul Sabatier 118, Route de Narbonne, 31062 Toulouse Cedex 04, France. [4]Department of Environmental Sciences, Copernicus Institute, Utrecht University, Post Office Box 80115, 3508 TC Utrecht, Netherlands. [5]Aquatic Food Webs Department, Netherlands Institute of Ecology, Rijksstraatweg 6, 3631 AC, Nieuwersluis, Netherlands.

*To whom correspondence should be addressed. E-mail: J.vandeKoppel@nioo.knaw.nl

S1). Pattern formation in our experiment can only be caused by interactions between individual mussels, as there was no heterogeneity in substrate, suspended algal food, or initial conditions.

To elucidate how interactions between individual mussels determine spatial pattern formation, we traced the movement of individual mussels during our experiments, and we related movement characteristics to the local density of conspecifics. The resulting description of mussel movement was incorporated into an individual-based model (IBM) to test if this description is sufficient to explain the observed patterns (*22*, *23*). At first, our analysis revealed a strong negative effect on movement of mussel densities in the direct neighborhood: Mussels moved less when surrounded by conspecifics (Fig. 2A). When this relation was included in the IBM, however, no regular patterns were produced after a day of simulation time (Fig. 2B and fig. S4A), and in the long run, the model predicted the formation of a few large clusters of mussels, distinctly different from what we had observed in the field and our lab experiments. This difference implies that additional behavior prevents the formation of such large clusters and possibly that mussels decide to move when cluster size becomes too large. This idea was confirmed by a multiple generalized linear model (GLM) analysis of the relationship between movement speed and mussel density that considered a range of scales: Apart from a clear negative effect of mussel density in the neighborhood on movement at a scale of 1.87 cm, we found a strong positive effect on movement at a scale of 7.5 cm (Fig. 2, C and D). Hence, mussel movement appeared to increase again when clusters became very large. When we incorporated this new relationship in the IBM, the model correctly predicted the observed patterns (Fig. 2E and see fig. S4 for a statistical characterization).

Our laboratory observations show that a scale-dependent feedback to the processes of aggregation (Fig. 2, C and D) explains the formation of patterns: Movement decreases when mussels aggregate to form small-scale clusters, attaching themselves to each other with byssal

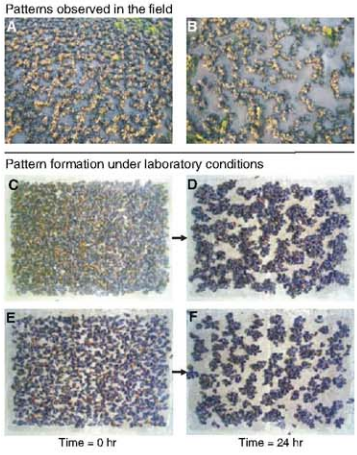


**Fig. 1.** Pattern formation in mussels in the field and under experimental laboratory conditions. **(A** and **B)** Small-scale, labyrinthlike spatial patterning in beds of the blue mussel *M. edulis*, as observed in the Menai Strait, near Bangor, UK. Scale is ~1.5 m wide. **(C** to **F)** Mussels that were laid out evenly under controlled conditions on a homogeneous substrate developed spatial patterns similar to those in the field within 24 hours. (C) and (D) versus (E) and (F): initial density of 6.0 and 3.8 kg/m$^2$, being ~1850 and ~1200 individuals, respectively. Images in (C) to (F) represent a surface of 60 × 80 cm. The development from (C) to (D) and (E) to (F) is shown in movies S1 and S2 in the supporting online material.

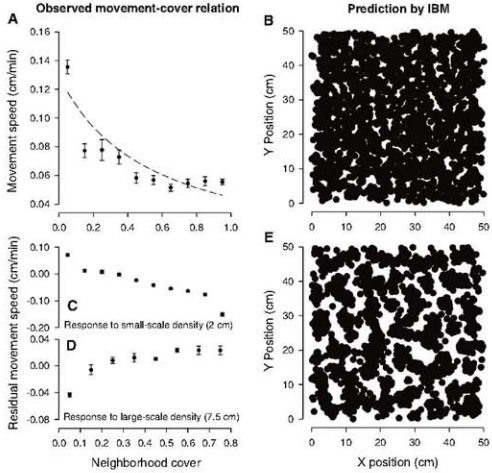


**Fig. 2.** Observed relationships between local mussel density and movement speed of mussels (left panels) and simulation results of IBMs that incorporate these relationships (right panels). **(A)** Relationship between movement speed of a particular tracked mussel and neighborhood cover within a 1.87-cm radius. The dashed line represents a univariate GLM fit with exponential distribution: $\beta = 1/(7.73 + 14.69\ C_{1.87})$; intercept: $z = 42.39$, $P < 0.001$; $C_{1.87}$-coefficient: $z = 22.09$, $P < 0.001$; $N = 4408$. **(C** and **D)** Residual deviance from a multiple GLM regression: $\beta = 1/(8.21 + 23.42\ C_{1.87} - 19.38\ C_{7.50})$; intercept: $z = 42.89$, $P < 0.001$; $C_{1.87}$-coefficient: $z = 23.19$, $P < 0.001$; $C_{7.50}$-coefficient: $z = -11.76$, $P < 0.001$; $N = 4408$. (C) Relationship between residual movement speed and neighborhood cover within 1.87-cm radius after removal of the effect of cover within 7.5-cm radius. (D) Relationship between residual movement speed and neighborhood cover at within 7.5-cm radius after removal of the effect of cover at 1.87-cm radius. **(B** and **E)**. An IBM simulation with 2025 (45 × 45) mussels with movement characteristics based on the single-regression fit did not reproduce the patterning after a 1-day simulation run, whereas the model based on the multiple regression fit closely reproduced the patterns observed in the laboratory experiment. Error bars indicate SEM.

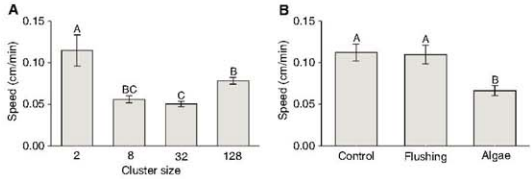


**Fig. 3.** Relationship between **(A)** cluster size and the movement speed of mussels and **(B)** mussel movement speed and addition of algae to large clusters of mussels. (A) Mussel movement speed initially decreases with cluster size but increases again when cluster size is increased from 32 to 128 individuals. (B) Supply of suspended algal food to clusters of 128 individuals decreases the movement speed significantly. The flushing treatment, a procedural control in which filtered seawater was supplied to mussels at the same rate as the algal supply treatment, was found to differ significantly from the algal supply treatment but not from the control treatment, indicating that the effect is caused by algal supply, not by flushing with seawater. Overall effects: (A) One-way analysis of variance (ANOVA): $F_{3,107}$ = 11.59, $N$ = 107, $P$ < 0.001; (B) one-way ANOVA: $F_{2,48}$= 7.68, $N$ = 48, $P$ = 0.001. Error bars represent SEM, whereas the characters on top of the bars denote significant differences based on Tukey's honest significant difference.

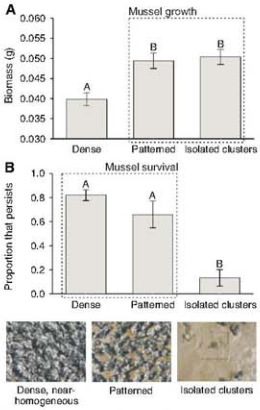


**Fig. 4.** Differences in **(A)** individual growth in terms of established size (Kruskal-Wallis rank sum test: $\chi^2$ = 23.60, $N$ = 800, $P$ < 0.001) and **(B)** persistence of mussels between dense, near-homogenous beds, patterned beds of intermediate-density, and low-density beds consisting of isolated clumps (one-way ANOVA: $F_{2,30}$ = 20.05, $N$ = 30, $P$ < 0.001). Error bars represent SEM, whereas the characters on top of the bars denote significant differences between the treatments based on pairwise Mann-Witney $U$ test for (A) and Tukey's honest significant difference post-hoc analysis of variance for (B).

threads to prevent predation or dislodgement, providing a positive feedback to the development of such small aggregates. When further aggregation leads to the formation of large-scale clusters, movement increases again, creating a negative feedback to further aggregation. This last mechanism is potentially related to competition because of the depletion of suspended algal food within the aggregates (*24*). Together, these mechanisms obey the general principle of scale-dependent activation-inhibition, which has been proposed to explain pattern formation in morphogenesis (*25*, *26*). We further investigated this hypothesis by determining the average movement speed of mussels in artificial clusters of 2, 8, 32, and 128 mussels. Our experiment revealed that mussel movement speed decreased with cluster size from 2 up to 32 mussels, but it increased again from 32 to 128 mussels per cluster (Fig. 3A), in agreement with the general principle of scale-dependent activation-inhibition. When suspended algal food was supplied to the center of large clusters of 128 individuals, movement dropped significantly, suggesting that algal depletion inhibits the formation of large clusters (Fig. 3B). This implies that mussels respond to both the local density of conspecifics within range of their foot (e.g., touch) and to the local availability of algal food. No evidence was found that other chemical signals influenced mussel movement in our experiments (*19*).

We performed a field study to investigate the emergent effects of self-organized pattern formation on the growth and survival of mussels under field conditions at the intertidal flats in the Menai Strait. At one location, fishermen seeded part of the intertidal flats with mussels of ~2 cm in size, 3 weeks before our field study. We observed strong variation in mussel density on the tidal flat, probably resulting from variation in seeding intensity. Mussel biomass on a square-meter basis was 20 to 30 kg fresh weight per square meter for dense homogeneous beds, 5- to 20-kg/m$^2$ for patterned beds, or <5 kg/m$^2$ for beds with isolated clumps. Our experiments revealed that mussels that occurred in isolated clumps had grown significantly more over these 3 weeks than those that occurred in dense, near-homogeneous beds (Fig. 4A), probably because of reduced competition. Mussel growth in patterned beds was significantly higher than in dense, near-homogeneous beds, but not significantly different from isolated mussels.

To investigate the effects of spatial patterns on persistence of mussels within the beds, we released 10 painted mussels in a group on open sediment, in patterned beds, and in dense near-homogeneous beds. After a week, >80% of the mussels were recovered from the dense bed, whereas <20% of the mussels on the open sediment remained (Fig. 4B). The local persistence of mussels released in patterned locations was significantly higher than those released as isolated clumps, but it did not differ significantly from those in dense beds. Experiments with mussel mimics (empty mussel shells filled and glued together with Blu-tac paste) yielded very similar results, indicating that most likely, physical disturbance due to water flow or wave action, rather than predation, is the cause of difference in persistence in dense or patterned mussel beds, as compared with the open areas. Hence, our experiments revealed a marked emergent effect of spatial patterns in mussel beds: It allows for high resilience of mussel beds to wave action and water flow and for high individual growth by reducing the effects of competition, properties that are incompatible in homogeneous beds.

Our results show that simple rules governing individual behavior of mussels explain the formation of spatial patterns at the population level. Spatial patterns were found to result from the interplay of positive and negative interactions between individual mussels at different spatial scales (*18*). Both growth and survival of mussels were found to be high in a patterned bed, a combination that cannot be achieved in a homogeneous bed. Hence, this is an emergent property of the spatial pattern, translating individual behavior to the functioning of mussel beds at the level of the population and ecosystem. This result has implications for our understanding of ecosystems, by showing that self-organized spatial patterns can determine their functioning, confirming the predictions of many conceptual (*27*) and theoretical studies (*3*, *6*, *28*). This is relevant to the conservation of many natural ecosystems, such arid ecosystems where human disturbance of spatial vegetation patchiness increased the loss of water from the landscape, leading to decreased productivity (*29*).

### References and Notes

1. C. A. Klausmeier, *Science* **284**, 1826 (1999).
2. P. Couteron, O. Lejeune, *J. Ecol.* **89**, 616 (2001).
3. M. Rietkerk *et al.*, *Am. Nat.* **160**, 524 (2002).
4. M. Rietkerk, S. C. Dekker, M. J. Wassen, A. W. M. Verkroost, M. F. P. Bierkens, *Am. Nat.* **163**, 699 (2004).
5. J. van de Koppel, C. M. Crain, *Am. Nat.* **168**, E136 (2006).
6. J. van de Koppel, M. Rietkerk, N. Dankers, P. M. J. Herman, *Am. Nat.* **165**, E66 (2005).

7. J. T. Wootton, *Nature* **413**, 841 (2001).
8. F. Guichard, P. M. Halpin, G. W. Allison, J. Lubchenco, B. A. Menge, *Am. Nat.* **161**, 889 (2003).
9. M. Rietkerk, J. Van de Koppel, *Trends Ecol. Evol.* **23**, 169 (2008).
10. O. N. Bjørnstad, M. Peltonen, A. M. Liebhold, W. Baltensweiler, *Science* **298**, 1020 (2002).
11. J. L. Maron, S. Harrison, *Science* **278**, 1619 (1997).
12. V. Castets, E. Dulos, J. Boissonade, P. De Kepper, *Phys. Rev. Lett.* **64**, 2953 (1990).
13. G. Nicolis, I. Prigogine, *Self-Organization in Nonequilibrium Systems* (Wiley, New York, 1977).
14. G. Theraulaz *et al.*, *Proc. Natl. Acad. Sci. U.S.A.* **99**, 9645 (2002).
15. H. Wager, *Philos. Trans. R. Soc. London Ser. B* **201**, 333 (1911).
16. J. J. Tyson, J. D. Murray, *Development* **106**, 421 (1989).
17. See the supporting online material for a literature review of experimental tests of self-organization and its mechanisms.
18. M. D. Bertness, S. D. Gaines, S. M. Yeh, *Ecology* **79**, 1382 (1998).
19. Materials and methods are available as supporting material on *Science* Online.
20. M. D. Bertness, E. Grosholz, *Oecologia* **67**, 192 (1985).
21. J. C. Gascoigne, H. A. Beadman, C. Saurel, M. J. Kaiser, *Oecologia* **145**, 371 (2005).
22. D. L. DeAngelis, W. M. Mooij, *Annu. Rev. Ecol. Evol. Syst.* **36**, 147 (2005).
23. V. Grimm *et al.*, *Science* **310**, 987 (2005).
24. P. R. Jonsson, J. K. Petersen, Ö. Karlsson, L.-O. Loo, S. Nilsson, *Limnol. Oceanogr.* **50**, 1989 (2005).
25. A. Gierer, H. Meinhardt, *Kybernetics* **12**, 30 (1972).
26. A. M. Turing, *Philos. Trans. R. Soc. London Ser. B Biol. Sci.* **237**, 37 (1952).
27. S. A. Levin, *Fragile Dominion: Complexity and the Commons* (Helix Books, Cambridge, MA, 1999).
28. R. V. Solé, J. Bascompte, *Self-Organization in Complex Ecosystems* (Princeton Univ. Press, Princeton, NJ, 2006).
29. J. A. Ludwig, B. P. Wilcox, D. D. Breshears, D. J. Tongway, A. C. Imeson, *Ecology* **86**, 288 (2005).


30. We thank A. Koutstaal, B. Koutstaal, A. Matkin, and J. van Soelen for their assistance during the field work and lab experiments; K. Mould and J. Wilson for access to their mussel lots; and A. Altieri, M. Bertness, T. Bouma, F. Guichard, M. de Jager, A.-M. Neutel, P. de Ruiter, and B. Silliman for critical discussions and reading of the manuscript. The field work at Bangor was supported by a grant from the Schure-Beijerinck-Popping fund of the Royal Dutch Academy of Sciences to J.v.d.K. The research of M.R. is supported by a personal Vidi grant from the Netherlands Organization of Scientific Research/Earth and Life Sciences (NWO-ALW). J.C.G. was supported by Biotechnology and Biological Sciences Research Council contract D18866. This is publication 4410 of the Netherlands Institute of Ecology (NIOO-KNAW).


**Supporting Online Material**

www.sciencemag.org/cgi/content/full/322/5902/739/DC1
Materials and Methods
SOM Text
Figs. S1 to S4
References
Movies S1 and S2

29 July 2008; accepted 26 September 2008
10.1126/science.1163952

# Natal Homing and Connectivity in Atlantic Bluefin Tuna Populations

**Jay R. Rooker,[1]*† David H. Secor,[2]* Gregorio De Metrio,[3] Ryan Schloesser,[1] Barbara A. Block,[4] John D. Neilson[5]**

**Atlantic bluefin tuna populations are in steep decline, and an improved understanding of connectivity between individuals from eastern (Mediterranean Sea) and western (Gulf of Mexico) spawning areas is needed to manage remaining fisheries. Chemical signatures in the otoliths of yearlings from regional nurseries were distinct and served as natural tags to assess natal homing and mixing. Adults showed high rates of natal homing to both eastern and western spawning areas. Trans-Atlantic movement (east to west) was significant and size-dependent, with individuals of Mediterranean origin mixing with the western population in the U.S. Atlantic. The largest (oldest) bluefin tuna collected near the northern extent of their range in North American waters were almost exclusively of western origin, indicating that this region represents critical habitat for the western population.**

Harvest strategies for marine fishes depend on fundamental assumptions about their complex life cycles, and management is often based on the "unit stock concept," which relies on the phenomenon of natal homing (return to spawning area) and limited or structured connectivity between populations (*1*). For Atlantic bluefin tuna, these assumptions are important because spawning populations in the western Atlantic are at 10% of the biomass prevailing when industrial fishing began, and recovery is confounded by trans-Atlantic movement across international jurisdictions (*2*). In assessments and management activities, the International Commission for the Conservation of Atlantic Tunas (ICCAT) has assumed that Atlantic bluefin tuna occur as two discrete populations that originate either in the Mediterranean Sea or the Gulf of Mexico; members of either population can undertake trans-Atlantic migrations, but adults will return to natal spawning regions; and trans-Atlantic migrations are relatively small in number, justifying the use of two broad management regions east and west of 45°W longitude. Despite four decades of regulation by ICCAT, bluefin tuna populations remain severely depressed, causing many to question the effectiveness of the current management regime (*3*, *4*). Although recent electronic tagging data demonstrated evidence for spawning site fidelity (i.e., return of adults repeatedly to the same spawning region) (*5*), the degree of natal homing in the populations and rate of exchange between eastern and western populations is unresolved. Without data on population structure and movement, there is no biological rationale for spatially explicit management, and thus rebuilding plans may be predisposed to fail.

Several approaches have been used to examine the population structure of Atlantic bluefin tuna (*2*), of which chemical traces in otoliths (ear stones) have considerable potential for quantifying natal homing and connectivity because otolith material deposited during the first year of life serves as a natural tag of the individual's place of

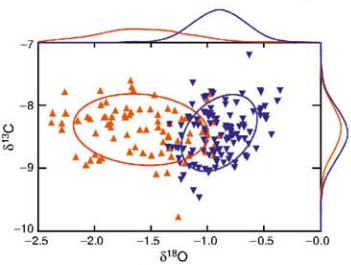


**Fig. 1.** Otolith $\delta^{13}C$ and $\delta^{18}O$ values for yearling Atlantic bluefin tuna collected from 1999 to 2004 in the eastern Atlantic Ocean/Mediterranean Sea (blue triangles) and western Atlantic Ocean (red triangles). Gaussian bivariate ellipses (one standard deviation of the mean) and normal distribution curves are shown. Yearlings ranged in age from 12 to 18 months. Two regions of the eastern Atlantic Ocean/Mediterranean Sea were sampled over the 6 years: the eastern Atlantic Ocean (Cantabrian Sea; 2000, 2001, and 2002) and the western/central Mediterranean Sea (Ligurian Sea to Adriatic Sea; 1999, 2000, 2002, 2003, and 2004) ($n = 113$). In the continental shelf waters of the U.S. Atlantic Ocean, yearlings were collected from Maryland to Massachusetts over a 6-year period ($n = 81$) [see S8 in (*8*)].

[1]Department of Marine Biology, Texas A&M University, 5007 Avenue U, Galveston, TX 77551, USA. [2]Chesapeake Biological Laboratory, University of Maryland Center for Environmental Science, Post Office Box 38, Solomons, MD 20688, USA. [3]Department of Animal Health and Well-Being, University of Bari, 70010 Valenzano, Bari, Italy. [4]Stanford University, Hopkins Marine Station, Oceanview Boulevard, Pacific Grove, CA 93950, USA. [5]Department of Fisheries and Oceans, Population Ecology Section, St. Andrews Biological Station, St. Andrews, NB, Canada.

*These authors contributed equally to this work.
†To whom correspondence should be addressed. E-mail: rookerj@tamug.edu

origin or nursery habitat (*6*, *7*). We determined the origin of bluefin tuna by means of carbon and oxygen stable isotope ratios ($\delta^{13}C$ and $\delta^{18}O$) in otoliths [see S1 in (*8*)]. Stable isotopes in otoliths and other biogenic carbonates represent a class of chemical tags for which associations with water mass properties are well understood (*9*). Global records of surface water stable carbon and oxygen isotopes indicate these natural markers vary regionally (*10*), and in otoliths these isotopes often serve as natal tags because they reflect water composition differences in nurseries, although fractionation due to kinetic and metabolic effects, particularly for $\delta^{13}C$, can influence isotopic composition (*11*).

The isotopic composition of otoliths from yearling (12 to 18 months of age) bluefin tuna was measured for individuals collected over 6 years (1999 to 2004) from both eastern (Mediterranean Sea/eastern Atlantic Ocean) and western (Gulf of Mexico/U.S. Atlantic Ocean) nurseries (Fig. 1). Otolith composition was distinct between yearlings from eastern and western nurseries [multivariate analysis of variance (MANOVA), $P < 0.01$; based on pooled years], and otolith $\delta^{18}O$ was significantly higher for yearlings from the eastern nursery in five of the years (all except 2001). Mean (SD) otolith $\delta^{18}O$ values for the eastern and western nurseries were −0.89‰ (0.23) and −1.66‰ (0.37), respectively. No significant differences in otolith $\delta^{13}C$ values were observed between eastern and western bluefin tuna in five of the six years sampled (exception 2002, ANOVA, $P < 0.05$) (Fig. 1). Using quadratic discriminant function analysis (QDFA) parameterized with otolith $\delta^{13}C$ and $\delta^{18}O$ values from all year classes, cross-validated classification success to eastern and western nurseries was high (87%), indicating that stable isotopes were useful markers of natal origin for bluefin tuna [see S2 in (*8*)].

Milled cores of otoliths were used to represent the yearling period of school (<60 kg), medium (60 to 140 kg), and giant (>140 kg) category bluefin tuna [see S3 in (*8*)], and maximum likelihood estimates were generated using a mixed-stock algorithm [see S4 in (*8*)] (*12*) to assign individuals to eastern and western nurseries. Although the temporal stability of the primary marker, $\delta^{18}O$, justified the pooling of years for establishing a baseline, temporal variability in otolith core $\delta^{13}C$ or $\delta^{18}O$ values was investigated because our calibration set of juveniles (baseline) did not match our adults. No differences were detected in otolith core $\delta^{18}O$ values between bluefin tuna with birthdates before or during our baseline period in either region, suggesting that the otolith $\delta^{18}O$ composition remained relatively constant over the years investigated [see S5 in (*8*)]. Changes in $\delta^{13}C$ values in otolith cores were detected, and depletion levels for $\delta^{13}C$ were significant and similar to reductions reported in the oceans due to release of $CO_2$ from the burning of fossil fuels (Suess Effect) (*13*). Otolith core $\delta^{13}C$ values were adjusted to account for such temporal variation, but estimates of origin were comparable to nonadjusted values [see S6 in (*8*)].

Natal homing, defined as the return of spawning adults to their region of origin, was high and remarkably similar for both eastern and western spawning regions: 95.8% for the Mediterranean Sea and 99.3% for the Gulf of Mexico [see S7 in (*8*)]. This work corroborates earlier indications of spawning fidelity from electronic tagging data that showed return migrations of both Mediterranean (*5*) and Gulf of Mexico (*5*, *14*) spawners over multiple years. Additionally, genetic differences have been observed between juveniles collected from the two regions (*15*). Documentation of natal homing in marine vertebrates is rare, and the size of natal areas for bluefin tuna are much larger than in systems where homing is better known (e.g., streams, lakes, and estuaries). Nevertheless, rates of return to eastern and western spawning areas by Atlantic bluefin tuna populations are at the upper end of ranges reported for teleosts, rivaling those of Pacific salmon (*16*). Although we could not document repeat spawning in this particular application, long-term archival tag deployments provide evidence of bluefin tuna returning to the same spawning sites over consecutive years (*2*, *5*).

Estimates of natal origin from otolith chemistry indicate that mixing occurs in North American waters, and our data confirm that U.S.

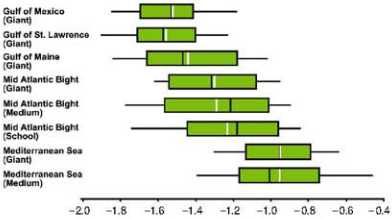


**Fig. 2.** Box plots showing otolith core $\delta^{18}O$ values of school (<60 kg), medium (60 to 140 kg), and giant (>140 kg) category Atlantic bluefin tuna from spawning areas (Mediterranean Sea, Gulf of Mexico), and foraging areas (Gulf of St. Lawrence, Gulf of Maine, Mid Atlantic Bight). Interquartile range (25th and 75th percentile) is shown by extent of boxes, and error bars represent 10th and 90th percentiles. Median (50th percentile) and mean values are shown in boxes as black and white lines, respectively. Collection dates: Mediterranean Sea (2003 to 2007), Gulf of Mexico (2004, 2007), Gulf of St. Lawrence (2006 to 2007), Gulf of Maine (1996, 1998), Mid Atlantic Bight (1997 to 2000).

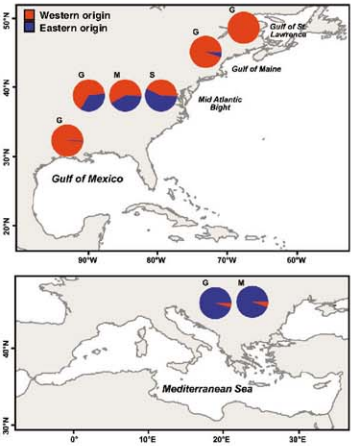


**Fig. 3.** Estimates of natal origin for school (S), medium (M), and giant (G) category Atlantic bluefin tuna from spawning areas (Mediterranean Sea, Gulf of Mexico) and foraging areas (Gulf of St. Lawrence, Gulf of Maine, Mid Atlantic Bight). Contribution rates (percentages) were determined by comparing milled otolith cores (corresponds to yearling period) to a baseline sample from eastern and western nurseries (east + west = 100%). Assignment to either eastern or western nursery was based on maximum likelihood estimations. Standard deviations (SD) were expressed as percentages of estimated proportions. Size classes were approximated based on weight or age (actual or derived from length): giant (>140 kg, ≥ age 10 years), medium (60 to 140 kg, age 5 to 9 years), and school (<60 kg, < age 5 years) category bluefin tuna. Percentage contribution of "western population" and standard deviation (SD) around estimated proportion per region and size category: Gulf of Mexico [giant: 99.3% (SD 1.7%), $n$ = 42]; Mediterranean Sea [giant: 4.2% (SD 3.1%), $n$ = 94; medium: 4.2% (SD 4.4%), $n$ = 38]; Gulf of St. Lawrence [giant: 100% (SD 0.0%), $n$ = 38]; Gulf of Maine [giant: 94.8% (SD 5.3%), $n$ = 72]; Mid Atlantic Bight [giant: 64.9% (SD 21.9%), $n$ = 12; medium: 55.7% (SD 10.4%), $n$ = 56; school: 42.6% (7.2%), $n$ = 86].

commercial and recreational fisheries are composed of both populations of bluefin tuna (Fig. 2). A large fraction of the school (57.4%) and medium (44.3%) category bluefin tuna present in the U.S. waters of the Mid Atlantic Bight were from the eastern population, and we observed that the occurrence of eastern bluefin tuna in the Mid Atlantic Bight decreased with increasing size (age) (Fig. 3). Our estimates of trans-Atlantic exchange were significantly higher than previous reports from conventional tags (*3*) and demonstrated substantial intermingling of individuals from eastern and western populations in U.S. waters, a finding supported with recent evidence from electronic tags (*5*). In contrast, giant category bluefin tuna collected from northern U.S (Gulf of Maine) and Canadian (Gulf of St. Lawrence) fisheries were almost entirely of western origin (94.8% and 100%, respectively). The mechanism(s) responsible for differences in stock composition of bluefin tuna samples from Mid Atlantic Bight (mixed populations) and Gulf of Maine/Gulf of St. Lawrence (western population) waters appears related to size (age) or reproductive state. The majority of our sample from the Mid Atlantic Bight was composed of adolescent bluefin tuna (<5 years of age), and tagging studies have demonstrated that young bluefin tuna are more likely to display trans-Atlantic movements that are linked to foraging than are adults (*2*). Ontogenetic shifts in dispersive behaviors often occur for marine vertebrates displaying natal homing, with exploratory movements associated with foraging decreasing at the onset of breeding (*17*, *18*). Similarly, our finding of stock homogeneity of giants (>140 kg, >10 years of age) in the Gulf of Maine and Gulf of St. Lawrence, and increasing contributions from the western population with age in the Mid Atlantic Bight, suggests that movement becomes more limited and structured after bluefin tuna become sexually mature.

Significant trans-Atlantic mixing of eastern adolescents on western foraging areas emphasizes the connectivity of Atlantic bluefin tuna populations. Under the current assessment framework that assumes limited mixing, a high degree of exchange evident from chemical signatures in otoliths indicates that past abundances of western Atlantic bluefin tuna may have been overestimated, particularly at younger age classes. In addition, exchange rates reported here show that U.S. fisheries for bluefin tuna appear dependent, to some extent, on recruits from the Mediterranean Sea. Because the eastern population is at least an order of magnitude higher in abundance than the western population (*19*), it is unlikely that west-to-east movement of adolescents from the western population contribute significantly to Mediterranean and other eastern Atlantic fisheries. Of greater concern is that adolescents from the western population show similar eastward dispersive behaviors across the 45°W management boundary. If this occurs at rates observed here for eastern adolescents, the smaller, less productive western population will be disproportionately affected by higher fishing rates in the eastern management zone.

The disparity between the eastern and western population sizes and the continued decline of the western stock suggests that some added level of protection is needed to ensure the sustainability of the smaller western component. Natal homing rates reported here were remarkably high to both regions and clearly show that the contribution of eastern adults to the western spawning area is inconsequential. Thus, spawning adults in the Gulf of Mexico appear to be entirely of western origin, and this region should be given high priority for conservation. High connectivity between foraging areas in the Gulf of Maine/Gulf of St. Lawrence and the Gulf of Mexico was also observed, signifying that this region of the northern Atlantic represents critical refugia for western giants. Due to the condition of the western population, a more conservative rate of exploitation of bluefin tuna, inclusive of eliminating bycatch in the Gulf of Mexico, will be required for the recovery of this population.

### References and Notes


1. D. Cushing, *Population Production and Regulation in the Sea* (Cambridge Univ. Press, Cambridge, 1995).
2. J. R. Rooker *et al.*, *Rev. Fish. Sci.* **15**, 265 (2007).
3. J. M. Fromentin, J. E. Powers, *Fish Fish.* **6**, 281 (2005).
4. A. Fonteneau, *Col. Vol. Sci. Pap. ICCAT* **60**, 1027 (2007).
5. B. A. Block *et al.*, *Nature* **434**, 1121 (2005).
6. G. R. Almany, M. L. Berumen, S. R. Thorrold, S. Planes, G. P. Jones, *Science* **316**, 742 (2007).
7. S. R. Thorrold, C. Latkoczy, P. K. Swart, *Science* **291**, 297 (2001).
8. Materials and methods are available as supporting material on *Science* Online.
9. S. R. Thorrold, S. E. Campana, C. M. Jones, P. K. Swart, *Geochim. Cosmochim. Acta* **61**, 2909 (1997).
10. A. N. LeGrande, G. A. Schmidt, *Geophys. Res. Lett.* **33**, L12604 (2006).
11. J. Ashford, C. Jones, *Geochim. Cosmochim. Acta* **71**, 87 (2007).
12. R. B. Millar, *Can. J. Fish. Aquat. Sci.* **44**, 583 (1987).
13. G. H. Rau, T. Takahashi, D. J. Des Marais, *Nature* **341**, 516 (1989).
14. S. L. H. Teo *et al.*, *Mar. Biol. (Berlin)* **151**, 1 (2007).
15. J. Carlsson, J. R. McDowell, J. E. L. Carlsson, J. E. Graves, *J. Hered.* **98**, 23 (2007).
16. T. P. Quinn, *Fish. Res.* **18**, 29 (1993).
17. J. R. Baker, G. A. Antonelis, C. W. Fowler, A. E. York, *Anim. Behav.* **50**, 237 (1995).
18. F. Maffucci, W. H. C. F. Kooistra, F. Bentivenya, *Biol. Conserv.* **127**, 183 (2006).
19. J. J. Magnuson *et al.*, *An Assessment of Atlantic Bluefin Tuna* (National Academy Press, Washington, DC, 1994).


20. We thank S. Campana, J. Graves, and R. D. Wells for insightful comments on earlier versions of the manuscript. Special thanks to A. Belmonte, A. Boustany, B. Campbell, A. Corriero, M. DeFlorio, D. Dettman, J. Kaufman, M. Lutcavage, E. Rodriguez-Marin, P. Mace, E. Prince, N. Santamaria, G. Skomal, M. Stokesbury, S. Teo, P. Thompson, S. Turner, V. Tičina, R. Wingate, NOAA Observer Program, T.F.M. Tuna Farms of the Mediterraneo S.L., Tuna Graso, S.A., and Fish and Fish Ltd. for their assistance. Funding for this study was provided by NOAA (Southeast Fisheries Science Center and Saltonstall-Kennedy Program), the International Fisheries Governance Program of Fisheries and Oceans Canada, Monterey Bay Aquarium, Tag-A-Giant Foundation, and the Large Pelagic Research Center (University of New Hampshire).


### Supporting Online Material

www.sciencemag.org/cgi/content/full/1161473/DC1
Materials and Methods
Fig. S1
References
SOM Data


6 June 2008; accepted 17 September 2008
Published online 2 October 2008;
10.1126/science.1161473
Include this information when citing this paper.


# Glia Are Essential for Sensory Organ Function in *C. elegans*


**Taulant Bacaj,* Maya Tevlin,* Yun Lu, Shai Shaham†**



**Sensory organs are composed of neurons, which convert environmental stimuli to electrical signals, and glia-like cells, whose functions are not well understood. To decipher glial roles in sensory organs, we ablated the sheath glial cell of the major sensory organ of *Caenorhabditis elegans*. We found that glia-ablated animals exhibit profound sensory deficits and that glia provide activities that affect neuronal morphology, behavior generation, and neuronal uptake of lipophilic dyes. To understand the molecular bases of these activities, we identified 298 genes whose messenger RNAs are glia-enriched. One gene, *fig-1*, encodes a labile protein with conserved thrombospondin TSP1 domains. FIG-1 protein functions extracellularly, is essential for neuronal dye uptake, and also affects behavior. Our results suggest that glia are required for multiple aspects of sensory organ function.**


Glia, the largest cell population in vertebrate nervous systems, are implicated in processes governing nervous system development and function (*1*). However, the functions of few glial proteins are characterized. Astrocytic glia are often positioned near synapses and can respond to and participate in synaptic activity (*2*, *3*), influencing the response of postsynaptic cells to presynaptic stimulation (*4*).

Sensory neurons convert environmental stimuli into neuronal activity, and their receptive endings are often associated with glia, such as retinal pig-


Laboratory of Developmental Genetics, The Rockefeller University, 1230 York Avenue, New York, NY 10065, USA.

*These authors contributed equally.
†To whom correspondence should be addressed. E-mail: shaham@rockefeller.edu

mented epithelial cells and Müller glia or olfactory ensheathing cells. Because sensory neurons are postsynaptic to the environment, their associated glia may affect sensory activity in ways analogous to synaptic astrocytes.

Sensory organs are conserved structures, exhibiting morphological, functional, and molecular similarities among diverged species (*5*). To understand glial contributions to sensory neuron functions, we studied the largest sensory organ of the nematode *Caenorhabditis elegans*, the amphid. This organ mediates responses to chemical, thermal, and tactile stimuli, promoting attractive and repulsive behaviors that are easily assayed. Each of the bilateral amphids comprises 12 neurons extending ciliated dendrites to the anterior tip (*5*). These neurons can be grouped based on association with the single amphid sheath glial cell: The dendritic receptive endings of four neurons are entirely surrounded by this glial cell in a hand-in-glove configuration, whereas remaining cilia are encased in a channel formed by the same glial cell and are exposed, through a pore, to the outside environment (*5*, *6*) (fig. S1).

We ablated sheath glia in first-stage larvae, after the amphid had formed, by either using a laser microbeam (*7*) or expressing the diphtheria toxin A gene from a sheath-glia–specific promoter (*8*). Ablation success was monitored by disappearance of a glia-specific green fluorescent protein (GFP) reporter, and by electron microscopy (EM) reconstruction of amphid sensory endings. We first examined the glia-embedded sensory neurons AWC, AWA, and AWB. Animals with bilateral sheath-glia ablation display severe defects in AWC-mediated chemotaxis toward benzaldehyde or isoamyl alcohol (*9*) (Fig. 1A), behaving comparably to *che-2(e1033)* mutants, which lack functional sensory cilia (*10*). Similarly, ablation also reduced chemotaxis toward AWA-sensed odorants (Fig. 1C). By contrast, AWB function was not affected by sheath glia ablation (Fig. 1E).

To confirm these neuron-selective effects of glia on odortaxis, we expressed the ODR-10 diacetyl receptor, normally found only in AWA (*11*), also in AWB neurons. As previously described (*12*), animals expressing ODR-10 in both neurons are less attracted to diacetyl than wild-type animals, reflecting the opposing behavioral outputs of these neurons (Fig. 1G). However, consistent with a defect in AWA, sheath-glia ablated animals expressing ODR-10 in both neurons are repelled by diacetyl (Fig. 1G). In glia-ablated animals, the extracellular environment of AWA and AWB is identical. The normal AWB response, therefore, suggests that odorant molecules can access and interact with odorant receptors in the absence of glia and that the presence of glia is required for integrating opposing environmental stimuli.

We also examined thermotaxis, a behavior mediated by the AFD sheath-glia embedded neuron. Whereas wild-type animals seek their cultivation temperature on a thermal gradient (*13*, *14*), inactivation of AFD by cell ablation or by the *ttx-1(p767)* mutation results in cryophilic/athermotactic behavior (*14*). Sheath-glia ablation does not seem to eliminate AFD function but results in thermophilic behavior (fig. S2), suppressible by *ttx-1(p767)* (fig. S2D).

The ciliated sensory receptive endings of AWC, AWA, AFD, and to a lesser extent AWB, were defective in sheath-glia ablated animals (Fig. 1). Sheath-glia ablation resulted in complete loss of the AWC wing-like cilium structure (Fig. 1B) ($n > 100$), and expansion of this structure in dauer animals was also blocked (fig. S3) ($n = 2$). Similarly, the highly branched processes of the AWA cilium were largely eliminated in sheath-glia ablated animals (Fig. 1D) ($n = 10$), as were the microvilli-like extensions of the AFD sensory ending (Fig. 1H) ($n = 15$). Ciliary localization of olfactory signaling proteins, including ODR-10 (AWB, Fig. 1F; AWA,

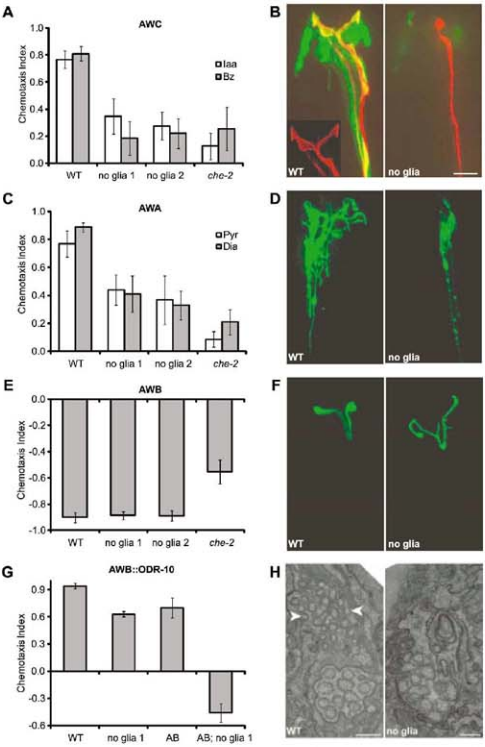


**Fig. 1.** Glia are required for behavior and cilium structure. **(A)** Glia-ablated animals have defective AWC-mediated odortaxis toward 1% isoamyl alcohol (Iaa) and 0.5% benzahldehyde (Bz), $P < 0.001$ (Student's *t* test). **(B)** A wild-type AWC cilium (red, *odr-1*::RFP) ensheathed by an amphid sheath glia (green, *vap-1*::GFP). Glia ablation in the contralateral amphid results in an amorphous cilium. Anterior, up. Scale bar, 5 μm. **(C)** Glia-ablated animals have defective AWA-mediated odortaxis toward 1% methyl pyrazine (Pyr) and 0.1% diacetyl (Dia), $P < 0.001$. **(D)** Glia removal decreases AWA cilium branching (*odr-3*::ODR-3p::GFP). **(E)** Glia are not required for AWB function, 10% 2-nonanone avoidance. **(F)** AWB cilium morphology appears grossly normal, although additional branching and failure of the two cilia to spread is often observed (*str-1*::ODR-10::GFP). **(G)** Animals expressing ODR-10 in AWA and AWB (AB) are attracted to diacetyl. However, dual-sensing animals lacking glia are repelled. **(H)** EM showing absence of AFD microvilli-like projections (arrowheads) in glia-ablated animals. Scale bar, 0.5 μm. WT, wild type; no glia, diphtheria-toxin-ablated glia; *che-2*, *che-2(e1033)* mutants; error bars, SD of 12 or more assays.

AWC, fig. S4), the G-alpha protein ODR-3 (AWA, Fig. 1D), and the cyclic-nucleotide-gated channel subunit TAX-4 (AWC, fig. S4), was unaltered.

We next examined behaviors mediated by amphid channel neurons. Sheath-glia ablation completely blocked chemotaxis toward NaCl (Fig. 2A), a behavior mediated by the ASE neurons (*15*). Avoidance of a high osmolarity barrier, mediated by ASH (*16*), was also entirely abrogated (Fig. 2B), as was long-range avoidance of 1-octanol (Fig. 2C), a behavior mediated in part by ADL (*12*). Surprisingly, sensory ending morphology, length, and microtubule organization of all channel neurons appeared normal in ablated animals (Fig. 2, D and E, and fig. S1). Furthermore, ciliary localization of intraflagellar transport components (CHE-11, DYF-11), or of ODR-10, expressed in ASH, was not disrupted by sheath-glia ablation (fig. S4).

We used G-CaMP to examine $Ca^{2+}$ level changes in ASH in response to high osmolarity. Whereas wild-type animals increase intracellular $Ca^{2+}$ after exposure to and removal of an osmotic stimulus (Fig. 3A and fig. S5) (*17*), sheath-glia ablated animals lacked these responses (Fig. 3B and fig. S5). To determine whether signaling downstream of $Ca^{2+}$ elevation was disrupted, we expressed the light-activated channel channelrhodopsin-2 (ChR2) (*18*) within ASH. In the presence of retinal, a ChR2 cofactor, glia-ablated (and wild-type) animals initiate backward locomotion (Fig. 3C), demonstrating that downstream signaling is intact and that glia are not required for ASH health/viability.

When *C. elegans* are soaked in lipophilic dyes (e.g., DiI), some channel neurons, and AWB, take up and concentrate the dye. DiI uptake was eliminated in all amphid neurons in glia-ablated animals (Fig. 2F). Thus, dye filling (defective in channel neurons and AWB), ciliary morphology (defective mainly in AWA, AWC, and AFD), and behavior generation (not defective in AWB) are independent properties of amphid sensory neurons, each requiring the presence of sheath glia.

To uncover glial factors controlling these neuronal properties, we compiled a list of amphid sheath-glia–enriched transcripts. mRNA from cultured GFP-expressing amphid-sheath glia was compared to mRNA from other cultured embryonic cells by hybridizing each population to an oligonucleotide gene array. We identified 298 unique transcripts with greater than fourfold enrichment (table S1), including the known glial genes *daf-6* and *vap-1* (*19*). Of 298 transcripts, 159 are predicted to encode transmembrane or secreted proteins that could potentially interact with amphid sensory neurons. These secreted proteins include $Ca^{2+}$ binding proteins and a KCl cotransporter, which may explain glial contributions to $Ca^{2+}$ elevation in ASH.

To validate our results, we generated GFP reporter fusion constructs to promoters of seven genes. Five were expressed exclusively in amphid sheath glia and phasmid sheath glia (an amphid-like tail sensory organ) (Fig. 4, A and B, and fig. S6).

We screened enriched genes by RNA interference (RNAi) for defects in amphid neuron dye filling (Dyf phenotype) and identified the gene F53B7.5, which we renamed *fig-1* (Dyf, expressed in glia). RNAi against *fig-1* resulted in dye-filling defects in amphids and phasmids (Fig.

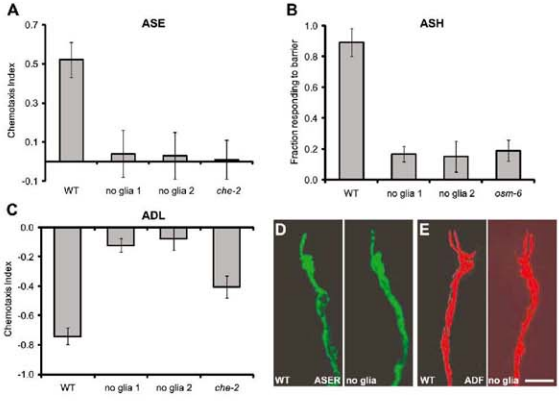


**Fig. 2.** Glia affect channel neuron function but not morphology. **(A)** Glia-ablated animals fail to detect 0.2 M NaCl ($P < 0.001$), an ASE-mediated behavior. **(B)** Glia-ablated animals fail to avoid a 4 M fructose ring ($P < 0.001$), an ASH-mediated behavior. *osm-6*, *osm-6(p811)* mutants. **(C)** Glia-ablated animals fail to avoid 1-octanol in a long-range assay ($P < 0.001$), a behavior partially mediated by ADL. **(D** and **E)** The morphology of amphid channel neurons is not affected by glia removal. ASER, *gcy-5*::GFP; ADF, T08G3.3::RFP). Scale bar, 5 μm. **(F)** Glia are required for neuronal uptake of DiI (red). Only the right amphid sheath glia is ablated. AWC (green, *odr-1*::YFP) indicates the location of the dendrite bundles. Error bars, SD of 12 or more assays.

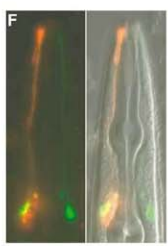


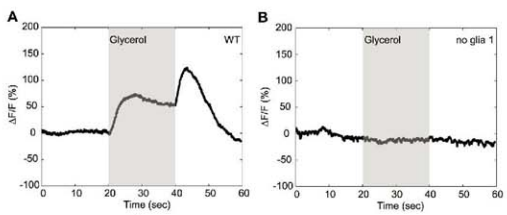


**Fig. 3.** Glia are required for $Ca^{2+}$ responses in ASH. **(A)** As determined by G-CaMP fluorescence, ASH responds to application and removal of 1M glycerol (*17*). Shaded region, stimulus duration. **(B)** ASH fails to respond to glycerol in glia-ablated animals. **(C)** Glia are not required for neuronal function downstream of $Ca^{2+}$ entry. Activation of ASH-expressed ChR2 by light causes animals to move backward; $n = 30$ for each.

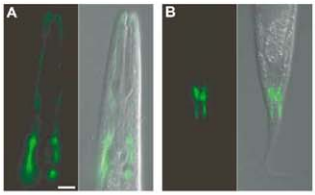


D

| Genotype | Normal Dye Filling (%) Amphid | Phasmid |
|---|---|---|
| WT | 100 | 100 |
| *fig-1* (RNAi) | 60 | 30 |
| *fig-1(tm2079)* | 18 | 0 |
| *fig-1(tm2079)*; C38G2 | 90 | 100 |
| *fig-1(tm2079)*; $P_{fig\text{-}1}$*fig-1* (long) | 50 | 44 |
| *fig-1(tm2079)*; $P_{fig\text{-}1}$*fig-1* (short) | 46 | 42 |
| *fig-1(tm2079)*; $P_{gla}$*fig-1* | 60 | 15 |
| *fig-1(tm2079)*; $P_{rnouron}$ *fig-1* | 80 | 0 |

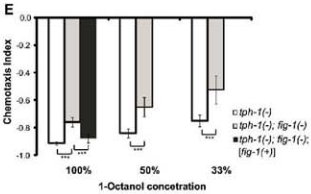


**Fig. 4.** Glial *fig-1* is required for neuronal dye filling and function. (**A** and **B**) *fig-1* is expressed in amphid (**A**) and phasmid (**B**) sheath glia. Anterior, up. Scale bar, 5 μm. (**C**) FIG-1 domain structure. Red, thrombospondin type 1 domain; green, C6 repeats; blue, EGF-like type II domain; bar, 200 amino acids. The predicted protein in the *fig-1(tm2079)* deletion is shown. (**D**) *fig-1* is required for DiI accumulation. One representative line shown for each condition: C38G2, cosmid containing *fig-1*; glial promoter, T02B11.3; neuronal promoter, *sra-6*; $n > 40$ for each. (**E**) *fig-1* is required for 1-octanol avoidance. Assays were performed in the *tph-1(mg280)* background, which suppresses movement defects of *fig-1(tm2079)* animals. *fig-1(tm2079)* mutants perform worse at all three concentrations, and these defects can be rescued by *fig-1(+)*. Asterisks, $P < 0.001$. Error bars, 95% confidence intervals. At least 24 assays for each condition.

4D). An 1117-bp deletion in *fig-1*, *tm2079*, also perturbed dye filling (Fig. 4C), and this defect was rescued by a cosmid spanning the *fig-1* locus. Interestingly, *fig-1(tm2079)* mutants exhibited normal neuronal and amphid sheath glia structure (fig. S1I), demonstrating that access to dye is not sufficient for dye filling and that glia-dependent neuronal properties are required for dye filling.

*fig-1*(RNAi) defects could be induced at all developmental stages and were observed within 24 hours of double-stranded RNA exposure (table S2), suggesting that although *fig-1* mRNA is highly expressed (table S1), FIG-1 protein must be labile, consistent with a nonstructural role.

Expression of a *fig-1* promoter::GFP reporter was detected exclusively within amphid and phasmid sheath glia (Fig. 4, A and B) and was first evident in late embryos, continuing throughout adulthood. Thus, FIG-1 expression may be required continuously for neuronal dye filling.

*fig-1* is predicted to generate two alternatively spliced mRNAs encoding proteins of 3095 (long) and 2892 (short) amino acids, the short isoform being sufficient for rescue (Fig. 4D). Both proteins contain an N-terminal signal sequence, a TSP1 thrombospondin domain, 18 C6 domains, and a second TSP1 domain (Fig. 4C). The larger protein is also predicted to contain an EGF-like type II motif at its C terminus (*8*). TSP1 and EGF-like motifs are characteristic domains found in astrocyte-secreted thrombospondin proteins implicated in synapse development (*20*).

To determine whether FIG-1 protein can act cell nonautonomously, we expressed a *fig-1*(short) cDNA transgene under either sheath glia (T02B11.3) or sensory neuron (*sra-6*; ASH, and weakly in ASI, PHA, and PHB) promoters. Both transgenes rescued *fig-1(tm2079)* mutants (Fig. 4D), as expected if FIG-1 acted extracellularly.

Finally, although *fig-1(tm2079)* mutants exhibited normal behavior toward most stimuli tested (fig. S7), we identified a modest but significant defect in 1-octanol avoidance (Fig. 4E), suggesting that *fig-1* also contributes to behavior generation.

We have demonstrated that *C. elegans* amphid sheath glia provide associated neurons with at least three separate activities and have identified a molecular mediator contributing to two of these functions. Recent studies suggest that *C. elegans* glia share developmental similarities with vertebrate glia (*21*). At least some of the glial functions we describe might, therefore, be conserved in other sensory systems.

Astrocyte-secreted thrombospondins play important postsynaptic roles in synapse assembly and function (*20*). Our studies of FIG-1, which contains domains also present in thrombospondins, demonstrate that this glial factor plays a key role in modulating sensory neuron properties. The rapid turnover of FIG-1 protein is intriguing, suggesting possible dynamic roles. Could FIG-1 and thrombospondins have related molecular functions? Sensory receptive endings share some similarities with postsynaptic neuronal endings. Both respond to diffusible cues by activating G protein–coupled receptors (*11*) or ligand-gated ion channels (*22*); postsynaptic dendritic spines are highly malleable in shape and size (*23*, *24*), as are sensory neuron receptive endings (*25*); and many vertebrate excitatory synapses are ensheathed by glia, as are sensory neuron receptive endings. These observations, together with the domain structure of FIG-1, suggest the highly speculative notion that analogies between the "sensory synapse" and true synapses might, in part, reflect molecular homologies. Our results provide strong evidence for essential glial contributions to sensory organ function.

### References and Notes


1. P. G. Haydon, *Nat. Rev. Neurosci.* **2**, 185 (2001).
2. G. Perea, A. Araque, *Science* **317**, 1083 (2007).
3. G. Perea, A. Araque, *J. Neurosci.* **25**, 2192 (2005).
4. R. Robitaille, *Neuron* **21**, 847 (1998).
5. S. Ward, N. Thomson, J. G. White, S. Brenner, *J. Comp. Neurol.* **160**, 313 (1975).
6. L. A. Perkins, E. M. Hedgecock, J. N. Thomson, J. G. Culotti, *Dev. Biol.* **117**, 456 (1986).
7. C. I. Bargmann, L. Avery, *Methods Cell Biol.* **48**, 225 (1995).
8. Materials and methods are available as supporting material on *Science* Online.
9. C. I. Bargmann, E. Hartwieg, H. R. Horvitz, *Cell* **74**, 515 (1993).
10. M. Fujiwara, T. Ishihara, I. Katsura, *Development* **126**, 4839 (1999).
11. P. Sengupta, J. H. Chou, C. I. Bargmann, *Cell* **84**, 899 (1996).
12. E. R. Troemel, B. E. Kimmel, C. I. Bargmann, *Cell* **91**, 161 (1997).
13. E. M. Hedgecock, R. L. Russell, *Proc. Natl. Acad. Sci. U.S.A.* **72**, 4061 (1975).
14. I. Mori, Y. Ohshima, *Nature* **376**, 344 (1995).
15. C. I. Bargmann, H. R. Horvitz, *Neuron* **7**, 729 (1991).
16. C. I. Bargmann, J. H. Thomas, H. R. Horvitz, *Cold Spring Harb. Symp. Quant. Biol.* **55**, 529 (1990).
17. M. A. Hilliard *et al.*, *EMBO J.* **24**, 63 (2005).
18. G. Nagel *et al.*, *Proc. Natl. Acad. Sci. U.S.A.* **100**, 13940 (2003).
19. E. A. Perens, S. Shaham, *Dev. Cell* **8**, 893 (2005).
20. K. S. Christopherson *et al.*, *Cell* **120**, 421 (2005).
21. S. Yoshimura, J. I. Murray, Y. Lu, R. H. Waterston, S. Shaham, *Development* **135**, 2263 (2008).
22. K. Sato, M. Pellegrino, T. Nakagawa, L. B. Vosshall, K. Touhara, *Nature* **452**, 1002 (2008).
23. J. T. Trachtenberg *et al.*, *Nature* **420**, 788 (2002).
24. K. K. Murai, L. N. Nguyen, F. Irie, Y. Yamaguchi, E. B. Pasquale, *Nat. Neurosci.* **6**, 153 (2003).
25. S. Mukhopadhyay, Y. Lu, S. Shaham, P. Sengupta, *Dev. Cell* **14**, 762 (2008).


26. We thank C. Bargmann and S. Chalasani for their generous help with G-CaMP imaging, N. Pokala for the ASH-ChR2 strain and advice on assays, H. Fares for a DT-A plasmid, S. Mazel for help with fluorescence-activated cell sorting, S. Mitani for the *tm2079* allele, A. North for help with microscopy, E. Nudleman for the thermotaxis apparatus, Shaham laboratory members for comments on the project and manuscript, and C. Bargmann, P. Sengupta, O. Hobert, and E. Jorgensen for strains. S.S. is a Klingenstein Fellow in the Neurosciences.


### Supporting Online Material

www.sciencemag.org/cgi/content/full/322/5902/744/DC1
Materials and Methods
Figs S1 to S7
Table S1 and S2
References

10 July 2008; accepted 18 September 2008
10.1126/science.1163074

# HARP Is an ATP-Driven Annealing Helicase

Timur Yusufzai and James T. Kadonaga*

DNA-dependent adenosine triphosphatases (ATPases) participate in a broad range of biological processes including transcription, DNA repair, and chromatin dynamics. Mutations in the HepA-related protein (HARP) ATPase are responsible for Schimke immuno-osseous dysplasia (SIOD), but the function of the protein is unknown. We found that HARP is an ATP-dependent annealing helicase that rewinds single-stranded DNA bubbles that are stably bound by replication protein A. Other related ATPases, including the DNA translocase Rad54, did not exhibit annealing helicase activity. Analysis of mutant HARP proteins suggests that SIOD is caused by a deficiency in annealing helicase activity. Moreover, the pleiotropy of HARP mutations is consistent with the function of HARP as an annealing helicase that acts throughout the genome to oppose the action of DNA-unwinding activities in the nucleus.

HARP (HepA-related protein; also known as SMARCAL1 and DNA-dependent ATPase A) is a member of the SNF2 family of adenosine triphosphate (ATP)–driven molecular motor proteins (*1*–*4*). The biological importance of HARP was revealed by the discovery that mutations in HARP are responsible for a pleiotropic disorder known as Schimke immuno-osseous dysplasia (SIOD) (*5*). However, the molecular function of the HARP ATPase activity is unknown.

We investigated how human HARP functions as an ATP-dependent molecular motor by synthesizing and purifying human HARP protein (fig. S1). In a gel mobility shift assay, HARP bound with higher affinity to fork DNA than to single-stranded DNA (ssDNA) or to double-stranded DNA (dsDNA) (Fig. 1A). In addition, the ATPase activity of HARP was stimulated to a much greater extent by fork DNA than by ssDNA or dsDNA (Fig. 1B) (*6*). These results are consistent with the finding that the HARP ATPase is activated by M13 ssDNA (*4*), which probably contains hairpin structures, as well as the observation that the HARP ATPase domain is stimulated by DNA structures that contain both ssDNA and dsDNA (*7*, *8*).

The stimulation of the HARP ATPase activity upon binding to fork DNA suggested that HARP may be an ATP-driven helicase that unwinds DNA. Helicases generate ssDNA regions that can be bound by ssDNA-binding proteins, such as replication protein A (RPA) in eukaryotes [e.g., (*9*)]. However, when we tested the ability of HARP to function as a helicase with several different assays and substrates, we did not observe any detectable helicase activity (e.g., fig. S2). Thus, HARP does not appear to be a helicase.

We therefore considered the possibility that HARP is an ATP-driven annealing helicase that anneals complementary RPA-bound ssDNA. To test this hypothesis, we devised an assay for annealing helicase activity (fig. S3). We generated a stable, partially unwound DNA substrate by adding RPA to plasmid DNA in the presence of topoisomerase I (*10*, *11*). Under these conditions, RPA binds to small transient bubbles and then wedges the DNA strands apart to form stable single-stranded bubbles in which RPA is bound to the unwound DNA (*12*). Upon addition of SDS (to inactivate enzymes such as topoisomerase I) and subsequent deproteinization, the RPA-unwound DNA yielded negatively supercoiled DNA (Fig. 2A, lanes 3 and 4). As a control, plasmid DNA was treated in an identical manner in the absence of RPA; the resulting DNA was relaxed, as expected (Fig. 2A, lanes 1 and 2). In addition, HARP protein did not alter DNA supercoiling in the presence or absence of ATP (Fig. 2A, lanes 5 and 6).

The addition of an annealing helicase to the partially unwound DNA substrate should yield circular DNA that is relaxed by topoisomerase I as a result of the elimination of the stable single-stranded regions within the dsDNA (fig. S3). In this assay, HARP catalyzed the ATP-dependent relaxation of the RPA-unwound DNA (Fig. 2A, compare lanes 7 and 8). This effect could be due to an ATP-dependent annealing helicase activity (fig. S4) or to the ATP-dependent removal of RPA from ssDNA by HARP. To distinguish between these two possibilities, we carried out gel mobility shift analyses with RPA-bound DNA and found that HARP did not catalyze the ATP-dependent displacement of RPA from DNA (Fig. 2B and figs. S5 and S6). These results thus reveal that HARP is an annealing helicase. In addition, we found that RPA did not directly stimulate the ATPase activity of HARP (fig. S7). These findings indicate that the properties of HARP are distinct from those of Mot1, a SNF2 family protein that removes TATA box–binding protein (TBP) from DNA and whose ATPase activity is stimulated by TBP (*13*, *14*).

We also investigated the possibility that the basis for the annealing helicase activity is translocation along dsDNA, which has been observed in some SNF2 family proteins such as Sth1 and Rad54 (*15*–*17*). To test this idea, we compared the properties of Rad54 and HARP. Rad54 is involved in homologous recombination that has been shown to translocate along DNA in both triple-helix strand-displacement assays (*16*) and single-molecule assays (*17*). In triple-helix strand-displacement assays, we found that Rad54 had a higher DNA translocation activity than did HARP (fig. S8). In contrast, Rad54 did not exhibit any detectable annealing helicase activity (Fig. 2C). Thus, the ability of a factor to translocate along dsDNA is not sufficient for the removal of RPA from the unwound DNA. We also tested two other SNF2 family proteins, ACF (which contains the ISWI ATPase) and Brg1, and found that neither protein exhibited annealing helicase activity (fig. S9). These results provide further evidence that the annealing helicase activity of HARP is not a general property of SNF2 ATPases.

To gain insight into the molecular basis of SIOD, we purified two mutant versions of HARP that are associated with the disease (fig. S10). The $Arg^{764} \rightarrow Gln$ (R764Q) mutation causes a severe form of SIOD, and the $Arg^{586} \rightarrow Trp$ (R586W) mutation results in a milder form of SIOD (*5*). Both of these mutations are in the conserved ATPase region of HARP. As seen with wild-type HARP (Fig. 1A), both mutant proteins bound selectively

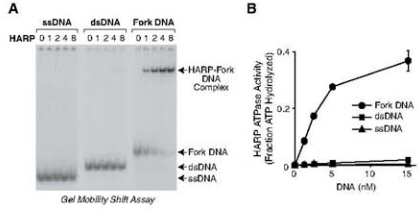


**Fig. 1.** HARP protein binds selectively to fork DNA. **(A)** HARP protein binds with higher affinity to fork DNA than to ssDNA or dsDNA. Gel mobility shift experiments were performed with a 30-nucleotide (nt) ssDNA, a 30–base pair dsDNA, and a 30-nt fork DNA that is identical to the dsDNA except for a 9-nt mismatch at one end. Relative concentrations of HARP are shown at tops of lanes; the actual concentrations of HARP are 0, 0.05, 0.1, 0.2, and 0.4 nM. **(B)** HARP ATPase activity is stimulated to a greater extent by fork DNA than by ssDNA or dsDNA. The DNA substrates used in the ATPase assays are identical to those used in (**A**), except that the DNA samples were not radiolabeled. Error bars represent SD ($N = 3$).

Section of Molecular Biology, University of California, San Diego, 9500 Gilman Drive, La Jolla, CA 92093, USA.

*To whom correspondence should be addressed. E-mail: jkadonaga@ucsd.edu

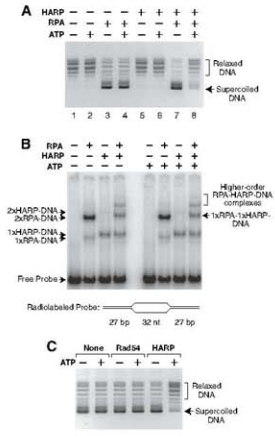


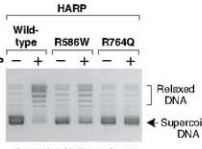


**Fig. 4.** Mutant HARP proteins are defective in annealing helicase activity. The R586W HARP protein has less annealing helicase activity than wild-type HARP, whereas the R764Q HARP protein has no detectable annealing helicase activity. Annealing helicase assays were performed as in Fig. 2. All reactions contained plasmid DNA, RPA, and topoisomerase I. UTP was used as a control for the absence of ATP.

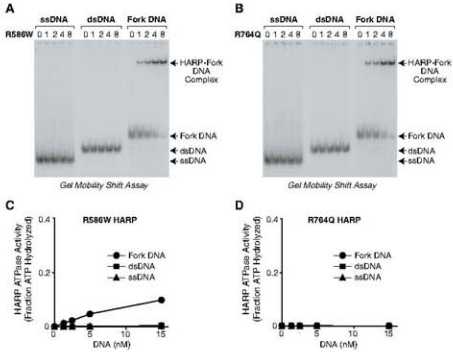


**Fig. 3.** Mutant HARP proteins bind selectively to fork DNA but exhibit less ATPase activity than wild-type HARP. The R764Q mutation results in a stronger SIOD phenotype than the R586W mutation (*5*). (**A** and **B**) The mutant HARP proteins bind with higher affinity to fork DNA than to ssDNA or dsDNA. These gel mobility shift experiments were performed as in Fig. 1A. (**C** and **D**) The R586W HARP protein has low ATPase activity, whereas the R764Q HARP protein has no detectable ATPase activity. ATPase assays were carried out as in Fig. 1B. Error bars represent SD ($N = 3$).

to fork DNA relative to ssDNA or dsDNA (Fig. 3, A and B). In addition, the wild-type and mutant HARP proteins bound with nearly the same affinity to fork DNA (fig. S11). However, in ATPase assays, the R586W HARP protein exhibited partial activity, whereas the R764Q HARP protein had no detectable activity (Fig. 3, C and D).

In the annealing helicase assay, R586W HARP exhibited less activity than wild-type HARP, whereas R764Q HARP had no detectable activity (Fig. 4). These results show that the two SIOD-associated mutations have little or no effect on DNA-binding by HARP; instead, the mutations reduce the ATPase and annealing helicase activities of HARP in a manner that correlates with the severity of the disease with which they occur. In addition, the studies of the mutant HARP proteins reveal that the DNA-binding activity of HARP is not sufficient for annealing helicase activity, because R764Q HARP was fully active for selective binding to fork DNA (Fig. 3B and fig. S11) yet was deficient in annealing helicase activity (Fig. 4).

HARP is an ATP-driven molecular zipper of complementary RPA-bound ssDNA (fig. S4). Whereas many helicases convert dsDNA into RPA-bound unwound DNA, HARP performs the opposite reaction. The annealing helicase activity of HARP is also distinct from fork regression activity [e.g., (*18*–*20*)], which involves the dissociation and annealing of four strands of DNA without any involvement of RPA (fig. S12).

The biological importance of HARP is revealed by its causal role in SIOD. The defects in the ATPase and annealing helicase activities of two SIOD mutant proteins correlate with the severity of disease. It is thus likely that SIOD is caused by a deficiency in annealing helicase activity. Moreover, SIOD patients exhibit a diverse range of symptoms. The pleiotropic nature of HARP mutations is consistent with the ubiquitous expression of HARP in mammalian tissues (*4*, *21*) and with the molecular function of HARP as an annealing helicase that acts throughout the genome to reanneal stably unwound DNA. There are many enzymes, such as helicases and polymerases, that unwind DNA. In addition, ssDNA bubbles could arise spontaneously, such as in A/T-rich sequences. Hence, there is considerable potential for the incomplete reannealing of DNA and formation of stable, RPA-bound DNA bubbles, which could be deleterious to the transcription of genes or may interfere with replication or repair processes. In this manner, HARP would be able to promote the proper functioning of the cell by catalyzing the rewinding of the stably unwound DNA. More generally, HARP would serve as an opposing force to the numerous DNA-unwinding activities in the nucleus.

### References and Notes

1. A. E. Gorbalenya, E. V. Koonin, *Curr. Opin. Struct. Biol.* **3**, 419 (1993).
2. J. A. Eisen, K. S. Sweder, P. C. Hanawalt, *Nucleic Acids Res.* **23**, 2715 (1995).
3. A. Flaus, D. M. Martin, G. J. Barton, T. Owen-Hughes, *Nucleic Acids Res.* **34**, 2887 (2006).
4. M. A. Coleman, J. A. Eisen, H. W. Mohrenweiser, *Genomics* **65**, 274 (2000).

5. C. F. Boerkoel *et al.*, *Nat. Genet.* **30**, 215 (2002).
6. The turnover number ($k_{cat}$) values (mean ± SD; $N = 4$) for HARP ATPase activity with fork DNA and dsDNA are approximately 1200 ± 270 $min^{-1}$ and 81 ± 29 $min^{-1}$, respectively. ATPase activity was not detectable in the absence of DNA or in the presence of ssDNA.
7. R. Muthuswami, P. A. Truman, L. D. Mesner, J. W. Hockensmith, *J. Biol. Chem.* **275**, 7648 (2000).
8. J. W. Hockensmith, A. F. Wahl, S. Kowalski, R. A. Bambara, *Biochemistry* **25**, 7812 (1986).
9. L. Wu, I. D. Hickson, *Annu. Rev. Genet.* **40**, 279 (2006).
10. A. Georgaki, B. Strack, V. Podust, U. Hübscher, *FEBS Lett.* **308**, 240 (1992).
11. K. Treuner, U. Ramsperger, R. Knippers, *J. Mol. Biol.* **259**, 104 (1996).
12. Y. Lao, C. G. Lee, M. S. Wold, *Biochemistry* **38**, 3974 (1999).
13. D. T. Auble, D. Wang, K. W. Post, S. Hahn, *Mol. Cell. Biol.* **17**, 4842 (1997).
14. J. J. Chicca 2nd, D. T. Auble, B. F. Pugh, *Mol. Cell. Biol.* **18**, 1701 (1998).
15. A. Saha, J. Wittmeyer, B. R. Cairns, *Genes Dev.* **16**, 2120 (2002).
16. M. Jaskelioff, S. Van Komen, J. E. Krebs, P. Sung, C. L. Peterson, *J. Biol. Chem.* **278**, 9212 (2003).
17. I. Amitani, R. J. Baskin, S. C. Kowalczykowski, *Mol. Cell* **23**, 143 (2006).
18. P. McGlynn, R. G. Lloyd, *Cell* **101**, 35 (2000).
19. C. Ralf, I. D. Hickson, L. Wu, *J. Biol. Chem.* **281**, 22839 (2006).
20. A. Blastyák *et al.*, *Mol. Cell* **28**, 167 (2007).
21. L. I. Elizondo *et al.*, *Am. J. Med. Genet.* **140A**, 340 (2006).


22. We thank B. Rattner, J.-Y. A. Hsu, T. Juven-Gershon, D. Urwin, and J. Theisen for critical reading of the manuscript; M. Coleman for the gift of HARP cDNAs in the early stages of this study; M. Wold for the human RPA expression vector; B. Cairns for the triple-helix plasmid; R. Kingston for the BRG1 expression vector; and M. Gellert for a helpful discussion on this work prior to publication. Supported by NIH grant GM058272 (J.T.K.) and by NIH National Research Service Award fellowship F32 GM76936 (T.Y.).


**Supporting Online Material**

www.sciencemag.org/cgi/content/full/322/5902/748/DC1
Materials and Methods
Figs. S1 to S13
References


2 June 2008; accepted 25 September 2008
10.1126/science.1161233


# Polycomb Proteins Targeted by a Short Repeat RNA to the Mouse X Chromosome


Jing Zhao,[1,2,3] Bryan K. Sun,[1,2,3] Jennifer A. Erwin,[1,2,3] Ji-Joon Song,[2,3] Jeannie T. Lee[1,2,3]*



To equalize X-chromosome dosages between the sexes, the female mammal inactivates one of her two X chromosomes. X-chromosome inactivation (XCI) is initiated by expression of *Xist*, a 17-kb noncoding RNA (ncRNA) that accumulates on the X in cis. Because interacting factors have not been isolated, the mechanism by which *Xist* induces silencing remains unknown. We discovered a 1.6-kilobase ncRNA (RepA) within *Xist* and identified the Polycomb complex, PRC2, as its direct target. PRC2 is initially recruited to the X by RepA RNA, with Ezh2 serving as the RNA binding subunit. The antisense *Tsix* RNA inhibits this interaction. RepA depletion abolishes full-length *Xist* induction and trimethylation on lysine 27 of histone H3 of the X. Likewise, PRC2 deficiency compromises *Xist* up-regulation. Therefore, RepA, together with PRC2, is required for the initiation and spread of XCI. We conclude that a ncRNA cofactor recruits Polycomb complexes to their target locus.


The mouse X-chromosome inactivation (XCI) center harbors several noncoding genes, including *Xist* (*1*, *2*) and its antisense repressor, *Tsix* (*3*). On the future Xa (active X), *Tsix* blocks *Xist* up-regulation and prevents the recruitment of silencing factors in cis. On the future Xi (inactive X), *Tsix* is down-regulated, which enables *Xist* transactivation and the spread of Xist RNA along the chromosome (*4*). The accumulation of *Xist* transcripts correlates with a cascade of chromatin changes (*5*), but how *Xist* directs these changes is unknown. In principle, the act of transcribing *Xist* could induce structural changes that could alter chromosomewide function (*1*). Alternatively, *Xist* could work as a transcript (*1*, *2*) by recruiting chromatin modifiers or by targeting the X to a specialized compartment (*6*). Although universally attractive, RNA-based models have remained hypothetical, as Xist-interacting proteins have yet to be identified.

To circumvent conventional difficulties with purifying Xist-interacting proteins, we carried out RNA immunoprecipitations (RIPs) and asked if Xist RNA can be found in a specific protein complex. We isolated nuclear RNAs and their binding proteins in the native state to avoid fixation artifacts and tested two cell types: mouse embryonic stem (ES) cells, which exist in the pre-XCI state but recapitulate XCI when induced to differentiate, and mouse embryonic fibroblasts (MEFs), which faithfully maintain Xi. Because trimethylation of histone 3 at $Lys^{27}$ (H3-K27me3) closely follows *Xist* up- and down-regulation (*6*–*9*), we asked if Xist RNA binds the H3-K27 methylase, PRC2—the Polycomb complex that includes Eed, Suz12, RbAp48, and the catalytic subunit, Ezh2 (*10*). Indeed, Ezh2 and Suz12 antibodies coimmunoprecipitated Xist RNA (Fig. 1, A to D). By contrast, Xist sequences were not consistently detected in cells treated with antibodies against H3-K27me3 or antibodies against acetylated H4, or in no-antibody controls. Pretreatment with ribonucleases (RNases) that digest single-stranded RNA (RNase I) and double-stranded RNA (RNase V1) abolished RIP signals, whereas pretreatment with RNase H (which digests RNA in RNA:DNA hybrids), DNase I, or no nucleases had no effect (Fig. 1E). By inference, the RIP products must be single- or double-stranded RNA.

In female cells, RNA could be detected in the complex even in the pre-XCI state (day 0) when there are <10 transcripts per cell (*11*). On day 0, PRC2 bound only Repeat A (R1), a motif required for silencing (*12*, *13*). Quantitative strand-specific RIP showed that both sense and antisense strands were highly enriched in the PRC2 complex (Fig. 1F). Not until cell differentiation and *Xist* up-regulation could PRC2 coimmunoprecipitate more 3′ regions of *Xist*, which suggested that other regions of Xist eventually come in contact with PRC2, though Repeat A remained the epicenter of binding (Fig. 1G). To determine when PRC2 is loaded onto chromatin, we performed DNA chromatin immunoprecipitation (ChIP) assays (Fig. 1H). While bound to RNA in day 0 wild-type cells, PRC2 was not enriched on DNA until differentiation (day 3, day 6) when Eed and/or Ezh2 levels increased ~10-fold. Accordingly, H3-K27me3 levels rose >10-fold. Together, RIP and ChIP showed that, although PRC2 bound Repeat A in pre-XCI cells, H3-K27me3 of chromatin was not evident until differentiation (Fig. 1, B and H). For males, PRC2 coimmunoprecipitated Xist sequences only in ES cells, not in MEFs (Fig. 1C), consistent with the absence of XCI. In $Tsix^{\Delta CpG/+}$ female cells, where XCI choice is predetermined and accelerated (*3*), PRC2 spreading occurred earlier, consistent with preemptive H3-K27me3 (Fig. 1, D and H) (*11*). Thus, PRC2 recruitment by RNA and its activity on chromatin are biochemically separable.

Examination of $Tsix^{\Delta CpG/+}$ cells enabled us to determine when *Xist* transactivation occurred relative to PRC2 recruitment. In this mutant, XCI always occurs on the mutated X, and H3-K27 methylation preempts *Xist* up-regulation, which indicated that H3-K27me3 and *Xist* transactivation are genetically separable (*11*). Indeed, DNA ChIP showed high Eed and Ezh2 enrichment on Repeat A on day 0 with accompanying H3-K27me3 (Fig. 1H). *Xist* expression remained low until differentiation (*11*). Therefore, in wild-type cells, PRC2 is recruited by RNA to *Xist*'s 5′ end on day 0, but PRC2


[1]Howard Hughes Medical Institute, Boston, MA 02115, USA. [2]Department of Molecular Biology, Massachusetts General Hospital, Boston, MA 02493, USA. [3]Department of Genetics, Harvard Medical School, Boston, MA 02115, USA.

*To whom correspondence should be addressed. E-mail: lee@molbio.mgh.harvard.edu

transfers to chromatin and catalyzes H3-K27me3 only after differentiation is triggered. These events occur before *Xist* transactivation.

Note that PRC2 preferentially associates with Repeat A across all time points (Fig. 1G), although PRC2 should theoretically coimmunoprecipitate all regions of an intact Xist molecule during native RIP, regardless of which RNA domain binds PRC2. To undertake higher-resolution analysis, we performed Xist-strand quantitative polymerase chain reaction (PCR) between *Xist* promoters P1 and P2 in ES cells and observed RNA levels at R7 and R8 three to four times as great as at R6 and R9 (Fig. 2, A and B). During differentiation, *Xist* up-regulated >100-fold in females but became barely detectable in males (Fig. 2C).

Quantitative differences at R6 to R9 hinted at a novel promoter activity. Indeed, RNA fluorescence in situ hybridization (FISH) detected a pinpoint signal on day 0 (Fig. 2D). Northern analysis revealed a ~1.6-kb transcript, with no obvious antisense counterparts other than known processed *Tsix* transcripts (Fig. 2E) (*14*). Rapid amplification of cDNA 3′ ends (3′ RACE) de-

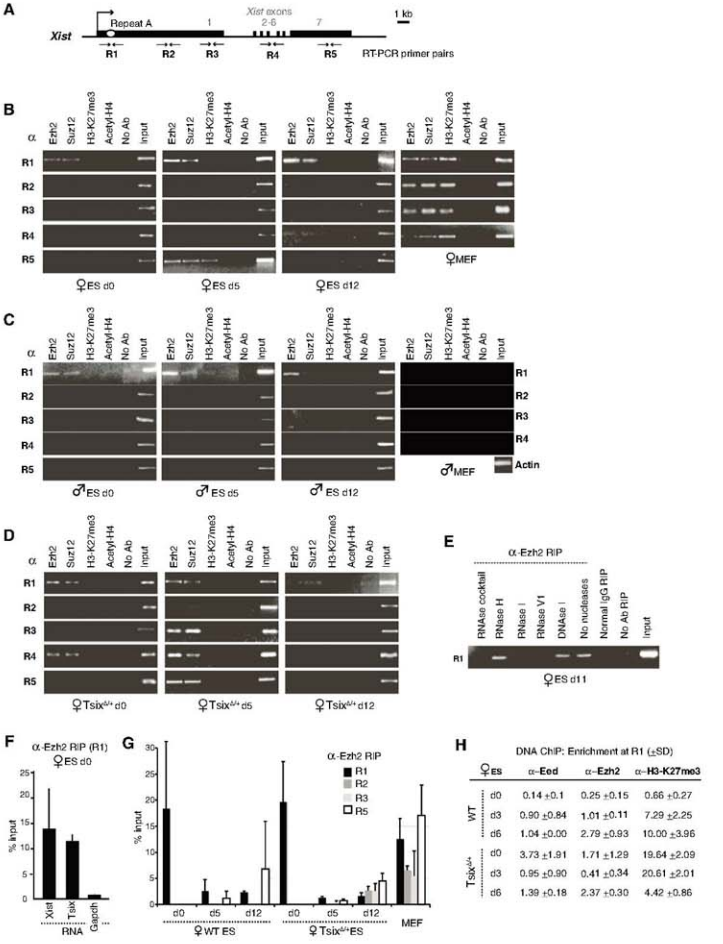


**Fig. 1.** The PRC2 complex contains Xist. **(A)** Map of *Xist*. **(B to D)** RIP in indicated cells. α, antibodies. **(E)** Effects of RNase pretreatment on RIP signals. **(F)** Strand-specific RIP at R1 by real-time PCR, normalized to input RNA. Error bar, 1 SD. **(G)** Quantitative RIP by real-time PCR at positions R1 to R5. **(H)** DNA ChIP using indicated antibodies, shown as a fraction of input and standardized to normal IgG ChIP. Day 0, d0, and so on.

fined its terminus at base pair (bp) 1948 downstream of P1 (Fig. 2F), which implied a transcription start site at ~bp 300. Luciferase reporter assays confirmed promoter activity within bp 79 to 320, appearing equally active in pre- and post-XCI cells, whereas P1 activity increased upon XCI (Fig. 2G). Competitive reverse transcription PCR (RT-PCR) previously revealed ~10 absolute copies of sense RNA in this region in day 0 female ES cells (*11*). The current stoichiometric data implied that three or four copies derive from full-length *Xist* and six or seven from Repeat A (Fig. 2B). Upon differentiation, Xist levels increased ~100-fold (Fig. 2C), whereas Repeat A levels increased 1.8-fold (Fig. 2E). Thus, Repeat A produces a small internal transcript, present in both male and female cells before XCI, but restricted to females after XCI. We designate the transcript "RepA" for Repeat A.

To test whether PRC2 is actually recruited by RepA, we generated doxycycline-inducible *RepA* transgenic female ES cells (Fig. 2H) and asked whether RepA could target PRC2 to ectopic autosomal sites independently of *Xist*. Indeed, for two clones (B5 and C5) of low transgene copy number, doxycycline induction resulted in about a threefold increase in RepA and commensurate increases in PRC2 binding (Fig. 2I). Thus, RepA is sufficient to recruit PRC2 in vivo without Xist, and recruitment depends on RepA transcription and/or RNA.

Does RepA RNA directly bind PRC2? To investigate, we tested whether RepA RNA oligomers could shift PRC2 in vitro in an electrophoretic mobility shift assay (EMSA). RepA comprises 7.5 tandem repeats of a 28-nucleotide (nt) se-

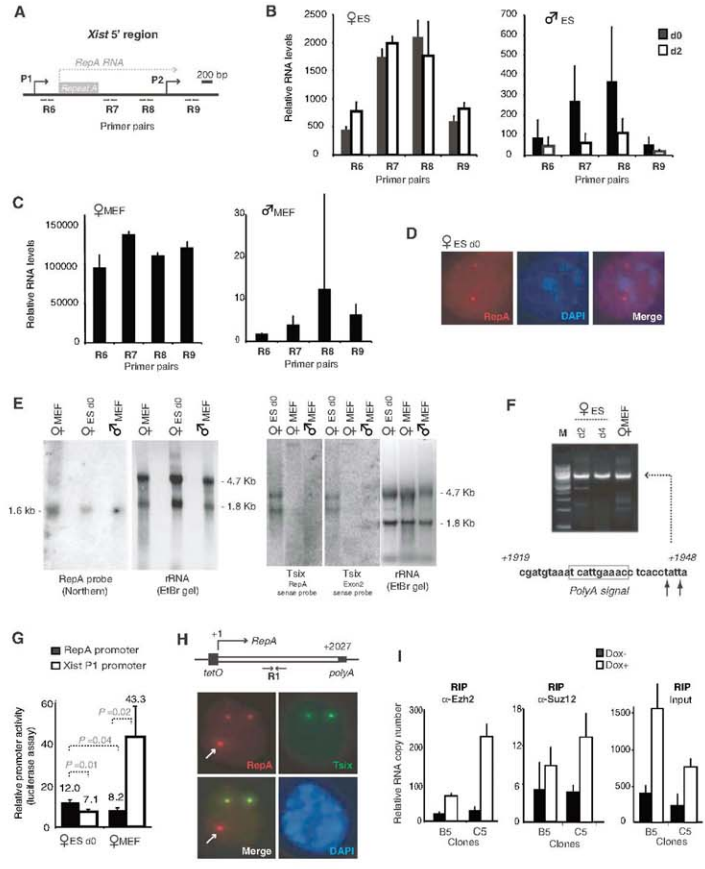


**Fig. 2.** A small RNA within *Xist*. **(A)** Map of *RepA* and the 5′ end of *Xist*. **(B** and **C)**. Strand-specific real-time PCR quantifies RNA copies at R6 to R9 in ES cells (B) or MEFs (C), normalized to standard curve. **(D)** RNA FISH using RepA probe. **(E)** Northern analysis of RepA and Tsix (5′ and 3′ positions). **(F)** 3′ RACE of RepA. **(G)** Transient transfection of luciferase reporter constructs comparing RepA (bp 79 to 320) versus *Xist* P1 promoters, each normalized to vector control. *P*, Student's *t* tests in indicated pairwise comparisons. **(H)** DNA FISH of *RepA* transgenic female ES cells. *Xist* P1 promoter is not in transgenes. Arrows, transgene. *Tsix* detected by pSx7. **(I)** Quantitative RIP in representative clones B5 and C5 ± doxycycline induction. No-antibody controls yielded no detectable RNA.

quence that folds into two conserved stem-loop structures (*13*) (Fig. 3A). A specific RNA-protein complex was observed when ES cell nuclear extract was incubated with wild-type sense probe (Fig. 3, B and C). It is noteworthy that a specific complex was also seen with antisense RNA, which harbors complementary stem-loop structures. In both cases, RNA-protein interactions were disrupted by excess cold wild-type, but not mutant or random, competitors. No shift was observed with a mutant probe lacking the conserved stem-loop structures or with random RNA oligomers (DsI and DsII). Therefore, a specific factor in ES cell nuclei binds RepA and Tsix.

To identify the factor, we asked if antibodies against Ezh2 could supershift the complex and found that preincubation in nuclear extract (day 4 female ES cells or MEFs) produced a supershift, whereas normal immunoglobulin IgG did not (Fig. 3D). Therefore, PRC2 directly binds RepA and Tsix, in agreement with RIP results (Fig. 1F). To confirm, we generated recombinant human PRC2 (hPRC2) containing EED, EZH2, SUZ12, and RBAP48 (*15*) and observed that hPRC2 shifted both sense and antisense RNAs but not mutated or random RNA [(Fig. 3, E and F) additional bands may indicate subcomplexes]. The hEED-hEZH2 subcomplex and the complete hPRC2 complex bound wild-type RNAs equally well. Ezh2 alone could also bind RNA, but hEED alone could not. Thus, Ezh2 must be the RNA-binding subunit of PRC2 (fig. S1). Given that Tsix also binds PRC2 and is a known *Xist* antagonist, Tsix could block XCI by titrating away PRC2. Indeed, RepA and Tsix oligomers competed with each other for PRC2 in vitro (Fig. 3C) and, in

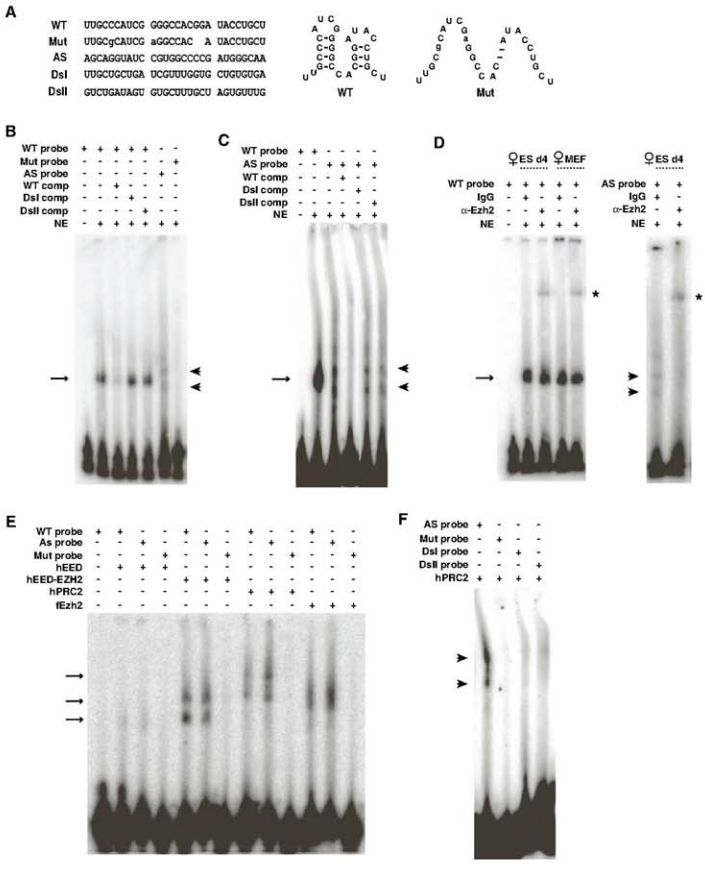


**Fig. 3.** RepA RNA directly binds PRC2 in vitro. **(A)** One Repeat A unit. WT, wild-type sense; mut, mutated; and AS, antisense. DsI and DsII, randomized *Xist* sequences. **(B)** EMSA using female ES cell nuclear extract (NE). Comp, competitors at 500× molar excess. Arrow, sense shift; arrowhead, antisense shift. **(C)** Antisense binding competed by sense RNAs but not nonspecific RNAs. **(D)** EMSA supershifts (*) with antibodies against Ezh2. **(E)** EMSA using recombinant hPRC2 (sub)complexes. fEzh2, *Drosophila* Ezh2. **(F)** hPRC2 bound by antisense but not by randomized probes.

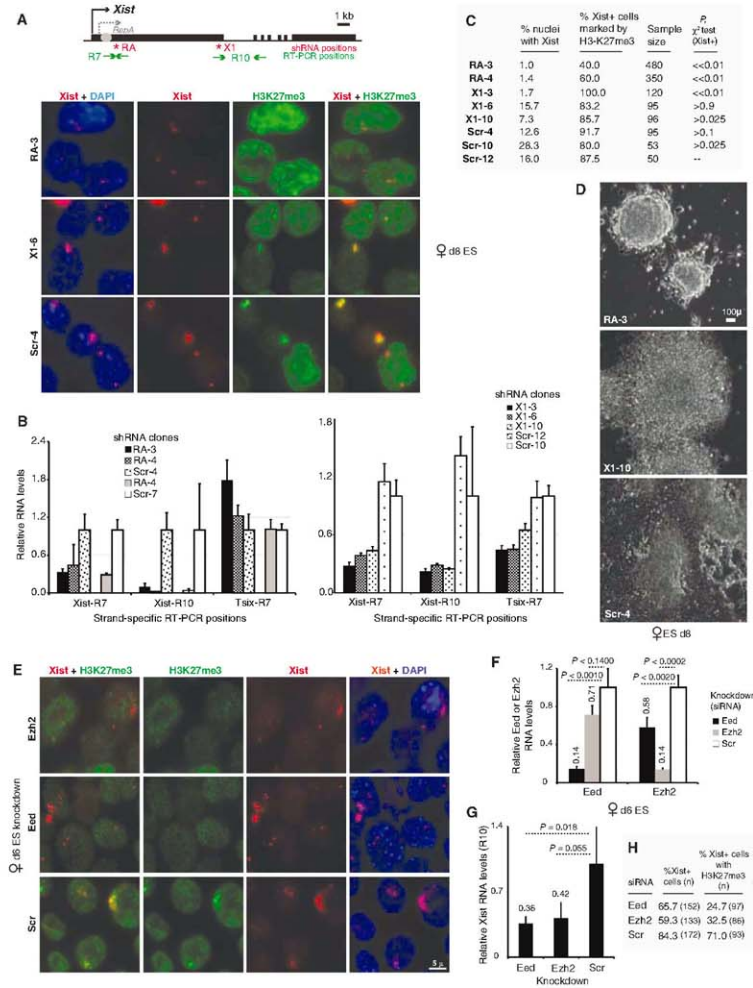


**Fig. 4.** RepA/PRC2 knockdowns compromise XCI initiation. **(A)** Xist RNA–H3-K27me3 immunoFISH in knockdown clones. ShRNA: RA, RepA. X1, *Xist* exon 1, Scr, scrambled control. **(B)** Xist and Tsix levels at indicated positions in knockdown clones. **(C)** ImmunoFISH: Frequency of *Xist* up-regulation (*Xist*$^+$) and H3-K27me3 foci. *P*, pairwise comparison against Scr-12 control for *Xist*$^+$ frequencies. **(D)** Embryoid body growth in shRNA clones. **(E)** Xist–H3-K27me3 immunoFISH after Eed, Ezh2, or control knockdown. **(F)** Eed and Ezh2 mRNA levels after knockdown in *Tsix*$^{\Delta/+}$ ES cells. *P*, *t* test. **(G)** Quantitative RT-PCR of Xist RNA after indicated knockdowns. *P*, *t* test. **(H)** ImmunoFISH: Frequency of *Xist* up-regulation and H3-K27 trimethylation after indicated knockdowns. *P* compares Xist foci numbers in controls ("expected") versus Eed/Ezh2 knockdowns.

the absence of Tsix in vivo ($Tsix^{\Delta CpG/+}$), H3-K27me3 occurred prematurely on day 0 (Fig. 1H). We propose that RepA directly interacts with Ezh2 and that Tsix competitively inhibits this interaction. As full-length Xist also contains the Repeat A motif, it is likely that Xist RNA also directly interacts with PRC2. Consistent with this idea, PRC2 coimmunoprecipitates both 5′ and 3′ domains of Xist RNA in RIP analysis (Fig. 1, B to D).

Previously, PRC2 seemed an unlikely direct target of Xist, as one report suggested that PRC2 is recruited without Repeat A (*7*). However, another report showed that PRC2 recruitment drops 80 to 90% in Repeat A mutants (*9*). To test if RepA functions in XCI, we created female ES clones carrying short hairpin RNA (shRNA) transgenes directed against *RepA* (RA clones) (Fig. 4A). Because RepA and Xist overlap, shRNA against RepA could potentially affect Xist. To distinguish RepA from Xist, we created shRNA against the end of *Xist* exon 1 (X1), which does not overlap RepA. Quantitative RT-PCR confirmed knockdown efficacy and specificity [(Fig. 4B) Xist contains the R7 sequence, so it may be affected by X1 knockdown; residual R7 levels may represent RepA].

Xist induction was severely compromised when RepA was depleted in clones RA-3 and RA-4, as few Xist foci were seen on day 8 when compared with X1 and scrambled (Scr) controls (Fig. 4, A to C). Thus, RepA RNA is required for *Xist* up-regulation. In 100% of RA-3 and RA-4 cells lacking Xist foci, H3-K27me3 was absent on the X (Fig. 4C). In a very small minority of RA-3 and RA-4 cells that up-regulated *Xist*, H3-K27me3 was also compromised, which indicated PRC2 recruitment defects—high Xist levels notwithstanding. Consistent with the failure of XCI, RepA-shRNA clones showed extremely poor embryoid body differentiation in contrast to controls (Fig. 4D). X1 clones showed an intermediate phenotype, consistent with intermediate expression of *Xist*. Although the X1 region is dispensable for silencing and localization (*13*), its knockdown could affect overall Xist stability and might explain the intermediate phenotype. We conclude that RepA RNA functions not only in Xist transactivation but also in H3-K27 methylation and XCI.

We next examined whether knocking down PRC2 subunits might have similar effects. Indeed, Eed and Ezh2 knockdown in day 6 female embryoid body led to significant reductions in Xist and H3-K27me3 foci (Fig. 4, E to H). Therefore, PRC2 also plays a role in *Xist* up-regulation and XCI. Consistent with previous studies (*16*, *17*), among $Xist^{\Delta}$ cells, PRC2 deficiency did not abrogate gene silencing (fig. S2), possibly because of functional redundancy of PRC2 and PRC1 (*17*). By our data (Figs. 1H and 4), the primary effect of the RepA-PRC2 knockdowns may be abrogation of preemptive H3-K27me3 on *Xist*, an event hypothesized to be

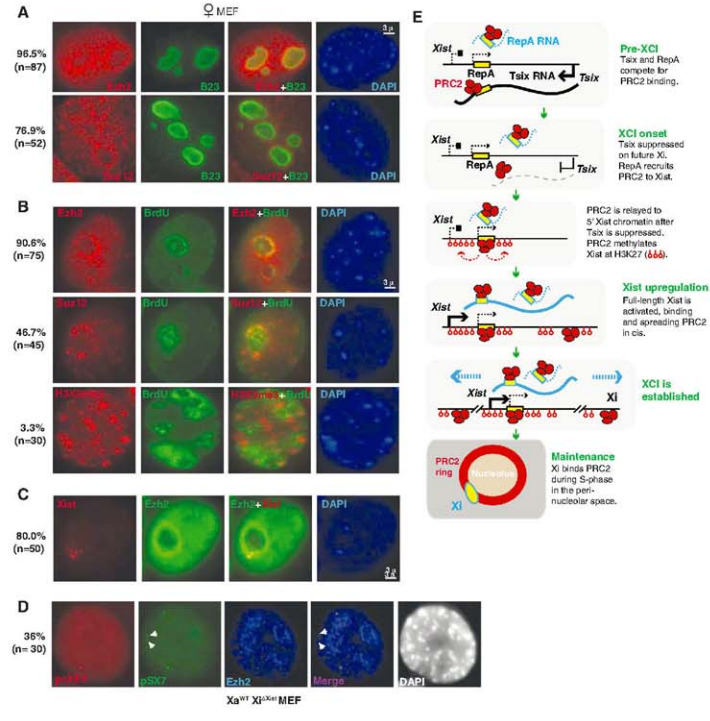


**Fig. 5.** PRC2 and Xi associate in the perinucleolar compartment after XCI. **(A)** Immunostain: Ezh2 and Suz12 concentrate around the nucleolus (B23+). **(B)** Ezh2 and Suz12, but not H3-K9me3, showed perinucleolar enrichment. **(C)** Xist RNA-Ezh2 immunoFISH. **(D)** *Xist* DNA-Ezh2 immunoFISH in $Xa^{WT}Xi^{\Delta Xist}$ MEFs (*6*). **(E)** Summary and model.

necessary for *Xist* induction (*11*). Therefore, RepA-PRC2 complex may act during XCI, firstly by inducing H3-K27me3 at *Xist* for its transactivation and secondly by enabling spread of H3-K27me3 along the Xi.

Given the importance of PRC2, it is odd that Xi is decorated by PRC2 only during initiation of XCI, though it stably retains H3-K27me3 thereafter (*7*, *8*). Given the hypothesis that Xi's epigenetic state is maintained by visiting a perinucleolar compartment during S phase (*6*), we wondered if PRC2 association during the maintenance phase may be likewise compartmentalized and transient. Indeed, we observed high levels of Ezh2 and Suz12 in this late-replicating perinucleolar compartment (Fig. 5, A and B), to which ~80% of Xi is associated in MEFs (Fig. 5C). When Xi has *Xist* deleted after XCI ($Xa^{W1}Xi^{\Delta Xist}$), the chromosome fails to relocalize to this compartment (*6*). In such cells, we observed that perinucleolar localization and H3-K27me3 were abolished (Fig. 5D) (*6*), which supports the idea that Xi in post-XCI cells associates with PRC2 and maintains H3-K27me3 by visiting the perinucleolar compartment during DNA replication.

In summary, we have discovered a small noncoding RNA (ncRNA) that is required to target PRC2 to a specific locus. Long suspected (*18*), an RNA cofactor may explain why no DNA binding subunit for mammalian Polycomb has emerged so far. Ezh2 is apparently the RNA binding PRC2 subunit. For XCI, the data provide new insight into how silencing is initiated on Xi (Fig. 5E). Given Tsix's established role as Xist antagonist (*3*), ability to bind PRC2 and to compete with RepA (Fig. 3), and molar excess over Xist, we propose that Tsix prevents RepA-PRC2 action in pre-XCI cells by titrating RepA away from PRC2, by blocking RepA-PRC2 transfer to chromatin, or by preventing PRC2 catalysis. The last two possibilities may explain why RepA-PRC2 interactions in males do not induce H3-K27me3 (Fig. 1D). In our model, when Tsix is down-regulated on the future Xi, RepA productively engages PRC2, methylates the *Xist* promoter in cis, and enables *Xist* transactivation. In support of this, abolishing Tsix ($Tsix^{\Delta CpG's}$) results in premature H3-K27 trimethylation (Fig. 1C) and elevated Xist levels (*11*). Full-length Xist also binds PRC2 (Fig. 1), so the spread of Xist RNA along Xi could distribute PRC2 and H3-K27me3 throughout the chromosome. As ectopic *Xist* transgenes are known to spread autosomal silencing (*13*), our data imply that *Xist*—perhaps *RepA* itself (Fig. 1)—serves as a nucleation center. After XCI, Xi maintains its association with PRC2 by means of the perinucleolar compartment in a RepA- and Xist-dependent manner. With evidence that RNA interference is required to localize Xist and target H3-K27me3 (*19*), involvement of small RNAs and RNA interference proteins may also be considered. Because another ncRNA ("HOTAIR") was recently identified in connection with PRC2 at a human HOX locus (*20*), RNA cofactors may emerge as universal requirements for Polycomb targeting.

### References and Notes


1. C. J. Brown *et al.*, *Cell* **71**, 527 (1992).
2. G. D. Penny, G. F. Kay, S. A. Sheardown, S. Rastan, N. Brockdorff, *Nature* **379**, 131 (1996).
3. J. T. Lee, N. Lu, *Cell* **99**, 47 (1999).
4. C. M. Clemson, J. A. McNeil, H. Willard, J. B. Lawrence, *J. Cell Biol.* **132**, 259 (1996).
5. J. C. Lucchesi, W. G. Kelly, B. Panning, *Annu. Rev. Genet.* **39**, 615 (2005).
6. L. F. Zhang, K. D. Huynh, J. T. Lee, *Cell* **129**, 693 (2007).
7. K. Plath *et al.*, *Science* **300**, 131 (2003).
8. J. Silva *et al.*, *Dev. Cell* **4**, 481 (2003).
9. A. Kohlmaier *et al.*, *PLoS Biol.* **2**, E171 (2004).
10. L. Ringrose, R. Paro, *Annu. Rev. Genet.* **38**, 413 (2004).
11. B. K. Sun, A. M. Deaton, J. T. Lee, *Mol. Cell* **21**, 617 (2006).
12. B. D. Hendrich, C. J. Brown, H. F. Willard, *Hum. Mol. Genet.* **2**, 663 (1993).
13. A. Wutz, T. P. Rasmussen, R. Jaenisch, *Nat. Genet.* **30**, 167 (2002).
14. T. Sado, Z. Wang, H. Sasaki, E. Li, *Development* **128**, 1275 (2001).
15. N. J. Francis, A. J. Saurin, Z. Shao, R. E. Kingston, *Mol. Cell* **8**, 545 (2001).
16. S. Kalantry, T. Magnuson, *PLoS Genet.* **2**, e66 (2006).
17. S. Schoeftner *et al.*, *EMBO J.* **25**, 3110 (2006).
18. S. Schmitt, R. Paro, *Genome Biol.* **7**, 218 (2006).
19. Y. Ogawa, B. K. Sun, J. T. Lee, *Science* **320**, 1336 (2008).
20. J. L. Rinn *et al.*, *Cell* **129**, 1311 (2007).


21. We thank R. Spencer and Y. Jeon for unpublished data and technical advice and Y. Ogawa for critical reading of the manuscript. Grant support: Massachusetts General Hospital Fund for Medical Discovery (J.Z.), NSF predoctoral award (J.A.E.), Jane Coffin Childs Fellowship (J.J.S.), and NIH-R01GM58839 (J.T.L.). J.T.L. is an Investigator of the HHMI. The transript "RepA" for Repeat A has GenBank accession number FJ361197.


### Supporting Online Material

www.sciencemag.org/cgi/content/full/322/5902/750/DC1
Materials and Methods
Figs. S1 and S2
References


10 July 2008; accepted 19 September 2008
10.1126/science.1163045


# Deletion of *Trpm7* Disrupts Embryonic Development and Thymopoiesis Without Altering $Mg^{2+}$ Homeostasis


**Jie Jin,[1,2]* Bimal N. Desai,[1]* Betsy Navarro,[1] Adriana Donovan,[2] Nancy C. Andrews,[2,3] David E. Clapham[1]†**



The gene *transient receptor potential-melastatin-like 7* (*Trpm7*) encodes a protein that functions as an ion channel and a kinase. TRPM7 has been proposed to be required for cellular $Mg^{2+}$ homeostasis in vertebrates. Deletion of mouse *Trpm7* revealed that it is essential for embryonic development. Tissue-specific deletion of *Trpm7* in the T cell lineage disrupted thymopoiesis, which led to a developmental block of thymocytes at the double-negative stage and a progressive depletion of thymic medullary cells. However, deletion of *Trpm7* in T cells did not affect acute uptake of $Mg^{2+}$ or the maintenance of total cellular $Mg^{2+}$. *Trpm7*-deficient thymocytes exhibited dysregulated synthesis of many growth factors that are necessary for the differentiation and maintenance of thymic epithelial cells. The thymic medullary cells lost signal transducer and activator of transcription 3 activity, which accounts for their depletion when Trpm7 is disrupted in thymocytes.


The transient receptor potential (TRP) superfamily comprises cation-permeant ion channels that have diverse functions (*1*–*3*). TRPM7 (*1*, *2*) and TRPM6 (*4*, *5*) proteins also contain a C-terminal kinase domain (*6*). TRPM7 is expressed in all examined cell types (*3*) and mediates the outwardly rectifying $Mg^{2+}$-inhibitable current (MIC) (*7*). TRPM6 and TRPM7 exhibit nearly identical current-voltage (*I-V*) relations, conducting only a few pA of inward current at physiological pH levels (*1*, *2*, *8*, *9*).

A chicken DT-40 B cell line targeted for *Trpm7* gene disruption was reported to require high concentrations of extracellular $Mg^{2+}$ (10 mM) for survival (*10*). Given the permeability of TRPM7 to $Mg^{2+}$, the results have been interpreted to indicate that TRPM7 was critical for cellular $Mg^{2+}$ homeostasis in vertebrates. A role for TRPM7 in vertebrate development was suggested by a *Danio rerio Trpm7* mutant that exhibited abnormal skeletogenesis and melanophore development, but whether this developmental defect is related to $Mg^{2+}$ homeostasis remains unclear (*11*).

We generated multiple mouse lines with a targeted deletion of the *Trpm7* gene (fig. S1A) (*12*). Mouse lines with disruption of *Trpm7* in all tissues (global deletion), generated using three different approaches, did not yield any live $Trpm7^{null/null}$ animals. Mendelian ratios of littermate genotypes indicated that $Trpm7^{null/null}$


[1]Department of Cardiology, Howard Hughes Medical Institute, Children's Hospital Boston, and Department of Neurobiology, Harvard Medical School, Enders Building 1309, 320 Longwood Avenue, Boston, MA 02115, USA. [2]Division of Hematology and Oncology, Children's Hospital Boston, Karp Family Building 8-125A, Boston, MA 02115, USA. [3]Department of Pediatrics and Department of Pharmacology and Cancer Biology, Duke University School of Medicine, Durham, NC 27702, USA.

*These authors contributed equally to this work.
†To whom correspondence should be addressed. E-mail: ddapham@enders.tch.harvard.edu

mice died prenatally (194 pups analyzed) (fig. S1, D and E). To rule out the possibility that embryonic viability was compromised by the disruption of maternoembryonic transport, we deleted *Trpm7* by using paternal *Sox-2 Cre*, which deletes the gene in the embryonic cells but not in extraembryonic visceral endoderm (*15*). Eight litters from this mating scheme failed to produce *Trpm7*$^{fl}$ (*Sox-2 Cre*) mice, indicating that embryonic lethality resulted from a requirement for TRPM7 in the developing embryo rather than a compromise of maternoembryonic nutrient transport. For further analysis, we used mice in which a β-geo cassette (coding for β-galactosidase) was inserted in the first intron of *Trpm7* (*Trpm7*$^{geo}$) (*12*). The β-geo transcript has a splice acceptor site but not a splice donor site; thus, barring alternative splicing, *Trpm7*$^{geo}$ generates a null allele of *Trpm7*. We isolated and analyzed embryos from *Trpm7*$^{geo/+}$ intercrosses at various times after fertilization and determined that *Trpm7*$^{null/null}$ embryos died before day 7.5 of embryogenesis (E7.5) (fig. S1F). LacZ staining of *Trpm7*$^{geo/+}$ embryos revealed a predominant expression in the fetal heart at E9.5, followed by a gradual and intense expansion of the expression across the ventral region at E10.5, peaking throughout the embryo at E11.5 and E12.5. The broad expression pattern was maintained through E14.5 (fig. S1G). Thus, TRPM7 is expressed in embryonic stem cells (fig. S1B), expression is increased in the early embryo, and the expressed TRPM7 has a non-redundant and vital role in the embryonic development of the mouse.

Using *lck-Cre* mice, we selectively deleted *Trpm7* in developing thymocytes. Deletions of *Trpm7*–exon 17, in thymocytes and mature T-lymphocytes isolated from *Trpm7*$^{-/fl}$ (*lck-Cre*) mice, were confirmed by reverse transcription polymerase chain reaction (RT-PCR) (fig. S2A) and quantified using quantitative RT-PCR directed against exon 17. Unmodified transcripts in thymocytes (8.9 ± 0.28% of normal) were lower than in T lymphocytes (16.8 ± 0.96% of normal) when compared with those in wild-type (*wt*) cells, which probably reflected the presence of contaminating cells of non–T cell lineage in Thy-1.2–directed immunoaffinity preparations from mouse spleens.

Whole-cell patch-clamp recordings revealed that MIC current ($I_{MIC}$) in thymocytes was potentiated by extracellular application of 10 mM $NH_4Cl$ (Fig. 1A) and reversibly inhibited by 10 mM $MgCl_2$ (Fig. 1A) or 100 μM 2-aminoethoxydiphenylborate (2-APB) (fig. S3A) (*7*, *14*). $I_{MIC}$ was abrogated in T cells derived from *Trpm7*$^{fl}$ (*lck-Cre*) mice (Fig. 1, B and C), whereas $K^+$ currents ($K_v1.3$, $K_v3.1$, and $K_{Ca}3.1$) (*15*–*18*) were unaffected (fig. S3B). $I_{MIC}$ was still present in a small population of T cells, probably because of incomplete *Cre* expression and inadvertent patch clamping of Thy-1.2+ splenocytes other than T lymphocytes.

We used a cell-permeable fluorescent indicator [KMG104AM (*19*)] to evaluate $Mg^{2+}$ influx in freshly isolated T cells from *wt* and *Trpm7*$^{fl}$ (*lck-Cre*) mice. T lymphocytes incubated with KMG104AM and maintained in a $Mg^{2+}$-free medium responded with an increased fluorescence intensity to extracellular perfusion with solutions containing 10 mM $MgCl_2$ but not to solutions containing 10 mM $CaCl_2$ (fig. S3C). $Mg^{2+}$ influx in *wt* T lymphocytes was insensitive to 0.5 mM 2-APB (Fig. 1D). Similarly, intracellular alkalinization induced by extracellular 50 mM $NH_4Cl$, which potentiates $I_{TRPM7}$ (*14*), did not result in higher $Mg^{2+}$ influx (fig. S3D). $Mg^{2+}$ influx in thymocytes freshly isolated from *Trpm7*$^{-/fl}$ (*lck-Cre*) mice was insensitive to deletion of TRPM7 (Fig. 1F), which indicates that TRPM7 does not mediate the observed $Mg^{2+}$ influx in T cells. To test the tissue $Mg^{2+}$-dependence on TRPM7, we used

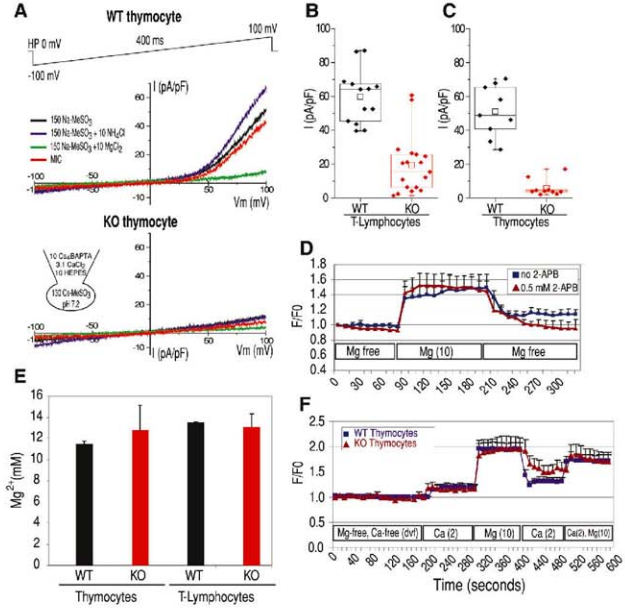


**Fig. 1.** $I_{MIC}$ and $Mg^{2+}$ homeostasis in *Trpm7*-deficient cells. **(A)** *I-V* relationship of $I_{MIC}$ in *wt* and *Trpm7*-deficient [knockout (KO)] thymocytes. **(B)** $I_{MIC}$ densities in *wt* ($n$ = 13 cells) and KO ($n$ = 18 cells) T lymphocytes ($P$ <0.0001, two samples independent $t$ test). Box charts are shown as a box (25 to 75 percentile), vertical bars (5 to 95 percentile), and data points (diamonds) overlap with the mean value (empty square) and median value (horizontal line in the box). **(C)** $I_{MIC}$ densities in *wt* ($n$ = 9 cells) and *KO* ($n$ = 10 cells) thymocytes ($P$ = <0.0001, two samples independent $t$ test). **(D)** $Mg^{2+}$ uptake in *wt* T lymphocytes loaded with KMG104AM, as indicated by the averaged ratio of fluorescence intensity $F$ at indicated time (seconds) over the initial fluorescence $F0$ at 0 s. $Mg^{2+}$ uptake in the absence (blue, $n$ = 25 cells) or presence (red, $n$ = 25 cells) of 0.5 mM 2-APB is shown. **(E)** ICP-MS quantitation of total $Ca^{2+}$ and $Mg^{2+}$ in $HNO_3$ extracts. Average concentration of total cellular $Mg^{2+}$ ($n$ = 3 mice) as calculated by normalizing to a $[K^+]$ of 120 mM is shown. Error bars indicate ± SD. **(F)** $Mg^{2+}$ uptake in *wt* (blue, $n$ = 117 cells) and *KO* (red, $n$ = 102 cells) thymocytes. $[Ca^{2+}]$ and $[Mg^{2+}]$ are in mM.

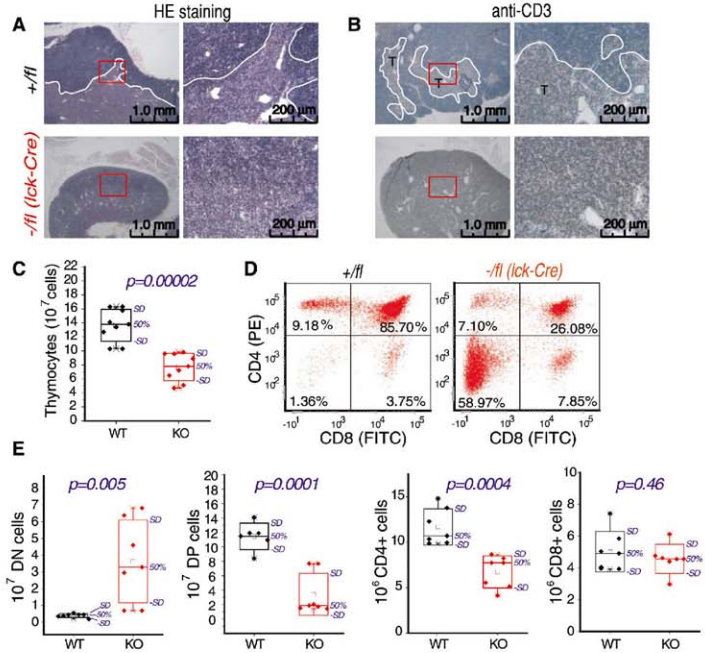


**Fig. 2.** Deletion of *Trpm7* in thymocytes leads to defective thymopoiesis. **(A)** Hematoxylin and eosin–staining of thymus sections from 12-week-old *wt* (top) and *KO* (bottom) mice at 4× (left) and 20× (right) magnification (red box). The boundary between medullary and cortical regions is highlighted with a solid white line where evident. **(B)** Thymocytes were immunolocalized by antibody-to-CD3 staining (brown) against a nuclear counterstain (blue) in the thymus sections obtained from *wt* (top) and *Trpm7*-deficient (bottom) mice. (Left) 4× magnification. Red boxes indicate the areas that are shown at 20× magnification to the right. The CD3+ T cell–enriched medullary regions are highlighted in a *wt* thymus (see fig. S6 for larger images). **(C)** Box chart showing the reduced number of thymocytes in *Trpm7*-deficient mice (red, $n = 9$ mice) as compared with *wt* mice (black, $n = 9$ mice). Box charts shown as a box (±SD), vertical bars (maximum-minimum values), and data overlap. The *P* values in all of the box charts were calculated using the two-sample independent *t* test. **(D)** Flow cytometry of CD4 and CD8 on thymocytes from *wt* and *KO* mice. **(E)** Box charts comparing the total number of thymocytes in the DN, DP, CD4+, and CD8+ thymocytes are shown ($n = 7$ mice).

inductively coupled plasma mass spectrometry (ICP-MS) to measure total $Mg^{2+}$ in freshly isolated T cells. The total [$Mg^{2+}$] in T cells obtained from *wt* and *Trpm7*$^{fl/fl}$ (*lck-Cre*) mice were not statistically different (Fig. 1E). These data indicate that TRPM7 is not essential for cellular $Mg^{2+}$ homeostasis in mice.

In the intestine of adult *Trpm7*$^{fl/fl}$ (*lck-Cre*) mice, T lymphocytes were readily detected at a density comparable to that of *wt* mice (fig. S7), whereas a small reduction in T cell density was evident in the lymph nodes (fig. S8) and spleen (fig. S4B) of *Trpm7*$^{fl/fl}$ (*lck-Cre*) mice. Flow cytometry of splenocytes isolated from *wt* and *Trpm7*$^{fl/fl}$ (*lck-Cre*) mice revealed a small reduction in the percentage and numbers of T cells but not of B cells (Fig. S4, C and D). Despite the decrease in the splenic T cell numbers, the results show that mature T lymphocytes in *Trpm7*$^{fl/fl}$ (*lck-Cre*) mice are able to survive and populate the periphery.

The thymi in *Trpm7*$^{fl/fl}$ (*lck-Cre*) mice developed morphological abnormalities with an 85% phenotypic penetrance ($n = 27$ mice), which suggests defective thymopoiesis. Histology of thymic sections derived from 12-week-old *Trpm7*$^{fl/fl}$ (*lck-Cre*) and *Trpm7*$^{+/fl}$ littermate controls showed abnormal thymic architecture in *Trpm7*$^{fl/fl}$ (*lck-Cre*) mice (Fig. 2A). The boundary between cortical and medullary areas was easily visible in *wt* thymi but not in *Trpm7*-deficient thymi (Fig. 2A and fig. S6A). In contrast to *wt* thymi, where the CD3+ T cells remained confined to the medulla (outlined and marked as T), the CD3+ cells in the thymi of *Trpm7*$^{fl/fl}$ (*lck-Cre*) mice were uniformly distributed across the thymic stroma (Fig. 2B and fig. S6B). Evaluation of thymic cellularity indicated a substantial reduction in the number of thymocytes in *Trpm7*$^{fl/fl}$ (*lck-Cre*) mice (Fig. 2C).

Thymocytes from *Trpm7*$^{fl/fl}$ (*lck-Cre*) mice contained a higher percentage (Fig. 2D) and number (Fig. 2E) of CD4– CD8– [double negative (DN)] cells than did thymocytes from *wt* controls, which indicates a partial developmental block in transition from the DN to double-positive (DP) stage. This developmental defect may account for the reduced number of T cells in *Trpm7*$^{fl/fl}$ (*lck Cre*) mice. Analysis of the DN population based on the cell-surface expression of CD44 and CD25 revealed a significantly higher percentage of DN thymocytes in the DN3 (CD44– CD25+) stage (Fig. 3A), which indicates a failure to down-regulate CD25 expression during T cell development. Because of the block at the DN stage, the cell number is significantly higher in *Trpm7*-deficient thymi. Overlays of CD25 expression of the total thymocyte population and of DN thymocytes show that the proportion of cells expressing CD25 was significantly higher in *Trpm7*-deficient thymi (Fig. 3B). We calculated the changes in percentages (Fig. 3C) and number (Fig. 3D) of DN cells in DN1 (CD44+ CD25–), DN2 (CD44+ CD25+), DN3 (CD44– CD25+), and DN4 (CD44– CD25–) stages. These data indicated that a portion of *Trpm7*-deficient thymocytes fails to down-regulate high-affinity interleukin-2 receptors (CD25), exhibiting a block during the transition from the DN3

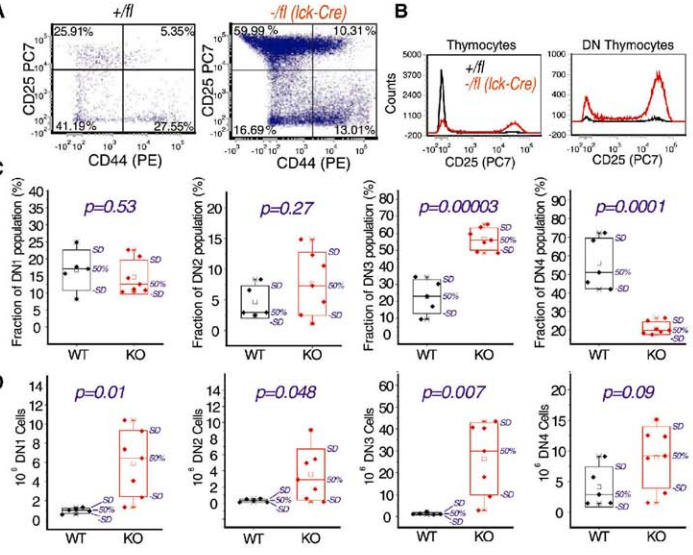


**Fig. 3.** *Trpm7*-deficient thymocytes are partially blocked at the DN3 stage. **(A)** Flow cytometry of CD44 and CD25 expression in DN (CD4– CD8–) thymocytes. Thymocytes were stained with antibody to CD4 [fluorescein isothiocyanate (FITC)], antibody to CD8 (FITC), antibody to CD44 [phycoerythrin (PE)] and antibody to CD25 [phosphatidylcholine 7 (PC7)]. FITC-negative cells (DN) were analyzed for CD44 and CD25 expression. **(B)** (Left) Overlay of cell-surface CD25 expression in *wt* (black) and *Trpm7*-deficient (red) thymocytes. (Right) Overlay of CD25 expression in DN thymocytes. **(C)** Box charts showing percentage of DN population found in the (left to right) DN1, DN2, DN3, and DN4 stages. **(D)** Box charts showing total number of thymocytes found in the (left to right) DN1, DN2, DN3, and DN4 stages.

to DN4 stage. Cell-surface expression of T cell receptor β (TCR-β) chain (fig. S5C) was not substantially altered, which suggests that the developmental defect was not due to a failure in TCR-β locus rearrangement.

We found a progressive loss of thymic medullary cells [cytokeratin 5+ (K5+); Fig. 4A, green] but not thymic cortical cells (K8+; Fig. 4A, red) in comparing 4- and 12-week-old *wt* and *Trpm7*$^{fl}$ (*lck-Cre*) mouse thymic sections. In *wt* mice, the CD3+ cells (Fig. 4B, green) were distributed preferentially within medullary regions of the thymus and showed minimal overlap with cortical thymic epithelial cells (TECs) (K8+; Fig. 4B, red). In contrast, the loss of medullary regions in *Trpm7*-deficient mice was accompanied by a uniform distribution of CD3+ thymocytes in the thymic cortex, as detected by an extensive overlap of K8 and CD3 staining (Fig. 4B).

We conducted a quantitative RT-PCR analysis of freshly isolated thymocytes for mRNA that encoded 82 growth factors with proposed roles in tissue growth and maintenance (fig. S9). We identified seven growth-factor mRNAs whose abundance increased by more than threefold and five growth-factor mRNAs present at <33% of normal levels in *Trpm7*-deficient thymocytes (Fig. 4C). Growth-factor mRNAs that were downregulated included fibroblast growth factor 13 (FGF-13), FGF-7, and midkine. FGF-7 is an important growth factor for thymic epithelial cells (*20*, *21*), and FGF receptors activate signal transducer and activator of transcription 3 (STAT3)–mediated transcriptional responses (*22*), a pathway crucial for the maintenance of thymic medullary cells (*23*). Midkine induces mesenchymal-epithelial transition through the activation of STAT3 (*24*, *25*).

Because STAT3 is autoregulated, the levels of STAT3 are a useful indicator of ongoing STAT3 activity (*26*). In *wt* mice, STAT3 was specifically expressed in medullary TECs (identified by expression of the K5 marker) and progressively lost in medullary TECs in *Trpm7*-deficient thymi (Fig. 4D). In 12-week-old *Trpm7*$^{fl}$ (*lck-Cre*) mice, STAT3 was not detectable in the remnants of the atrophic thymic medulla. Similarly, although activated phospho-STAT3 was readily detected immunohistochemically in the nucleus of *wt* medullary TECs, there was no evidence of activated phospho-STAT3 in *Trpm7*-deficient medullary TECs (Fig. 4E). These data show that deletion of *Trpm7* in thymocytes results in reduced STAT3 activity and abundance in thymic medullary cells, which is expected to lead to a progressive loss of thymic architecture.

TRPM7 is the first TRP channel to be identified with a nonredundant role in embryogenesis and the only ion channel known to be necessary for thymopoiesis. The most notable feature of TRPM7 is the permeation of $Ca^{2+}$, $Mg^{2+}$, and trace metals in the very same structure that contains a kinase. TRPM7 mediates exceedingly low inward conductance, which suggests that the actions of the permeant species are localized and do not substantially affect global $Mg^{2+}$ levels. Our work is now concentrated on how this bifunctional protein mediates these effects on cell-differentiation processes.

### References and Notes


1. L. W. Runnels, L. Yue, D. E. Clapham, *Science* **291**, 1043 (2001).
2. M. J. Nadler *et al.*, *Nature* **411**, 590 (2001).
3. I. S. Ramsey, M. Delling, D. E. Clapham, *Annu. Rev. Physiol.* **68**, 619 (2006).
4. K. P. Schlingmann *et al.*, *Nat. Genet.* **31**, 166 (2002).
5. R. Y. Walder *et al.*, *Nat. Genet.* **31**, 171 (2002).
6. H. Yamaguchi, M. Matsushita, A. C. Nairn, J. Kuriyan, *Mol. Cell* **7**, 1047 (2001).
7. M. Prakriya, R. S. Lewis, *J. Gen. Physiol.* **119**, 487 (2002).
8. J. A. Kozak, H. H. Kerschbaum, M. D. Cahalan, *J. Gen. Physiol.* **120**, 221 (2002).
9. M. Li, J. Jiang, L. Yue, *J. Gen. Physiol.* **127**, 525 (2006).
10. C. Schmitz *et al.*, *Cell* **114**, 191 (2003).
11. M. R. Elizondo *et al.*, *Curr. Biol.* **15**, 667 (2005).
12. Material and methods are available as supporting material on *Science* Online.
13. A. Donovan *et al.*, *Cell Metab.* **1**, 191 (2005).
14. J. A. Kozak, M. Matsushita, A. C. Nairn, M. D. Cahalan, *J. Gen. Physiol.* **126**, 499 (2005).
15. R. S. Lewis, M. D. Cahalan, *Science* **239**, 771 (1988).
16. M. D. Cahalan, K. G. Chandy, T. E. DeCoursey, S. Gupta, *J. Physiol.* **358**, 197 (1985).
17. T. E. Decoursey, K. G. Chandy, S. Gupta, M. D. Cahalan, *J. Gen. Physiol.* **89**, 379 (1987).
18. S. Grissmer, A. N. Nguyen, M. D. Cahalan, *J. Gen. Physiol.* **102**, 601 (1993).
19. H. Komatsu *et al.*, *J. Am. Chem. Soc.* **126**, 16353 (2004).

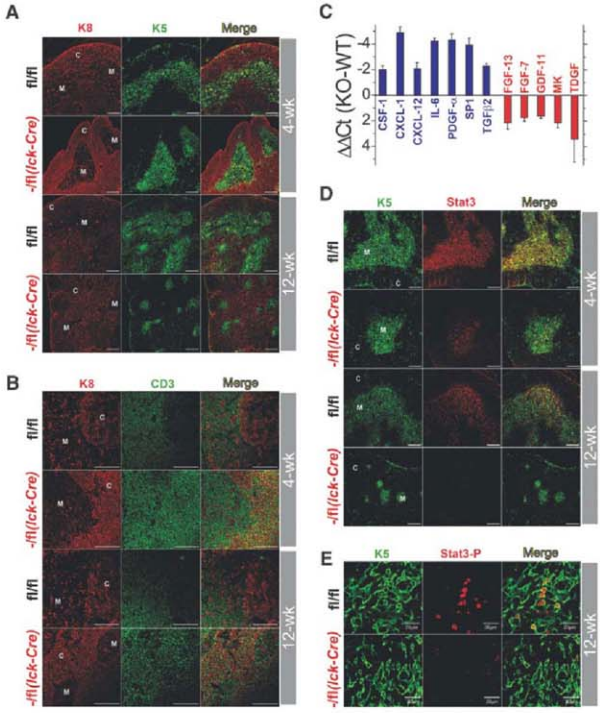


**Fig. 4.** Deletion of *Tpm7* in thymocytes results in progressive loss of medullary epithelial cells. **(A)** Immunofluoresence staining of thymus sections with antibodies to thymic epithelial markers K8 (red) and K5 (green). Letters indicate thymic cortex (C) and medullary (M) regions. Scale bar, 200 μm. **(B)** Staining of thymus sections to CD3 (green) and K8 (red). **(C)** Dysregulated mRNA encoding growth factors in knockout thymocytes relative to *wt* thymocytes identified by quantitative RT-PCR. Growth factors with increased (blue) or decreased (red) mRNA abundance are presented as average ΔΔCt values ($n$ = 3 mice). Error bars indicate SD. A complete list of quantitative RT-PCR results is in fig. S9. **(D)** Immunofluoresence staining of thymus sections with antibody to STAT3 (red) and K5 (green). **(E)** Immunofluoresence staining of phospho-STAT3 (Tyr705) (red) and K5 (green) in thymus sections. Scale bar, 20 μm.


20. M. Erickson *et al.*, *Blood* **100**, 3269 (2002).
21. S. Rossi *et al.*, *Blood* **100**, 682 (2002).
22. K. C. Hart *et al.*, *Oncogene* **19**, 3309 (2000).
23. S. Sano *et al.*, *Immunity* **15**, 261 (2001).
24. Y. Huang *et al.*, *Cell Cycle* **7**, 1613 (2008).
25. E. R. Cernkovich, J. Deng, K. Hua, J. B. Harp, *Endocrinology* **148**, 1598 (2007).
26. M. Ichiba, K. Nakajima, Y. Yamanaka, N. Kiuchi, T. Hirano, *J. Biol. Chem.* **273**, 6132 (1998).



27. This work was supported by the NIH and NIH postdoctoral fellowship T32HL007572-20 (B.N.D.). We thank F. Alt, H. von Boehmer, M. Fleming, G. Krapivinsky, and M. Delling for helpful discussions. Technical assistance from Y. Fujiwara (Division of Hematology Transgenic core facility), D. Campagna (identification of bacterial artificial chromosome clones), G. Losiyev (Brigham Women's Hospital Flow Cytometry core facility), R. Bronson (mouse necropsy), and Z. Chen (ICP-MS) is deeply appreciated.


**Supporting Online Material**

www.sciencemag.org/cgi/content/full/322/5902/756/DC1
Materials and Methods
SOM Text
Figs. S1 to S9
References


21 July 2008; accepted 25 September 2008
10.1126/science.1163493

## Microplate Sealing Film

A new gas-permeable rayon microplate sealing film has been shown to improve culturing of mammalian cells, bacteria, and yeast culture by up to 70 percent compared with an impermeable seal. Manufactured from high-permeability, medical-grade rayon, the new heat-sealing film provides a uniform air and carbon dioxide exchange with all microplate wells, unlike plate lids, which favor exchange for wells near the plate edges. The membrane also reduces evaporation, enhancing longer term incubation experiments. Designed for use with both manual and automated heat sealers, the new sealing film makes use of a noncytotoxic adhesive to minimize sample cross-contamination.

Porvair Sciences
For information +44-1372-824290
www.porvair-sciences.com

## Syringe Filters

The regenerated cellulose (RC) syringe filters remove particulates from the sample, which prevents buildup and blockage in chromatography columns and frits while minimizing wear and tear on injection valves. Sample filtration can reduce system downtime and component replacement. The new RC membranes deliver clean sample with no detectable leachates and are compatible with high-performance liquid chromatography, gas chromatography, immunochromatography, and capillary electrophoresis analysis. The filters offer wider chemical compatibility compared with traditional nylon membranes.

Phenomenex
For information 310-212-0555
www.phenomenex.com

## Universal Cell Migration Kit

The Oris Universal Cell Migration Kit offers a 96-well format in which cell seeding stoppers replace cumbersome membrane-based, cell culture inserts to generate real-time results. Unlike the original Oris Cell Migration Kit, the new universal assembly kit allows scientists to coat the 96-well plate with any extracellular matrix component to create a migration or invasion assay. A two-dimensional closure assay can be designed by leaving the plate uncoated. The Oris Cell Seeding Stoppers are then inserted into each well, where the stopper tip creates a protected 2-mm round zone in the center of each well. Cells are seeded and allowed to adhere, and then the stoppers are removed, exposing a detection zone into which cells can move. An overlay of an extracellular matrix on the cells after stopper removal provides a three-dimensional environment for studying invasion. Cell movement can be monitored in real time by staining and viewing cells with a microscope or digital imaging system.

Platypus Technologies
For information 608-237-1270
www.platypustech.com

## Metabolomics Resource Website

A comprehensive online resource center for metabolomics researchers provides tools and technical advice to help scientists studying small-molecule metabolite profiles. The Metabolomics Solutions Center enables users to tap into Thermo Fisher's extensive knowledge of metabolomics in a single, easy-to-navigate location. It includes application notes, scientific posters, technical guides, webinars, and customer articles from leading researchers in the fields of agriculture, environmental toxicology, disease, nutrition, microorganisms, lipidomics, and general applications.

ThermoFisher Scientific
For information 800-532-4752
www.thermo.com/metabolomics

## Warmed Microscope Platforms

Warmed platforms are available for 35-mm and 50-mm petri dishes, glass slides, and chambered slides. The WP-10 and WP-16 warmed platforms are constructed of aluminum to allow temperature control from 25°C to 65°C and are available in 10-mm and 16-mm aperture sizes. These platforms provide excellent mechanical access from below and have good heat conductivity. They are black anodized for corrosion protection and to minimize stray light reflectance. Control is provided by the TC-124A and TC-144 temperature controllers.

Warner Instruments
For information 800-599-4203
www.warnerinstruments.com

## Parallel Synthesizer

The Carousel 12 Plus Reaction Station is designed to provide busy chemistry laboratories with an easy-to-use productivity tool that simultaneously heats or cools, stirs and refluxes up to 12 samples (1–20 ml) under an inert atmosphere. The Carousel Plus features a new removable reflux and gas distribution head that can be easily transferred, with tubes in situ, between the Carousel's heated base, cooling reservoir, and support stand, providing a unique modular system. The Carousel Plus includes a fluoropolymer insulation plate that sits over the heated base to act as a barrier to heat loss. Viewing slots in the heated base provide a view of the reaction tube contents and stirring performance. The instrument operates from ambient to 180°C (220°C for short periods), and with the addition of a cooling reservoir, to -78°C.

Radleys
For information +44-1799-513320
www.radleys.com

Electronically submit your new product description or product literature information! Go to **www.sciencemag.org/products/newproducts.dtl** for more information.

Newly offered instrumentation, apparatus, and laboratory materials of interest to researchers in all disciplines in academic, industrial, and governmental organizations are featured in this space. Emphasis is given to purpose, chief characteristics, and availability of products and materials. Endorsement by *Science* or AAAS of any products or materials mentioned is not implied. Additional information may be obtained from the manufacturer or supplier.

- Probe the evolution of emotions, language, morality, and microbes.
- Join leaders who are tackling the climate change crisis.
- Learn how the U.S. elections will shape policy and funding.

**Register now and obtain program details at http://www.aaas.org/meetings.**

**Reporters: The EurekAlert! Web site hosts the AAAS Meeting Newsroom. Reporters can obtain details at www.eurekalert.org/aaasnewsroom.**

AAAS
ADVANCING SCIENCE, SERVING SOCIETY

# 2009 Annual Meeting

## *Our Planet and Its Life: Origins and Futures*

12–16 February • Chicago

Dear Colleagues,

The 2009 AAAS Meeting will bring together an exceptional array of speakers addressing some of the most crucial and timely areas of science, technology, and engineering.

The meeting's theme — Our Planet and Its Life: Origins and Futures — recognizes that 2009 is the 200th anniversary of Charles Darwin's birth and the 150th anniversary of the publication of his book, *On the Origin of Species by Means of Natural Selection*. New understanding of the processes that fascinated Darwin continues to be the focus of intense research 150 years later. Indeed every discipline can demonstrate its own unique evolutionary path and speculate on where it may lead.

Attendees from more than 50 countries will have the opportunity to choose among a broad range of activities, including nearly 175 symposia, seminars, and career development workshops as well as plenary and topical lectures by some of the world's leading scientists and engineers.

Typically the meeting includes thousands of participants and hundreds of members of the international and national media. It offers unparalleled networking opportunities. More details can be found at www.aaas.org/meetings, including how sustainability science, an emerging field, has found a home.

The Annual Meeting reflects tremendous efforts from the AAAS sections, divisions, and committees, which we gratefully acknowledge. I also extend a personal thanks to the members of the Scientific Program Committee who reviewed and assembled the many excellent ideas and proposals into this outstanding meeting.

I urge you to join us in Chicago,

James J. McCarthy, Ph.D., AAAS President and
Alexander Agassiz Professor of
Biological Oceanography, Harvard University

## President's Address

### James J. McCarthy

**AAAS President; Alexander Agassiz Professor of Biological Oceanography, Harvard University, Cambridge, Mass.**

McCarthy received his Ph.D. degree from Scripps Institution of Oceanography and B.S. degree in biology from Gonzaga University. He teaches courses in ocean and climate science and oversees Harvard's program in Environmental Science and Public Policy. His research interests relate to marine plankton, biogeochemical cycles, and climate. He has served on and led many national and international groups charged with planning and implementing studies of global change, including chair of the international scientific committee that establishes research priorities and oversees implementation of the International Geosphere–Biosphere Program from 1986 to 1993; founding editor for the American Geophysical Union's *Global Biogeochemical Cycles;* co-chair of the Intergovernmental Panel on Climate Change (IPCC), Working Group II, which had responsibilities for assessing impacts of and vulnerabilities to global climate change for the Third IPCC Assessment (2001); lead author of the Arctic Climate Impact Assessment; and vice-chair of the Northeast Climate Impacts Assessment. He has been elected a fellow of AAAS and the American Academy of Arts and Sciences and a foreign member of the Royal Swedish Academy of Sciences.

*President's Reception: Immediately following*

## Plenary Speakers

### Sean B. Carroll

**Professor of Molecular Biology and Genetics, University of Wisconsin, Madison**

***Remarkable Creatures: Epic Adventures in the Search for the Origins of Species***

Until recently, scientists studying evolution relied on fossil records and morphology to painstakingly piece together a picture of how animals evolved. Today, scientists are now using DNA evidence collected from modern animals to find new clues. Molecular biologist Sean Carroll focuses on the way new animal forms have evolved, and his studies of a wide variety of animal species have dramatically changed the face of evolutionary biology. Major discoveries from his laboratory have been featured in *Time, US News & World Report, The New York Times, Discover,* and *Natural History.* Carroll is the author of *Endless Forms Most Beautiful* (2005) which was a finalist for the *Los Angeles Times* Book Prize, and *The Making of the Fittest* (2006) which won the Phi Beta Kappa Science Book Award. His most recent book, *Remarkable Creatures: Epic Adventures in the Search for the Origins of Species,* will be published in 2009. He is a member of the National Academy of Sciences and an AAAS Fellow. He received his bachelor's degree at Washington University and his Ph.D. degree in immunology from Tufts University.

### Susan W. Kieffer

**Center for Advanced Study Professor of Geology and Physics, and Walgreen University Chair, University of Illinois, Urbana-Champaign**

***Celebrating the Earth: Its Past, Our Present, A Future?***

Planetary scientist Susan Kieffer has degrees in math, physics, geology, and planetary science, which is apparent in the interdisciplinary nature of her work. She is internationally renowned and a leading authority on the mechanisms of meteorite impact, geyser dynamics, volcanic eruptions, and river floods. She was the first scientist to describe the physics and chemistry involved in the eruptions on Jupiter's moon Io, the lateral blast associated with the eruption of Mt. St. Helens, the dynamics of Old Faithful as seen by a micro video camera lowered into the geyser between violent eruptions, and the hydraulics of the rapids of the Colorado River. With colleagues, she described the dynamics of the Chixculub meteor impact that caused vaporization of limestone, which resulted in massive amounts of carbon dioxide in the atmosphere and ultimately resulted in a major extinction event 65 million years ago. Kieffer is a member of the National Academy of Sciences, a MacArthur Fellow, and has received numerous awards and honors. She attended Caltech, University of Colorado, Boulder, and Allegheny College.

### Svante Pääbo

**Director of the Department of Genetics, Max-Planck-Institute for Evolutionary Anthropology, Leipzig, Germany**

***A Neanderthal Perspective on Human Origins***

A biologist specializing in evolutionary genetics, Svante Pääbo is known as one of the founders of paleogenetics, a discipline that uses the methods of genetics to study early humans and other ancient populations. He is conducting some of the most exacting work ever attempted on the DNA of human and nonhuman primates. His track record of discoveries began in 1985 when he isolated DNA from a 2,400-year-old Egyptian mummy. In 2006, after decoding fragments of DNA from the remains of Neanderthal, he announced plans to reconstruct the entire genome. In 1992, he received the Gottfried Wilhelm Leibniz Prize of the Deutsche Forschungsgemeinschaft, which is the highest honor awarded in German research. Pääbo's department in August 2002 published findings about the evolution of the "language gene," FOXP2, which is lacking or damaged in some individuals with language disabilities. He was born in Stockholm and earned his Ph.D. degree from Uppsala University. He is a member of the National Academy of Sciences.

# Topical Lecture Series

**Colin F. Camerer**
Robert Kirby Professor of Behavioral Economics, California Institute of Technology, Pasadena
***Interface Between Cognitive Psychology and Economics***

**Ekaterina Dadachova**
Sylvia and Robert Olnick Faculty Scholar in Cancer Research, and Associate Professor of Nuclear Medicine and Microbiology and Immunology, Albert Einstein College of Medicine of Yeshiva University, Bronx, NY
***New Approaches to the Therapy of Infectious Disease***

**T. Conrad Gilliam**
Marjorie I. and Bernard A. Mitchell Professor and Chair of the Department of Human Genetics, University of Chicago, Ill.
***Human Genetics***

**Lene Vestergaard Hau**
Mallinckrodt Professor of Physics and of Applied Physics, Harvard University, Cambridge, Mass.
***Wizardry with Light: Freeze, Teleport, and Go!***

**Amory Lovins**
Co-Founder, Chairman, and Chief Scientist, Rocky Mountain Institute, Snowmass, Colo.
***Profitable Solutions to the Oil, Climate, and Proliferation Problems***

**Daniel G. Nocera**
Professor of Energy and of Chemistry, Massachusetts Institute of Technology, Cambridge
***Harnessing the Sun and Oceans To Meet the World's Energy Demands***

**Timothy D. White**
Professor of Integrative Biology, University of California, Berkeley
***Evolution of Early Humans***

**Jeanette Wing**
Assistant Director, National Science Foundation, Arlington, Va.
***Computational Thinking***

2009 George Sarton Memorial Lecture

**Ken Alder**
Professor of History and Milton H. Wilson Professor in the Humanities, Northwestern University, Evanston, Ill.
***A History of the International Scientific Conference***

2009 John P. McGovern Award Lecture in the Behavioral Sciences

**Elizabeth Loftus**
Distinguished Professor, University of California, Irvine
***Illusions and Delusions of Memory***

## Topical Panel

***North-South Scientific International Cooperation—Meeting Global Challenges***

**Lord Martin Rees,** President of the Royal Society, Master of Trinity College, and Professor of Cosmology and Astrophysics, University of Cambridge, U.K.

**József Pálinkás,** President, Hungarian Academy of Sciences, Budapest *(Invited)*

**Jacob Palis,** President, Academy of Sciences for the Developing World, Rio de Janeiro, Brazil *(Invited)*

# Seminar Tracks

Day-long seminars address topics at the intersection of science and society: assessing and responding to climate change, human evolution, and nanotechnology

## Assessing and Responding to Climate Change

**Equity, Sustainability, and Governance of Mixed-Use Landscapes**
*Organized by Ashwini Chhatre, University of Illinois, Urbana-Champaign*
Sustainability has emerged as a necessary objective of policy interventions. The future of life on Earth depends on our ability to devise governance systems that guide nature-society interactions toward more sustainable trajectories. Moving beyond the role of institutions in dealing with trade-offs among competing land uses along different outcome dimensions — income generation, biodiversity conservation, ecosystem services provision, greenhouse gas emissions, and carbon sequestration — speakers will discuss the challenge of devising complex multi-level governance systems for mixed-use landscapes.

**Risky Business: Assessing and Dealing with Extremes in a Changing Climate**
*Organized by Claudia Tebaldi, Climate Central, Palo Alto, Calif.*
Extreme events are arguably the most crucial aspect of climate change, threatening to have the largest impacts on social and natural systems. They pose tough questions, often with heavy financial and legal implications, about the distinction between natural and human causes. This

## Discount Airfares

United Airlines is the official carrier for the 2009 AAAS Annual Meeting.

For details about airfare discounts, visit www.aaas.org/meetings and select ···› Travel Information.

session explores what can and cannot be reliably said about the influence of global warming on several aspects of extreme events: hurricanes, temperature and precipitation extremes over North America, and the attribution of specific historic events to human-caused warming. Speakers will discuss what kind of scientific information can help us better understand past, present, and future patterns of extreme events, while taking steps to protect our resources and adapt to a dynamic climate.

**U.S. Cities: Responding to Concerns About Climate Change**
*Organized by Donald J. Wuebbles, University of Illinois, Urbana-Champaign*
Cities cover only 0.4 percent of the Earth's surface but generate the bulk of the world's emissions of carbon dioxide, making urban areas key to alleviating the concerns about global warming. Many cities are already taking action by developing climate adaptation and mitigation strategies for their own communities. Several efforts are already underway to attack the climate issue, for example, by enhancing urban planning, reexamining city policies, improving energy efficiency, and reevaluating local transportation systems. The green roofs in Chicago are one such response. Speakers will discuss the ongoing efforts within U.S. cities toward adaptation and mitigation of climate change.

## Human Evolution

**The Evolution of Human Diets**
*Organized by Matt Sponheimer, University of Colorado, Boulder*
Recent changes in human diet have been implicated in the etiology of modern diseases including Type II diabetes, arteriosclerosis, and several forms of cancer. As a result, many have argued that our dietary recommendations should be informed by our knowledge of the feeding behavior of human ancestors and our close primate kin. In this session, researchers will examine the evolution of human diets through the lenses of archaeology, morphology, biogeochemistry, ethology, genetics, and energetics. Assembling scientists who address similar questions in different ways will underscore areas of growing consensus and controversy and in so doing should considerably advance our knowledge of hominin dietary adaptations.

**The Origin of the Human Species**
*Organized by Leslie C. Aiello, Wenner-Gren Foundation for Anthropological Research, New York City*
In *On the Origin of Species by Means of Natural Selection*, Charles Darwin famously said that "light will be thrown on the origin of man and his history." Although there were no widely accepted human fossils at the time of publication (1859), today there are more than 20 fossil hominin species spanning over 6 million years of prehistory. This session brings together leading international experts to discuss what the extensive fossil and archaeological record can tell us about six major periods in human biological and cultural evolution.

## Nanotechnology

**Driving Beyond Our Nano-Headlights?**
*Organized by Joel G. Pounds, Pacific Northwest National Laboratory, Richland, Wash.*
Nanotechnology has enormous potential to benefit society and the economy. It also might yield unanticipated, negative environmental change. DDT had long-term ecological side effects that were not understood until organisms failed to adapt. And, commercial development of genetically modified organisms was delayed by the perception that risks from these organisms outweighed their benefits. Speakers will explore where the science of nanotoxicology is heading, the challenges in understanding and predicting long-term effects, approaches to nanotoxicological research, and the policy framework required.

**From Donuts to Drugs: Nano-Biotechnology Evolution or Revolution?**
*Organized by Rodney A. Hill, University of Idaho, Moscow*
The foods we eat and the drugs we take in the future could be more revolutionary than evolutionary, if research at the nano-bio interface continues at its current pace. Imagine targeted drugs and guilt-free food; or treatments that make you even better than new. Nanotechnology is driving the development of tools to understand biology better and materials to promote good health. Where is bio-nanoscience heading and how can science and citizens work together to ensure its success? This session will turn to the interface between nanomaterials and humans, and highlight provocative, cutting-edge science.

# Special Sessions

## 2009 Forum for Sustainability Science Programs

One of the biggest challenges that the planet faces is how to balance the needs of human development with the needs of the environment. Policy-makers at all levels of governance increasingly look to scientists and engineers to provide guidance in creating sustainable societies. Universities are increasingly responding by developing academic and research programs in Science and Technology for Sustainable Development or "Sustainability Science" that undertake practical, place-based research to provide decision-support for addressing sustainability challenges.

Since the inaugural Forum at the 2007 AAAS Annual Meeting in San Francisco, the AAAS Center for Science, Technology, and Sustainable Development has convened key university actors in Sustainability Science to dialogue on collaborative approaches to building this emerging field. Though participants from the United States and abroad hail from diverse perspectives and institutions, most are experiencing similar challenges as they develop interdisciplinary programs, which combine both basic and applied research methods.

As a follow-up to previous sessions which identified key challenges and opportunities (2007) and began to identify opportunities to further connect these universities (2008), the 2009 Forum will tackle a number of common concerns for these programs including:

- Curriculum Development
- Sustainability Science and Decision-Making
- Support for Interdisciplinary Sustainability Research

The Forum will include a series of roundtable discussions, led by key actors in the sustainability science community.

## 2009 Forum for School Science

The quality of science and mathematics education is high on the list of concerns in most countries of the world. Scientists and educators in many countries are developing and testing programs and practices, including a number they have adapted from U.S. initiatives. Many states are visiting programs in other countries and attempting to benchmark those that show high levels of performance on international assessments.

In some cases, economical, cultural, and social differences result in different ideas, strategies, and adaptations. In other countries, where elements of U.S.-developed programs are implemented, lessons can be learned from their results, especially to inform the work of transformation in the United States. The Forum for School Science will offer a series of "global" conversations with U.S. and international presenters. The discussions will include examples of programs and current thinking in each area and reflect on symposia to be offered in the symposium track, Learning and Literacy. Areas to be covered include:

- Rethinking U.S. reforms of the curriculum core (sharing, adapting, and delivering materials)
- Implementing what we know (policy, research, and scaling)
- Restructuring undergraduate and graduate STEM education
- Engaging the public with science and education.

## Welcome to China, Greece, Italy, Mexico, Poland, and Russia.

In other words, welcome to Chicago. Easy access, big business, lots of science, and great diversity make Chicago one of the truly global cities.

# Symposium Tracks

## Brain and Behavior

**Beyond the Beagle: Evolutionary Approaches to the Study of Social Behavior**
*Organized by* Jill Mateo, University of Chicago, Ill.

**Comparative Cognition: The Science of Mental Evolution**
*Organized by* Edward A. Wasserman, University of Iowa, Iowa City

**Embodied Language and Cognition: Brains, Mouths, and Hands**
*Organized by* Philip Rubin, Haskins Laboratories, New Haven, Conn.

**Expression of Emotions: Biocultural Perspectives**
*Organized by* Carl A. Maida, University of California, Los Angeles

**Languages Without Ancestors**
*Organized by* Karen Emmorey, San Diego State University, Calif.

**Post-Traumatic Stress Disorder and the Military**
*Organized by* Stephanie J. Bird, Massachusetts Institute of Technology, Cambridge, Mass.

**Post-Traumatic Stress Disorder: The New Battle for Veterans**
*Organized by* Virginia R. G. Carson, Chapman University, Orange, Calif.

**The Science of Kissing**
*Organized by* Albert H. Teich, AAAS Science and Policy Programs, Washington, D.C.

**Social Emotion and the Brain**
*Organized by* John T. Cacioppo, University of Chicago, Ill.

## Evolution and Revolution

**Animal Body Plan Evolution of Development**
*Organized by* Christopher J. Lowe, University of Chicago, Ill.

**Celebrating Darwin at 200: Explaining How Human Morality Evolved**
*Organized by* Douglas Allchin, University of Minnesota, Minneapolis

**Evolution Makes Sense of Biology**
*Organized by* Eugenie C. Scott, National Center for Science Education, Oakland, Calif.

**Evolution of Mammalian Retroelement Activity**
*Organized by* Robert C. von Borstel, University of Alberta, Canada

**Genetics Meets Anthropology: How DNA Unravels the Roots of Human Society**
*Organized by* Eamonn Cahill, Office of the Chief Scientific Adviser to the Government of Ireland, Dublin

**Host-Pathogen Interactions: Evolution of Immune Defenses**
*Organized by* Nancy E. Beckage, University of California, Riverside

**The Invisible Woman in Evolution: Natural Selection and Life-Cycle Events**
*Organized by* Marquisa LaVelle, University of Rhode Island, Kingston

**The Last Piece of Darwin's Puzzle: The Evolution of the Social Mind**
*Organized by* Dario Maestripieri, University of Chicago, Ill.

**Microbes in a Changing World: The Lessons of Darwin**
*Organized by* Roberto G. Kolter, Harvard Medical School, Boston, Mass.

**Origins of Complex Societies in Primates and Humans**
*Organized by* Robert D. Martin, Field Museum of Natural History, Chicago, Ill.

**Studying Vertebrate Genomes: Reading Evolution's Notebooks**
*Organized by* Eric D. Green, National Human Genome Research Institute, Bethesda, Md.

**Symbiosis as an Evolutionary Driver: Mergers of Cells and Genomes**
*Organized by* Jeffrey D. Palmer, Indiana University, Bloomington

## Feeding a Hungry Planet

**Adulteration, Counterfeiting, and Smuggling: How Safe Is Our Imported Food?**
*Organized by* Ewen C. D. Todd, Michigan State University, East Lansing

**Aquaculture Impacts, Standards, and Sustainability**
*Organized by* Angela T. Bednarek, Lenfest Ocean Program, Washington, D.C.

**Beyond the Obituaries: Successful Fish Stories in Ocean Conservation**
*Organized by* Jeremy B. C. Jackson, Scripps Institution of Oceanography, La Jolla, Calif.

**Foods of the Future**
*Organized by* Clare M. Hasler, University of California, Davis

**Green, Gene, Growing Machines: The Evolutionary Shaping of Plant Form**
*Organized by* David A. Baum, University of Wisconsin, Madison

**A Hunger for Power: The Global Nexus of Energy and Food**
*Organized by* Michael E. Webber, University of Texas, Austin

**Living Soil, Food Quality, and the Future of Food**
*Organized by* Preston K. Andrews, Washington State University, Pullman

**Nanofood for Healthier Living?**
*Organized by* Aidan Gilligan, European Commission, Brussels, Belgium

**Protecting Our Planet Against Food Riots in the Future**
*Organized by* Ronald L. Phillips, University of Minnesota, St. Paul

**The Promise of Translational Research for Sustainable Agriculture: Darwin on Steroids**
*Organized by* Daniel Bush, Colorado State University, Fort Collins

## Global Partnerships

**Advancing Women in Physics Internationally**
*Organized by* Beverly K. Hartline, Delaware State University, Dover

**Ambitious Materials for Energy 2020: European Cooperation for Major Breakthroughs**
*Organized by* Carlos Saraiva Martins, European Commission, Brussels, Belgium

**Building a Diversified Portfolio: The Roles of Nonprofits in Biomedical Research**
*Organized by* Maria T. Vassileva, Foundation for the National Institutes of Health, Bethesda, Md.

**East Asian Science Policies and New Global Realities**
*Organized by* Yaeko Mitsumori, National Institute of Science and Technology Policy, Tokyo, Japan

**Geologic Storage of Carbon Dioxide: The Regional Carbon Sequestration Partnerships Initiative**
*Organized by* Sean I. Plasynski, U.S. Department of Energy, Pittsburgh, Pa.

**Internationalization of Science: Looking Ahead**
*Organized by* Gianpietro van de Goor, European Research Council–European Commission, Brussels, Belgium

**New Partnerships for Science in the Cradle of Humanity**
*Organized by* Sarah Banas, AAAS International Office, Washington, D.C.

**New Tools in Diplomacy: Environmental Change, Conservation, and Conflict**
*Organized by* Alex O. Dehgan, U.S. Department of State, Washington, D.C.

**Science for Diplomacy: Building Scientific Cooperation with North Korea**
*Organized by* Linda Staheli, U.S. Civilian Research and Development Foundation, Arlington, Va.

**Thirsting for Daily Sustenance: Public-Private Partnerships for Global Water Access**
*Organized by* Usha R. Balakrishnan, CARTHA, Iowa City, Iowa

## Innovations for a Healthy Society

**21st Century Medical Challenges: Issues of Development and Delivery**
*Organized by* Paul H. Fagette, Illinois Institute of Technology, Chicago

**Adult Stem Cells: From Scientific Process to Patient Benefit**
*Organized by* Norbert Riedel, Baxter International, Deerfield, Ill.

**Emerging Genomic Tools for Predicting Adverse Drug Reactions: Promises and Challenges**
*Organized by* Danny D. Shen, University of Washington, Seattle

**Epigenetics: Mechanisms and Impact on Biomedicine**
*Organized by* Walter Doerfler, University of Cologne, Germany

**Fighting the Rising Tide of Antibiotic Resistance: Causes and Cures in the Sea**
*Organized by* Carolyn Sotka, NOAA Oceans and Human Health Initiative, Charleston, S.C.

**Genetics of Addiction: What We Can Learn from Genes?**
*Organized by* Indridi Benediktsson, European Commission, Brussels

**Is the World's Drug Supply Safe?**
*Organized by* Darrell R. Abernethy, United States Pharmacopeia, Rockville, Md.

**Medicines for Children**
*Organized by* Indridi Benediktsson, European Commission, Brussels, Belgium

**Origins of the Perfect Face: Extreme Makeovers**
*Organized by* Mary MacDougall, University of Alabama, Birmingham

**Preimplantation Genetic Diagnosis: Beyond Natural Selection?**
*Organized by* Aidan Gilligan, European Commission, Brussels, Belgium

**Species and Individual Differences in Response to Drugs**
*Organized by* Margaret O. James, University of Florida, Gainesville

## Learning and Literacy

**Celebrating Year of Science 2009: Efforts To Improve Public Engagement in Science**
*Organized by* Sheri Potter, American Institute of Biological Sciences, Sarasota, Fla.

**College Science Courses: Remembering C.P. Snow**
*Organized by* Jon D. Miller, Michigan State University, East Lansing

**Conceptual Interference in Chemistry and Biology Instruction**
*Organized by* Melanie M. Cooper, Clemson University, S.C.

**Concern for the Future: Civic Leadership in Advancing Science Education**
*Organized by* Julie Parente, Museum of Science and Industry, Chicago, Ill.

**Discipline-Based Science Education Research**
*Organized by* David E. Meltzer, Arizona State University, Mesa

**Inquiry or Direct? Research-Based Practices in Science Education**
*Organized by* William W. Cobern, Western Michigan University, Kalamazoo

**K-12 Engineering Education in the United States**
*Organized by* Greg Pearson, National Academy of Engineering, Washington, D.C.

**Mathematical Biology, the New Frontier: Educating the Next Generation**
*Organized by* Bonnie Shulman, Bates College, Lewiston, Maine

**A New Kind of Scientist: Professional Master's Education and U.S. Competitiveness**
*Organized by* Brad Wible, Northwestern University, Evanston, Ill.

**Science Cafés: Taking Science to Public Places**
*Organized by* Mikkel Bohm, Danish Science Communication, Copenhagen

**Science Policy 101: Taking Science Policy Out of Washington and into the Classroom**
*Organized by* Tobin L. Smith, Association of American Universities, Washington, D.C.

**Visualizing Earth: Teaching Geoscience Using New Technologies**
*Organized by* Marilyn J. Suiter, National Science Foundation, Arlington, Va.

## Machines, Systems, and Knowledge

**Analyzing Virtual Worlds: Next Step in the Evolution of Social Science Research**
*Organized by* Jaideep Srivastava, University of Minnesota, Minneapolis

**Big, Small, and Everything in Between: Simulating Our World Using Scientific Computing**
*Organized by* Thomas H. Dunning, University of Illinois, Urbana-Champaign

**Casting New Light on Ancient Secrets**
*Organized by* Silvana Damerell, Diamond Light Source, Didcot, U.K.

**Earth's History and Future Revealed at the Frontier of Scientific Computing**
*Organized by* Norman Chonacky, Yale University, New Haven, Conn.

**The Grid, the Cloud, Sensor Nets, and the Future of Computing**
*Organized by* Michael R. Nelson, Georgetown University, Washington, D.C.

**How Telescopes Made the Earth a Planet: 400 Years After Galileo**
*Organized by* Virginia Trimble, University of California, Irvine

**Information and Communications Technology and Sustainable Infrastructure**
*Organized by* Priscilla P. Nelson, New Jersey Institute of Technology, Newark

**Interdisciplinary Approaches to the Study of Large-Scale Human Networks**
*Organized by* David Lazer, Harvard University, Cambridge, Mass.

**The Mathematical Twists and Turns of Data Sets**
*Organized by* Robert Ghrist, University of Pennsylvania, Philadelphia

**New Computing Platforms for Data-Intensive Science**
*Organized by* Ian Foster, Argonne National Laboratory, Chicago, Ill.

## Managing Environmental Challenges

**Basic Research for Global Energy Security: A Call to Action**
*Organized by* James Misewich, Brookhaven National Laboratory, Upton, N.Y.

**Biofuels Ablaze**
*Organized by* Susan E. Cozzens, Georgia Institute of Technology, Atlanta

**Biofuels, Tropical Deforestation, and Climate Policy: Key Challenges and Opportunities**
*Organized by* Holly Gibbs, University of Wisconsin, Madison

**Chicago Wilderness: Integrating Biological and Social Diversity into the Future**
*Organized by* Sir Peter Crane, University of Chicago, Ill.

**Drake's Well to Solar Cells: 150 Years of Energy Transitions**
*Organized by* Audra J. Wolfe, Chemical Heritage Foundation, Philadelphia, Pa.

**Environmental Justice and Climate Change**
*Organized by* Nicky Sheats, Thomas Edison State College, Trenton, N.J.

**Food for Thought: Feeding Ourselves, Feeding the Climate Crisis**
*Organized by* Astrid J. Scholz, Ecotrust, Portland, Ore.

**The Future of the U.S. Climate-Observing Capability**
*Organized by* Thomas P. Ackerman, University of Washington, Seattle

**Global Trade and the Homogecene: Lessons from the Great Lakes for the World**
*Organized by* David M. Lodge, University of Notre Dame, Ind.

**Keeping the Lights on: The Revival of Nuclear Energy for Our Future**
*Organized by* Aidan Gilligan, European Commission, Brussels, Belgium

**Plug-in Hybrids and Other Electric Vehicles: Key to Planetary Mobility?**
*Organized by* Tina Kaarsberg, U.S. Department of Energy, Washington, D.C.

**What Is New and Surprising Since the IPCC Fourth Assessment?**
*Organized by* Berrien Moore, University of New Hampshire, Dover

## Oceans, Earth, and Air

**21st Century Water: Friend or Foe?**
*Organized by* Charles J. Vorosmarty, City College of New York, New York City

**Crossing the Plate Boundary: Probing Earthquakes at the Source**
*Organized by* Charna E. Meth, Consortium for Ocean Leadership, Washington, D.C.

**Disaster Scene Investigation: Lessons of the Wenchuan Earthquake**
*Organized by* Richard A. Stone, AAAS/*Science*, Washington, D.C.

**Emerging Threats and Research Challenges for Global Ecosystems**
*Organized by* William F. Laurance, Smithsonian Tropical Research Institute, Panama City, Panama

**Facing Our Uncertain Future: The Reality of Climate-Change Adaptation in the Ocean**
*Organized by* Emily Pidgeon, Conservation International, Arlington, Va.

**Life in the Extreme: The Deep Biosphere's Influence on Global Processes**
*Organized by* Charna E. Meth, Consortium for Ocean Leadership, Washington, D.C.

**Our Changing Planet: Achievements of the International Polar Year**
*Organized by* Rolf Sinclair, Chevy Chase, Md.

**Solutions for Resuscitating Dead Zones: From Chicago to the Gulf of Mexico and Beyond**
*Organized by* Donald F. Boesch, University of Maryland Center for Environmental Science, Cambridge, Md.

**Water: Who Gets the Last Drop?**
*Organized by* Deon Stuthman, University of Minnesota, St. Paul

## On the Brink of Discovery

**Artificial Cells: Models of the Simplest Life**
*Organized by* Christine Keating, Pennsylvania State University, State College

**Beyond E=mc$^2$: Unveiling the Early Universe with High-Intensity Accelerators**
*Organized by* Kurt Riesselmann, Fermi National Accelerator Laboratory, Batavia, Ill.

**Closing in on High-Energy Physics Discoveries: From the Tevatron to the Large Hadron**
*Organized by* Maria Spiropulu, European Organization for Nuclear Research (CERN), Geneva, Switzerland

**Cosmic Cradle of Life**
*Organized by* Mark T. Adams, National Radio Astronomy Observatory, Charlottesville, Va.

**From Enlightenment Lunar Theories to the Discovery of Extra Solar Planets**
*Organized by* Ronald S. Calinger, Catholic University of America, Washington, D.C.

**Exciting Research at the Fermi National Accelerator Laboratory**
*Organized by* David M. Cook, Lawrence University, Appleton, Wis.

**Microbial Communication: Single Cells Gain a Voice**
*Organized by* Clay Fuqua, Indiana University, Bloomington

**Origin and Evolution of Planets**
*Organized by* Gilbert W. Collins, Lawrence Livermore National Laboratory, Livermore, Calif.

**Origins and Endings: From the Beginning to the End of the Universe**
*Organized by* Lawrence M. Krauss, Case Western Reserve University, Cleveland, Ohio

**Quest for the Perfect Liquid: Connecting Heavy Ions, String Theory, and Cold Atoms**
*Organized by* Peter Steinberg, Brookhaven National Laboratory, Upton, N.Y.

**Synthetic Life**
*Organized by* Christina Smolke, California Institute of Technology, Pasadena

**Weird Life**
*Organized by* Jill C. Tarter, SETI Institute, Mountain View, Calif.

## Research Techniques and Resources

**Bright Light for Better Health**
*Organized by* Silvana C. Damerell, Diamond Light Source, Didcot, U.K.

**Evolution of Knowledge Production: Exploring Creativity, Innovation, and Networks**
*Organized by* Gretchen B. Jordan, Sandia National Laboratories, Albuquerque, N.M.

**Frontiers in the Plant Tree of Life**
*Organized by* Michael Donoghue, Yale University, New Haven, Conn.

**The Future of U.S. Accelerator Science**
*Organized by* Cherry A. Murray, Lawrence Livermore National Laboratory, Livermore, Calif.

# CELTIC STRENGTH:
## SCIENCE IN IRELAND

Lush green hills, miles of rugged coastline, a vibrant history, charming neighbors, a pub at every corner, and a prospering economy ... Sounds like an idyllic place to live, but would you want to do your research there?
**By Laura Bonetta**

A decade ago the answer likely would have been "no" for most scientists, but today Ireland is carving a place for itself among those countries leading the world in scientific research and development. A significant commitment by the government to develop a "knowledge economy" has resulted in greater opportunities for scientists and engineers. "We are in a totally different world," says **David McConnell,** head of the genetics department at Trinity College Dublin (TCD). "Now we have the government behind us."

In 2007 the Irish government and European Union invested €995 million (US$1.328 billion) in research. This is a considerable investment in a country with a population of just over 4 million people. And the results are easy to spot. A growing number of research institutes/centers and biotech companies are popping up across the country, and more Irish students are obtaining graduate degrees than ever before. As Ireland's science enterprise begins to establish itself, it is providing researchers with challenges, as well as unparalleled opportunities.

### The Switch to Irish Funding

Until about 10 years ago, there was next to no funding for research in Ireland. "The real lift-off began in 2000," says **Patrick Cunningham,** the government's chief scientific adviser since 2007. "In the subsequent seven years the government spending on research went up by 264 percent. That means that the growth rate in research and development increased at twice the rate of the economy, which is growing at a rate of 7 percent a year in Ireland."

The Irish government announced in June 2006 a Strategy for Science, Technology and Innovation involving an investment of €8.2 billion (US$10.9 billion) over the next seven years. The purpose of the strategy was to turn Ireland into a knowledge economy as the best way forward for economic development. "It was a very deliberate policy change," explains Cunningham.

Historically many pharmaceutical companies had established a presence in Ireland because of favorable corporate tax breaks and relatively cheap labor. "But the government realized that, if we were to remain attractive for foreign investment, our people would have to be trained to perform higher level functions," says Cunningham.

In 2006, the seven Irish universities and a number of institutes of technology awarded 979 Ph.D.s, 565 of which were in science and engineering disciplines. One of the targets under the Strategy for Science, Technology and Innovation is to increase the annual Ph.D. output to 1,300 by 2013. Additional goals are to "increase the number of research teams led by internationally competitive principal investigators" and to "develop sustainable career paths for researchers." continued »

> "The growth rate in research and development increased at twice the rate of the economy."

From Top: Ireland's coastline; **Issault Lynch; Patrick Cunningham;** The CRANN SFI CSET Building at Trinity College Dublin

**UPCOMING FEATURES**

Regenerative Medicine (online only) — November 7
Diversity: GLBT (online only) — December 5
Faculty 1: Choosing the Right Postdoc for Your Lab — February 6

"The country is extremely well placed to be a leader in this area."
—Frank Gannon


These tasks fall in the hands of the Science Foundation Ireland (SFI), the country's main research funding agency—a cross between the National Institutes of Health (NIH) and the National Science Foundation (NSF) in the United States. SFI was established in 2000 to support researchers working in those fields of science and engineering that underpin biotechnology, information and communications technology, and sustainable energy and energy-efficient technologies development. "SFI's mandate is to invest in basic science in areas related to the economy," says Cunningham.

SFI has a budget of €1.4 billion (US$1.9 billion) to spend over 2007–2013, translating to about €200 million (US$267 million) per year. "SFI is a component of a national economic program. We are focused on scientific excellence rather than short-term results," says **Frank Gannon,** who became SFI director general in July 2007, after leaving his post as executive director of the European Molecular Biology Organization (EMBO).

A major area of research funding for SFI is "interdisciplinary" research—a catchword for many granting bodies but, says Gannon, a good match for Ireland. "The country is extremely well placed to be a leader in this area. We have many leading pharmaceutical and software companies in a small country with strong social networks. At SFI we look to develop programs in convergence areas," says Gannon. "In many other countries research programs have grown more in silo fashion."

## A Changing Landscape

People who have worked in Ireland for many years have seen a huge change. "After graduating from Caltech [California Institute of Technology] in 1970, I came back to Ireland," recalls McConnell. "But it was not a good idea from the point of view of a scientific career. In fact it was a silly move." McConnell left for Harvard University, where he worked 1976–1977, but then returned to Ireland once again because "it looked as if things were going to change," he says.

McConnell joined the department of genetics at Trinity College Dublin in the late 1970s, a department that had been founded in 1958 with money from the Irish Sugar Company. At the time, it was difficult to obtain funds to conduct the kind of research McConnell had been used to doing in the United States.

By 1979, the European Commission (EC) started providing some grants for research. McConnell and colleagues at Trinity became very adept at obtaining these grants. "We relied heavily on EC funding for many years and built a lot of contacts with European scientists," recalls McConnell. With EC funding, geneticists at Trinity were able to participate in three of the early genome sequencing projects in yeast, *Arabidopsis*, and *Bacillus subtilis*.

After the year 2000, Irish scientists began to switch from EC funding to grants from SFI and other Irish agencies. "Today the funding is outstanding," says McConnell. "It is sufficient to allow you to compete internationally." McConnell's department—which moved to the Smurfit Institute of Genetics in 1998 with support from various philanthropies—currently receives €7 million (US$9.3 million) in annual research funding to support 15 groups and a total of about a hundred researchers. This year the department celebrated its fiftieth anniversary with a symposium held on 17–20 September with James Watson as a guest of honor.

**Ciaran Regan** also returned to Ireland in the pre-SFI days, after having worked many years in The Netherlands and London. "The transformation has been phenomenal," says Regan, a professor of neuropharmacology at University College Dublin (UCD). Regan's lab is located in UCD's Conway Institute of Biomolecular and Biomedical Research, a new building constructed in 1999 with funds from government and private donors. "It is the most magnificent and largest research center in Ireland," says Regan. "Working in this building has an unimaginable impact. It brings pressure to deliver and maintain a certain standard of research, but also an incredible sense of pride."

Regan's research focuses on synaptic plasticity—the ability of connections between neurons to change in strength—and its role in learning and memory. In addition to running his own lab, he directs the Applied Neurotherapeutic Research Group, a collaborative research initiative funded jointly by SFI and Wyeth, to understand the molecular underpinnings of changes in behavior and to identify new drug targets for diseases such as schizophrenia.

This type of collaboration is not unique. GlaxoSmithKline is investing up to €14.6 million (US$19.5 million) in a collaboration with TCD and the National University of Ireland (NUI) Galway to discover new therapies for Alzheimer's disease.

## Investing in R&D

Industry and academic partnerships are a common theme of Irish research. It is not surprising considering that the small country has a very high concentration of major pharmaceutical companies: Genzyme, Pfizer, Amgen, GlaxoSmithKline, Merck Sharp & Dohme (part of the US company Merck & Co.), Boston Scientific, Wyeth, Johson & Johnson, Abbott, and others have substantial operations in Ireland. According to the Industrial Development Agency (IDA), Ireland has established itself as the most popular destination for development and manufacture outside the United States. In 2006 the pharmaceutical and biotech industries brought in the bulk of the €2.6 billion (US$3.5 billion) the region saw in capital investment projects. continued »

CREDIT: PHOTO COURTESY OF SFI

Focus on Ireland

Researcher at Trinity College

## Featured Participants

**Applied Neurotherapeutics Research Group**
www.ucd-neurotherapeutics.com/~conway

**European Commission (EC)**
ec.europa.eu

**Industrial Development Agency**
www.idaireland.com

**National Institute for Bioprocessing Research and Training**
www.nibrt.ie

**National University of Ireland (NUI)**
www.nuigalway.ie

**Science Foundation Ireland (SFI)**
www.sfi.ie

**Trinity College Dublin (TCD)**
www.tcd.ie

**University College Dublin (UCD)**
www.ucd.ie

Regent House at Trinity College Dublin

Several factors make Ireland attractive to foreign investors. The country has one of the world's lowest rates of corporation tax, with the maximum rate for trading profits of 12.5 percent. It also provides many economic incentives for intellectual property developed and licensed from the country, such as patent royalty exemption and a research and development tax credit.

But another attraction is that Ireland has a skilled labor force, according to **Daniel Hoey** and **Bryan Meehan,** managers at two Merck, Sharp and Dohme facilities in Ireland. The plant in Ballydine, established in 1976, currently employs 340 people. Merck is now investing €100 million (US$133 million) to expand the plant and create 120 new positions over the next three years. "We will now start doing late-stage process and analytical development as well as the launch of new products from this site," says Hoey.

Plans are also under way to establish a new €200 million (US$267 million) vaccine facility in Carlow Town with the support of IDA Ireland. The plant, which will develop and manufacture human vaccines, is expected to launch in 2011 and will create 170 new jobs. "We decided to build the plant here after considering a number of sites worldwide," says Meehan, adding that key considerations included government collaboration, access to top scientists, and a proven track record in Ballydine. "We are just starting to hire now and the talent we are seeing is first class."

And Merck is not unique in its expansion efforts. Pfizer will build a €190 million (US$252.7 million) biotechnology factory in Cork to make drugs the US company is testing to replace older medicines. The plant will be Pfizer's sixth in the country. In December 2006, Eli Lilly and Company announced it was to invest up to €400 million (US$532 million) in a program to establish a biopharmaceuticals development and manufacturing facility in Kinsale. "Until 10 years ago most companies only did production in Ireland. Most carried out no development," says **Barry O'Dowd,** IDA Ireland's manager for pharmaceuticals and biotechnology. "Today 70 percent of companies are doing some development work."

In addition, an increasing number of startups are popping up in Ireland. Opsona Therapeutics, for example, a drug development company focusing on the regulation of the human immune system, was founded in Dublin in 2004 by three immunologists at Trinity College Dublin. One of Opsona's main investors is the California-based biotech company Genentech.

### A Developing Science Environment

An indication that Ireland provides a favorable research environment is that researchers from the United States, UK, Germany, and other European countries are moving there. To facilitate the move SFI provides awards to established researchers relocating to Ireland—up to €500,000 (US$665,000) per year for up to two years to set up a new lab.

After obtaining one of these awards, **Kevin Sullivan** left his lab at the Scripps Research Institute in sunny San Diego, where he had spent close to 20 years, to join NUI Galway on the west coast of Ireland.

In 2004, Noel Lowndes at Galway was gearing up to form a center of excellence for the study of chromosome biology, Sullivan's field of expertise. The prospect of joining that group, which today comprises 10 labs in the Center for Chromosome Biology, combined with increased science funding in Ireland and a gloomy funding scene in the United States prompted Sullivan to move. "It is a very collegial environment," he says. "Here at the center, there is a desire to inform and participate in each other's research."

One of the goals of the Center for Chromosome Biology is to establish screening techniques using small interfering RNAs (siRNAs) to find new targets for anticancer drugs, as well as gain a better continued »


Pauline Rudd

"Here at the center, there is a feeling to inform and participate in each other's research."
—Kevin Sullivan

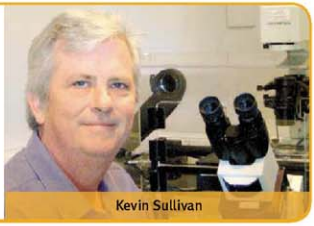
Kevin Sullivan

understanding of fundamental cancer mechanisms. While Sullivan is optimistic that this kind of research can be done in Ireland, he bellieves that the expensive and extensive infrastructure it requires is not yet in place. "We budget about €15,000 (US$19,950) operating expenses for each researcher per year. To do one of the siRNA screens you need about €50,000 (US$66,500), more than three years worth of operating expenses for an individual," he explains. "This type of science is a big investment and, while the return in terms of basic science can come rapidly and with high impact, the translation to biotechnologies is less certain and certainly longer term."

While in the United States there is a long history of funding basic science and there are many large and established centers that researchers can tap into, Ireland's research enterprise is still in its budding stages. "Ireland is still very youthful in its drive to become an internationally competitive center for biomedical research," says Sullivan. That can be a source of some frustration at times, but being in a position to impact positively on Ireland's scientific development is an attraction to many people.

**Pauline Rudd** at UCD is one of them. "There is a real sense that you can help make a difference. A few weeks ago I met the minister of the Department of Enterprise, Trade and Employment [Jimmy Devins] and he actually knew who I was. That would be unlikely to happen in a country like the UK," she says. "Here, you can influence the direction that science is taking because you are close to the people making the decisions."

## Collaborations Take Center Stage

Rudd moved to UCD from the Glycobiology Institute at the University of Oxford in the UK to join the National Institute for Bioprocessing Research and Training (NIBRT). The goal of this newly established institute, funded to the tune of €72 million (US$95.76 million) by IDA Ireland, is to support the biopharmaceutical industry at all levels. "If a company decides to move to Ireland and has specific scientific issues they are grappling with, they can come to NIBRT and we will help them solve their problems," says Rudd.

NIBRT scientists will provide training in the whole spectrum of bioprocessing activities as well as undertake research projects to advance current knowledge of bioprocessing technologies and techniques. "It is always a dream for academics to see practical applications of their work," says Rudd. "It would be a privilege to know that we contributed to the development of a drug that is helping patients."

Rudd is a world-renowned expert in glycobiology, or the study of sugar molecules, a field that is becoming increasingly important to the pharmaceutical industry. Many of the new biological drugs, or biologics, currently being manufactured are glycoproteins, i.e., proteins with attached sugar molecules. It is thus important to have ways to quickly establish the glycosylation status of a protein at all stages of bioprocessing. For example, about 40 percent of the hormone erythropoietin has to be discarded during manufacturing because of inappropriate glycosylation.

Rudd also carries on an independent research program at NIBRT and has a joint appointment at UCD. She has found that Ireland provides wider opportunities for academic collaboration than in the UK. "Most research grants in Ireland involve being in big interdisciplinary clusters," says Rudd. "It forces you to relate your expertise to a completely different field."

This spirit of collaboration led to the launch of a new network of academic researchers with multimillion euros of funding, called GlycoScience Ireland, in April 2008. The network is planning a research collaboration to understand how specific bacteria colonize the human gut by modifying the sugars attached to cells that line the intestines—the results of which will have implications for the milk production industry since some bacteria in milk become part of the human intestinal flora.

"This kind of collaboration would be unlikely to happen in England," says Rudd. "In the UK, collaborations tend to be between a small number of laboratories and we would ask relatively focused, academic-type questions. Here many more labs participate and the questions we ask are more global in relevance. It is exciting and challenging."

There is no doubt that in a short time Ireland has undergone a dramatic change. Although the research enterprise is still just developing, today moving to Ireland can be a positive career move for many. "If you want to move to a cosmopolitan city, join a university that is over 400 years old and do first-class science, you should come for a visit," says Trinity College's McConnell. And for anyone worried about the unpredictable weather, McConnell says there is plenty of Guinness to go around to make up for it!

*Laura Bonetta is a scientist turned freelance writer based in the Washington, D.C., area.*

DOI: 10.1126/science.opms.r0800064

CREDIT (LEFT): PHOTOGRAPHER: KILLIAN O'DRISCOLL (NIBRT)